Chiral lanthanide complexes

Rachel Sarah Dickins

CHIRAL LANTHANIDE COMPLEXES

Rachel Sarah Dickins

A thesis submitted in part-fulfilment of the degree of Doctor of Philosophy
of the University of Durham
October 1997

Research carried out at the Department of Chemistry
1994-1997

CHIRAL LANTHANIDE COMPLEXES

Rachel Sarah Dickins

ABSTRACT

The use of chiral lanthanide complexes as probes to investigate interactions with other chiral molecules and macromolecules is of particular interest. A key step in the development of such systems is the preparation of a single, rigid enantiomer of the complex which is conformationally rigid on the NMR timescale or the lifetime of the metal-based emission. Chiral europium and terbium complexes are of particular concern as they may function as emissive probes and are amenable to analysis by circular dichroism and circularly polarised luminescence.

Charge neutral and cationic complexes of N-substituted 1,4,7,10-tetraazacyclododecane, functionalised with three phosphinate and one amide pendent arms, or two, three and four pendent amide arms containing a remote chiral centre, have been prepared. The chirality of the remote stereocentre determines the helicity of the arrangement of the pendent arms and the conformation of the 12-membered macrocycle.

The chiral europium and terbium complexes of the tetraamide complexes exist as single, rigid enantiomers, exhibiting a well-defined metal-based circularly polarised emission. Circular dichroism studies reveal that exciton coupling occurs between adjacent pairs of 1-naphthyl chromophores of tetraamides, whereas the constitutional 2-naphthyl isomers exhibit excimer formation.

The behaviour of the di-, tri-, and tetraamide complexes in the presence of added anions has been investigated. The measurement of the luminescent lifetime of the excited state and the circularly polarised emission exhibited by the enantiopure complexes in aqueous solution affords a novel way of signalling the presence of selected oxy-anions.

University of Durham, October 1997

Declaration

The research described in this thesis was undertaken at the Department of Chemistry of the University of Durham between October 1994 and September 1997. All of the work is my own, except where specifically stated otherwise. No part of it has been submitted previously for a degree at this or any other University.

Statement of Copyright

ACKNOWLEDGEMENTS

I would like to express my sincere thanks to all the people with whom I have worked during my time at Durham.

It has been a pleasure and privilege to have worked for Professor David Parker who has provided not only a wealth of knowledge and sound advice, but much enthusiasm and encouragement throughout the years.

I would like to thank Professor Silvio Aime and Dr. Mauro Botta, Turin, for providing NMR analysis of some of the paramagnetic complexes, Professor Jim Riehl, Michigan, and Dr. Bob Peacock, Glasgow, for performing the circularly polarised luminescence, Dr. Giuliano Siligardi, Birkbeck, for the circular dichroism measurements and Dr. Lorenzo di Bari, Pisa, for the near infra-red CD spectrum.

The technical staff have provided support and efficient services and have also been friendly faces in the department, especially my 'Dads in Durham', Ray and Gordon.

Dr. Gareth Williams has been a kind, patient co-worker whose experience and help has been invaluable and greatly appreciated. The postgraduate and postdoctoral workers within the department have not only provided much help, experience and encouragement but also laughter, circuit training, great Friday nights out in Klute and, above all, friendship.

I should like to thank all my friends at D.A.R.C., especially Michael, for their kindness, considerable support and greatly appreciated distractions from work.

Finally my utmost thanks must go to my parents, sister Caroline and Gran who have supported my every move, provided me with the most wonderful opportunities and have given me the best gift of all, their unconditional love.

To Mum and Dad

CONTENTS

ABBREVIATIONS

Compounds

$12N_4$	1,4,7,10-tetraazacyclododecane
DMF	N,N-dimethylformamide
DMSO	dimethylsulfoxide
DNA	deoxyribonucleic acid
DOTA	1,4,7,10-tetraazacyclododecane-1,4,7,10-tetraacetic acid
dpm	dipivaloylmethane
DTPA	diethylenetriamine-N, N, N'', N', N'-pentaacetic acid
EDTA	ethylenediamine-N, N, N', N',-tetraacetic acid
$Eu(facam)_3$	europiumtris(3-trifluoroacetyl-d-camphorato)
MES	2-[N-morpholino]ethanesulfonic acid
MOPS	3-[N-morpholino]propanesulfonic acid
1-Np	1-naphthyl
2-Np	2-naphthyl
Ph	phenyl
TFA	trifluoroacetic acid
THF	tetrahydrofuran

Techniques and Spectroscopy

$[\alpha]_D$		optical rotation
CD		circular dichroism
	g_{abs}	absorption dissymmetry factor
CPL		circularly polarised luminescence
	g_{em}	emission dissymmetry factor
	PEM	photoelastic modulator
HPLC		high performance liquid chromatography
IR		infra-red spectroscopy
	br	broad

	m	medium
	s	strong
	str	stretching vibration
	w	weak
m.p.		melting point
MS		mass spectroscopy
	DCI	desorbed chemical ionisation
	ESMS	electrospray mass spectrometry
	ES+	electrospray ionisation using positive ion detection mode
	ES-	electrospray ionisation using negative ion detection mode
	FAB	fast atom bombardment
	M	molecular ion
MRI		magnetic resonance imaging
NMR		nuclear magnetic resonance
	COSY	correlation spectroscopy
	EXSY	exchange spectroscopy
	br	broad
	d	doublet
	m	multiplet
	s	singlet
	t	triplet
	VT	variable temperature
NMRD		nuclear magnetic dispersion profile
TLC		thin layer chromatography
u.v.		ultraviolet

Miscellaneous

Ln	generic symbol for a lanthanide ion
LMCT	ligand to metal charge transfer
M	mol dm^{-3}

CHAPTER 1

INTRODUCTION

CHAPTER 1

INTRODUCTION

This thesis describes the work carried out in the synthesis and characterisation of enantiopure lanthanide complexes, and a study of their physicochemical properties in solution.

Lanthanide complexes have been studied intensively due to their potential use in radiopharmaceuticals[1], as contrast agents in magnetic resonance imaging[2,3], as luminescent probes in biochemical analyses[4,5] and as shift reagents in NMR.[6,7] Of major concern is the investigation of the behaviour of these metal complexes *in vivo* and their interactions with large molecules such as DNA and proteins. In biological systems, the remarkable specificity in the interaction between molecules and in their chemical reactions is largely determined by charge and chirality.

1.1 Complex design

1.1.1 Charge

The kinetic stability of a complex is dependent, among other factors, upon its charge. The major kinetic pathway for metal ion dissociation is likely to be acid or cation promoted[8], therefore it is preferable to synthesise charge neutral or cationic metal complexes where the tendency for protonation or encounter with other cations is disfavoured. For example, the neutral gadolinium complex of monoamide **(1a)** dissociates eight times more slowly than the complex of the anionic analogue **(2a)**.[9]

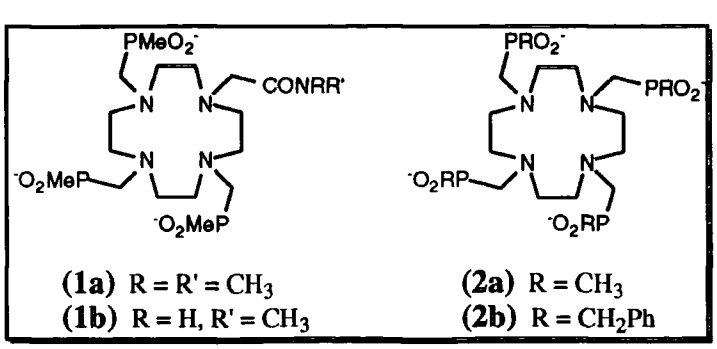

(1a) R = R' = CH_3
(1b) R = H, R' = CH_3

(2a) R = CH_3
(2b) R = CH_2Ph

The charge of a complex is also critical in determining its biodistribution. If passive diffusion into cells and penetration of the blood-brain barrier or the nuclear membrane of a cell is required, charge neutral complexes are desirable. The charge neutral technetium complexes (**3**)[10] and (**4**)[11], for example, are stereoselective imaging agents for the brain whereas cationic compexes such as (**5**) and (**6**) are found to be targeted to the heart.[12,13]

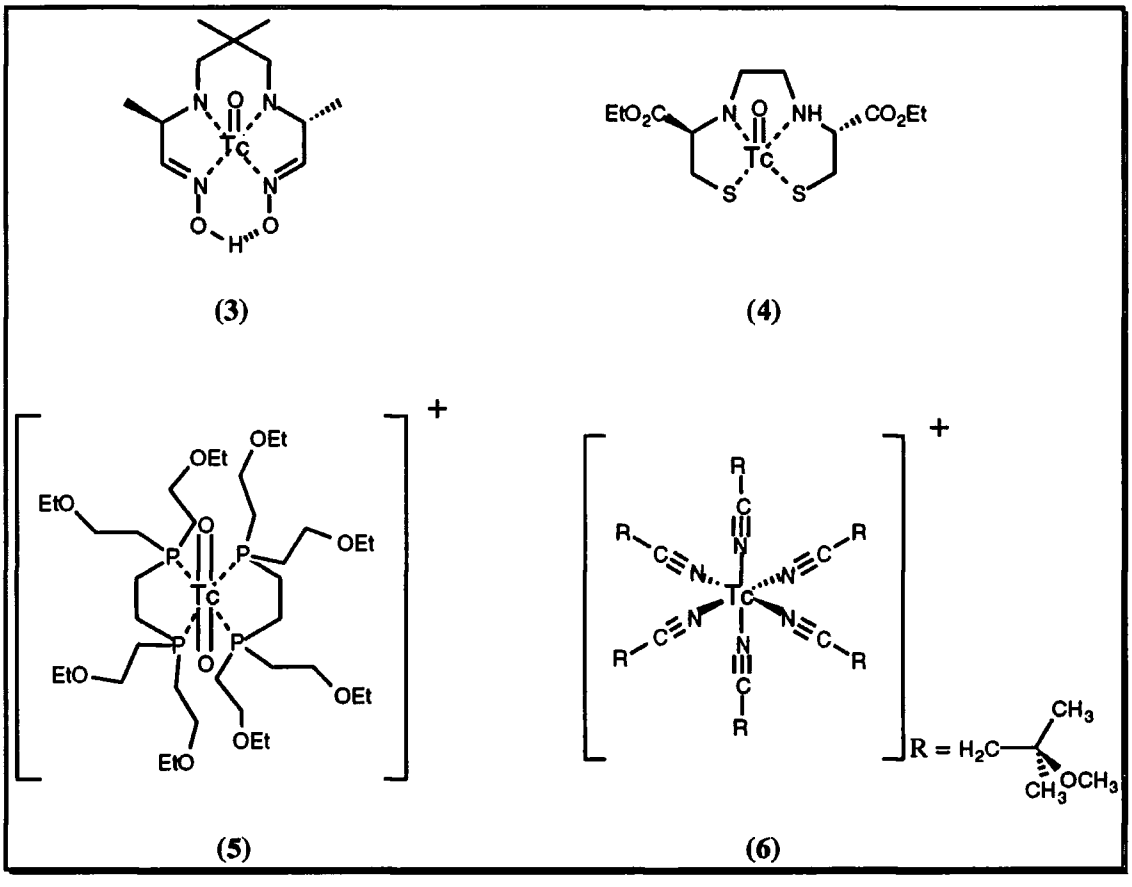

The anionic gadolinium complex of (**2b**), exhibits biliary clearance whereas related neutral and cationic complexes clear via the renal system thereby providing enhanced imaging possibilities for the liver / gall bladder / intestine.[14,15]

1.1.2 Chirality

In nature, precise molecular recognition and specific reactions are achieved using chiral molecules. For example, the natural enzyme chymotrypsin reacts efficiently with only one enantiomer, L-tryptophan methyl ester, to catalyse its hydrolysis whereas the D-tryptophan methyl ester is a competitve inhibitor.[16] This specificity displayed in nature

is not at all surprising as specific binding interactions and chiral discrimination will be governed by stereochemistry and the molecular architecture of the binding site. This is evident from the comparison of the binding of enantiomers of the chiral intercalator, ruthenium trisphenanthroline complexes, $Ru(phen)_3^{2+}$, to 'B'-DNA[17] **(Figure 1.1)**.

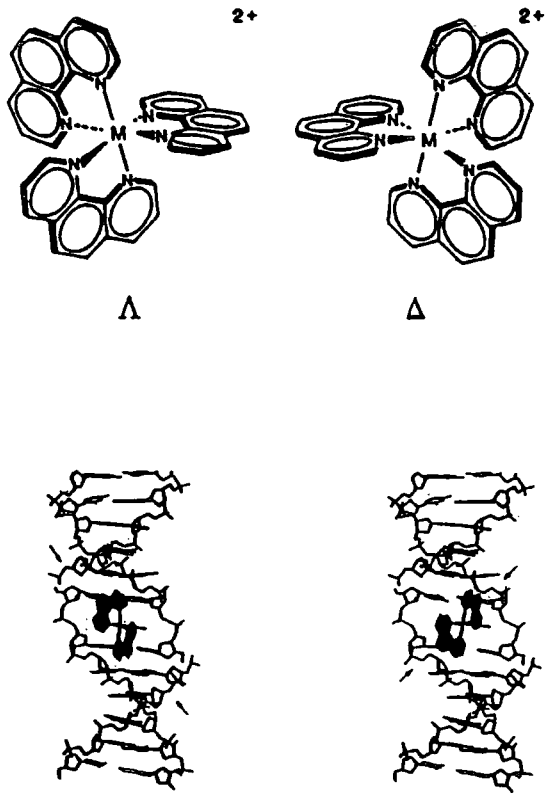

Figure 1.1. The Λ- and Δ-enantiomers of a tris(phenanthroline) metal complex and their models of intercalation in a 'B'-DNA helix. The arrows indicate the disposition of the non-intercalated ligands with respect to the helical groove.[17]

Binding favours the Δ-isomer as with one phenanthroline group intercalated into the DNA helix the remaining phenanthroline groups lie along the groove of the right-handed DNA in a complementary fashion. However, for the Λ-isomer, with one phenanthroline group intercalated steric repulsions are evident between the non-intercalated phenanthroline hydrogen atoms and phosphate atoms on the helix, the

arrangement of non-intercalated groups therefore opposing the right-handed DNA groove. This chiral discrimination depends on matching the chirality of the complex to that of the helix. Similarly, enantiomeric selectivity has also been observed in the covalent binding of chiral complexes to DNA through hydrophobic binding or coordination sites along the groove, and the chiral discrimination favours structures whose symmetry is complementary to that of the DNA helix.[18]

1.1.3 Ligand structure

The lanthanide ions are classified as hard acids and therefore prefer hard donor atoms such as O and N. More polarisable amine nitrogens are preferred to ether oxygens and donors with large ground state dipole moments such as carboxamides and sulphoxides are better donors than less polar substituents such as alcohols. As the lanthanide-ligand coordination is predominantly ionic in nature, negatively charged donor groups such as carboxylates, phosphonates and phosphinates are highly suitable. Water is an extremely strong ligand for lanthanides and this restricts complex stability in aqueous media as other ligands must compete for coordination. Coordination numbers from 6 to 12 have been reported in the solid state for lanthanides but 8 and 9 coordinate complexes are most common in solution.

Complex stabilities may be enhanced by incorporating the donor atoms into chelating rings. This is known as the chelate effect.[19] For lanthanide ions, 5-membered chelate rings are favoured over 6-membered chelates.[20] Incorporating the donor atoms into a macrocycle gives rise to additional stability.[21] This 'macrocyclic effect' is due to enthalpic and entropic factors which vary according to metal ion and macrocycle.[22] Suitable ligand systems for lanthanide ions will therefore be based on octadentate macrocycles containing some O and N donor atoms which are able to form 5-membered chelate rings.

Macrocyclic ligands based on 1,4,7,10-tetraazacyclododecane with functionalised pendent arms are ideally suited to bind lanthanides and a number of such complexes

have been reported. Representative examples include complexes of the anionic **(7)**[23,24], **(2)**,[25,26] neutral **(1)**[9] and cationic **(8)**[26,27] systems.

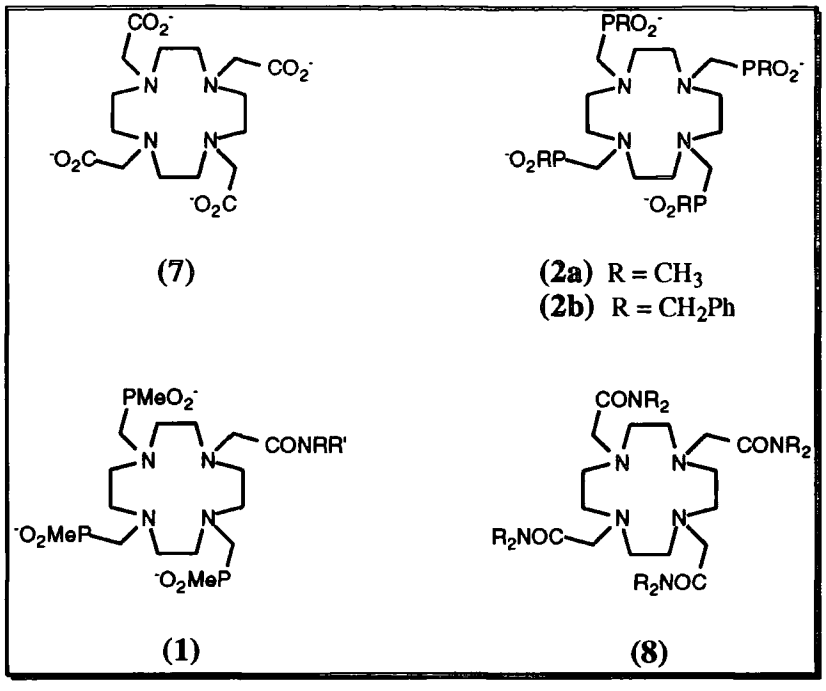

The anionic gadolinium complex of DOTA, **(Gd.7)**$^{-}$, developed by Desreux, is a clinically used extracellular contrast agent in magnetic resonance imaging. Lanthanide complexes of tetrabenzylphosphinates, **(2b)**, are shown to bind strongly to proteins such as albumin ($K_d = 3 \times 10^{-4}$ dm^3 mol^{-1}) and are recognised *in vivo* by the 'organic anionic transporter' found in liver cells which usually handles species such as bilirubin, leading to predominant biliary rather than renal clearance of the complex.[28,29] Neutral lanthanide complexes such as **(1)**[9] are advantageous for use *in vivo* as the lower osmolality reduces pain incurred on injection compared to anionic systems and the complexes are kinetically stable with respect to acid catalysed dissociation. The cationic complexes of **(8)**, have been shown to act as extracellular ^{31}P NMR shift reagents through their binding to inorganic phosphate in serum, allowing intra- versus extracellular phosphate concentration to be monitored.[30]

1.2 Stereoisomerism

1.2.1 Dota

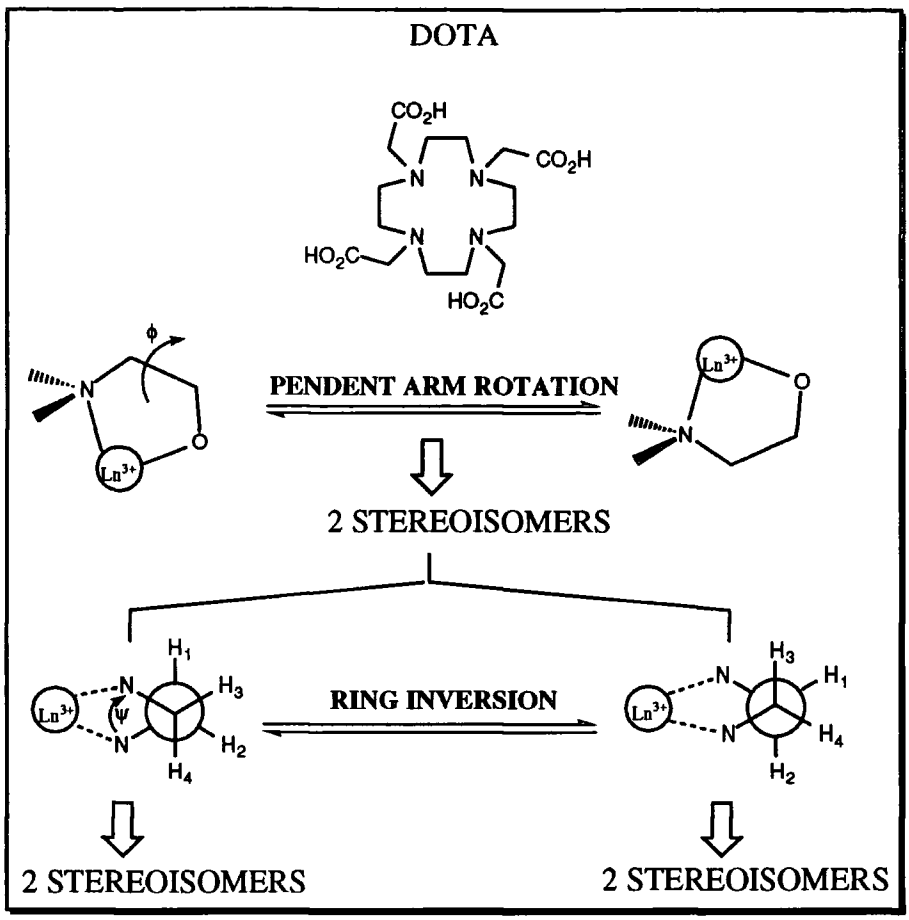

Figure 1.2. *Stereoisomerism exhibited by DOTA-like complexes.*

X-ray solid state structures of **(Ln.DOTA)**$^-$, **(Ln.7)**$^-$, complexes (Ln = Eu[24], Gd[31], Lu[32]), the simplest of the complexes based on 1,4,7,10-tetraazacyclododecane, show that the octadentate ligand, with four N and four O donor atoms, is arranged in a square antiprismatic geometry with a ninth axial coordination site occupied by a water molecule. The N atoms are arranged in a gauche conformation and the protons in the ethylenediamine bridges are staggered, giving rise to two possible ring conformations which may be described, following the nomenclature of Corey[33], as the ($\lambda\lambda\lambda\lambda$) or the enantiomeric ($\delta\delta\delta\delta$) conformation. Furthermore, the acetate pendent arms may be arranged in either a clockwise or an anticlockwise fashion resulting in a Λ or Δ conformation.[34] These two structurally independent features of chirality exhibited by such complexes based on 1,4,7,10-tetraazacyclododecane (**Figure 1.2**) gives rise to two

enantiomeric pairs of diastereoisomers for **(Ln.DOTA)**$^-$ complexes (M_1, M_2 and m_1, m_2), the structure and dynamics of which are depicted in **Figure 1.3.**

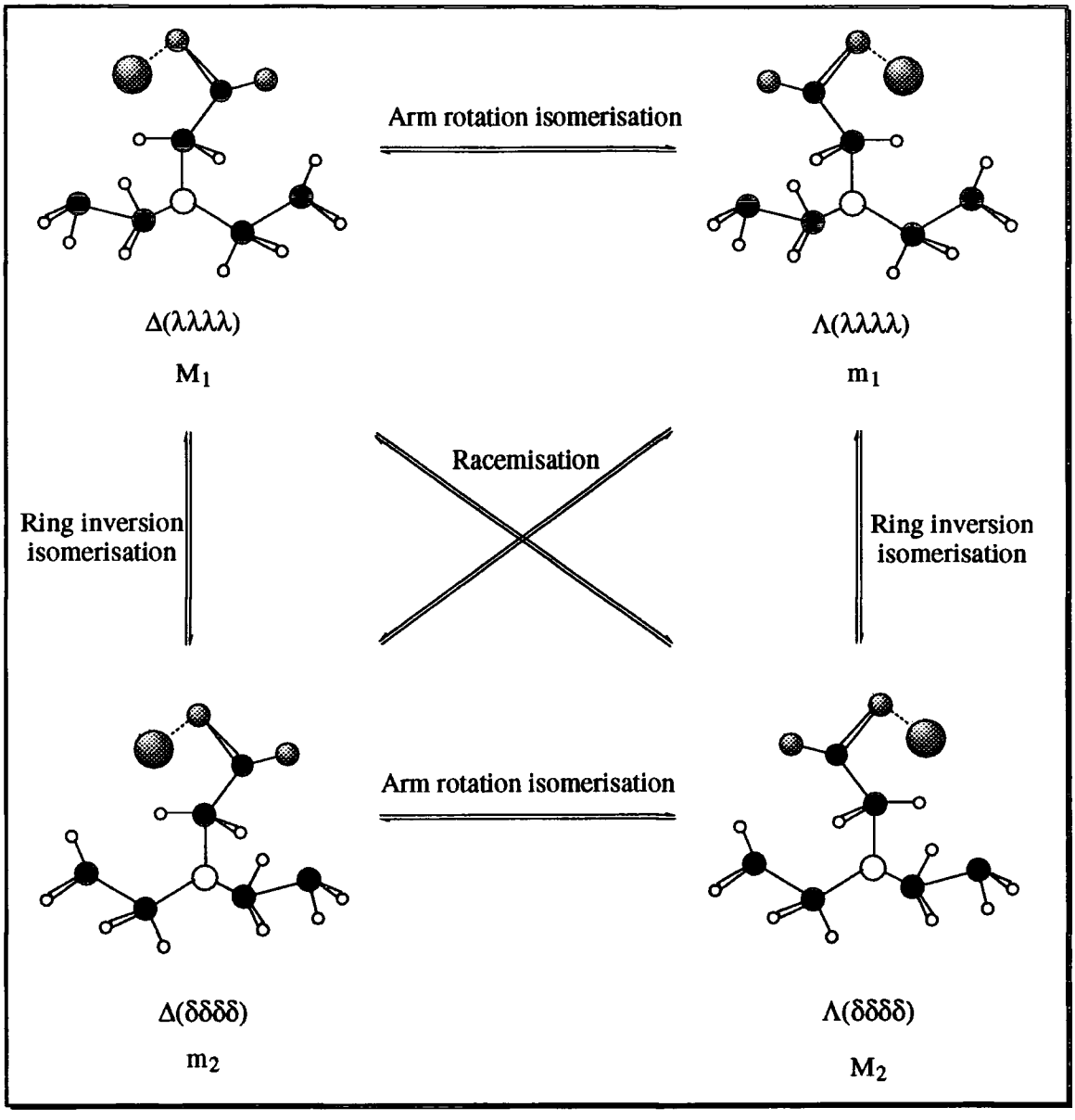

Figure 1.3. *Schematic representation of the diastereoisomers of* ***(Ln.DOTA)***$^-$ *complexes, showing the geometry about only one bound N-*CH_2*-COO group, and the possible exchange mechanisms.*

M_1 and M_2 have regular square antiprism structures, where the twist angle around the four-fold axis is 40°, whereas m_1 and m_2, with twist angles of 29°, have twisted square antiprism structures (**Figure 1.4**).

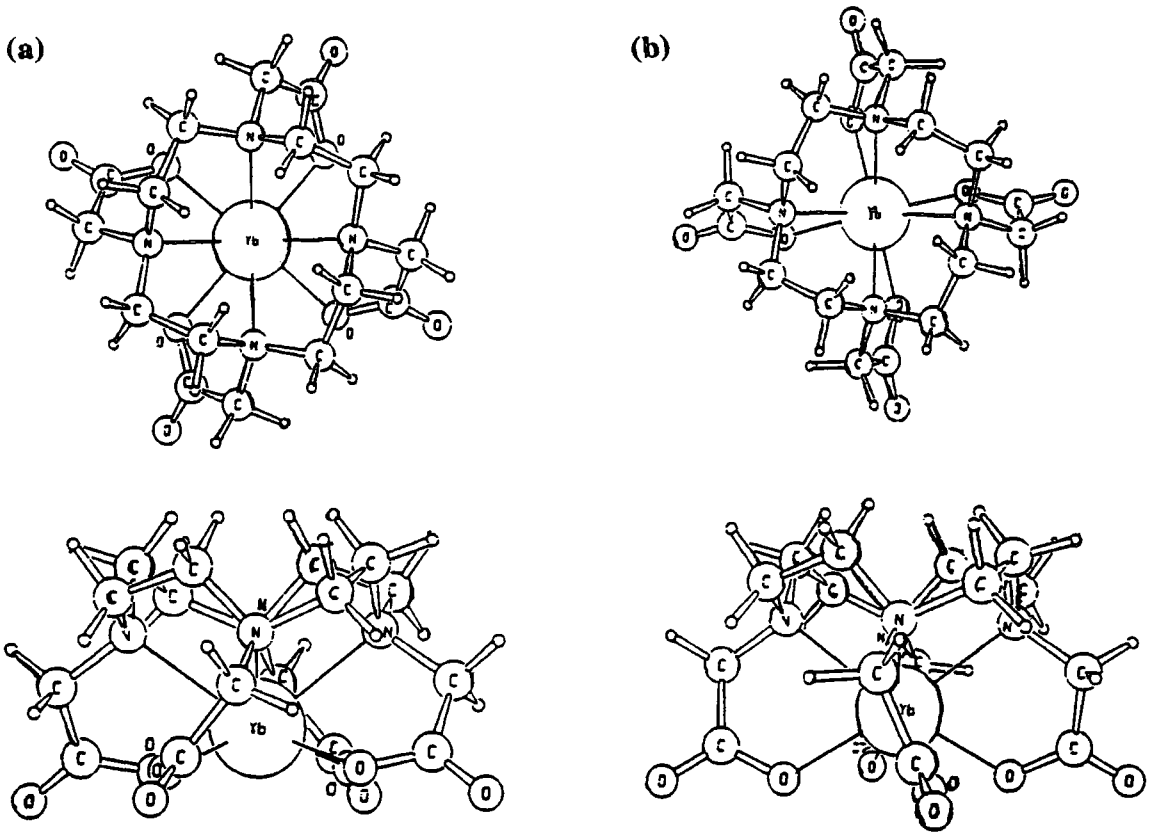

Figure 1.4. Top and side views of the structures for the **(a)** M and **(b)** m isomers as obtained by analysis of the dipolar shifts for the **(Yb.DOTA)**$^-$ complex.[35]

In the solid state, DOTA complexes of Eu, Gd, Lu and Y[36] have a $\Delta(\lambda\lambda\lambda\lambda)$, ($M_1$), or the enantiomeric $\Lambda(\delta\delta\delta\delta)$, ($M_2$), structure. However, in solution ^1H and ^{13}C NMR show the existence of both diastereoisomers (M and m) for all **(Ln.DOTA)**$^-$ complexes, which are in slow exchange at room temperature.[35] The relative proportions of the two isomers varies across the Ln series as shown in **Figure 1.5**.[37,38]

For the DOTA complexes of the larger ions, La, Ce and Pr, the m isomer is the more abundant. The two isomers appear in comparable amounts for **(Nd.DOTA)**$^-$, and moving across the Ln series the abundance of the M isomer increases, reaching a maximum for **(Ho.DOTA)**$^-$. For lanthanides heavier than Ho, the mole fraction of M decreases again with decreasing ionic radius.

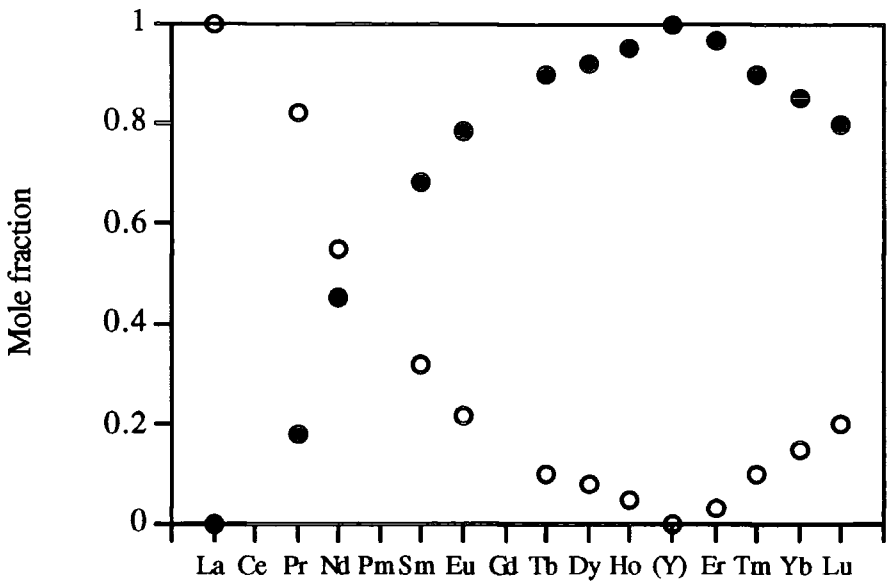

Figure 1.5. *Molar fractions of the isomers m (open circles) and M (filled circles) as a function of complexed metal ion determined from ^1H NMR spectroscopy. Data is taken from references 37 and 38.*

The m isomer has a larger 'effective' cavity size than the M isomer due to a reduction in the acetate-N-CH_2 torsion angle caused by steric hindrance between the acetate proton and neighbouring axial ring protons, and therefore is favoured for the larger lanthanides. The M isomer, with its smaller 'effective' cavity, becomes more favourable as the size of the lanthanide ion decreases. The reversal of the trend observed towards the end of the series has been attributed to the presence of a third species present in solution, M' or m', representing the loss of the inner sphere water on the complex which results in a further decrease in the 'effective' cavity size.[37] A coordination equilibrium (**Figure 1.6**) is therefore superimposed on the conformational equilibrium shown in **Figure 1.3**.

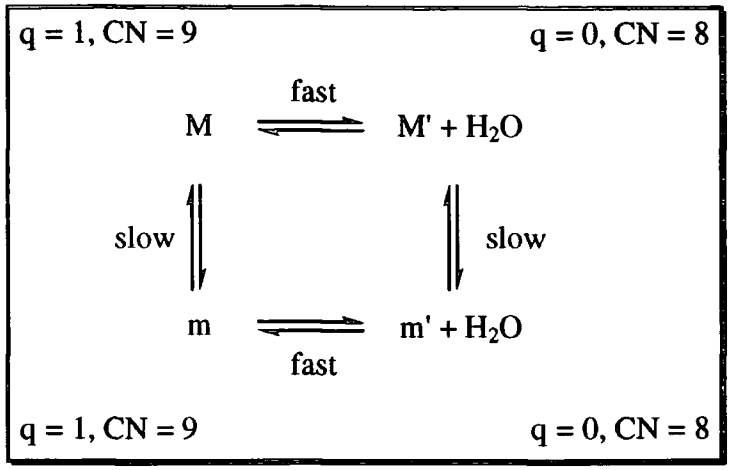

Figure 1.6. *Schematic representation of the coordination and conformational equilibria in solution. Enantiomeric pairs are not shown.*

The coordination equilibrium between bound (M, m) and unbound (M', m') water is fast on the NMR time scale (10^5 - 10^8 s^{-1})[39], and therefore not distinguishable by this technique, whereas the conformational equilibria are slow giving rise to differing proton spectra for the M and m isomers.[35] Evidence for the coordination equilibrium arises from variable-pressure studies.[37] Near-zero reaction volumes were observed for the isomerisation of **(Nd.DOTA)**$^-$ and **(Eu.DOTA)**$^-$ indicating that the isomerisation proceeds without a change in coordination, whereas large positive reaction volumes were observed for the isomerisation of **(Yb.DOTA)**$^-$ and **(Lu.DOTA)**$^-$ suggesting the isomerisation proceeds with the decrease of coordination from 9 to 8.

The cavity size of the isomers decreases in the order m > M > m' > M', and the isomers predominate in this same order as the lanthanide (III) ionic radius decreases. Hence the decrease in mole fraction of the M isomer apparent from Er^{3+} onwards can be attributed to the increasing presence of the m' isomer.

2D-EXSY spectra show that each proton in one isomer exchanges with a proton in that same isomer and with two protons in the other isomer, one of them being located in a similar environment (eg. $M_{ax} \rightarrow m_{ax}$) and one being orientated differently (eg. $M_{ax} \rightarrow m_{eq}$).[35,38,40] The possible exchange mechanisms, isomerisation or racemisation, are depicted in **Figure 1.3**. Isomerisation may occur by a rotation of the

acetate arms whilst the ring maintains a fixed conformation, or via inversion of the ring ethylenic groups keeping the acetate arms in a fixed position. Racemisation may occur by an intramolecular mechanism or by rotation of the acetate arms followed by inversion of the ring conformation. Variable temperature ^{1}H NMR spectra of **(Pr.DOTA)**$^{-}$ and ^{13}C NMR spectra of **(Nd.DOTA)**$^{-}$ show that the isomerisation process occurs more quickly than the racemisation process.[35] However the studies were unable to ascertain whether the isomerisation process occurs through an arm rotation or a ring inversion. 2D-EXSY spectra of **(Nd.DOTA)**$^{-}$ show that the two isomerisation processes, arm rotation and ring inversion, occur at the same rates and are characterised by the same thermodynamic parameters, suggesting a possible concerted mechanism for the isomerism.[40]

Summarising, for **(Ln.DOTA)**$^{-}$ complexes there exists two enantiomeric pairs of diastereoisomers in solution, observable by NMR, which are in exchange and interconverting through either a pendent arm rotation, ring inversion or some combined synchronous motion.

1.2.2 Tetraphosphinates

Another class of octadentate lanthanide complexes based on 1,4,7,10-tetraazacyclododecane to be considered is the tetraphosphinates.[28] The complexes display the arm rotation and ring inversion isomerism exhibited by DOTA complexes (**Figure 1.3**) but an additional degree of chirality is introduced into such systems, as upon metal binding, chiral centres are created at the P atoms. This results in the formation of 24 possible stereoisomers, 8 of which will be enantiomeric pairs, therefore only 16 of the stereoisomers will be distinguishable by NMR analysis, in principle (**Figure 1.7**).

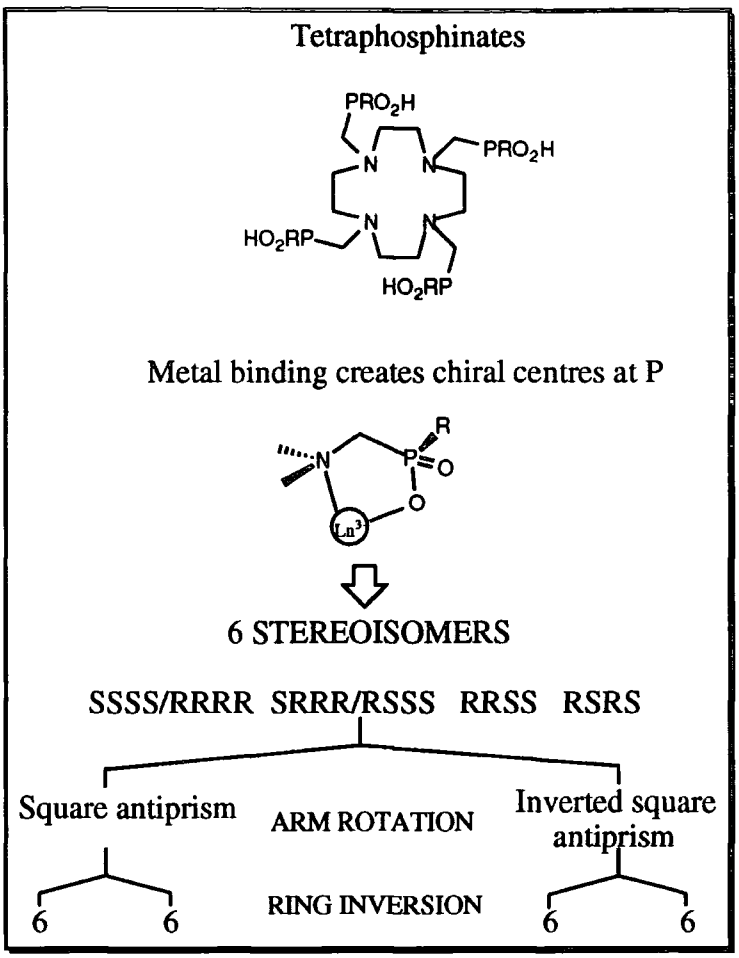

Figure 1.7. *Stereoisomerism exhibited by tetraphosphinate complexes.*

X-ray solid state structures of Ln^{3+} tetraphosphinates[41] (Ln = Yb, Gd, Eu) show that all the complexes, with four O and four N donor atoms, are arranged in a twisted square antiprismatic geometry (m). The earlier lanthanides and La are 9 coordinate with a water molecule bound to the metal centre, whereas the middle and later lanthanides are 8 coordinate and lack a bound water molecule. The complexes exist in two enantiomeric forms with an RRRR or SSSS configuration at P.

Solution NMR analysis shows that one diastereoisomer, out of the 16 possibilities, is largely predominant (»90%).[42] The ^1H chemical shifts for the Yb complex are remarkably similar to those observed for the minor isomer of **(Yb.DOTA)**$^-$.[35] It is well known that Yb^{3+} causes paramagnetic shifts that are essentially free of any contact contribution[43], therefore ^1H NMR shifts may be correlated directly to structure which suggests that in solution the Yb^{3+} tetraphosphinate complex adopts a twisted square

antiprismatic structure. The diastereoisomer has two enantiomeric forms, presumably RRRR and SSSS with respect to P as these minimise steric constaints. The two enantiomeric complexes of the tetrabenzylphosphinates (**2b**), may be distinguished upon the addition of β-cyclodextrin which acts as a chiral solvating agent in aqueous media.[42] Furthermore, variable temperature ^1H NMR studies (5 - 80 °C) of Y^{3+}, Eu^{3+} and Yb^{3+} complexes indicate a high degree of stereochemical rigidity in the systems. On passing from an acetate pendent arm in DOTA to a sterically more demanding phosphinate group, the isomerisation processes involving arm rotation and ring inversion have been frozen out.

1.2.3 Monoamidotriphosphinates

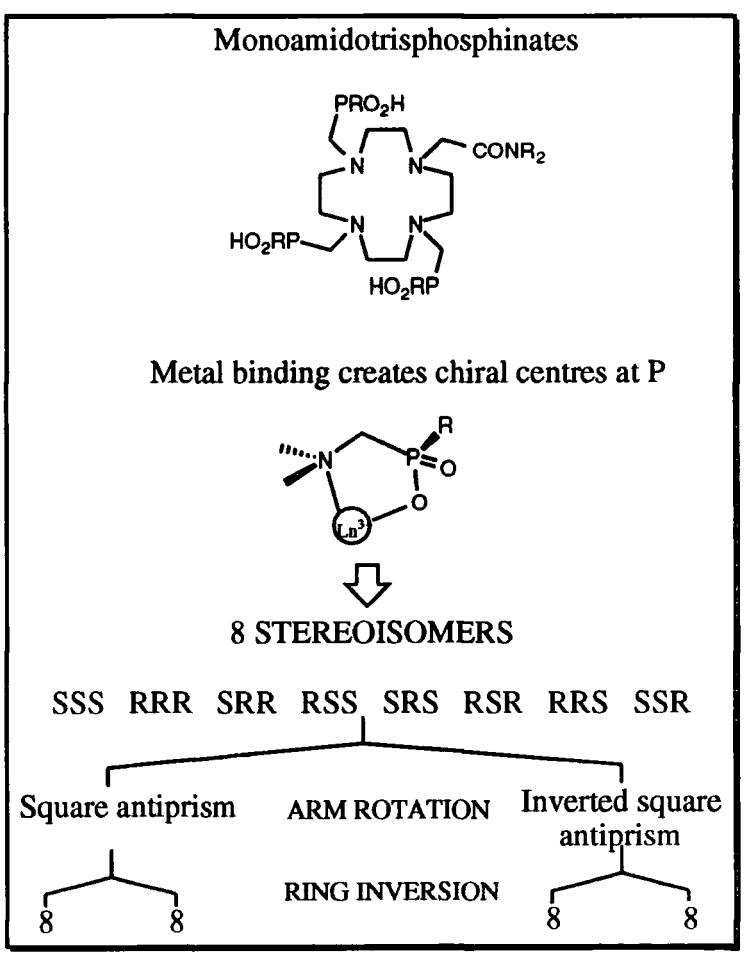

Figure 1.8. *Stereoisomers of monoamidotrisphoshinate complexes.*

When one of the phosphinate groups is replaced by a neutral carboxamide substituent then the number of possible stereoisomers increases to 32 (**Figure 1.8**). There are 16

pairs of enantiomers, therefore only 16 of the stereoisomers will be distinguishable by NMR analysis, in principle.

Again largely one, rigid diastereoisomer predominates in solution with suggested RRR and SSS configuration at P.[42]

1.3 Paramagnetic NMR

When a paramagnetic ion interacts with an NMR active nucleus, the presence of the unpaired electrons results in an enhanced relaxation of the nucleus, broadening and sometimes shifting of the resonances.[44] The large magnetic moments of the lanthanide ions results in expanded chemical shift ranges and ^1H shifts of 200 ppm or more are not unusual. The unpaired electrons also cause large perturbations in the distribution of the local magnetic fields which result in nuclear relaxation and line broadening. This signal broadening is very severe for many lanthanides such as dysprosium and terbium and, as a result, multiplets arising from spin-spin splitting may be lost.

1.3.1 Chemical shift

The interaction of a nucleus with an unpaired electron can involve direct dipole-dipole coupling or indirect (scalar) coupling. A dipolar, or pseudocontact shift, δ_p, is a result of a through-space interaction between the electron and nuclear magnetic dipoles, and may be described[45] as

$$\delta_p = \frac{C_j \beta^2}{60 (k T)^2} \quad \frac{[A (3 \cos^2\theta - 1) + A' (\sin^2\theta \cos 2\phi)]}{r^3} \qquad \textbf{(1.1)}$$

$$\text{where } C_j = g^2 J(J+1)(2J-1)(2J+3) \langle J | a | J \rangle$$

The terms A and A' are crystal-field coefficients and $\langle J | a | J \rangle$ is a numerical coefficient. The lanthanide independent constants, A and A', may be combined with C_j to give a much simplified form of equation **(1.1)**.

$$\delta_p = \frac{D'(3\cos^2\theta - 1)}{r^3} + \frac{D''(\sin^2\theta \cos 2\phi)}{r^3} \qquad (1.2)$$

Scalar interactions result in Fermi or contact shifts, δ_c, and involve the interaction of the nuclear moment with the electric currents arising from the electron density at the nucleus. For electrons in spherical environments

$$\delta_c = \frac{2\pi A g_s \beta S(S+1)}{3hkT\gamma_I} \qquad (1.3)$$

However, for lanthanides spin-orbital coupling must be considered hence

$$\delta_c = \frac{2\pi A g_j (g_j - 1) \beta_j J(J+1)}{3hkT\gamma_I} \qquad (1.4)$$

where A is the hyperfine splitting constant, g the Lande splitting factor, β the Bohr magneton and γ the magnetogyric ratio.

The overall chemical shift for a paramagnetic system is given as a contribution of three terms

$$\delta = \delta_0 + \delta_c + \delta_p \qquad (1.5)$$

where δ_0 is the diamagnetic shift.

For lanthanides, the pseudocontact contribution usually predominates as the unpaired electrons in the 4f orbitals are largely shielded from the valence orbitals involved in bonding between the metal and the ligand. The unpaired electron spin density therefore largely resides on the lanthanide ion and shifts are mainly due to through-space interactions. These depend on the orientation of the resonating nucleus with respect to the lanthanide and can therefore give useful structural information.[6]

The shifting abilities of the lanthanides have been studied[46,47] and **Figure 1.9** shows the chemical shift of the most shifted resonance of n-hexanol in the presence of lanthanide (III) complexes of tris(dipivaloylmethanato), $Ln(dpm)_3$.

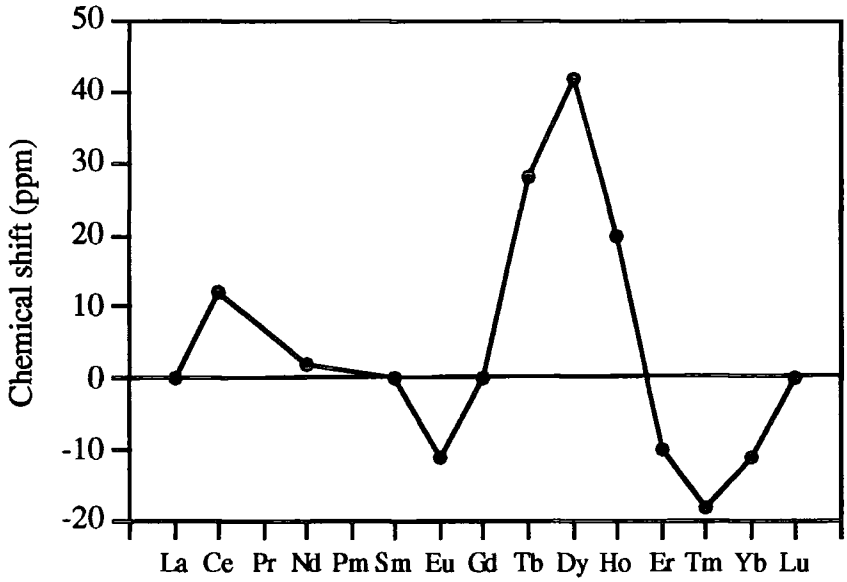

Figure 1.9. *Isotropic shifts of the most shifted resonance of n-hexanol in the presence of $Ln(dpm)_3$. Data from reference 44.*

Of the early lanthanides, Pr^{3+} and Eu^{3+} produce relatively large shifts to lower and higher frequency respectively, both occurring with negligible line broadening. Nd^{3+} and Sm^{3+} produce small and negligible shifts to lower frequency respectively. Gd^{3+} is not a shift reagent and as $\delta_p = 0$, due to the isotropic distribution of the 7 unpaired f electrons, this provides evidence in favour of the largely dipolar origin of the lanthanide shifts. Tb^{3+}, Dy^{3+} and Ho^{3+} all induce huge shifts to lower frequency with severe line broadening whereas Er^{3+}, Tm^{3+} and Yb^{3+} produce large shifts to higher frequency. Of course, the diamagnetic La^{3+} and Lu^{3+} complexes produce no shifts at all.

1.3.2 Relaxivity

Paramagnetic compounds catalyse the nuclear relaxation of nearby nuclei through time dependent fluctuations of the magnetic field due to dipolar and scalar interactions. The relaxation rates[48] of water protons are increased, typically by a factor of 10^6, when the

oxygen atom is coordinated to a highly paramagnetic ion such as Gd^{3+}. The ability of paramagnetic complexes to increase water proton relaxation rates is termed relaxivity. It is highly sensitive to structural, electronic and dynamic features of the complex. The observed longitudinal relaxation rate of water protons in a solution containing a paramagnetic complex is given by

$$R_1^{obs} = R_{1p}^{is} + R_{1p}^{os} + R_1^{o} \qquad \textbf{(1.6)}$$

where R_{1p}^{is} and R_{1p}^{os} are the inner and outer sphere contributions respectively and R_1^{o} is the water relaxation rate in the absence of a paramagnetic complex.

The inner sphere contribution involves dipolar coupling between the paramagnetic ion and the proton nuclei of the directly coordinated water molecules and depends on the correlation times that define molecular reorientation (τ_R), electron spin relaxation (τ_S), and chemical exchange of water (τ_M). The latter contribution is usually sufficiently fast for Gd^{3+} complexes (1-10 ns), to allow propagation of the effect to the bulk solvent. The inner sphere contribution is described by the Solomon-Bloembergen-Morgan theory[49] summarised by the equations **(1.7)** and **(1.8)**.

$$R_{1p}^{is} = \frac{C\,q}{55.6}\,\frac{1}{T_{1M} + \tau_M} \qquad \textbf{(1.7)}$$

$$T_{1M} = \frac{K}{r^6}\, f(\tau_C, \omega_I, \omega_S) \qquad \textbf{(1.8)}$$

where C is the molar concentration of paramagnetic complex, q is the number of water molecules directly coordinated to the metal and τ_M is the mean residence lifetime in the coordinated sites.

The term T_{1M} is the longitudinal proton relaxation time and depends on the inverse of the sixth power of the distance between the metal ion and water protons, the Larmor frequency for proton (ω_I) and electron (ω_S) and on the correlation time, τ_C, for the modulation of the dipolar interaction which is dependent on τ_R, τ_M and τ_S.

$$\frac{1}{\tau_C} = \frac{1}{\tau_R} + \frac{1}{\tau_S} + \frac{1}{\tau_M} \qquad \textbf{(1.9)}$$

The outer sphere contributions are due to a modulation of the electron-nuclear magnetic dipole caused by solvent molecules diffusing in the outer coordination sphere of the complex. The contribution depends on the relative translational diffusion of solute and solvent, D, and the electronic relaxation time, τ_S and is given by Freed's equation[50]

$$R_{1p}^{os} = \frac{32}{405} \gamma_H^2 g^2 \mu_B^2 S(S+1) \frac{N_A}{1000} \frac{C}{aD} f(\tau_S, \tau_D, \omega_I, \omega_S) \qquad \textbf{(1.10)}$$

where N_A is the Avogadro number, a is the distance of closest approach of the water molecule to the paramagnetic ion and $\tau_D = a^2/D$.

The longitudinal water proton relaxation rate is magnetic field dependent and can be measured over the magnetic field range corresponding to Larmor frequencies of 0.01 to 50 MHz using the field-cycling relaxometer developed by Koenig and Brown.[51] The nuclear magnetic relaxation dispersion (NMRD) profiles obtained represent a fingerprint of the relaxation properties of the metal chelates and may be analysed using the equations above to yield valuable structural and dynamic information. The relaxivity in the high magnetic field region is mainly controlled by τ_R, which depends on the relative size of the complex, whereas in the low magnetic field region τ_S is the dominant contributor, which is sensitive to symmetry and the chemical nature of the coordinating groups.

1.3.3 Applications

Shift reagents

There has been much interest in the use of lanthanide complexes as shift reagents in NMR since they were first introduced by Hinckley in 1969.[52] Shift reagents, when added to a solution of the compound under investigation, effect spectral simplification and resolution enhancement. This results in separation of the chemical shifts of

overlapping resonances without destruction of spin-spin coupling patterns. Shift reagents may be used with a majority of organic molecules that possess lone pairs available for coordination to the lanthanide ion. Research into lanthanide shift reagents has been focussed on Eu^{3+} and Pr^{3+} as these ions produce sizeable shifts with usually negligible line broadening of the resonances.[44,53]

Contrast agents

Although Gd^{3+} complexes are not suitable as shift reagents in NMR due to the large degree of broadening to which they give rise, they are perfect for use as contrast agents in magnetic resonance imaging (MRI).[2,3,54] MRI is a diagnostic technique relying upon the detection of spatially localised NMR signals of water protons. The signal intensity is dependent upon a number of factors but in particular the water proton relaxation times. Spatial resolution and detail of the NMR images of tissues can be greatly enhanced by the addition of a paramagnetic agent able to significantly decrease this relaxation time. The Gd^{3+} ion couples a large magnetic moment (S = 7/2) with a long electronic spin relaxation time ($\approx 10^{-9}$ s), two properties that ensure an optimum efficiency for nuclear spin relaxation.[55] As the free ion is highly toxic and therefore undesirable in the body, Gd^{3+} must be administered as a kinetically stable complex of high relaxivity, low toxicity, good water solubility and low osmolality. Other general requirements are the rapid excretion after administration, ensuring the complex is well-tolerated and current research is aimed at the targeting of suitably functionalised complexes to allow the selective imaging of certain tissues and organs.

1.4 Lanthanide Luminescence

1.4.1 General luminescence

Luminescence is the radiative process occurring when electrons, having absorbed energy to enter excited states, revert back to their ground states, losing energy by emitting light. The radiative pathway occurring between two levels of the same spin multiplicity ($\Delta S = 0$) is termed fluorescence, and typically takes 10^{-9} - 10^{-6} s. When the radiative process involves intersystem crossing, ($\Delta S \neq 0$) then phosphorescence occurs

which is essentially a forbidden process and therefore longer-lived, normally lasting 10^{-4} - 10^{2} s. The emission processes may be represented in a Jablonski diagram (**Figure 1.10**).

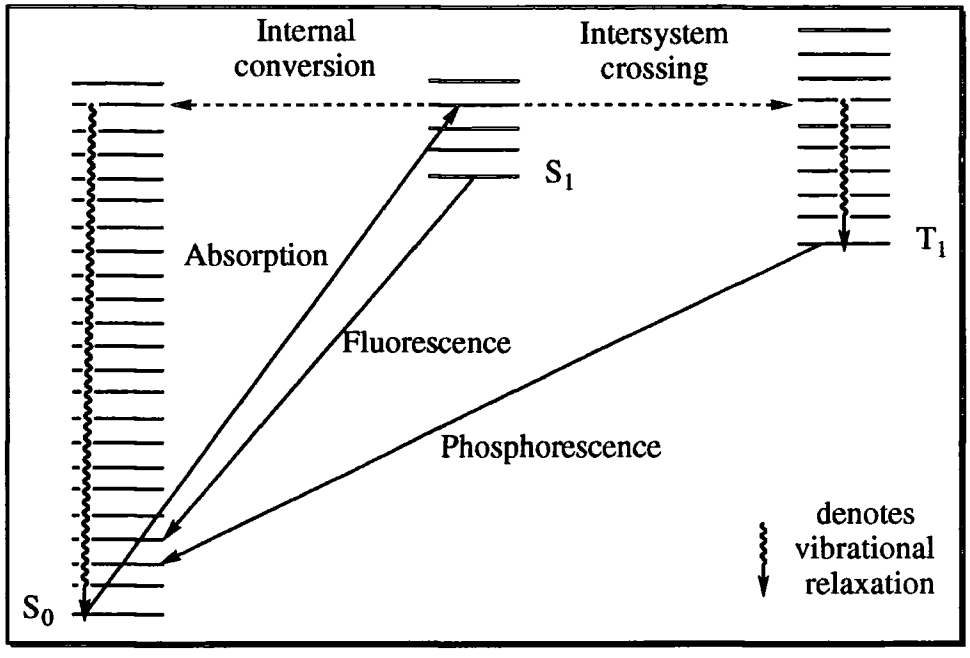

Figure 1.10. *A simplified Jablonski diagram showing absorption and emission processes of fluorescence and phosphoresence.*

Luminescence occurs if it can compete with non-radiative deactivation pathways.

Most of the lanthanide (III) ions are known to luminesce, particularly in the solid state under anhydrous conditions, as demonstrated in the application of lanthanide luminescence in phosphors[56] for television screens and in the ubiquitous Nd-YAG laser.[57] The lowest lying excited states of the lanthanides comprise of $4f^n$ configurations. The 4f electrons are shielded from the environment by the outer core 5s and 5p electrons and therefore are minimally involved in bonding. As a consequence, the total ligand field splitting of an f-electron term spans only a few hundred wavenumbers compared to transition metals' d-electron term energy splittings of the order 25 000 cm^{-1}. Therefore non-radiative deexcitation processes are relatively inefficient for lanthanide complexes due to inefficient interactions between the ligand

and metal f orbitals, allowing the emission of radiation as luminescence to compete in many instances. The energy levels of the lanthanides are shown in **Figure 1.11**.

In order to observe luminescence, a relatively large energy gap between the highest ground state and the lowest excited state level, ΔE, is required. La^{3+} and Lu^{3+} do not exhibit luminescence due to the empty and filled 4f shell respectively. Pr^{3+}, Nd^{3+}, Ho^{3+}, Er^{3+} and Tm^{3+} show weak luminescence as ΔE is relatively small, allowing efficient non-radiative deactivation pathways. The ions Sm^{3+}, Eu^{3+}, Gd^{3+}, Tb^{3+}, Dy^{3+} and Yb^{3+} are the most likely to exhibit strong luminescence due to their relatively large energy gaps of 7400, 12 500, 32 000, 14 800, 7850, 10 200 cm^{-1} respectively.

Lanthanide luminescence may be studied by two spectroscopic procedures. Emission spectroscopy involves excitation of the sample at a suitable wavelength, λ_{ex}, while the emission monochromator is scanned and gives information on the probability and structure of transitions from the emissive level to various levels in the ground state manifold. Excitation spectroscopy involves monitoring the emission at a suitable wavelength, λ_{em}, while the excitation monochromator is scanned and gives information regarding transitions from the ground state to the emissive and higher states. The excitation spectrum closely resembles the absorption spectrum, with the exception of some Eu^{3+} systems where the excitation may be complicated by the tendency of Eu^{3+} to undergo a photoreduction to Eu^{2+} via a ligand to metal charge transfer process.[59]

1.4.2 Sensitised emission

Although most lanthanides absorb u.v. or visible light, the molar absorptivities are low (1 - 10 $dm^3\ mol^{-1}\ cm^{-1}$) as a consequence of the parity forbidden transitions within the 4f shell, hence the excited states are not readily populated with conventional light sources. This limitation can be overcome by directly exciting the lanthanide with a powerful laser source which generates intense light with narrow bandwidths (typically < 0.02 nm). Alternatively, the effective molar absorptivity of the lanthanide may be increased by sensitised emission[60], where the lanthanide is indirectly excited by energy

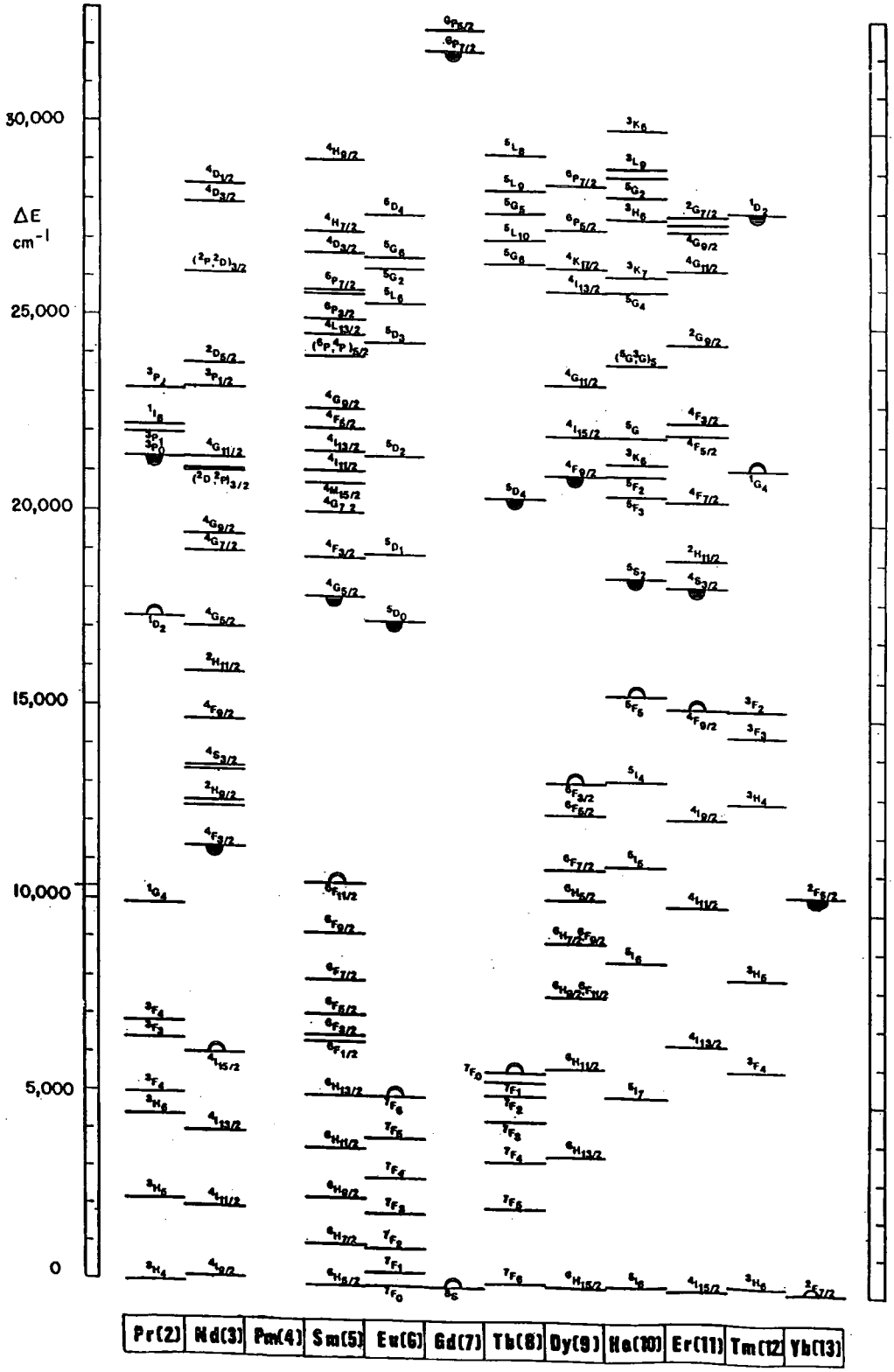

Figure 1.11. *Energy level diagram for the lanthanides. Filled circles represent lowest luminescent levels and open circles represent highest levels of the ground state manifold.*[58]

transfer from a neighbouring chromophore. The chromophore may be present in solution, be incorporated into a ligand system which binds to the lanthanide ion, or be directly coordinated to the ion, and must absorb strongly at a suitable wavelength and give rise to efficient energy transfer to the metal centre, as depicted in the Jablonski diagram in **Figure 1.12.**

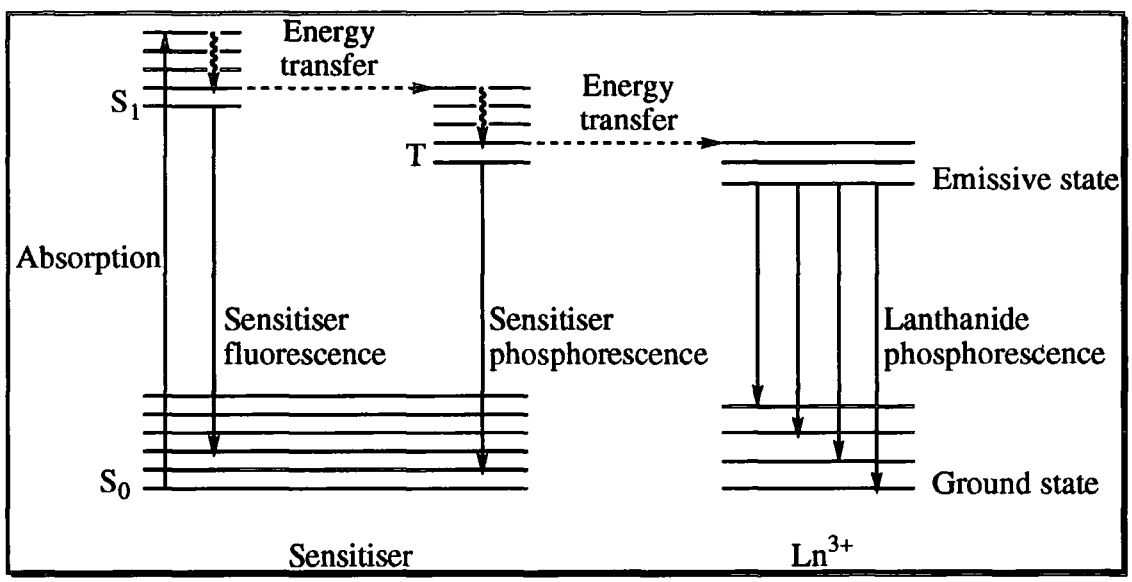

Figure 1.12. *Jablonski diagram for sensitised emission.*

The energy transfer is favoured by a short distance between the sensitiser and the lanthanide ion and the efficiency is dependent on the energy difference between the higher lying triplet state of the sensitiser and the emissive state of the lanthanide.[61] This energy difference should be ≥ 1500 cm^{-1} to prevent thermally activated back energy transfer from the lanthanide to the triplet state occurring.[63,64]

This energy transfer may occur via a Förster[63] or a Dexter mechanism. The Förster mechanism is a coulombic interaction arising when the dipole of the excited sensitiser induces a dipole in the acceptor. The process is purely 'through space' and does not require any physical contact between the sensitiser and acceptor. The Dexter mechanism is an exchange interaction involving mutual electron exchange between sensitiser and acceptor, as depicted in **Figure 1.13**, with conservation of total spin

multiplicity of the system. It occurs via their overlapping electron clouds and therefore requires physical contact.

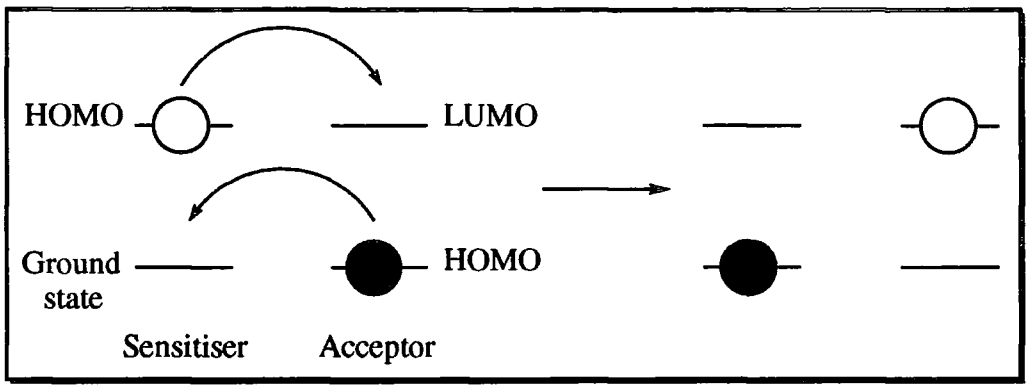

Figure 1.13. *Energy transfer from sensitiser to acceptor through mutual electron exchange.*

Both processes require spectral overlap between the emission spectrum of the sensitiser and the absorption spectrum of the acceptor.

1.4.3 Europium and terbium luminescence

Most studies on lanthanide luminescence have focussed on the behaviour of Eu^{3+} and Tb^{3+} complexes which emit relatively strongly in the visible region of the spectrum, the energy levels for which are shown in **Figure 1.14.**[65] The emission spectra can be obtained by exciting the emissive level of Eu^{3+} ($^5D_0$) and Tb^{3+} ($^5D_4$) with light at 579 and 488 nm respectively (**Figure 1.15**).

The narrow nature and position of the transitions does not change significantly from complex to complex, although the intensities and ligand field-induced fine structure are sensitive to the coordination environment of the binding site and provide a characteristic signature of the binding domain. Individual J levels are well separated from one another due to the large spin orbital coupling of the lanthanides. With the exception of the $^7F_0$ and $^5D_0$ states of Eu^{3+} which are non-degenerate, ligand fields split the J levels even further, amounting to a few hundred cm^{-1}.

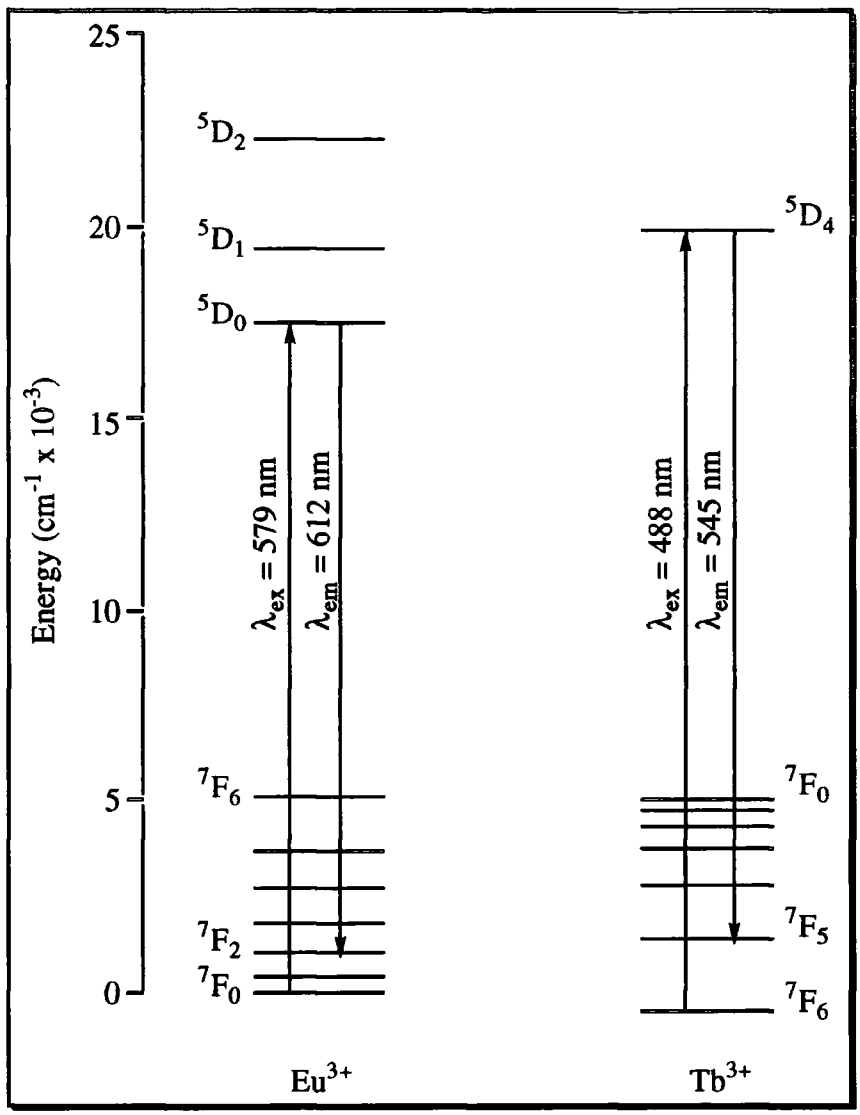

Figure 1.14. *Energy levels for Eu^{3+} and Tb^{3+} showing the excitation wavelength and the most intense emissive transition for the ions. Each level is labelled according to the $^{2S+1}L_J$ Russell-Saunders scheme.*[65]

For Eu^{3+} complexes in solution, the strongest emissions generally arise from $^5D_0 \rightarrow {}^7F_{1,2}$ transitions at 590 and 620 nm respectively, the relative intensities of which are highly sensitive to the ligand environment reflecting the hypersensitive nature of the $^5D_0 \rightarrow {}^7F_2$ transition. These transitions are highly informative as their spectral splitting patterns are relatively simple. Note that the $^5D_0 \rightarrow {}^7F_2$ transition is absent if Eu lies on an inversion centre. The $^5D_0 \rightarrow {}^7F_4$ transition is also relatively intense whereas the remaining $^5D_0 \rightarrow {}^7F_J$ transitions are generally rather weak or unobservable. The $^5D_0 \rightarrow {}^7F_1$ is magnetic dipole in character, its radiative transition probability being little affected by the ligand environment and the transition being very

sensitive to the symmetry of the complex. Two bands are observed if a C_3 or C_4 axis is present. However, the $^5D_0 \rightarrow {}^7F_2$ and $^7F_4$ transitions are predominantly electric dipole in character and therefore the radiative transition probabilities are highly sensitive to the ligand environment. The $^5D_0 \rightarrow {}^7F_0$ transition is formally allowed in low symmetry systems, is predominantly electric dipole in character, and although weak, its intensity is sensitive to the ligand environment. As the $^7F_0$ level is non-degenerate, only a single transition is possible for each Eu ion environment, hence the transition is also a probe of Eu^{3+} coordination homogeneity. In solution, emission from the $^5D_1$ excited state is usually weak and luminescence from the upper levels is efficiently quenched

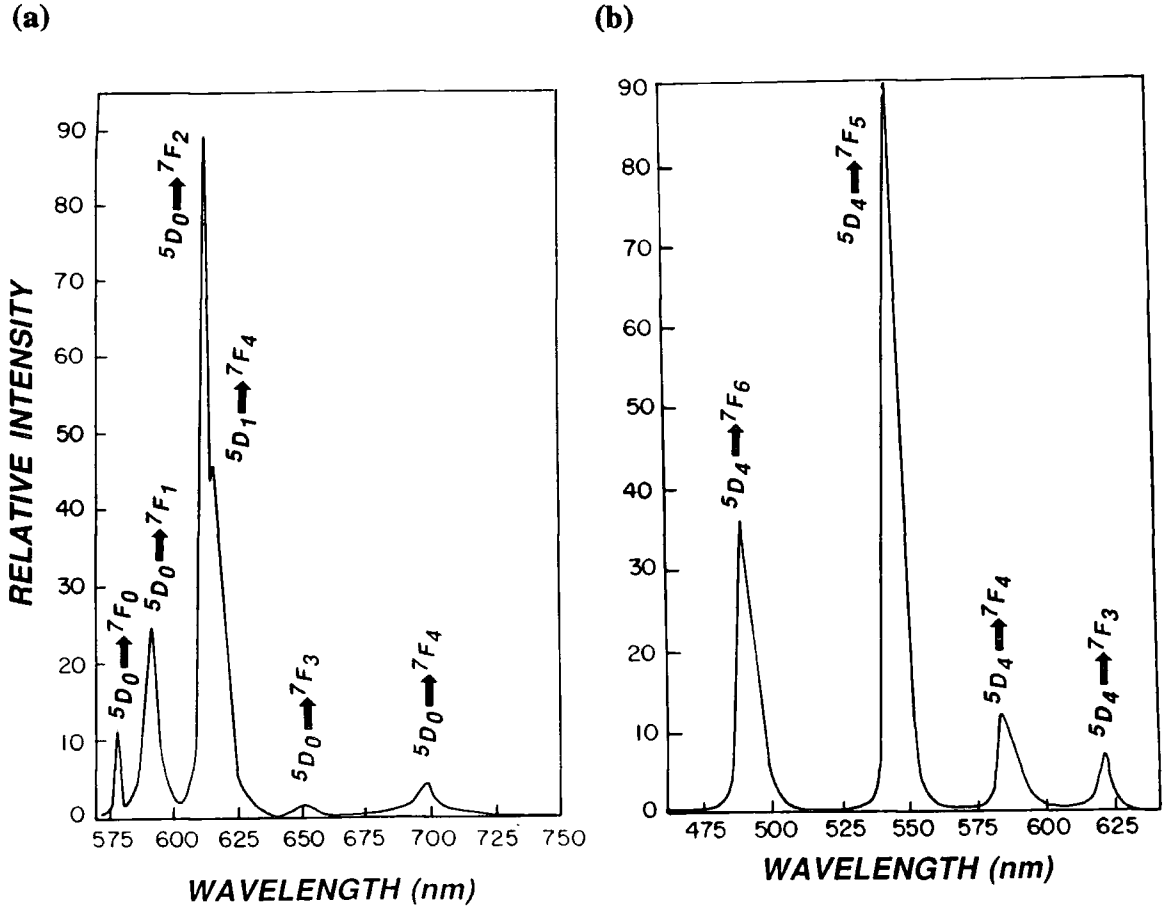

Figure 1.15. Emission spectra of **(a)** Eu^{3+} and **(b)** Tb^{3+} in acetic acid sensitised by 4-methylbenzophenone.[66]

For Tb^{3+} complexes in solution, all emissions arise from the $^5D_4$ level. The $^5D_4 \rightarrow {}^7F_5$ transition (545 nm) is the most intense emission band observed. The $^5D_4 \rightarrow {}^7F_{0,1}$ emissions are always very weak and the relative intensities of the remaining transitions are generally of the order $^5D_4 \rightarrow {}^7F_6 > {}^7F_4 > {}^7F_3 > {}^7F_2$. The $^5D_4 \rightarrow {}^7F_{6,4,2}$ transitions show some sensitivity to the nature of the bonded ligands and the $^5D_4 \rightarrow {}^7F_{5,3}$ transitions are magnetic dipole in character, but owing to the degeneracy of the $^5D_4$ level they cannot be used directly to probe structure.

1.4.4 Deactivation of the excited state

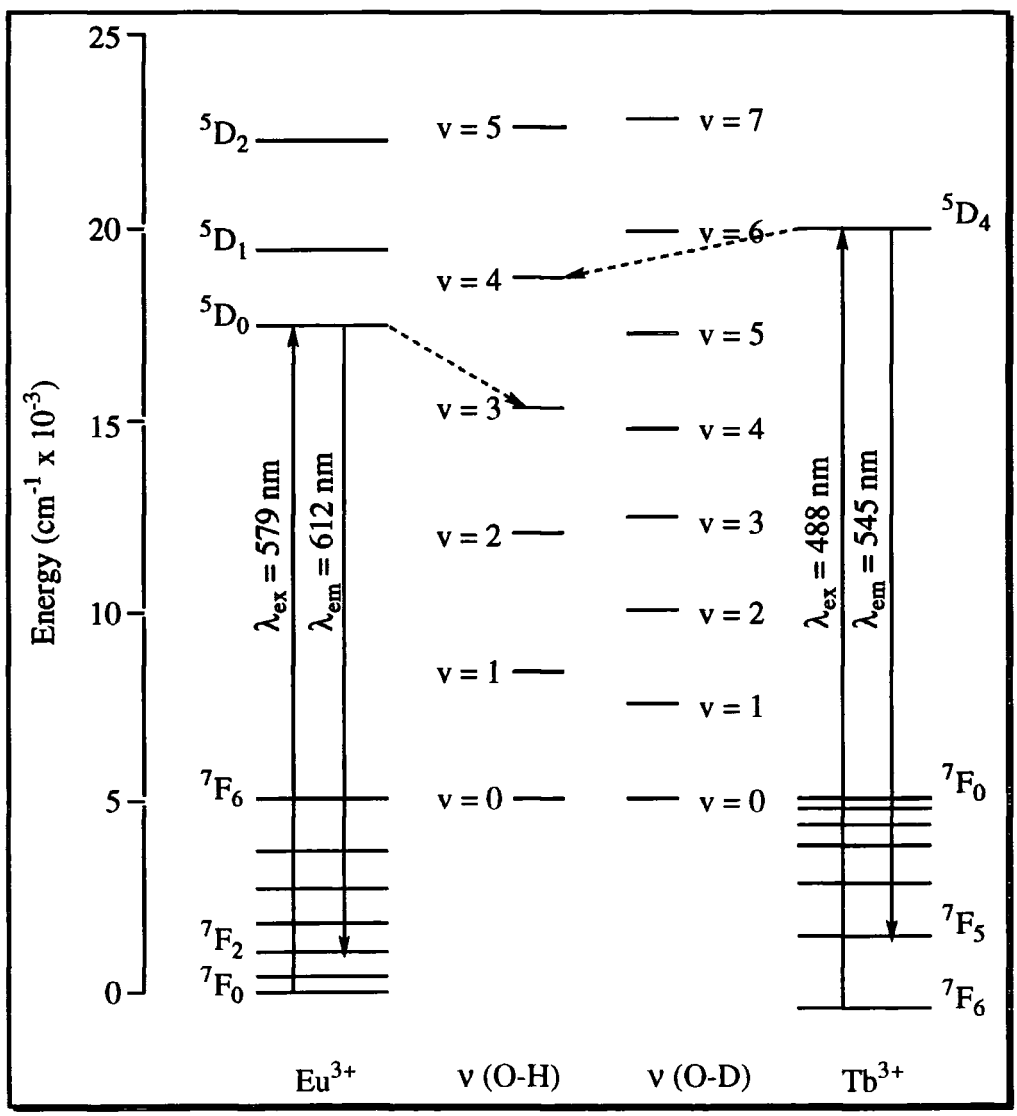

Figure 1.16. *Electronic energy levels of Eu^{3+} and Tb^{3+} appropriately juxtaposed to the vibrational energy levels of O-H and O-D.*[4]

The luminescence lifetimes in aqueous solution for the emissive $^5D_0$ state of Eu^{3+} and $^5D_4$ state of Tb^{3+} typically lie in the range 0.1-1.0 ms and 0.4-5.0 ms respectively.[14] There are other non-radiative processes that compete to varying extents, resulting in a decrease in the lifetimes. Lifetimes are sensitive to the metal's environment and it was first recognised by Kropp and Windsor[67] that the presence of coordinated water molecules provides a facile non-radiative de-excitation pathway through energy transfer to the O-H vibrational manifold of water. Such a pathway was found to be much less efficient in D_2O which can be explained by comparing the electronic energy levels and energy gaps of Eu^{3+} and Tb^{3+} to the O-H and O-D vibrational 'ladders' of coordinated molecules (**Figure 1.16**). The de-excitation process occurs, despite the apparent mismatch of the energy levels, as hydrogen-bonding results in a 'blurring' of the O-H and O-D vibrational manifold.

The energy of separation from the highest J level of the ground state manifold, to the emissive level, is the energy gap, and it is this gap that must be bridged by a vibrational ladder in order to provide a deexcitation pathway. Non-radiative processes of this type are less efficient the higher up a vibrational ladder one must go to bridge the gap due to the poorer Frank-Condon overlap of the two wavefunctions at these higher levels. Therefore energy transfer into O-D vibrations is much less efficient than into O-H vibrations as O-D oscillators have smaller stretching frequencies and bridging the energy gap requires excitation into a higher vibrational level for D_2O than H_2O. This theory also accounts for the variation in the deuterium isotope effect observed within the lanthanide series. The energy transfer into O-H or O-D vibrations becomes less probable as the energy gap increases. Therefore the effect is much more pronounced for Eu^{3+} (ΔE = 12 300 cm^{-1}) compared to Tb^{3+} (ΔE = 14 700 cm^{-1}) and is found to be absent for Gd^{3+} (ΔE = 32 000 cm^{-1}).

1.4.5 Hydration state

The deactivating effect of coordinated water molecules may be partitioned from the other modes of depopulation of the emissive state to give equation **(1.11)**.

$$k_{obs}^{H_2O} = k_{nat} + \Sigma k_{nr} + k_{OH} \qquad (1.11)$$

where $k_{obs}^{H_2O}$ is the observed luminescence decay constant in water, k_{nat} is the natural radiative rate constant, Σk_{nr} is the sum of the rate constants for non radiative processes and k_{OH} is the rate constant for non radiative energy transfer to the O-H oscillators in water.

The k_{OH} term may be neglected in D_2O resulting in equation **(1.12)**.

$$k_{obs}^{D_2O} = k_{nat} + \Sigma k_{nr} \qquad (1.12)$$

Heller,[68] Haas and Stein[69] showed that each O-H oscillator acts independently in quenching the lanthanide excited state.

$$\Delta k_{obs} = k_{obs}^{H_2O} - k_{obs}^{D_2O} = k_{OH} \qquad (1.13)$$

This relationship has been exploited by Horrocks and Sudnick[70] in the estimation of q, the number of water molecules coordinated to the lanthanide ion.

$$q = A_{Ln} (\tau_{H_2O}^{-1} - \tau_{D_2O}^{-1}) = A_{Ln}\ \Delta\tau^{-1} \qquad (1.14)$$

where τ is the luminescent lifetime in ms (reciprocal of k) and A_{Ln} is a proportionality constant specific to the lanthanide ion reflecting its sensitivity to vibronic quenching. Proportionality constants for Eu^{3+} and Tb^{3+} were determined from plots of $\Delta\tau^{-1}$ versus q for well characterised crystalline solids in which q was known from X-ray crystallography. The plots were found to be linear with high correlation coefficients and the proportionality constants obtained were $A_{Eu} = 1.05$ and $A_{Tb} = 4.2$. Thus,

excited state lifetime measurements in H_2O and D_2O may be used to estimate the apparent hydration state, q, of a complex in solution, with an estimated uncertainty of ±0.5.

1.4.6 Luminescent probes

Luminescent lanthanide probes have been used extensively to solve structural problems ranging from the determination of local symmetries and structure in inorganic crystalline materials and glasses[36], including a group theoretical analysis of the observed splittings of the f-f transitions[4], to an investigation of biological systems[71] including inter-metal distances[72] and distances between energy donors and acceptors[73,74], and even to studies probing metal binding sites[73,75,76] in biological media by isomorphous replacement of Ca^{2+}.

The use of luminescent lanthanide complexes in solving analytical problems has been studied intensively recently.[14,77] Immunological procedures for the determination of biological materials in low concentration and for the clinical investigation and interactions of, for example, enzymes, antibodies and drugs, are far superior to any other techniques. The general principle involves the selective binding of a targeting system, which may be an immunologically raised antibody fragment or protein, to the target molecule of interest. The use of a radioactive or luminescent reporter group covalently attached to the targeting system gives a means of detecting the analyte through measurement of the radioactivity or luminescence. Radioimmunoassays[78,79] are used for such purposes but suffer from a number of drawbacks such as the inherent risk to health, high disposal costs, handling licences and short shelf life. Labelling samples with a luminescent probe offers an attractive alternative.[80,81] Not only do these relatively inexpensive fluoroimmunoassays offer improved sensitivity and specificity, they eliminate problems with handling radioactive materials, are amenable to microscopic detection and allow the measurement of luminescence in a time-resolved mode to be employed (**Figure 1.17**).

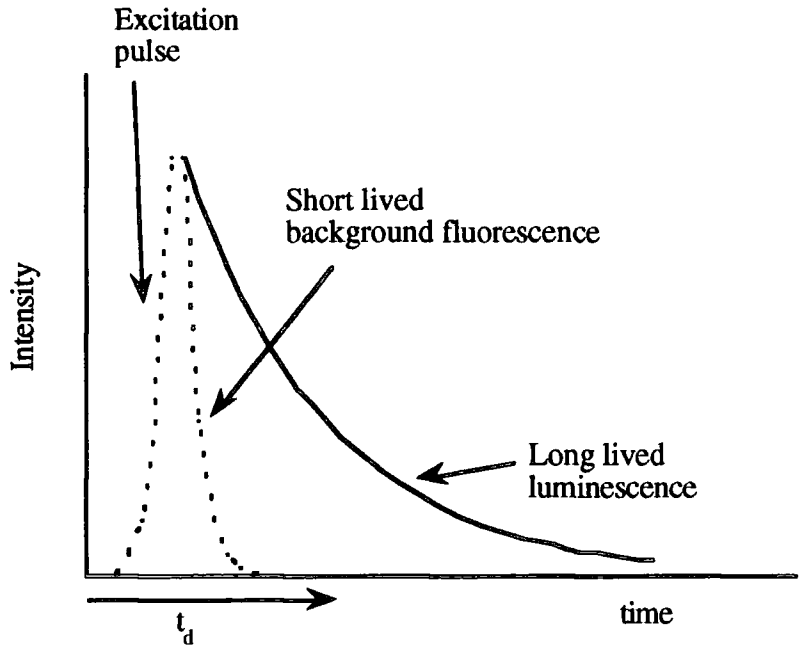

Figure 1.17. *Schematic representation of time-resolved detection.*

Time-resolved detection minimises interference arising from the background luminescence of biological media such as proteins. On excitation, both the background fluorescence and luminescence of the lanthanide rise rapidly. The background fluorescence decays quickly, typically on the nanosecond timescale, whereas the lanthanide luminescence decays over a much longer timescale, of the order of milliseconds. The luminescence is therefore monitored after a time interval, t_d, during which time all the background fluorescence and scattered light have decayed to zero. For systems where the lifetime is independent of the environment, the measured luminescence is directly proportional to the concentration of the analyte present.

The binding of the analyte may also have a direct effect on the luminescence which may be observed as a quenching or enhancement of the emission, or a shift in the excitation or emission wavelength. Luminescent lanthanide complexes suitable for attachment to biological substrates have been developed in order to monitor interactions and the fate of biomolecules within cells.[82,83]

Luminescent lanthanide complexes form attractive probes, as the use of sensitised emission gives rise to exceptionally large Stokes shifts, $\lambda_{em} \gg \lambda_{ex}$, typically in the range 250 - 350 nm, which eliminates problems of self-absorption of emitted light. The emission bands are very narrow, characteristic of the metal and little affected by changes in the environment, the wavelengths shifting no more than ±2 nm on changing the temperature or coordination site. They exhibit long lived luminescence at room temperature allowing time-resolved detection to be employed.

There are several general requirements of luminescent lanthanide complexes for use as probes in biochemical analyses. As most studies will be performed in aqueous solution at physiological pH (7.4), good water solubility and a high kinetic and thermodynamic stability are essential. A high quantum yield is required, therefore the ligand must shield the lanthanide ion from water molecules which quench the excited state of the lanthanide resulting in decreased luminescence. The ligand must also incorporate a suitable chromophore which can sensitise the lanthanide luminescence. As biological samples absorb strongly below 330 nm, and the cut off point to avoid 'all quartz' optics is 340 nm, excitation wavelengths above this are desirable to ensure that the incident light will be absorbed by the complex, resulting in high sensitivity. The complex must be readily modified to allow covalent linkage into the targeting molecule. The targeting molecule may be a protein or antibody, raised by immunological methods to recognise selectively and specifically bind to the target species, or a simpler molecule such as a DNA intercalator[84], peptide[85] or cyclodextrin[86] for example. This coupling process should not diminish the immunoreactivity of the labelled substance nor increase its specific binding. The interactions with other biological components should also be minimal.

1.5 Chiroptical methods

An advantage of studying chiral complexes is that chiroptical techniques such as optical rotation, circular dichroism (CD) and circularly polarised luminescence (CPL) may be employed. Chiroptical methods are particularly sensitive to stereochemical and

electronic features of molecular systems and, as different mechanisms are used to determine band intensities compared to conventional spectroscopy, further selectivity is available.

1.5.1 Optical rotation

Plane polarised light may be resolved into a superposition of right and left circularly polarised components. On entering a chiral medium the two components propagate at different rates. The difference in refractive indices of right and left circularly polarised light is dependent on whether or not the electric field of the incident radiation rotates in the same sense as the helical nature of the chiral medium. On passing through the chiral medium, one component propagates faster than the other, and as a result, their electric vectors are in phase at a different angle when they leave the sample and their superposition gives rise to a plane polarised beam rotated through an angle, α, relative to the incoming beam (**Figure 1.18**). This optical rotation[87,88] is dependent on optical pathlength, wavelength of light used, temperature and the concentration of the chiral substance.

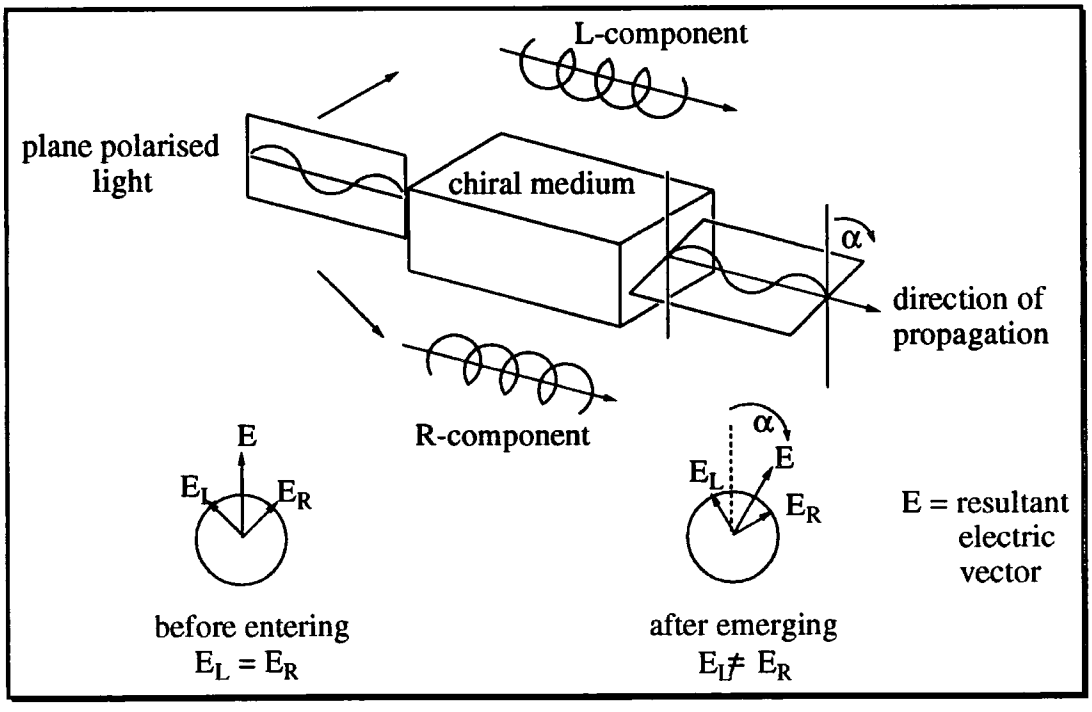

Figure 1.18. *Pictorial representation of optical rotation.*

1.5.2 Circular dichroism

Not only do right and left circularly polarised light have different refractive indices in chiral media, the degree of absorption experienced by each component is also modified. In absorption, the electric field or the magnetic field (or both) of the radiation rearranges the electron density of the molecule from the initial state to one of higher energy. The electric field causes a net linear displacement of the electron density and produces an electric dipole transition moment, μ. The magnetic field induces a circular rearrangement of the electron density known as the magnetic dipole transition moment, m. In an achiral molecule the net electron redistribution during a transition is always planar. However, in a chiral molecule, μ and m, having parallel polarisations, combine to yield a helical electron redistribution. As there are no planes of symmetry, the electrons are moving in some kind of helical arrangement and the interaction with the right and left circularly polarised light will therefore be different. This differential absorption is termed circular dichroism (CD)[89], and when the two projections of right and left circularly polarised light are recombined after leaving the chiral medium, they no longer produce plane polarised light but elliptically polarised light, whose major axis lies along the angle of rotation.

The measurement of circular dichroism is based on instrumentation designed by Grosjean and Legrand.[90] Linearly polarised light is passed through a quarter wave plate, a material that produces a 90° phase difference between left and right circularly polarised components, which may be a Pockels cell or a photoelastic modulator. This modulates the linearly polarised light alternately into left or right circularly polarised light which is detected by a photomultiplier tube, the output of which is converted into two signals. One signal is due to the differential absorption of one component over the other and is proportional to the circular dichroism, whereas the other signal is averaged and related to the mean light absorption. The ratio of these signals is the absorption dissymmetry factor, g_{abs}, which is the quantity of interest.

$$g_{abs}(\lambda) = \frac{\Delta\varepsilon}{\varepsilon} = \frac{\varepsilon_L - \varepsilon_R}{1/2\ (\varepsilon_L + \varepsilon_R)} \qquad \textbf{(1.15)}$$

where ε_L and ε_R correspond to extinction coefficients for left and right circularly polarised components of the emitted radiation.

An absorption spectrum is a measure of the probability of a transition occurring at a given energy. A CD spectrum is a plot of $\Delta\varepsilon$ versus wavelength. Since different electronic transitions involve the redistribution of electrons of different handedness, any one molecule may give rise to both positive and negative CD signals.

CD spectra not only prove the existence of enantiomers but in some cases can be used to determine absolute configuration of substrates as demonstrated by Nakanishi.[91] CD probes the chirality of molecular ground states giving rise to structural information and is often used to probe changes in conformation and interactions of biological molecules[89] such as DNA[92] and proteins.[93]

1.5.3 Circularly polarised luminescence

Circularly polarised luminescence (CPL) is the emission analogue of circular dichroism and probes the chirality of the emitting excited state. It is the spontaneous emission of right and left circularly polarised light by chiral systems. There are two experimentally measureable parameters, namely the emission circular intensity differential

$$\Delta I(\lambda) = I_L(\lambda) - I_R(\lambda) \qquad \textbf{(1.16)}$$

and the emission dissymmetry factor

$$g_{em}(\lambda) = \frac{2\,\Delta I(\lambda)}{I(\lambda)} \qquad \textbf{(1.17)}$$

where $I(\lambda) = I_L(\lambda) + I_R(\lambda)$ and I_L and I_R correspond to the intensities of the left and right circularly polarised components of the emitted radiation.[94,95]

There are currently no commercially available instruments for the measurement of CPL and research groups have constructed their own instruments following similar designs

based on the photon-counting spectrometer developed by Schipper, van den Beukel and Dekkers.[96] In the basic experiment, the sample is excited at 90° from the detection source with an incident excitation beam which may be circularly polarised, linearly polarised or unpolarised light. The emitted light passes through a photoelastic modulator driven at 50 kHz which acts as an oscillating quarter wave plate. During one half-cycle of modulation left circularly polarised light is converted to linearly polarised light, and during the other half-cycle right circularly polarised light is converted. The light is selected by the linear polariser, wavelength resolved by the monochromator and detected by the photomultiplier. The detected signal is passed on to an amplifier which outputs photopulses to a differential photon counter. This is linked to the photoelastic modulator in such a way that the counter adds the photopulses that enter when left circularly polarised light is passing through the photomultipler and subtracts when right circularly polarised light enters. This counter provides a reading which is proportional to ΔI. A second counter adds every pulse thereby giving a reading proportional to I.

A CPL spectrum is a plot of ΔI versus wavelength. CPL is a very sensitive technique as it combines the specificity of natural optical activity with the measurement sensitivity of optical emission techniques. It can be used to provide information on the structure and chirality of the excited state. Several reviews have been published on CPL and its potential uses.[94,95]

1.5.4 Circular dichroism and circularly polarised luminescence of lanthanides

In order to use circular dichroism and circularly polarised luminescence to probe the chirality of lanthanide complexes, absorption and emission transitions should be selected that obey selection rules for lanthanide optical activity.[95,97] The magnitude and sign of the optical activity is determined by the rotatory strength, R_{ab}.

$$R_{ab} = |\mu||m|\cos\tau_{ab} \qquad (1.18)$$

for the transition a ⟶ b, where τ_{ab} is the angle between electric vector, μ, and magnetic vector, m.

The intensity of CD and CPL bands is therefore dependent on the magnetic and electric dipole strengths of the transition. Dissymmetry factors are measures of the degree of optical activity associated with electronic absorption or emission transitions and are determined by the relative magnetic dipole 'allowedness' versus the electric dipole 'allowedness' of the transition. Selection rules for large CD or CPL intensities and large dissymmetry factors are different. The largest CD or CPL intensities are exhibited by transitions which are both electric dipole and magnetic dipole allowed, whereas large dissymmetry factors occur with transitions that are magnetic dipole allowed but electric dipole forbidden. CD and CPL spectra are therefore determined by the magnitude of the rotatory strength of the transition and the dissymmetry factor.

For lanthanides, the CD and CPL sensitive transitions have $|\Delta J| \leq 1$ (excluding J=J'=0). For Eu^{3+} there are a number of available transitions in both absorption and emission, the accessible transitions being the $^7F_0 \longrightarrow {}^5D_1$ and $^7F_1 \longrightarrow {}^5D_0$ excitations and $^5D_0 \longrightarrow {}^7F_1$ emission. In CD studies, the $^7F_0 \longrightarrow {}^5D_1$ and $^7F_0 \longrightarrow {}^5D_2$ transitions exhibit comparable CD intensities whereas g_{abs} for the latter is some ten times smaller. Similarly in CPL, the intensities of the $^5D_0 \longrightarrow {}^7F_1$ and $^5D_0 \longrightarrow {}^7F_2$ transitions are approximately the same, with $^5D_0 \longrightarrow {}^7F_1$ showing greater sensitivity to changes in ligand environment and having a g_{em} value an order of magnitude larger. In fact Eu^{3+} complexes display extraordinarily large dissymmetry factors compared to other optically active systems, and the largest g_{em} value reported to date is that observed for $Eu(facam)_3$ (g_{em} = -0.78, λ = 595 nm, DMSO).[94]

For Tb^{3+} complexes the CD sensitive transitions are $^7F_{3,4,5} \longrightarrow {}^5D_4$. However, these transitions are not accessible in the visible region for direct excitation. It is possible to efficiently excite Tb^{3+} and Eu^{3+} indirectly through neighbouring chromophores but these allowed transitions have very low g_{abs} values and poor CD. The largest

dissymmetry factors for emission are observed for $^5D_4 \rightarrow {}^7F_{3,4,5}$ transitions. The CPL intensity and g_{em} value for $^5D_4 \rightarrow {}^7F_5$ transition is found to be 3-10 times greater than $^5D_4 \rightarrow {}^7F_{3,4}$ due to crystal field effects.[95]

As the ^7F_J and $^5D_4$ states are split extensively by ligand fields, the sign and splitting patterns associated with Tb^{3+} transitions are exceedingly complex and therefore not amenable to structural analysis. CPL spectra of Eu^{3+} systems are considerably easier to interpret as they exhibit very few crystal field components to the transitions. Europium is therefore the lanthanide of choice for determining structural information.

CPL is particularly useful in the study of chiral lanthanide complexes as the poor absorptivity of the lanthanide ions means corresponding CD spectra are weak. The sensitivity of the measurement allows studies to be conducted at very low concentrations and the sign and magnitude of the CPL are highly sensitive to stereochemical and electronic structural details of the system. However, full exploitation of CPL in structural studies awaits the development of spectra-structure relationship.

References for Chapter 1

1. A.R. Fritzberg, 'Radiopharmaceuticals : Progress and Clinical Perspectives', C.R.C. Press, Boca Raton, 1986, vols. 1 and 2.
2. M.F. Tweedle in 'Lanthanide Probes in Life, Chemical and Earth Sciences', eds., J.- C.G. Bünzli and G.R. Choppin, Elsevier, Amsterdam, 1989, Chapter 5.
3. R.B. Lauffer, *Chem. Rev.*, 1987, **87**, 901.
4. J.-C.G. Bünzli in 'Lanthanide Probes in Life, Chemical and Earth Sciences', eds., J.-C.G. Bünzli and G.R. Choppin, Elsevier, Amsterdam, 1989, Chapter 7.
5. B. Alpha, J.-M. Lehn and G. Mathis, *Angew. Chem., Int. Ed. Engl.*, 1987, **26**, 266.

6. A.D. Sherry and C.F.G. Geraldes in 'Lanthanide Probes in Life, Chemical and Earth Sciences', eds., J.-C.G. Bünzli and G.R. Choppin, Elsevier, Amsterdam, 1989, Chapter 4.

7. R.M. Sink, D.C. Buster and A.D. Sherry, *Inorg. Chem.*, 1990, **29**, 3645.

8. D. Parker, *Chem. Rev.*, 1990, **19**, 271.

9. K. Pulukkody, T.J. Norman, D. Parker, L. Royle and C.J. Broan, *J. Chem. Soc., Perkin Trans. 2*, 1993, 605.

10. S. Jurisson, E.O. Schlemper, D.E. Troutner, L.R. Canning, D.P. Nowotnik and R.D. Neirinckx, *Inorg. Chem.*, 1986, **25**, 543.

11. J. Leveille, G. Demenceau, M. DeRoo, R.A. Morgan, D. Kupranick and R.C. Walovitch, *J. Nucl. Med.*, 1980, **30**, 1892.

12. A.G. Jones, M.J. Abrams, A. Davison, J.W. Brodack, A.K. Toothaker, S.J. Adelstein and A.I. Kassis, *Int. J. Nucl. Med. Biol.*, 1984, **11**, 225.

13. A.M. Forster, A.D. Sherry, C.M Archer, K.N. Nagle, F.S. Booker, B. Edwards, H.R. Gill, J.D. Kelly and M. McPartlin, *J. Nucl. Med.*, 1992, **33**, 850.

14. D. Parker, K. Pulukkody, T.J. Norman, A. Harrison, L. Royle and C. Walker, *J. Chem. Soc., Chem. Commun.*, 1992, 1441.

15. A. Harrison, C.A. Walker, K.A. Pereira, D. Parker, L. Royle, K. Pulukkody and T.J. Norman, *Magn. Reson. Imag.*, 1993, **11**, 761.

16. G. E. Hein and C. Niemann, *J. Am. Chem. Soc.*, 1962, **84**, 4487.

17. J.K. Barton, *Science*, 1986, **33**, 727.

18. J.K. Barton and E. Lolis, *J. Am. Chem. Soc.*, 1985, **107**, 708.

19. G. Schwarzenbach, *Helv. Chim. Acta*, 1952, **35**, 2344.

20. R.D. Hancock and A.E. Martell, *Chem. Rev.*, 1989, **89**, 1875.

21. D.K. Cabbiness and D.W. Margerum, *J. Am. Chem. Soc.*, 1969, **91**, 6540.

22. L.F. Lindoy, 'The Chemistry of Macrocyclic Ligand Complexes', Cambridge University Press, Cambridge, 1989.

23. J.F. Desreux, *Inorg. Chem.*, 1980, **19**, 1319; X. Wang, T. Jin, V. Comblin, A. Lopez-Mut, E. Merciny and J.F. Desreux, *Inorg. Chem.*, 1992, **31**, 1095.

24. M. Spirlet, J. Rebizant, J.F. Desreux and M.F. Loncin, *Inorg. Chem.*, 1984, **23**, 359.

25. J.P.L. Cox, K. Jankowski, R. Kataky, D. Parker, N.R.A. Beeley, B.A. Boyce, M.A. Eaton, K. Miller, A.T. Millican, A. Harrison and C.A. Walker, *J. Chem. Soc., Chem. Commun.*, 1989, 797; C.J. Broan, J.P.L. Cox, A.S. Craig, R. Kataky, D. Parker, A. Harrison, A.M. Randall and G. Ferguson, *J. Chem. Soc., Perkin Trans. 2*, 1991, 87.

26. H. Maumela, R.D. Hancock, L. Carlton, J.H. Reibenspies and K.P. Wainwright, *J. Am. Chem. Soc.*, 1995, **117**, 6698.

27. S. Amin, J.R. Morrow, C.H. Lake and M.R. Churchill, *Angew. Chem., Int. Ed. Engl.*, 1994, **33**, 773; S. Amin, D.A. Voss, W.De W. Horrocks, C.H. Lake, M.R. Churchill and J.R. Morrow, *Inorg. Chem.*, 1995, **34**, 3294.

28. S. Aime, A.S. Batsanov, M. Botta, J.A.K. Howard, D. Parker, K. Senanayake and J.A.G. Williams, *Inorg. Chem.*, 1994, **33**, 4696.

29. C.J. Broan, J. Jankowski, R. Kataky and D. Parker, *J. Chem. Soc., Chem. Commun.*, 1990, 1739; 1991, 204.

30. S. Aime, M. Botta, R.S. Dickins, A. de Sousa and D. Parker, unpublished work; see also N. Sabbatini, M. Guardigli, J.-M. Lehn and G. Mathis, *J. Alloys Compd.*, 1992, **180**, 363.

31. J.P. Dubost, J.M. Leger, M.H. Langlois, D. Meyer and M. Schaefer, *C.R. Acad. Sci., Ser. 2*, 1991, **312**, 349.

32. S. Aime, A. Barge, M. Botta, M. Fasano, J.D. Ayala and G. Bombieri, *Inorg. Chim. Acta*, 1996, **246**, 423.

33. E.J. Corey and J.C. Bailar, *J. Am. Chem. Soc.*, 1959, **81**, 2620.

34. D.H. Metcalf, J.M.M. Stewart, S.W. Synder, C.M. Grisham and F.S. Richardson, *Inorg. Chem.*, 1992, **31**, 2445.

35. S. Aime, M. Botta and G. Ermondi, *Inorg. Chem.*, 1992, **31**, 4291.

36. C.A. Chang, I.C. Francesconi, M.F. Malley, K. Kumar, J.Z. Gougoutas, M.F. Tweedle, D.W. Lee and L.J. Wilson, *Inorg. Chem.*, 1993, **32**, 3501.

37. S. Aime, M. Botta, M. Fasano, M.P.M. Marques, C.F.G.C. Geraldes, D. Pubanz and A.E. Merbach, *Inorg. Chem.*, 1997, **36**, 2059.

38. S. Hoeft and K. Roth, *Chem. Ber.*, 1993, **126**, 869.

39. N. Graeppi, D.H. Powell, G. Laurenczy, L. Zekany and A.E. Merbach, *Inorg. Chim. Acta*, 1995, **235**, 311.

40. V. Jacques and J.F. Desreux, *Inorg. Chem.*, 1994, **33**, 4048.

41. S. Aime, A.S. Batsanov, M. Botta, R.S. Dickins, S. Faulkner, C.E. Foster, A. Harrison, J.A.K. Howard, J.M. Moloney, D. Parker, L. Royle and J.A.G. Williams, *J. Chem. Soc., Dalton Trans.*, October 1997.

42. S. Aime, M. Botta, D. Parker and J.A.G. Williams, *J. Chem. Soc., Dalton Trans.*, 1995, 2259.

43. J.P. Jesson in 'NMR of Paramagnetic Molecules : Principles and Applications', eds., G.N. LaMar, W.De W. Horrocks, Jr. and R.H. Holm, Academic Press, London, 1973, Chapter 1.

44. W.De W. Horrocks, Jr. in 'NMR of Paramagnetic Molecules, Principles and Applications', eds., G.N. LaMar, W.De W. Horrocks, Jr., and R.H. Holm, Academic press, London, 1973, Chapter 12.

45. B. Bleaney, *J. Magn. Reson.*, 1972, **8**, 91.

46. W.De W. Horrocks, Jr. and J.P. Sipe, *Science*, 1972, **177**, 994.

47. W.De W. Horrocks, Jr. and J.P. Sipe, *J. Am. Chem. Soc.*, 1971, **93**, 6800.

48. F. Block, *Phys. Rev.*, 1946, **70**, 460.

49. I. Solomon, *Phys. Rev.*, 1955, **99**, 559; N. Bloembergen and L.O. Morgan, *J. Chem. Phys.*, 1961, **34**, 842.

50. J.H. Freed, *J. Chem. Phys.*, 1978, **68**, 4034.

51. S.H. Koenig and R.D. Brown in 'Relaxometry of Tissue in NMR Spectroscopy of Cells and Organisms', ed., R.M. Gupta, C.R.C. Press, Boca Raton, Florida, 1987, vol. 2, 75-114.

52. C.C. Hinckley, *J. Am. Chem. Soc.*, 1969, **92**, 5160.

53. J. Reuben, *J. Am. Chem. Soc.*, 1980, **102**, 2232; J. Reuben and G.A. Elgavish, *J. Magn. Reson.*, 1981, **42**, 242; R. Hazama, K. Umakoshi, C. Kubuto, K. Kabuto and Y. Sasaki, *Chem. Commun.*, 1996, **1**, 15.

54. B.L. Engelstad and G.L. Wolf in 'Magnetic Resonance Imaging', eds., D.D. Stark and W.G. Bradley, C.V. Mosby Company, St. Louis, 1988.

55. S.H. Koenig and R.D. Brown, *Prog. NMR Spectr.*, 1990, **22**, 487.

56. K.A. Gschneidner and L. Eyring, 'Handbook of the Physics and Chemistry of the Rare Earths', North Holland, Amsterdam, 1979, vols. 3 and 4.

57. R. Reisfeld and C.K. Jorgensen, 'Lasers and Excited States of Rare Earths', Springer, Berlin, 1977.

58. G. Stein and E. Würzberg, *J. Chem. Phys.*, 1975, **62**, 208.

59. D. Parker and J.A.G. Williams, *J. Chem. Soc., Perkin Trans. 2,* 1995, 1305.

60. S.A. Weissmann, *J. Chem. Phys.*, 1942, **10**, 214.

61. W.De W. Horrocks, Jr. and M. Albin, *Prog. Inorg. Chem.*, 1984, **31**, 1.

62. G.J. McCarthy and J.J. Rhyne, 'The Rare Earths in Modern Science and Technology', Plenum, New York, 1978, vol. 1.

63. T. Förster, *Discuss. Faraday Soc.*, 1959, **27**, 7.

64. A. Beeby, D. Parker and J.A.G. Williams, *J. Chem Soc., Perkin Trans. 2,* 1996, 1565.

65. W.De W. Horrocks, Jr. and D.R. Sudnick, *Acc. Chem. Res.*, 1981, **14**, 384.

66. W.D. Heller and E. Wasserman, *J. Chem. Phys.*, 1965, **42**, 949.

67. J.L. Kropp and M.W. Windsor, *J. Chem. Phys.*, 1963, **39**, 2769; 1965, **42**, 1599; 1966, **45**, 761.

68. A. Heller, *J. Am. Chem. Soc.*, 1966, **88**, 2058.

69. Y. Haas and G. Stein, *Chem. Phys. Lett.*, 1971, **11**, 143; *J. Phys. Chem.*, 1971, **75**, 3677.

70. W.De W. Horrocks, Jr. and D.R. Sudnick, *J. Am. Chem. Soc.*, 1979, **101**, 334.

71. C.F. Meares and T.G. Wensel, *Acc. Chem. Res.*, 1984, **17**, 202.

72. C.F. Meares and J.E. Ledbetter, *Biochemistry*, 1977, 16, 5178.

73. J. Bruno, W.De W. Horrocks, Jr. and R.J. Zaukor, *Biochemistry*, 1992, **31**, 7016.

74. W.De W. Horrocks, Jr. and W.E. Collier, *J. Am. Chem. Soc.*, 1981, **103**, 2856.

75. F.S. Richardson, *Chem. Rev.*, 1982, **82**, 541.

76. W.De W. Horrocks, Jr. and D.R. Sudnick, *Acc. Chem. Res.*, 1981, **14**, 384.

77. E.F.G. Dickson, A. Pollak and E.P. Diamandis, *Photochem. Photobiol.*, 1995, **27**, 3; E. Lopez, C. Chypre, B. Alpha, G. Mathis, *Clin. Chem.*, 1993, **39**, 196; V.-M. Mukkala, C. Sund, M. Kwiakowski, P. Pasanen, M. Högberg, J. Kankare, H. Takalo, *Helv. Chim. Acta.*, 1992, **75**, 1621.

78. R.S. Yallow and S.A. Berson, J. *Clin. Invest.*, 1959, **38**, 1996.

79. H.G. Eckert, *Angew. Chem.*, 1976, **88**, 565; *Angew. Chem., Int. Ed. Engl.*, 1976, **15**, 525.

80. E. Soini and I. Hemmilä, *Clin. Chem.*, 1979, **25**, 353.

81. A. Meyer and S. Neuenhofer, *Angew. Chem., Int. Ed. Engl.*, 1994, **33**, 1044.

82. R.A. Evangelista, A. Pollak, B. Allore, E.F. Templeton, R.C. Morton and E.P. Diamandis, *Clin. Biochem.*, 1988, **21**, 173.

83. V.-M. Mukkala, H. Takalo, P. Little, J. Kankare, S. Kuusela, H. Lönnberg, 'Metal Based Drugs', 1994, **1**, 201.

84. K. Shinozuko, Y. Seto and H. Sawai, *J. Chem. Soc., Chem. Commun.*, 1994, 1377.

85. P. Gottlieb, E. Hazum, E. Tzehoval, M. Feldman, S. Segal, M. Fridkin, *Biochem. Biophys. Res. Commun.*, 1984, **119**, 201.

86. D.M. Gravett and J.E. Guillet, *J. Am. Chem. Soc.*, 1993, **115**, 5970.

87. W. Weller in 'Physical Methods of Chemistry', eds., A. Weissberger and B.W. Rossiter, John Wiley and Sons, New York, 1972, vol. 1, Chapter 2.

88. H.G. Brittain in 'Lanthanide Probes in Life, Chemical and Earth Sciences', eds., J.-C.G. Bünzli and G.R. Choppin, Elsevier, Amsterdam, 1989, Chapter 8.

89. A. Rodger and B. Nordén, 'Circular Dichroism and Linear Dichroism', Oxford University Press, New York, 1997.

90. L. Velluz, M. Legrand and M. Grosjean, 'Optical Circular Dichroism : Principles, Measurements and Applications,' Verlag Chemie, Weinheim, 1965.

91. K. Nakanishi and J. Dillon, *J. Am. Chem. Soc.*, 1971, **93**, 4058.

92. P.G. Arscott, C. Ma, J.R. Weller and V.A. Bloomfield, *Biopolymers,* 1995, **36**, 345; C.W. Patterson, S.B. Singham, G.C. Salzman and C.J. Bustamente, *J. Chem. Phys.*, 1986, **84**, 1916.

93. N. Greenfield and G.D. Fasman, *Biochemistry*, 1969, **8**, 4108.

94. J.P. Riehl and F.S. Richardson, *Methods Enzymol.,* 1993, **226**, 539.

95. J.P. Riehl and F.S. Richardson, *Chem. Rev.*, 1986, **86**, 1; 1977, **77**, 773.

96. P.H. Schippers, A. van den Beukel and H.P.J.M. Dekkers, *J. Phys. E*, 1984, **15**, 945.

97. F.S. Richardson, *Inorg. Chem.,* 1980, **19**, 2806.

CHAPTER 2

NEUTRAL LANTHANIDE COMPLEXES OF MONOAMIDETRIPHOSPHINATE TETRAAZAMACROCYCLES

CHAPTER 2

NEUTRAL LANTHANIDE COMPLEXES OF MONOAMIDETRIPHOSPHINATE TETRAAZAMACROCYCLES

2.1 Introduction

Achiral lanthanide complexes based on **(1a)** and **(1b)** have been studied previously within the research group at Durham.[1] The use of phosphinates as coordinating groups allows the control of lipophilicity and solubility through variation of the substituent at the pentavalent P and allows the possibility of studying such complexes by ^{31}P NMR. The carboxamide group is a good donor for lanthanides and provides a site for further functionalisation. Neutral systems exhibit enhanced kinetic stability with respect to acid catalysed dissociation compared to anionic systems and *in vivo* studies[2] have shown lanthanide complexes of **(1)** to have high kinetic stabilities comparable to **(Y.DOTA)$^-$**, **(Y.7)$^-$**.

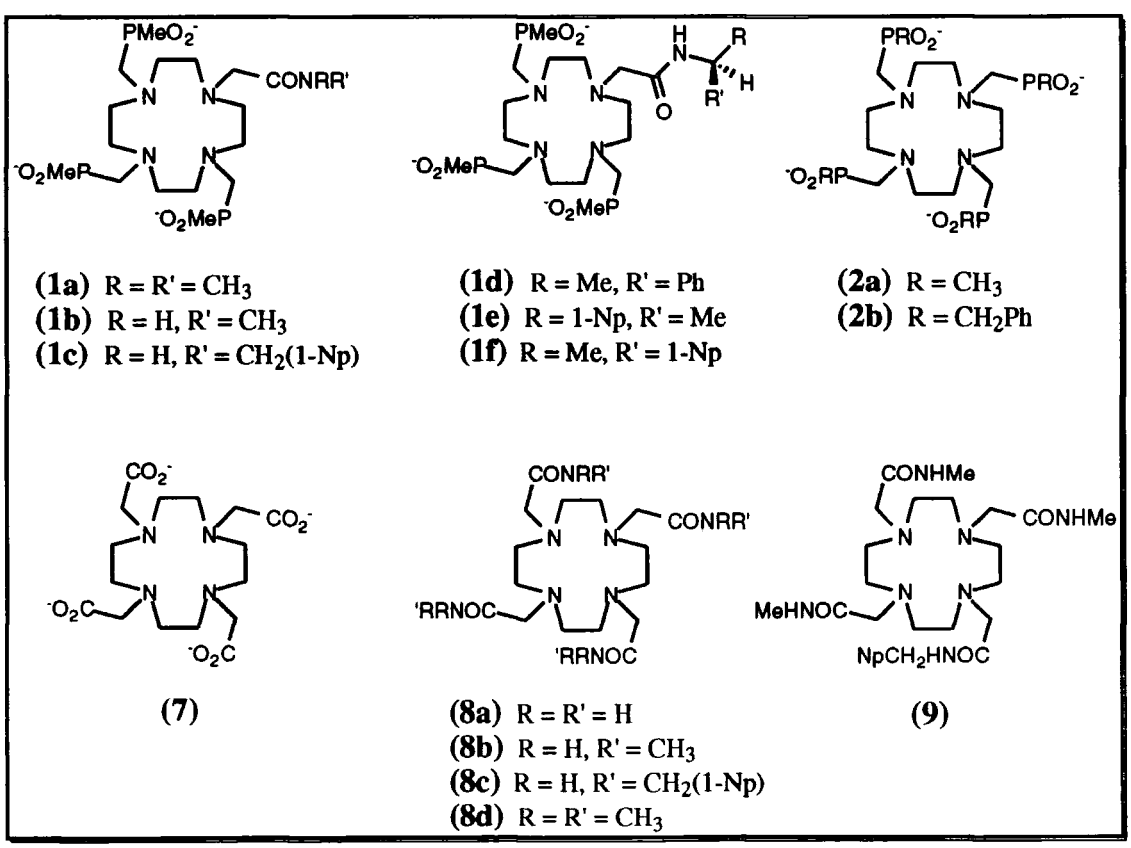

Figure 2.1 *Lanthanide complexes discussed in this chapter.*

Solution NMR studies of **(Ln.1a)** and **(Ln.1b)** show that the achiral complexes exist largely as one diastereoisomer in solution, consisting of 2 enantiomeric forms.[1] The diastereoisomer in solution is conformationally rigid on the NMR timescale and over the lifetime of the metal based emission. A chiral analogue (**Figure 2.1**), of such complexes would therefore be advantageous in the study of *in vivo* interactions. Resolution of the enantiomers has been unsuccessful to date and an alternative approach to enantiopure systems is thus desirable. It was decided to synthesise a chiral analogue by addition of a chiral group to the pendent carboxamide arm in the hope that this remote chiral centre will favour the formation of one enantiomeric complex.

2.2 Synthesis

The complexes were prepared according to the synthetic procedure outlined in **Scheme 2.1**.

The selective monoalkylation of $12N_4$ was achieved through the protection of three of the ring nitrogen atoms by reaction with molybdenum hexacarbonyl in dibutyl ether.[2] The reaction is quantitative resulting in the formation of the octahedral molybdenum tricarbonyl complex of $12N_4$, in which three of the four nitrogen atoms are bound to the molybdenum leaving the fourth available for reaction. This protection approach has been found to be preferable to the use of the analogous tricarbonyl-chromium complex reported earlier.[3] Reaction of the molybdenum complex in dry *N,N*-dimethylformamide with the appropriate chiral chloroamide, (itself formed by reacting the chiral amine with chloroacetylchloride at -20 °C), followed by decomplexation of the molybdenum moiety in aqueous acid, yielded the monoalkylated macrocycle. Condensation with paraformaldehyde yielded an imine which was trapped by reaction with diethoxymethylphosphine, prepared from the reaction of diethoxychlorophosphite with methylmagnesium bromide. An Arbuzov rearrangement gave the triphosphinate esters, which were selectively hydrolysed under mildly basic conditions (10% KOH) to yield the corresponding triphosphinate acids. Metal complexation was achieved by heating the ligand with the appropriate metal acetate in boiling water.

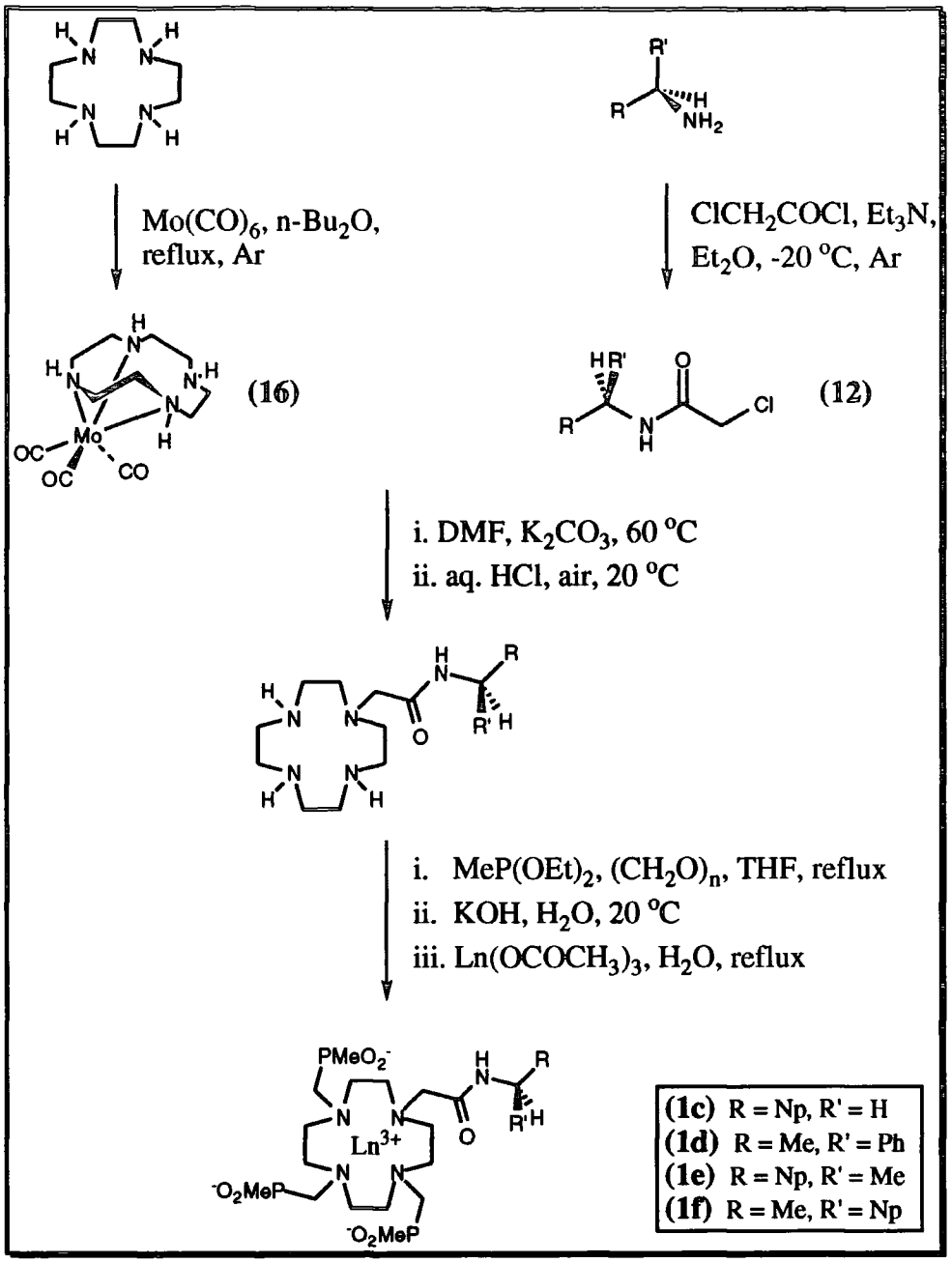

Scheme 2.1. *Procedure for the synthesis of monoamidotriphosphinate tetraazamacrocyclic complexes.*

2.3 NMR analysis

The stereoisomerism exhibited by achiral monoamidotriphosphinates, as depicted in Chapter 1.2, gives rise to 32 possible stereoisomers, 16 of which will be distinguishable by NMR analysis. The presence of a chiral amide pendent arm renders all 32 stereoisomers diastereomeric, therefore all 32 isomers may be distinguished by NMR analysis, in principle.

2.3.1 Europium complexes

Europium complexes are highly suited for analysis by NMR as they combine the large chemical shift range typical of paramagnetic species with a limited line broadening. All the resonances are therefore well separated which aids in the interpretation of the spectra. **Figure 2.2** shows the $^{31}P\{^{1}H\}$ NMR spectra for europium complexes **(Eu.1d)** and **(Eu.1e)**. The presence of six intense resonances may be immediately discerned, indicating the existence of two dominant isomers out of the 32 possibilities. Smaller peaks corresponding to at least two minor isomers are also evident. The actual ratio of the major isomers is dependent on the size of the chiral amide group, being 2:1 for the phenyl analogue **(Eu.1d)** and 4:1 for the naphthyl analogue **(Eu.1e)**. The bulkier naphthyl group therefore acts as a better stereodifferentiating group.

The two diastereoisomers are enantiomerically pure as shown by the addition of the chiral solvating agent, β-cyclodextrin. β-Cyclodextrin is itself a chiral molecule and forms inclusion compounds with aryl guests in which the aromatic groups bind inside the cyclodextrin cavity. Upon binding to aromatic moieties present in a pair of enantiomers, diastereoisomeric complexes are formed which may therefore be distinguished by NMR analysis. The $^{31}P\{^{1}H\}$ NMR spectrum for the achiral europium complex **(Eu.1c)** is shown in **Figure 2.3** in the absence and presence of β-cyclodextrin. In the absence of any chiral solvating agent, just 3 phosphorus peaks are evident corresponding to one major diastereoisomer in solution. However, on addition of β-cyclodextrin, enantiodifferentiation occurs and each of the resonances is shifted and split into two, suggesting that the diastereoisomer has two enantiomeric forms. By considering steric constraints and by comparison to the X-ray structure of the tetrabenzylphosphinate analogue **(2b)**[4], the most probable isomers are those with a twisted square antiprismatic structure in which the P-CH_3 groups are directed outside the coordination cage and the configuration at P is RRR and SSS. **Figure 2.3** also shows the $^{31}P\{^{1}H\}$ NMR spectrum for **(Eu.1d)** in the presence of β-cyclodextrin. Slight shifts in the frequency of the resonances are observed on inclusion, as expected, but the number of resonances remains the same strongly suggesting that each

diastereoisomer is enantiomerically pure. It is postulated that the two diastereoisomers will have the same ring conformation and layout of the pendent arms but differ in the configuration at P. Therefore the two diastereoisomers of **(Eu.1d)** are likely to be SSSS and SRRR with respect to configuration at the chiral C and P respectively. Similarly, for **(Eu.1e)** the diastereoisomers will be RRRR and RSSS and for **(Eu.1f)** SSSS and SRRR with respect to configuration at the C and P respectively, which is consistent with the identical $^{31}P\{^{1}H\}$ NMR spectra observed for **(Eu.1e)** and **(Eu.1f)**.

The transverse relaxation times, T_2, of the proton resonances in the europium complexes are sufficiently long to enable the detection of coupling patterns at low magnetic fields (90 MHz) and the detection of cross peaks in the 2D homonuclear COSY experiment. **Figure 2.4** shows the ^{1}H spectrum and 2D homonuclear COSY spectrum for **(Eu.1d)**. The spectra are complicated by the presence of the two isomeric species but a partial assignment of the resonances was possible. A heteronuclear C-H COSY experiment is required for full assignment of the ^{1}H resonances. Several broad triplets at high frequency can be attributed to axial ring protons coupled to a geminal equatorial proton and a vicinal axial proton of the same ethylenediamine group. Equatorial protons appear as doublets due to coupling with a geminal axial proton. The COSY spectrum allows the resonances of the ring protons to be assigned within each of the ethylenediamine groups. The 3 doublets of relative intensity three and relative intensity 1.5 correspond to the P coupled methyl groups of the major and minor isomers respectively. A feature to note is that the coupling patterns are lost at higher magnetic field strengths due to an increase in line broadening.[5] At 400 MHz most of the ^{1}H signals appear as singlets, therefore the usual higher degree of resolution provided by using high field instruments is not applicable to europium complexes. The shifting ability of the complexes is sufficient to provide enhanced resolution at lower magnetic field strengths.

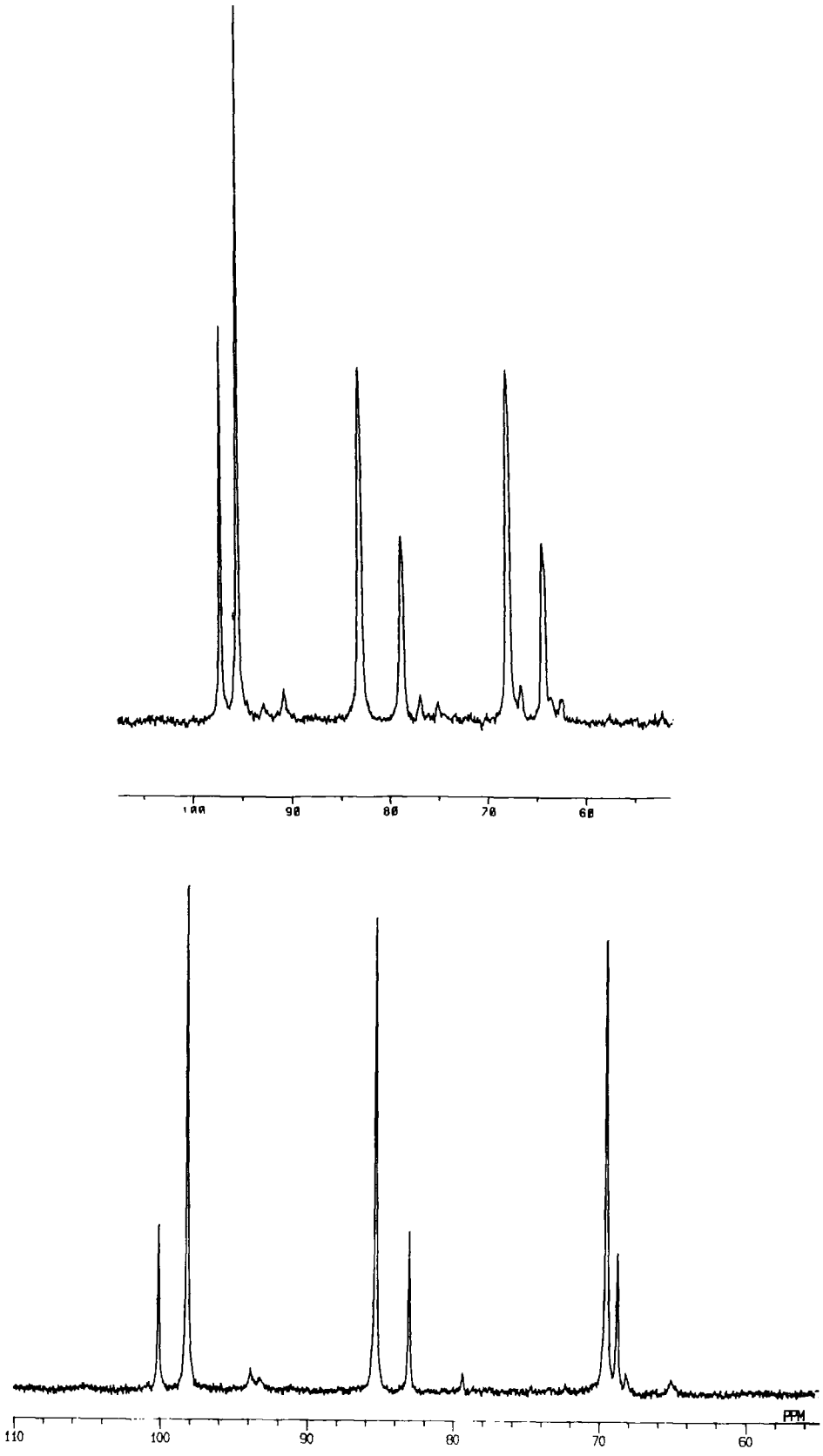

Figure 2.2 *$^{31}P\{^{1}H\}$ spectra for* ***(Eu.1d)*** *(upper) and* ***(Eu.1e)*** *(lower) (101.2 MHz, D_2O, 298 K).*

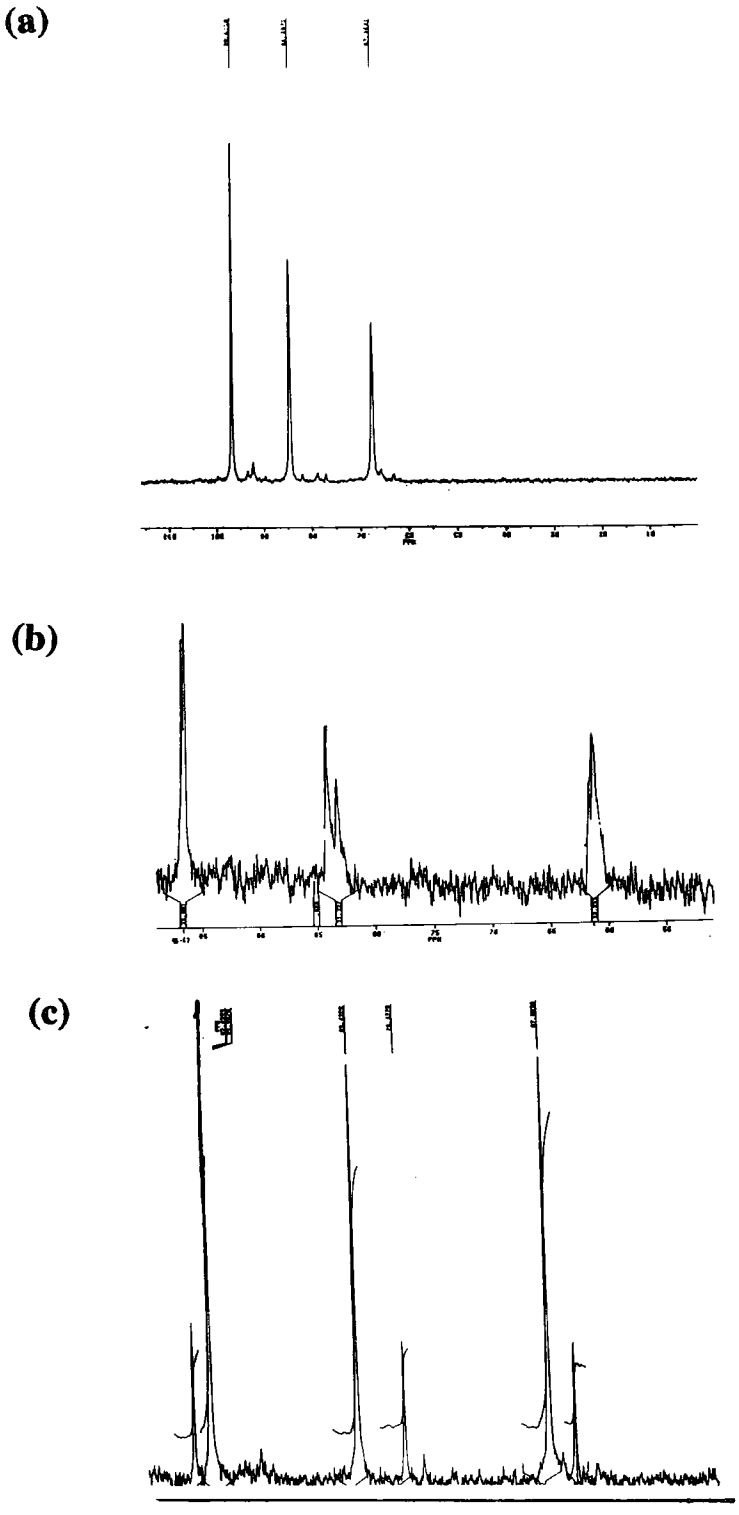

Figure 2.3 *$^{31}P\{^{1}H\}$ spectra for* ***(a) (Eu.1c)****,* ***(b) (Eu.1c)*** *in the presence of β-cyclodextrin and* ***(c) (Eu.1d)*** *in the presence of β-cyclodextrin (101.2 MHz, D_2O, 298 K).*

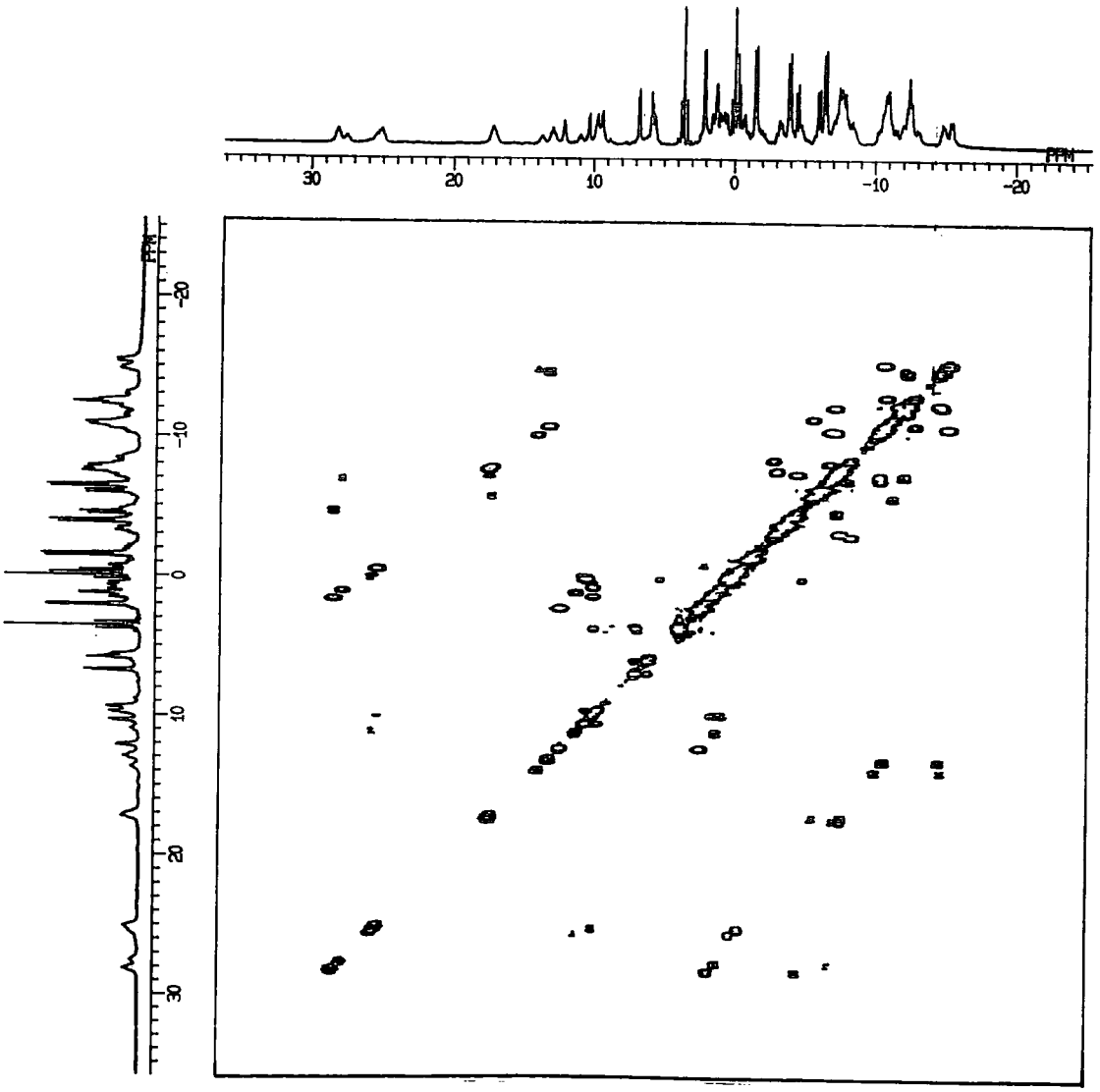

Figure 2.4 *^1H spectrum and 2D homonuclear COSY spectrum for* ***(Eu.1d)*** *(90 MHz, D_2O, 298 K).*

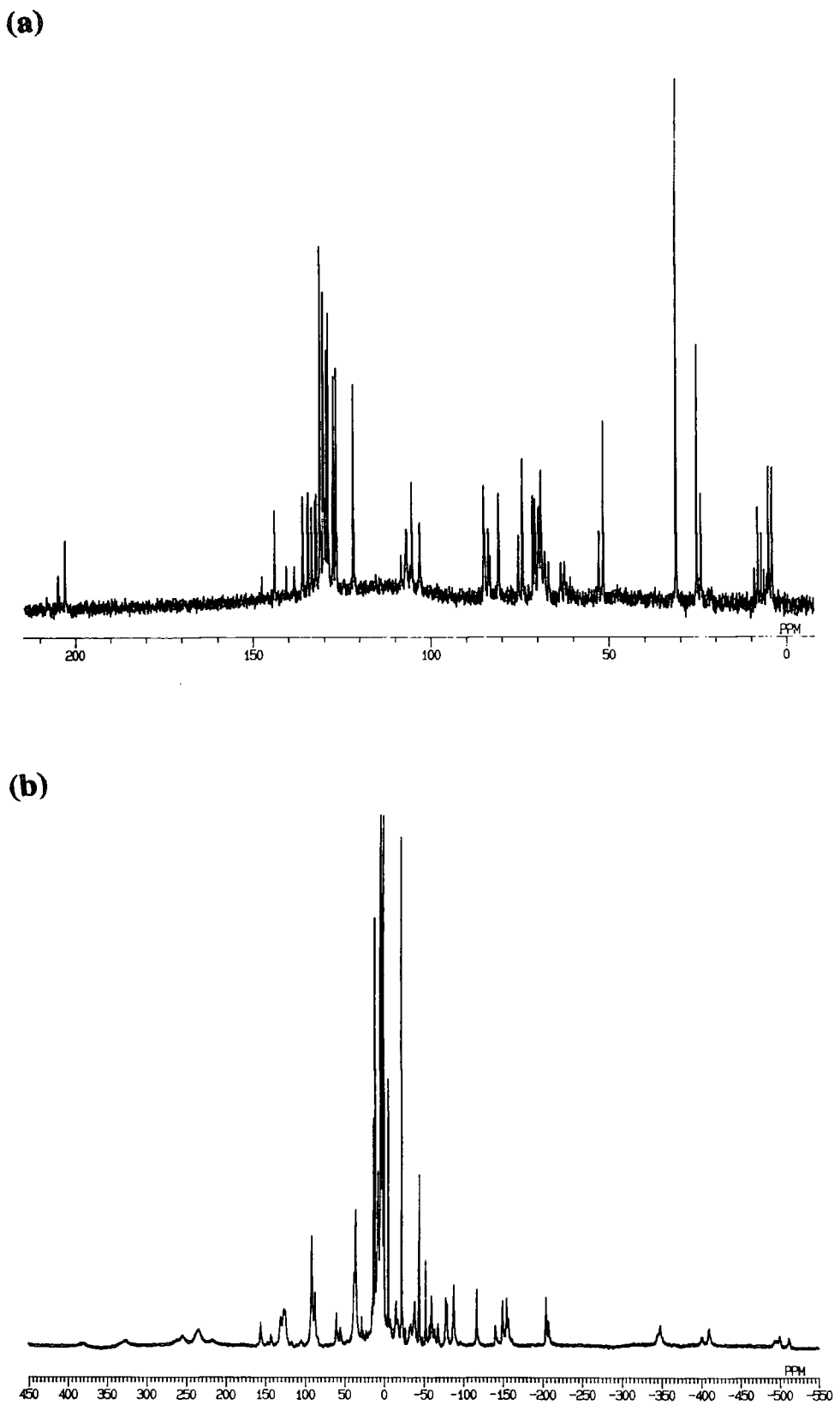

Figure 2.5 *(a)* $^{13}C\{^{1}H\}$ *spectrum for* ***(Eu.1d)*** *(100 MHz,*D_2O*, 298 K).*

(b) ^{1}H *spectrum for* ***(Tb.1d)*** *(90 MHz,* D_2O*, 298 K).*

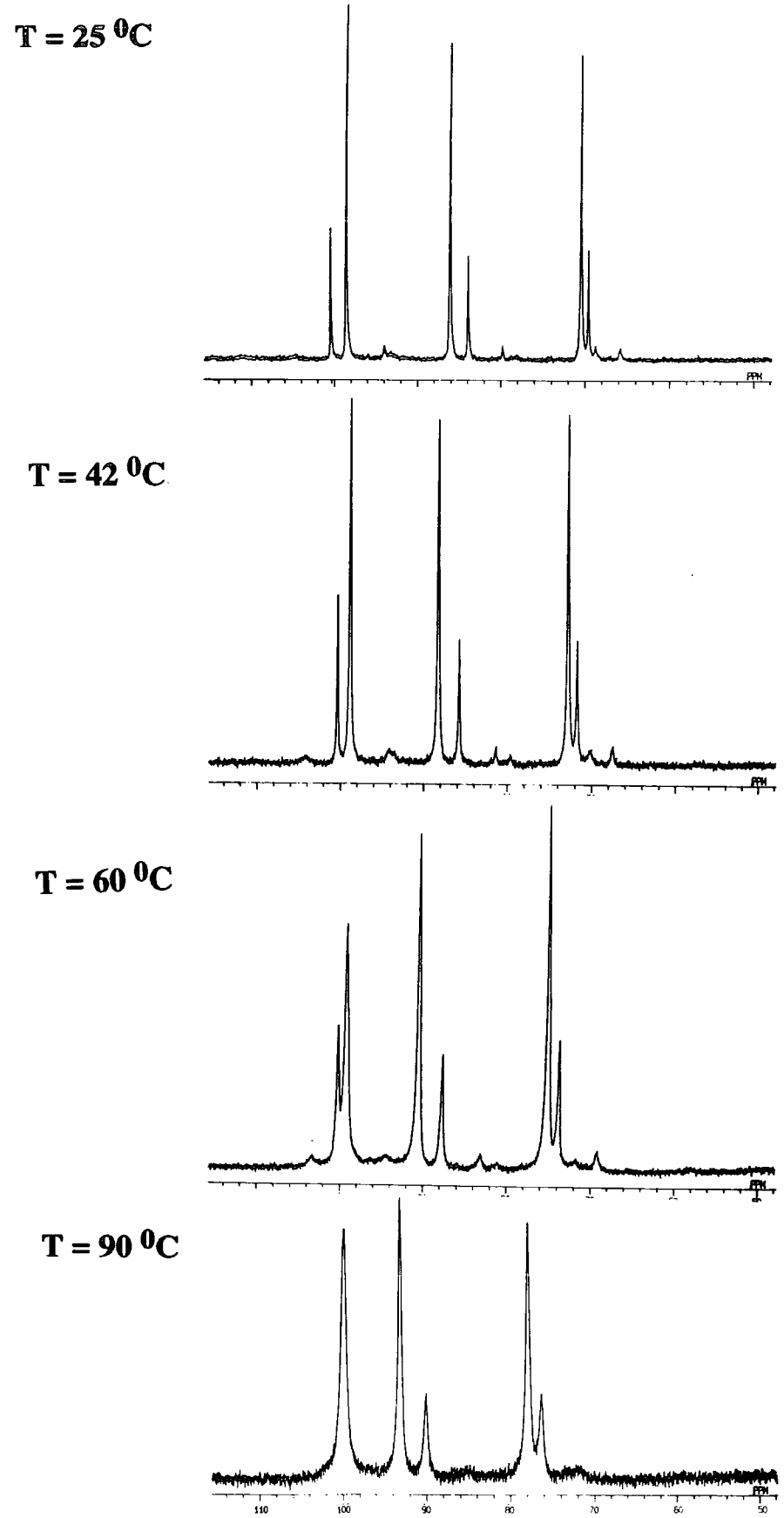

Figure 2.6 *Variable temperature $^{31}P\{^{1}H\}$ spectra for* ***(Eu.1e)*** *at 298, 315, 333, 363 K (161.9 MHz, D_2O).*

A typical $^{13}C\{^1H\}$ spectrum is shown in **Figure 2.5**. The paramagnetic effect of the nearby europium ion causes the ring-CH_2 carbon resonances to be spread over a considerable range, resulting in the separation of each individual resonance. The aromatic groups must lie outside the coordination cage, as predicted, since the carbon resonances are little affected by the presence of the europium ion and the paramagnetic shifting effects have a $1/r^6$ dependency (Chapter 1.3).

Variable temperature ^1H and $^{31}P\{^1H\}$ NMR studies in the range 298-363 K indicate that an exchange process was occurring between the isomers. There are two possible exchange mechanisms. A concerted sliding motion of the pendent arms over the lanthanide ion surface, or a configurational inversion of the ring whilst the Ln-O bond remains intact, will exchange isomers but only those with the same configuration at P. Alternately, if the Ln-O bond is labile, then all the isomers may exchange through a bond breaking and reforming process. The $^{31}P\{^1H\}$ variable temperature NMR spectra of **(Eu.1e)**, depicted in **Figure 2.6**, revealed a broadening of the minor isomer resonances as the temperature was increased to 42 °C, whereas the resonances of the 2 major isomers remain sharp and well defined. Increasing the temperature to 60 °C resulted in a slight broadening of the major isomer resonances. At 90 °C the 2 highest frequency resonances of the major isomers broadened sufficiently as to overlap whereas the lower frequency resonances broadened but did not coalesce. This indicates that the two major isomers are not in exchange with one another, and that the broadening is due to exchange of these isomers with other minor isomers in solution. This suggests that exchange occurs via a pendent arm rotation and ring inversion whilst the Ln-O bond remains intact. This behaviour is consistent with previous studies on similar systems which had indicated a remarkable lack of lability of the Ln-O bond.[6]

2.3.2 Terbium complexes

The analysis of NMR data for terbium complexes is complicated by the high degree of broadening associated with the metal ion. The short transverse relaxation time prohibits the detection of coupling patterns and cross peaks in 2D experiments. The

resonances are greatly shifted and broadened, as exemplified in **Figure 2.5** where the ^1H chemical shift range for the terbium complex of **(Tb.1d)** is of the order of 1000 ppm.

2.3.3 Gadolinium complexes

The long electronic relaxation time for the Gd^{3+} ion gives rise to a high degree of signal broadening which prevents the measurement of high resolution NMR spectra for gadolinium complexes. However, this long electronic relaxation time coupled with the large magnetic moment of the Gd^{3+} ion (S = 7/2), gives rise to efficient nuclear spin relaxation and renders the complexes suitable as relaxation agents as discussed in Chapter 1.3.

The $1/T_1$ NMRD profiles for **(Gd.1d)** and **(Gd.1e)** have been recorded in Turin by Professor S. Aime and coworkers. The two recorded profiles have similar shapes, as shown in **Figure 2.7**, which are typical of low molecular volume gadolinium complexes with a single bound water molecule. Quantitative analysis of the NMRD profiles using the equations discussed in Chapter 1.3, allows the calculation of relaxation parameters **(Table 2.1)**. Relaxivity values, R_{1p}, (20 MHz, 298 K) of 3.65 $mmol^{-1}$ s^{-1} and 3.45 $mmol^{-1}$ s^{-1} were measured for **(Gd.1d)** and **(Gd.1e)** respectively. The relaxivity remains fairly constant over the pH range 2-12, emphasising the stability of the complexes, and only increases with time at pH < 2 when dissociation of the complex becomes apparent. The values are considerably higher than those reported for the tetrabenzyl **(Gd.2b)**$^-$ (R_{1p} = 1.85 $mmol^{-1}$ s^{-1}, 20 MHz, 298 K) and tetramethyl **(Gd.2a)**$^-$ (R_{1p} = 2.44 $mmol^{-1}$ s^{-1}, 20 MHz, 298 K) derivatives, which have no directly coordinated water molecules.[4]

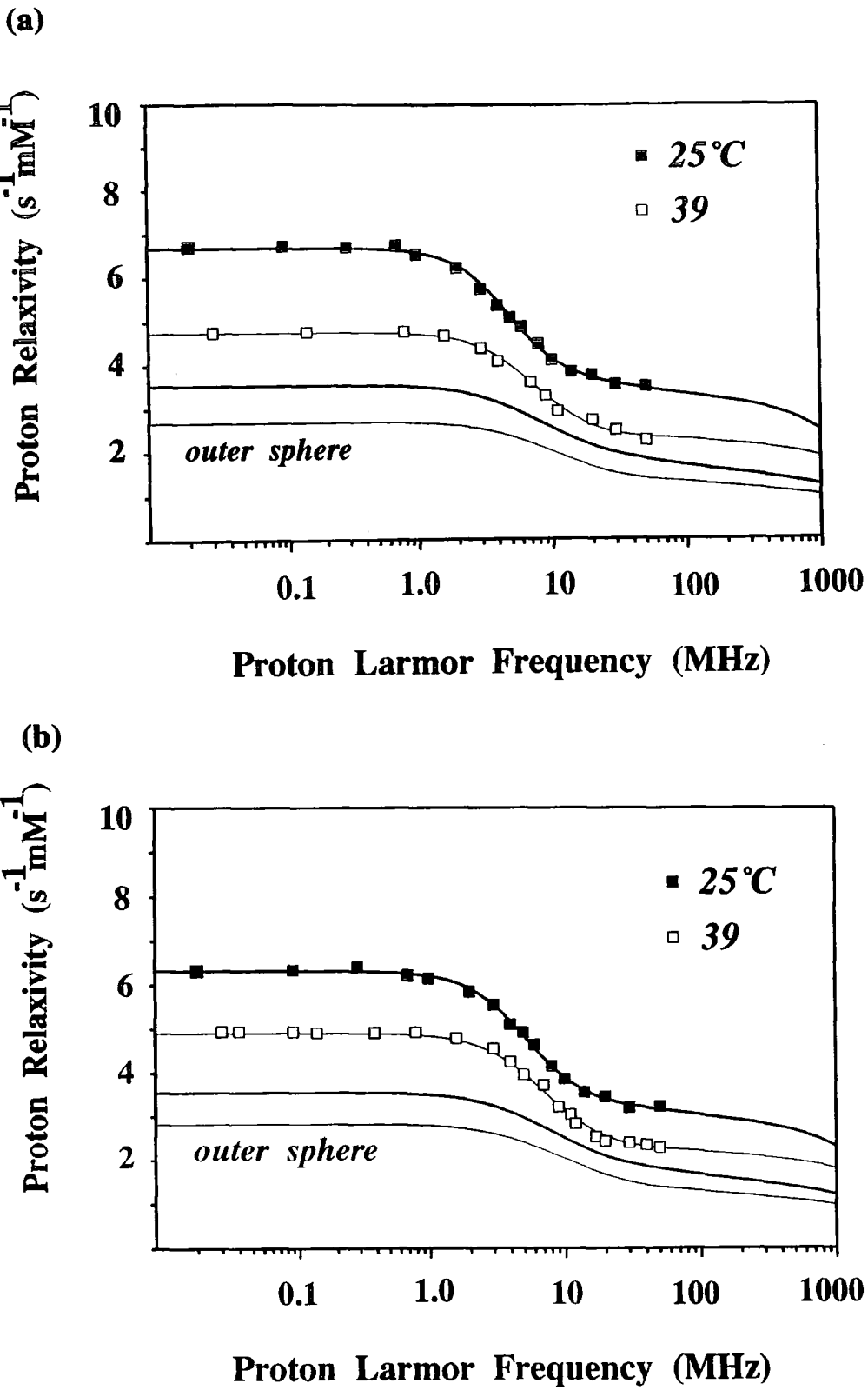

Figure 2.7. *NMRD profiles for* ***(a) (Gd.1d)*** *and* ***(b) (Gd.1e)****. The solid line through the points represents the simulated behaviour generated using a best fitting procedure to relaxation theory discussed in Chapter 1.3. The lower curves show the outer sphere contributions to the observed relaxivity.*

	(Gd.1d)		**(Gd.1e)**		
	Temperature (K)		Temperature (K)		
Parameter	298	312	278	298	312
τ_{S0} (ps)	122	91	118	124	113
τ_V (ps)	18.3	9.1	24.4	15.7	8.4
τ_R (ps)	100	61	190	91	60
τ_M (ns)	0.9	0.5	1.3	0.8	0.6
q	1	1	1	1	1
r (Å)	3.40	3.40	3.44	3.44	3.44
a (Å)	4.0	4.0	4.0	4.0	4.0
D ($cm^2\ s^{-1}$). 10^5	2.40	3.15	1.00	2.40	3.15

Table 2.1. *Relaxation parameters obtained by fitting relaxation theory for the gadolinium complexes* ***(Gd.1d)*** *and* ***(Gd.1e)*** *to the experimental NMRD profiles.*

The data suggests that in the complexes of **(Gd.1d)** and **(Gd.1e)** there are both inner sphere and outer sphere contributions to the relaxivity. The steric encumbrance of the complex is decreased on replacement of a phosphinic acid group with a carboxamide group, therefore a water molecule may enter into the coordination sphere. This second coordination sphere contribution may result from the ability of the carboxamide oxygen to undergo hydrogen bonding with the water molecule (**Scheme 2.2**), thereby bringing the water molecule close enough to the metal centre to affect the solvent relaxation and result in partial hydration of the metal ion.

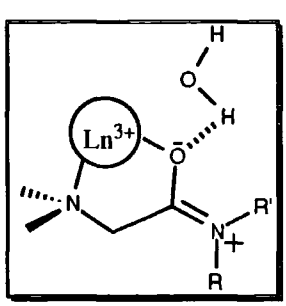

Scheme 2.2

Recent work has suggested that inner (q = 1) and outer (q = 0) sphere water molecules represent boundary conditions for the hydration state, q, of a complex.[7] A complex may possess any intermediate value, $0 \leq q \leq 1$, with the distance of closest approach of the water molecule to the ion varying between 3.0 Å (q = 1) to > 4.5 Å (q = 0). The separation of the inner sphere water protons to the gadolinium ion, r, was calculated to be 3.40 Å and 3.44 Å for **(Gd.1d)** and **(Gd.1e)** respectively, from a fitting of the NMRD profiles. The relaxivity of **(Gd.1d)** is greater than that of **(Gd.1e)** as the smaller phenyl group is less sterically demanding, enabling the water molecule to approach more closely to the metal centre. The hydration state, q, will therefore depend upon the steric demands of the ligand. Comparing the relaxivity values for the tetrabenzyl **(Gd.2b)**$^-$ and tetramethyl **(Gd.2a)**$^-$ derivatives it may be inferred that the hydrophobicity of the local ion environment, which depends upon the nature of the substituents at N or P, also determines the value of the relaxivity.

The addition of β-cyclodextrin to **(Eu.1e)** resulted in the formation of an inclusion compound as shown by the observed shift of the P atoms upon binding. The strength of the interaction may be evaluated by calculation of the dissociation constant, K_d, for the **(Gd.1e)**-β-cyclodextrin adduct through the proton relaxation enhancement technique.[8] This involves monitoring the increase in relaxivity at a fixed Larmor frequency when a fixed concentration of the gadolinium complex is titrated with increasing amounts of β-cyclodextrin. On formation of the inclusion adduct, the size of the gadolinium complex is increased which results in a slower rotational correlation time, τ_R, and therefore an increase in relaxivity (Chapter 1.3). The titration data is reported as a plot of the relaxivity enhancement factor, ε*, which represents the ratio of the paramagnetic relaxation rates in the presence and absence of β-cyclodextrin, as a function of β-cyclodextrin concentration. The data is analysed according to equation **(2.1)**.[4]

$$\varepsilon^* = \frac{1}{\varepsilon_b} \frac{C_T + n M_T + K_d - [(C_T + n M_T + K_d)^2 - 4 n M_T C_T]^{0.5}}{2 C_T} + 1 \qquad \textbf{(2.1)}$$

where C_T = total concentration of complex, M_T = total concentration of β-cyclodextrin, n = number of binding sites (= 1), ε_b = relaxivity for the fully bound complex.

A value of the dissociation constant, $K_d = 2.62 \times 10^{-2}$ dm^3 mol^{-1}, was obtained from a best fitting procedure of the data (**Figure 2.8**) to equation **(2.1)**. This is a relatively weak interaction in comparison to the interaction of β-cyclodextrin with 1-methylnaphthalene[9], for which $K_d = 3.23 \times 10^{-3}$ dm^3 mol^{-1}.

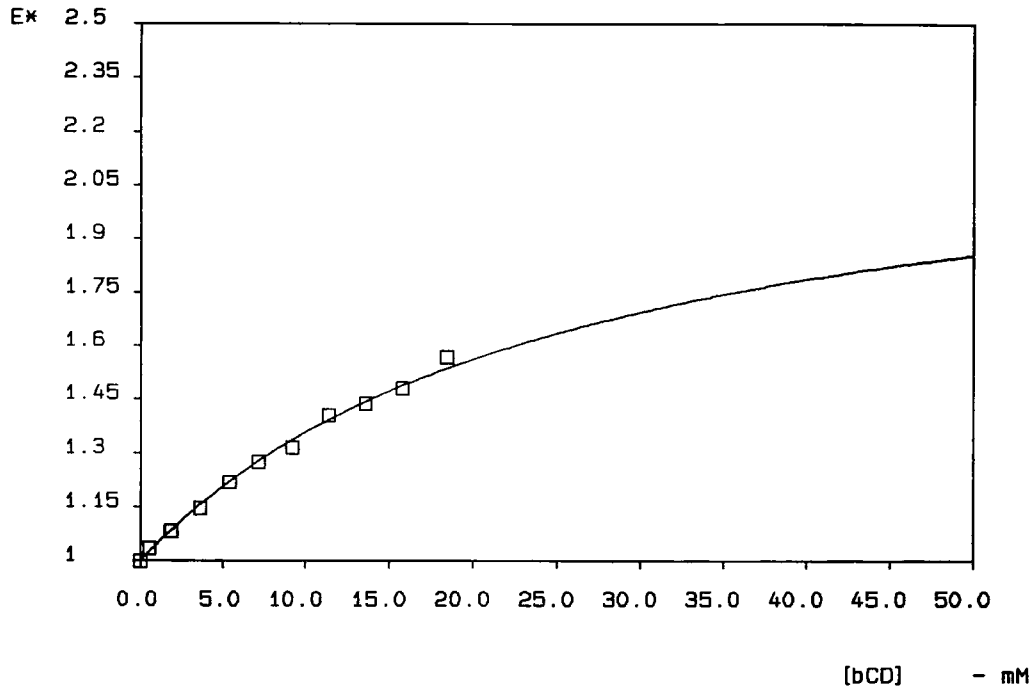

Figure 2.8. *Proton relaxation enhancement for* ***(Gd.1e)*** *(0.2 mmol, 20 MHz, 298 K) as a function of added β-cyclodextrin. The solid line represents the best fit to equation* ***(2.1)****.*

2.4 Luminescence properties of monoamidetriphosphinate complexes

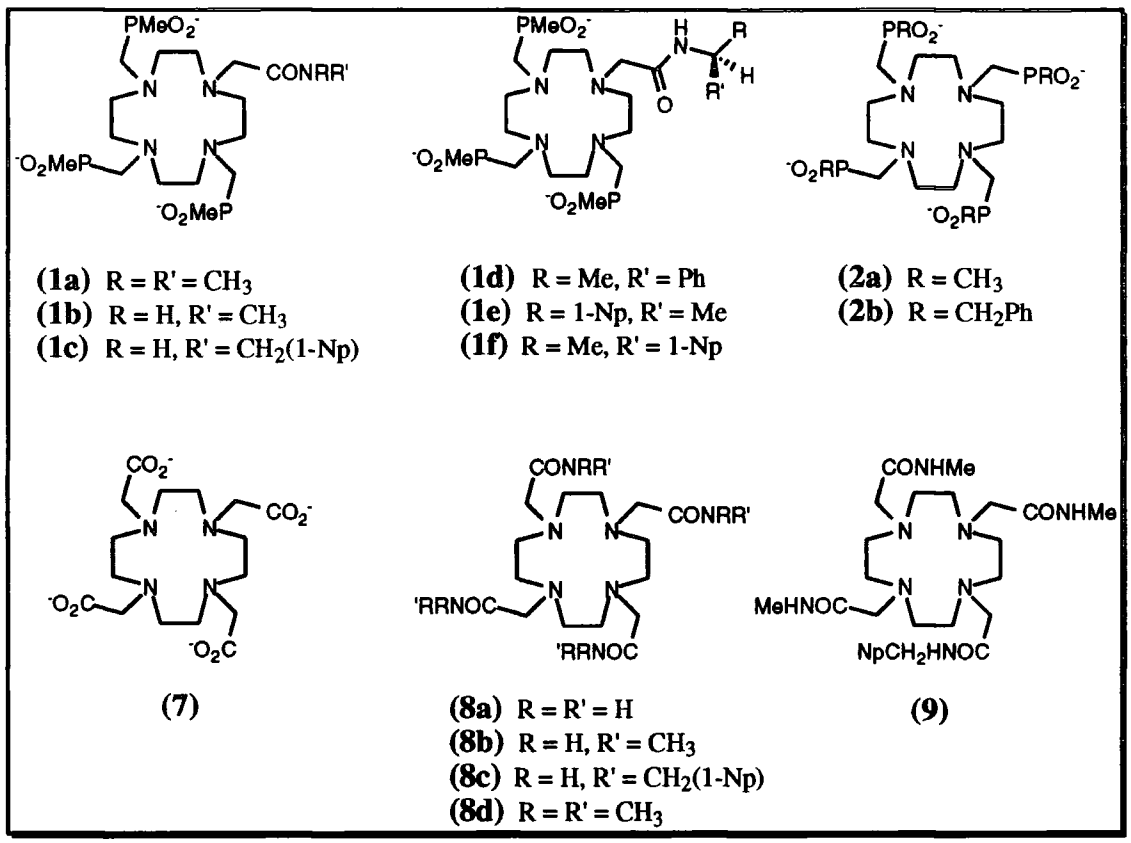

Figure 2.1 *Lanthanide complexes discussed in this chapter.*

2.4.1 Europium emission spectra

The corrected phosphorescence emission spectra for the complexes **(Eu.1d)** and **(Eu.1e)** have been recorded (298 K, H_2O) following excitation at 254 nm and 278 nm respectively. A representative spectrum for **(Eu.1e)** is shown in **Figure 2.9** and the $^5D_0 \longrightarrow {}^7F_n$ transitions have been assigned.

The $^5D_0 \longrightarrow {}^7F_0$ (Δ J = 0) transition is forbidden by electronic selection rules[10] but is formally allowed in systems of low symmetry and acquires its intensity via an electric-dipole mechanism. The monoamidetriphosphinate complexes lack axial symmetry therefore a weak transition is expected at 579 nm. On close inspection of the spectrum, a tiny peak is evident at this wavelength. This peak becomes more apparent on increasing the excitation and emission monochromator slit widths to their maximum values which maximises the amount of light getting into the sample and the detector.

However, this results in loss of resolution and the 579 nm peak is swamped by the $^5D_0 \longrightarrow {}^7F_1$ transition, therefore a compromise between the sensitivity of detection and degree of fine structure observed has to be made. The $^5D_0 \longrightarrow {}^7F_0$ transition is a probe of the Eu^{3+} ion homogeneity, as both states are non-degenerate, therefore only one component will be observed for the transition. As the complexes **(Eu.1d)** and **(Eu.1e)** both exist as two isomers in solution observation of two components to the transition are expected. Obviously the $^5D_0 \longrightarrow {}^7F_0$ transition is far too weak for the complexes for any analysis to be made. However, a highly resolved spectrum using laser excitation and sensitive photon-counting equipment could reveal the existence of two bands for the transition.

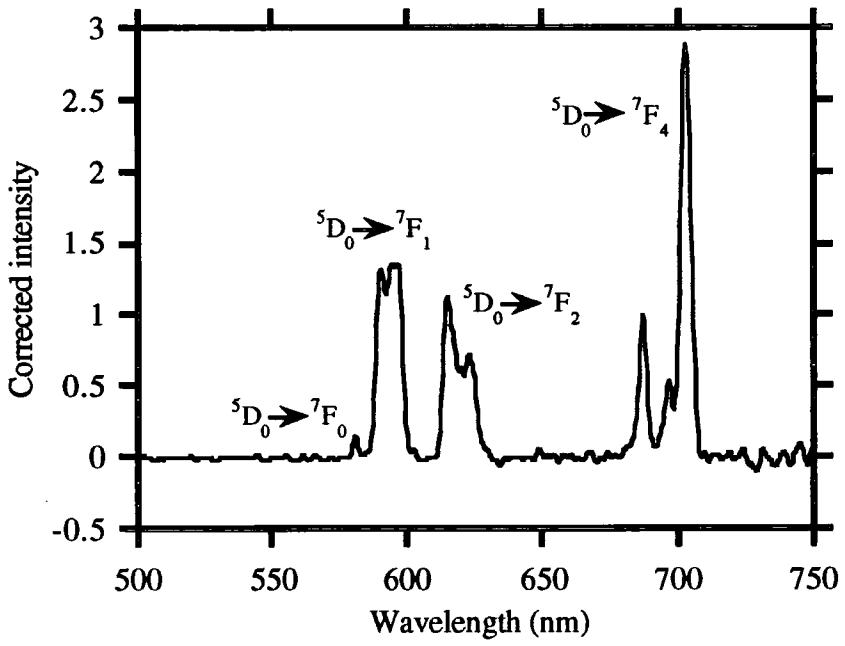

Figure 2.9. *Corrected phosphorescence emission spectrum for* ***(Eu.1e)*** *(298 K, H_2O) following excitation at 274 nm.*

The $^5D_0 \longrightarrow {}^7F_1$ (Δ J = 1) transition for **(Eu.1e)**, being magnetic dipole in character, is little affected by the ligand environment. As the complex does not possess axial symmetry, 3 components to the transition are expected.[11,12] The observed transition occurs at 594 nm and is very broad, exhibiting only very slight structuring. Once again,

in order to maximise the amount of light passing in and out of the sample, the monochromator slits were adjusted accordingly and the increased sensitivity of detection resulted in loss of resolution, therefore the fine structure of the transition was lost.

The hypersensitive $^5D_0 \longrightarrow {}^7F_2$ (Δ J = 2) transition is a very sensitive probe of ligand environment as discussed in Chapter 1.4. Two components are resolved at 615 nm and 624 nm. The $^5D_0 \longrightarrow {}^7F_3$ (Δ J = 3) transition was absent but the $^5D_0 \longrightarrow {}^7F_4$ (Δ J = 4) transition was relatively intense, exhibiting some fine structure.

In the case of **(Eu.1d)**, similar transition frequencies were observed but the relative intensities of the transitions are different, trends that have also become apparent in related europium complexes.[7] The intensity of the hypersensitive transition Δ J = 2 to that of Δ J = 1 has been found to vary according to the metal environment. In addition there is a variation in the relative intensity ratio of the components of the Δ J = 2 transition. It appears that **(Eu.DOTA)$^-$**, **(Eu.7)$^-$** and the tetrabenzylphosphinate **(Eu.2b)$^-$** complexes represent two limiting cases. The Δ J = 2 transition is weaker than that of Δ J = 1 for **(Eu.DOTA)$^-$**, and the component of the Δ J = 2 transition at lower wavelength is much more intense. For **(Eu.2b)$^-$** the reverse is true. This may be related to the different solution structures of the complexes. **(Eu.DOTA)$^-$** adopts a square antiprismatic geometry whereas **(Eu.2b)$^-$** adopts a twisted square antiprismatic structure. The neutral monoamidotriphosphinates display characteristics between these two limiting cases and the relative ratios of the transitions and transition components depends upon the nature of the substituents at N.

2.4.2 Terbium emission spectra

A representative corrected phosphorescence emission spectra of the terbium complex **(Tb.1d)** is shown in **Figure 2.10** and the $^5D_4 \longrightarrow {}^7F_n$ transitions have been assigned.

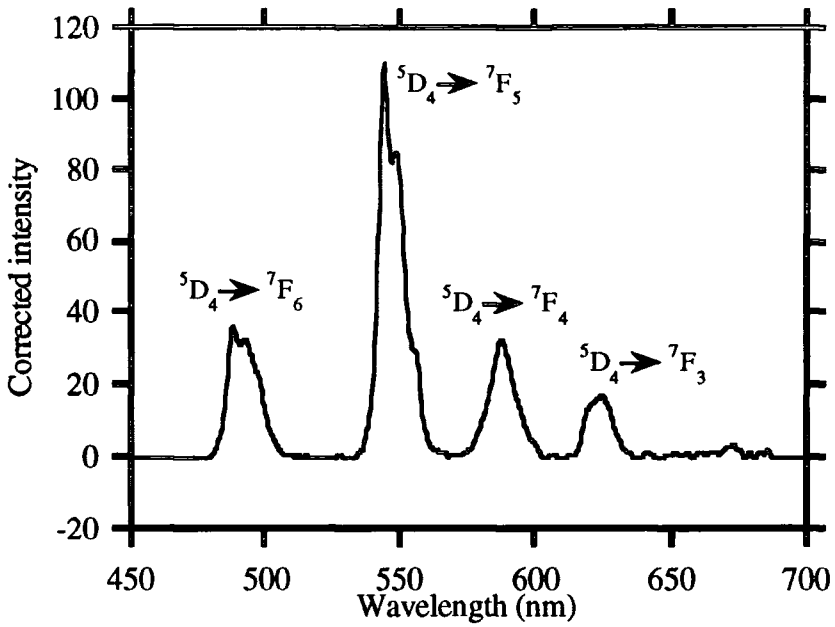

Figure 2.10. *Corrected phosphorescence emission spectrum for (**Tb.1d**) (298 K, H_2O) following excitation at 254 nm.*

Immediately obvious are the higher intensities of the transitions compared to the europium spectra. Emission is often much weaker for europium complexes compared to terbium complexes due to a competitive charge transfer mechanism of energy capture by the europium ion.[13] The four intense bands observed arise from transitions from the emissive $^5D_4$ state to $^7F_{6,5,4,3}$ levels of the ground state manifold. The large J values associated with the transitions mean that each one will be split into many components. For example, the $^5D_4 \longrightarrow {}^7F_5$ transition will give rise to $2J+1 = 9$ levels for $^5D_4$ and $2J + 1 = 11$ levels for $^7F_5$ resulting in a possible 99 components to the transition. Of course, many of these components will have the same or similar energies, due to the very small separation of the J sub levels, therefore terbium emission bands will not be fully resolved but just display some degree of fine structuring. Thus, terbium spectra cannot be used to extract structural information in the same way that europium spectra may be analysed.

2.4.3 Absorption and excitation spectra

As discussed in Chapter 1.4, the lanthanide ions have very poor molar absorptivities, typically $\varepsilon > 1\ M^{-1}\ cm^{-1}$, therefore the u.v. absorption spectra is largely dominated by the phenyl absorbance at 254 nm ($\varepsilon = 204$ per Ph group) or the naphthyl absorbance at 286 nm ($\varepsilon = 9300$ per Np group). For all the complexes there is a good match between the absorption and excitation spectra indicating that sensitised emission and energy transfer from the aromatic chromophore to the lanthanide ion is occurring.

For the terbium complex (**Tb.1d**), the observed excitation band lacked vibrational fine structure which suggests that some other absorption process along with that for the aromatic chromophore is taking place. For Eu^{3+} there exists a ligand to metal charge transfer band (LMCT) due to the ease of reduction of $Eu^{3+} \longrightarrow Eu^{2+}$ ($E^o = -0.35$ V). This process is unfavourable for Tb^{3+} as the reduction potential for $Tb^{3+} \longrightarrow Tb^{2+}$ is -2.3 V. However, a ligand to metal charge transfer band may arise from the transfer of an electron from the metal to the π^* orbital of the amide carbonyl group. The superposition of this amide-Tb LMCT band with the phenyl absorption may account for the loss of fine structure.

2.4.4 Quantum yields

The Stark and Einstein law "*if a species absorbs radiation then one particle is excited for each quantum of radiation absorbed*" led to the concept of quantum yield, ϕ. Quantum yield is a measure of the efficiency of the use of radiation for a particular process. The quantum yield of emission, ϕ_{em}, is defined as the ratio of the number of photons emitted to the number of photons absorbed and is the ratio of the radiative rate constant, k_o, to the sum of all the rate constants for processes that deactivate the emitting state.

$$\phi_{em} = \frac{k_o}{k_o + \Sigma k_i^{nr}} \qquad (2.2)$$

Σk_i^{nr} is the sum of all the rate constants for non radiative deactivation of the emitting state.

The term $(k_o + \Sigma k_i^{nr})^{-1}$ is the observed luminescence lifetime, τ_{obs} hence

$$\phi_{em} = k_0 \tau_{obs} \qquad (2.3)$$

Therefore the quantum yield of emission has a direct dependency on the lifetime of the excited state and upon non-radiative deactivation pathways that may compete with the luminescence.

The phosphorescence quantum yields for europium and terbium complexes were measured in aqueous solution relative to the standards $[Ru(bipy)_3]Cl_2$ and quinine sulphate (in 1 mol dm^{-3} H_2SO_4) respectively[14] and are reported in **Table 2.2.**

	H_2O	D_2O
(Eu.1d)	1.0×10^{-3}	2.0×10^{-3}
(Tb.1d)	0.12	0.18
(Eu.1e)	0.8×10^{-3}	1.7×10^{-3}
(Tb.1e)	-	-

Table 2.2. *Phosphorescence quantum yields for europium and terbium complexes in H_2O and D_2O.*

The quantum yield for **(Tb.1d)** is much greater than those for the europium complexes. This may be attributed to the ease of reduction of $Eu^{3+} \longrightarrow Eu^{2+}$ (E^o = -0.35 V) which gives rise to an efficient non-radiative deactivation pathway via a photoinduced electron transfer from the chromophore to the metal, resulting in the formation of Eu^{2+} and a radical cation. Evidence for such a process has been provided by measurement of the fluorescence spectra of Eu^{3+}, Gd^{3+} and Tb^{3+} complexes of **(9)** which show that the fluorescence intensity of the naphthyl group in the case of Eu^{3+} is only 10% of that measured for the other complexes, indicating that in the case of europium there is indeed an alternative deactivation pathway for the excited state.[12] The processes

$Gd^{3+} \longrightarrow Gd^{2+}$ and $Tb^{3+} \longrightarrow Tb^{2+}$ are relatively inaccessible therefore photoinduced electron transfer is disfavoured for these ions.

The terbium complex, **(Tb.1e)** displays very weak emission in aerated aqueous solution. This may be attributed to a back energy transfer process occurring from the metal emissive state to the naphthyl triplet state. Such an effect has been observed with similar systems[15] and other sensitising chromophores.[16] Due to the relatively high energy of the terbium emissive state, the energy gap between the naphthyl triplet and the $^5D_4$ emissive state is very small, estimated to be only 4-5 kJ mol^{-1}, therefore this back energy transfer process becomes very efficient. The emission intensity is substantially increased on degassing the sample. Although molecular oxygen has little direct effect on quenching the excited state of lanthanide ions, it may do so indirectly via subsequent quenching of the naphthyl triplet state after this back energy transfer has occurred. Removing molecular oxygen from the system eliminates this deactivation pathway and hence strong emission is then observed.

In order to achieve high quantum yields, efficient energy transfer from the chromophore to the metal, which is favoured by a good match of donor and acceptor energy levels and the close proximity of the chromophore, is required along with a high quantum yield for the formation of the chromophore triplet state and minimal non-radiative deactivation pathways (eg. vibrational quenching by H_2O oscillators) available for the lanthanide emissive state.

2.4.5 Excited state lifetimes

The phosphorescence of the complexes **(Eu.1d)**, **(Tb.1d)** and **(Eu.1e)** decays exponentially over several milliseconds following pulsed excitation which is consistent with first order kinetics of deactivation of the emissive state. The lifetimes of the emissive state, τ, were determined in H_2O and D_2O by observing the intensity of luminescence afer a range of delay times and are reported in **Table 2.3**.

	τ_{H_2O} ms	τ_{D_2O} ms	k_{H_2O} $(ms)^{-1}$	k_{D_2O} $(ms)^{-1}$	Δk $(ms)^{-1}$	ΣOH s^{-1}	NH s^{-1}	CH s^{-1}	q
(Eu.2b)$^-$	1.59	2.08	0.63	0.48	0.15	150	-	-	0.16
(Eu.[$^2H_7$]-2b)$^-$	1.67	2.27	0.60	0.44	0.16	160	-	-	0.17
(Eu.2a)$^-$	0.25	1.85	0.80	0.54	0.26	260	-	-	0.27
(Eu.8a)$^{3+}$[18]	0.52	2.17	1.93	0.46	1.47	1062	51	-	1.54
(Eu.8b)$^{3+}$	0.55	2.13	1.82	0.47	1.35	1058	73	-	1.42
(Eu.8c)$^{3+}$	0.59	2.38	1.69	0.42	1.27	978	73	-	1.33
(Eu.8d)$^{3+}$	0.63	1.85	1.60	0.54	1.06	1060	-	-	1.11
(Eu.7)$^-$	0.63	1.85	1.60	0.54	1.06	1060	-	26	1.11
(Eu.[$^2H_7$]-7)$^-$	0.71	2.78	1.41	0.36	1.05	1050	-	-	1.10
(Eu.1a)	0.84	1.97	1.19	0.51	0.68	680	-	-	0.71
(Eu.1b)	0.76	1.85	1.32	0.54	0.78	680	100	-	0.82
(Eu.1d)	0.68	1.74	1.47	0.57	0.9	800	100	-	0.94
(Eu.1e)	0.73	1.70	1.37	0.59	0.78	680	100	-	0.82
(Tb.7)$^-$	1.51	2.54	0.66	0.39	0.27	270	-	-	1.10
(Tb.2a)$^-$	2.96	3.71	0.34	0.27	0.07	70	-	-	0.28
(Tb.2b)$^-$	4.13	4.44	0.24	0.23	0.02	16	-	-	0.07
(Tb.1a)	3.53	4.30	0.28	0.23	0.05	50	-	-	0.21
(Tb.1b)	3.20	4.30	0.31	0.23	0.08	50	30	-	0.34
(Tb.1d)	3.00	4.00	0.33	0.25	0.08	50	30	-	0.35

Table 2.3. *Lifetimes and rate constants for the excited states of europium and terbium complexes and the estimated individual contributions of XH oscillators (k values were reproducible to ±0.03 $(ms)^{-1}$). The XH oscillator contributions to Δk are estimated within ± 15%.*

The lifetimes of the terbium complexes are longer than their europium analogues due to the larger energy gap between the emissive state and the highest J level of the ground state manifold which reduces the efficiency of non-radiative deactivation pathways.

The lifetimes in D_2O are also significantly longer than those in H_2O due to the occurrence of efficient energy transfer to the O-H vibrational manifold of water, a deactivation process that is absent in D_2O and is much more pronounced for Eu^{3+} than Tb^{3+} as discussed in Chapter 1.4.

By comparing the vibrational stretching frequencies of an O-H group ($\nu_{OH} \approx 3400\ cm^{-1}$) with those of N-H ($\nu_{OH} \approx 3300\ cm^{-1}$) and C-H ($\nu_{OH} \approx 2950\ cm^{-1}$), it may be envisaged that the higher vibrational levels of these oscillators may lie close in energy to the excited state of the lanthanide ion thereby providing additional deactivation pathways. Partitioning these deactivating processes from the other modes of depopulation of the emissive state gives equation **(2.4)**.

$$k_{obs}^{H_2O} = k_{nat} + k_{nr} + \Sigma k_{XH} \qquad \textbf{(2.4)}$$

where k_{nat} is the natural radiative rate constant, k_{nr} is the rate constant for non-radiative deactivation and Σk_{XH} is the sum of the rate constants for energy transfer to proximate energy matched XH oscillators.

The lower stretching frequency of O-D, N-D and C-D oscillators means that they are much less efficient at deactivation and therefore their contribution to the observed rate constant in D_2O may be neglected.

$$k_{obs}^{D_2O} = k_{nat} + k_{nr} \qquad \textbf{(2.5)}$$

Hence

$$\Delta k = k_{obs}^{H_2O} - k_{obs}^{D_2O} = \Sigma k_{XH} \qquad \textbf{(2.6)}$$

Table 2.3 lists the experimentally measured rate constants for deactivation of the excited state of some appropriate europium and terbium complexes along with estimated contributions due to XH oscillators present and the corresponding apparent q values.

OH Oscillator quenching

The crystal structure of the europium complex of the tetrabenzylphosphinate ligand **(Eu.2b)**$^{-}$, shows that it does not possess any metal-bound water, the nearest water molecule being in the crystal lattice some 5.6 Å from the metal centre (**Appendix 3**). The apparent q value of 0.16 must therefore be attributed to water molecules diffusing in the outer sphere of the complex, close enough to the europium ion to cause some vibrational deactivation. Supporting evidence arises by comparison to the q value obtained for **(Eu.2a)**$^{-}$. This tetramethylphosphinate complex is less hydrophobic thereby allowing the outer sphere water molecules to diffuse more closely to the metal centre giving rise to an increased q value of 0.27. Indeed this is consistent with NMRD studies on the related gadolinium complexes[4] which suggest the nearest water molecule is some 0.42 Å closer for **(Gd.2a)**$^{-}$. Crystallographic data on similar nine coordinate europium complexes with bound water molecules shows there to be little variation in Eu-O distances.[13] Therefore differences observed in Δk due to OH oscillator contributions are due to changes in the distance of closest approach of closely diffusing water molecules.

NH Oscillator quenching

The effect of NH/ND exchange is evident by comparing the Δk and q values for the europium complexes of **(8)** which are known to possess one bound water molecule from crystallographic and NMRD analyses of gadolinium complexes.[17] The complex **(Eu.8d)**$^{3+}$ has no NH bonds and therefore Δk may be ascribed to the contribution from bound and closely diffusing water only. The Δk value increases by 0.29 $(ms)^{-1}$ by the introduction of 4 NH groups in **(Eu.8b)**$^{3+}$, each NH contributing ~73 s^{-1} to the observed rate constant assuming the contribution from bound and closely diffusing water is the same for both complexes. Likewise, comparison to **(Eu.8a)**$^{3+}$ which has 8 NH bonds increases the Δk value by 0.41 $(ms)^{-1}$, each NH contributing an average of ~51 s^{-1} to the observed rate constant.[18] The Δk value for **(Eu.8a)**$^{3+}$ with 8 NH bonds is not double that for **(Eu.8b)**$^{3+}$ with 4 NH bonds. The primary amide NH groups in **(Eu.8a)**$^{3+}$ are diastereotopic and are likely to have different stretching frequencies and

therefore may be expected to have different quenching abilities. The quenching abilities of the NH oscillators in **(Eu.8b)**$^{3+}$ and **(Eu.8c)**$^{3+}$ are expected to be similar. The difference observed in Δk can be attributed to the varying distance of closest approach of closely diffusing water molecules. Complex **(Eu.8c)**$^{3+}$ is much more hydrophobic than **(Eu.8b)**$^{3+}$, therefore Σk_{OH} contributions will be less significant, accounting for the decreased Δk value observed.

^{1}H NMR analysis demonstrated that NH/ND exchange occurs rapidly at room temperature at pD 6, the ease of exchange being attributed to the europium ion which may act as an effective charge sink and thereby promote amide enolisation[19] (**Scheme 2.3**).

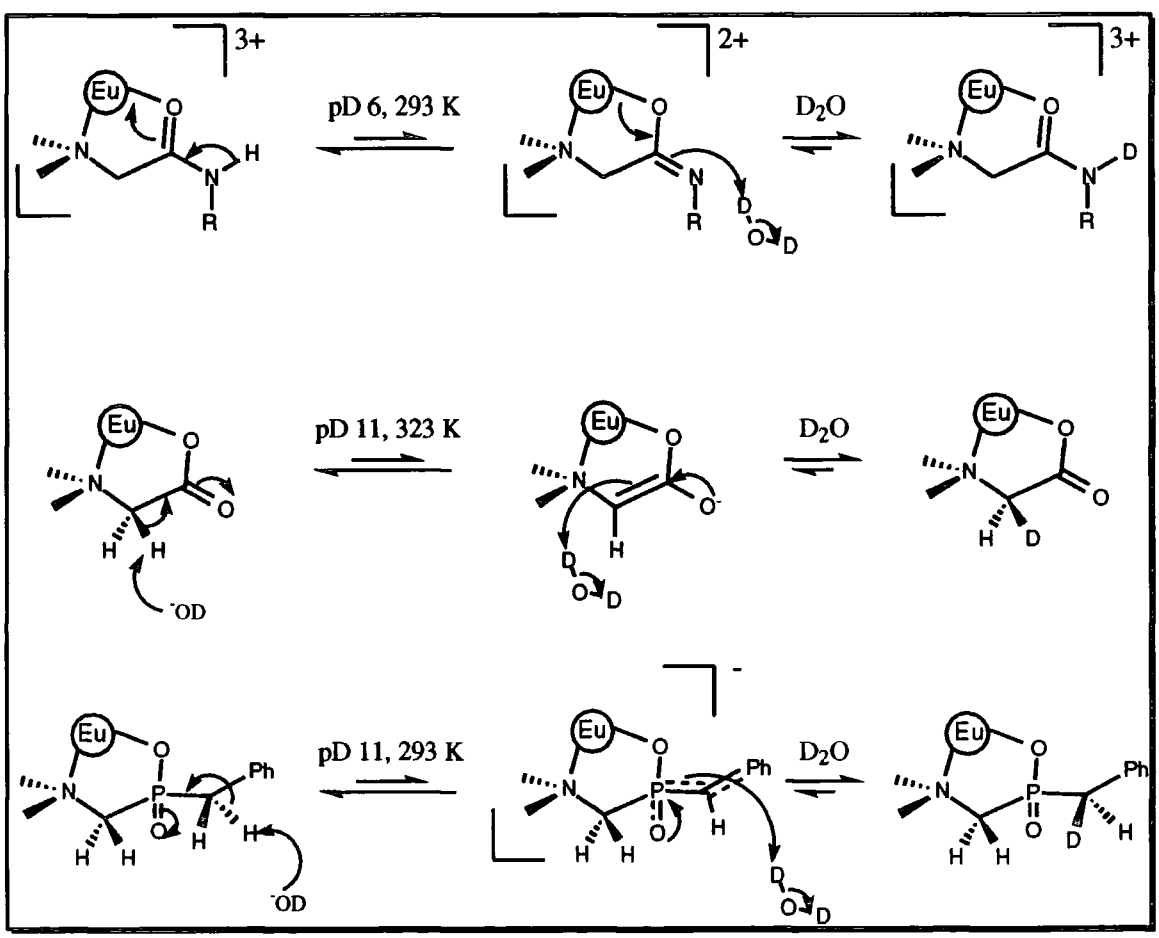

Scheme 2.3. *Possible H/D exchange mechanisms.*

CH Oscillator quenching

The methylene acetate protons of **(Eu.7)**$^{-}$ were exchanged for deuterium following heating at 323 K at pD 11 (KOD) in D_2O for 18 hours. ^1H NMR analysis of the residual diastereotopic C-H resonances at δ -16.4 and -18.1 (293 K, pD 6) and analysis of the isotope pattern of the negative ion electrospray mass spectrum revealed that 90 (2) % deuterium incorporation had occurred corresponding to 7.2 out of the 8 protons having undergone deuterium exchange. **Scheme 2.3** depicts a possible mechanism for the exchange.

H/D Exchange of the benzylic protons of **(Eu.2b)**$^{-}$ was achieved by heating the corresponding ethyl ester of **(2b)** with CD_3OD and CD_3ONa at room temperature for 24 hours. Subsequent ester hydrolysis by treatment with DCl followed by complexation with europium acetate (D_2O, pD 6, reflux) yielded **(Eu.2b)**$^{-}$ with 7 out of the 8 benzylic hydrogens exchanged with deuterium. This 87 (3) % incorporation was assessed by observing the residual diastereotopic CH resonances at δ -1.0 and -2.4 (293 K, pD 6) and by negative ion ESMS. H/D Exchange occurred at the benzylic position as opposed to the N-methylene position due to the extra resonance stabilisation of the intermediate anion promoted by the neighbouring phenyl ring (**Scheme 2.3**).

By comparison of the k values in H_2O and D_2O for **(Eu.7)**$^{-}$ and **(Eu.2b)**$^{-}$ and their deuterium exchanged forms, **(Eu.[$^2H_7$]-7)**$^{-}$ and **(Eu.[$^2H_7$]-2b)**$^{-}$ respectively, the contribution due to CH oscillators may be assessed. On H/D exchange the k values in H_2O or D_2O for **(Eu.7)**$^{-}$ and **(Eu.[$^2H_7$]-7)**$^{-}$ decreased by ~0.18 $(ms)^{-1}$. This decrease is due to the exchange of 7 CH bonds for 7 CD bonds therefore each CH oscillator contributes ~0.18 / 7 = 26 s^{-1} to Δk. A similar analysis on **(Eu.2b)**$^{-}$ and **(Eu.[$^2H_7$]-2b)**$^{-}$ suggests that each CH oscillator contributes ~5 s^{-1} to Δk. The distance between the oscillator and the europium centre, r, will determine the quenching ability and will have a $1/r^6$ dependence. Therefore the smaller effect observed on deuteration of **(Eu.2b)**$^{-}$ compared to **(Eu.7)**$^{-}$ can be attributed to the greater distance between the CH oscillators and the metal. Crystallographic data show that the distance between the methylene

CH_2 and the metal centre in **(Eu.7)**$^-$ is 3.5 Å [4], whereas in **(Eu.2b)**$^-$ the distance between the benzylic CH_2 and the metal is 4.1 Å.[20]

The effect of NH/ND exchange on the monoamidotriphosphinate complexes **(Eu.1e)** and **(Eu.1d)** can be analysed by comparison to **(Eu.1a)** and **(Eu.1b)**. The complex **(Eu.1a)**, which contains no NH bonds, gives rise to a contribution to Δk from bound and closely diffusing water molecules of 340 s^{-1}. Introduction of one NH group as in **(Eu.1b)** increases the Δk value by 0.1 $(ms)^{-1}$. The contribution due to NH oscillators in **(Eu.1a)**, **(Eu.1e)** and **(Eu.1d)** are expected to be similar and therefore the difference in Δk will be due to the varying distance of closest approach of water molecules to the europium ion in the complexes. The larger Δk value observed for **(Eu.1d)** compared to **(Eu.1e)** is consistent with the more hydrophobic nature of the **(Eu.1e)** complex, which limits the approach of water to the ion resulting in a decreased quenching ability. The approach of a water molecule is less sterically hindered in **(Eu.1d)** compared to **(Eu.1b)** as the large phenyl group α to the amide NH may be directed away from the coordination cage, therefore accounting for the lower Δk value for the latter complex. Although the naphthyl group may also be directed outside the coordination cage, it is a bulkier group and hinders the approach of a water molecule, hence it displays a Δk value comparable to **(Eu.1b)**.

Summary

In order to achieve a more accurate estimation of the hydration state, q, of a complex, the quenching role of closely diffusing water, NH and CH oscillators must also be considered.[21]

The apparent non integral q values observed for the monoamidotriphosphinate complexes **(Eu.1d)** and **(Eu.1e)** suggest partial hydration of the europium ion. This is consistent with the longer than usual distance of closest approach of a water molecule to the lanthanide ion, determined by relaxivity measurements on the corresponding gadolinium complexes, as discussed in Chapter 2.3.

The Δk values observed for the terbium complexes are smaller than their europium analogues. This may be due, in part, to the larger energy gap for Tb^{3+} which restricts the deactivation pathways available for the excited state. As the Tb^{3+} emissive state is higher in energy than the Eu^{3+} emissive state, the matched vibrational energy levels of XH oscillators will be of higher energy where the Frank-Condon overlap is poor and hence the non-radiative processes are less efficient. The apparent q values for terbium complexes will therefore be lower than their europium analogues. For terbium complexes of monoamidotriphosphinates, however, the q values are substantially lower than expected. This cannot be attributed to deactivation by NH oscillators alone, as a much reduced q value is observed with **(Tb.1a)** where there are no NH bonds present. It therefore appears that the deactivation by water in europium complexes of this type is much greater than in the terbium complexes. The greater ionic radius of Eu^{3+} (94.7 pm) compared to Tb^{3+} (92.3 pm), which allows the water molecule to approach more closely, superimposed onto the greater OH deactivation effect for Eu^{3+} could account for this difference. Indeed, Eu^{3+} complexes are found to be more hydrated than Tb^{3+} complexes as a direct consequence of the lanthanide contraction which sometimes gives rise to an apparent change in the coordination in the solution hydration number halfway along the lanthanide series at gadolinium, "the gadolinium break".[22] It has been suggested that a 9 coordinate tricapped trigonal prismatic geometry for the larger lanthanide ions and their complexes may switch to a more compact 8 coordinate square antiprismatic geometry around gadolinium.[22]

2.5 Circularly polarised luminescence

The chiroptical technique of circularly polarised luminescence (CPL) has been utilised to probe the chiral ligand environment about the lanthanide ion. Professor J. Riehl and coworkers at Michigan Technological University have examined the CPL exhibited by the terbium complexes **(Tb.1d)** and **(Tb.1e)**. **Figure 2.11 (a)** shows the total emission spectrum and also the total emission spectrum (lower trace) and CPL spectrum (upper trace) for the $^5D_4 \longrightarrow {}^7F_5$ **(b)**, $^7F_4$ **(c)** and $^7F_3$ **(d)** transitions for **(Tb.1d)**.

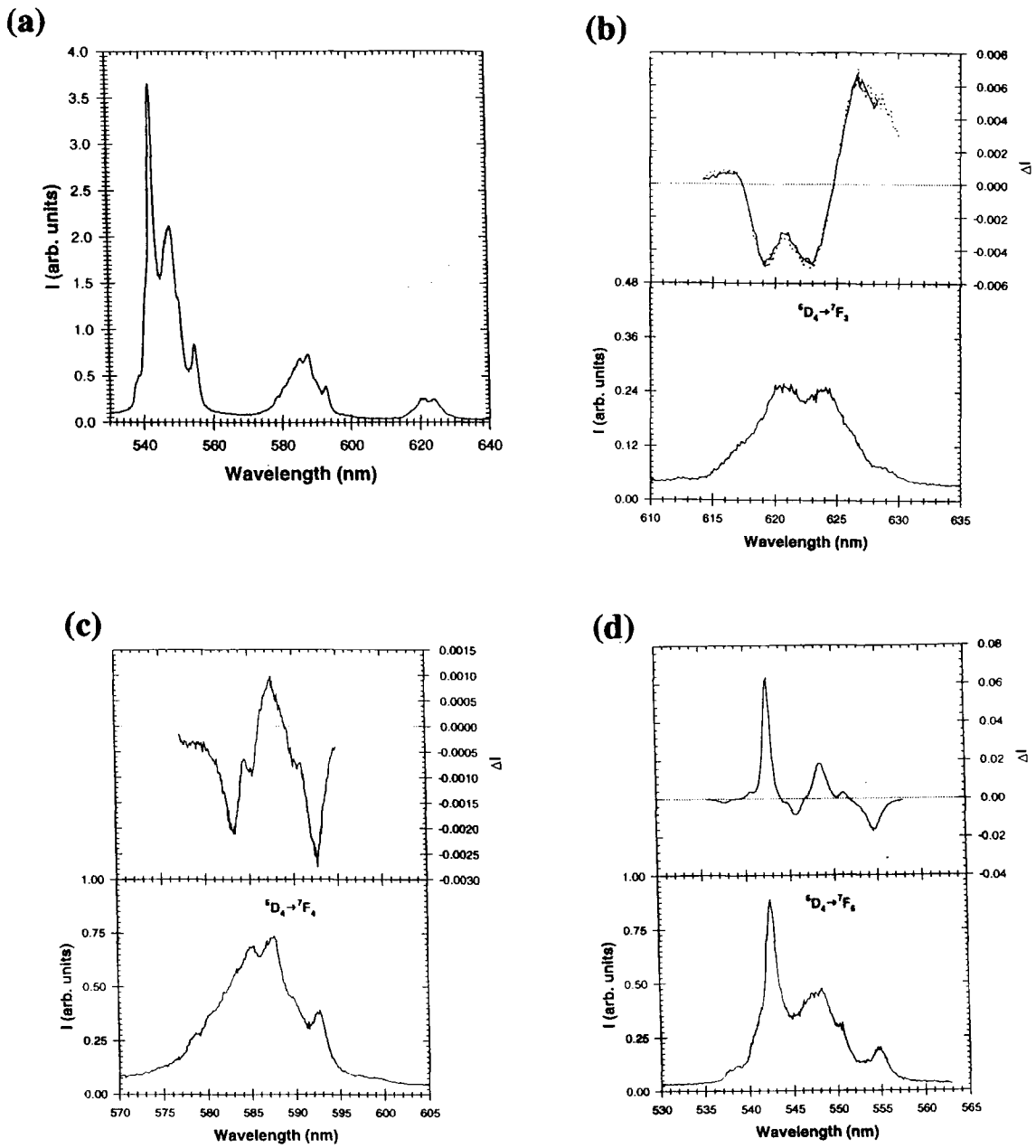

Figure 2.11 *(a) Total emission spectrum for (**Tb.1d**). Total emission spectrum (lower trace) and CPL spectrum (upper trace) for the ΔJ = 1 (**b**), ΔJ = 0 (**c**), ΔJ = -1 (**d**) transitions of (**Tb.1d**) in aqueous solution following excitation at 488 nm (298 K).*

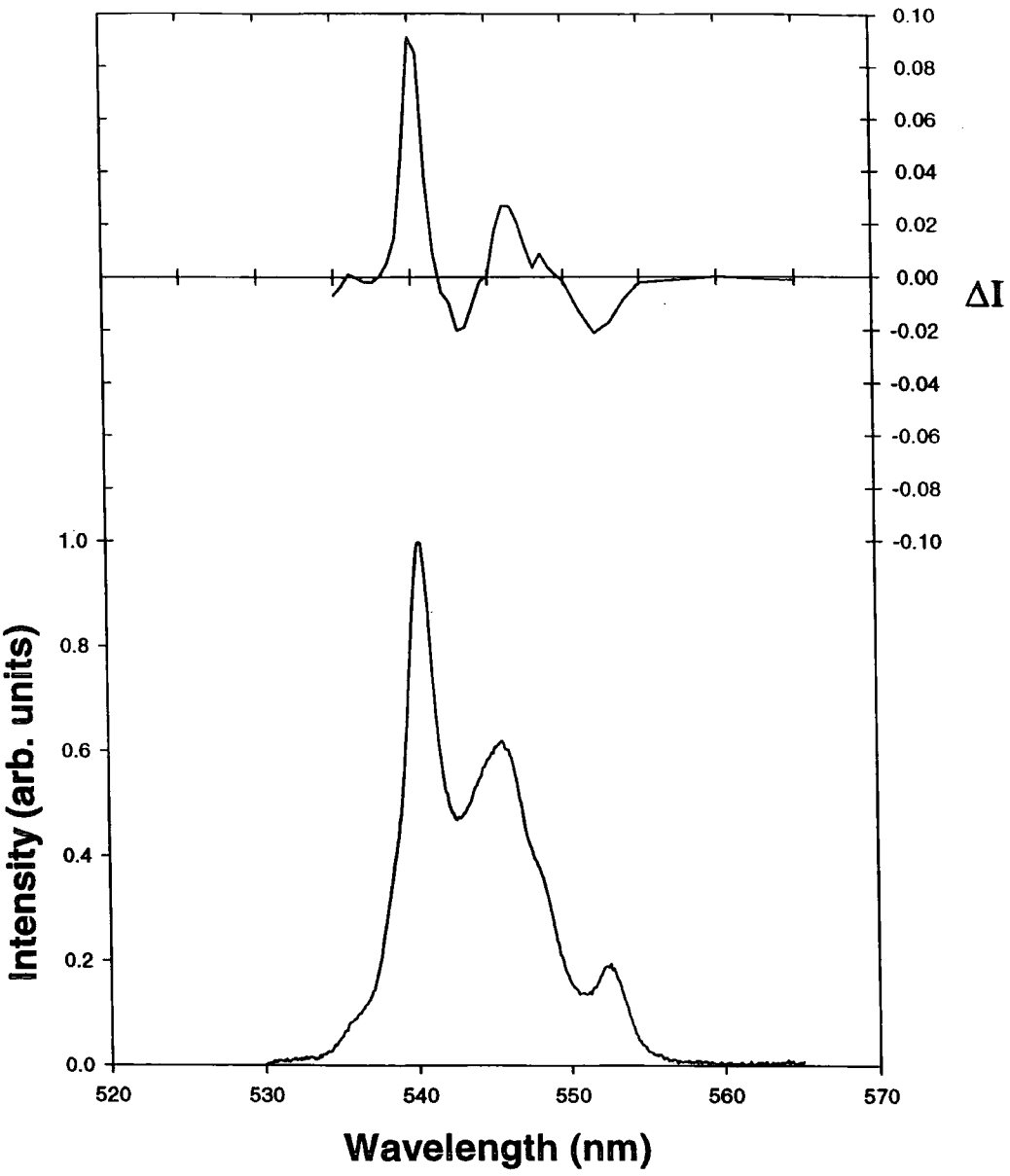

Figure 2.12 *Total emission spectrum (lower trace) and CPL spectrum (upper trace) for* ***(Tb.1e)*** *in aqueous solution for the* $\Delta J = 1$ *transition following u.v. excitation (298 K).*

CPL was observed following direct excitation of the terbium $^7F_6 \longrightarrow {}^5D_4$ transition using an argon ion laser (λ_{ex} = 488 nm). The CPL is relatively strong for the $^5D_4 \longrightarrow {}^7F_5$ transition with a value of the emission dissymmetry factor of $g_{em}{}^{\lambda\,543}$ = 0.17. Weaker CPL was also observed for the $^5D_4 \longrightarrow {}^7F_4$ and $^7F_3$ transitions with corresponding emission dissymmetry factors of $g_{em}{}^{\lambda\,584}$ = -0.06 and $g_{em}{}^{\lambda\,621}$ = -0.12 respectively.

Due to the complex nature of the terbium transitions as discussed in Chapter 1.5. no structural information may be ascertained from the spectra. However, the spectra do show that the environment around the metal ion in its excited state is indeed chiral! In **Figure 2.11 (b)**, the CPL was obtained following excitation with left circularly polarised light (solid line) and right circularly polarised light (dotted line). The two spectra appear identical. Considering a chiral species in solution, there will be preferential absorption of right or left circularly polarised light on excitation. However, the CPL spectra will be independent of the handedness of the excitation source used as on absorption of right or left circularly polarised light by the lanthanide ion the same metal-based excited state is formed, which can then undergo emission. It is only the nature of the chiral environment around the metal that will determine the sign and magnitude of the CPL.

Strong CPL was exhibited by **(Tb.1e)** following sensitised emission by u.v. excitation (λ_{ex} = 300 nm) into the proximate naphthyl chromophore. The solutions were degassed prior to measurement to eliminate the efficient deactivation pathway of the excited state via back energy transfer to the naphthyl triplet state and subsequent quenching by molecular oxygen. **Figure 2.12** shows the total emission (lower trace) and the CPL (upper trace) for the $^5D_4 \longrightarrow {}^7F_5$ transition for which a dissymmetry factor of $g_{em}{}^{\lambda\,540}$ = 0.18 was calculated. The CPL spectrum is remarkably similar to that of the $^5D_4 \longrightarrow {}^7F_5$ transition for **(Tb.1d)**. This is not at all surprising since the complexes only differ in the substituent at the remote amide pendent arm, the environment around the metal ion being identical in every respect.

CPL has been observed from racemic mixtures following excitation by circularly polarised light.[23,24] Circularly polarised excitation preferentially excites one enantiomer over the other, giving rise to an excess of this enantiomer in the excited state, so that net circularly polarised emission is observed. Excitation of the racemic tetrabenzylphosphinate analogue, **(Tb.2b)**$^-$, with right circularly polarised light gave an exact mirror image CPL spectrum to that obtained from excitation with left circularly polarised light.[13,25] On excitation with right or left circularly polarised light one enantiomer is excited preferentially and undergoes circularly polarised emission as if there were an excess of this enantiomer in solution. The CPL spectra obtained following excitation by right and left circularly polarised light correspond to the two enantiomers and will therefore be equal and opposite.

^{1}H NMR studies on the corresponding europium complexes reveal that two diastereoisomers exist in solution in a ratio of 2:1 for **(Eu.1d)** and 4:1 for **(Eu.1e)**. By comparing the g_{em} values for **(Tb.1d)** and **(Tb.1e)** information may be ascertained on the relative structures of the two diastereoisomers present in each complex. If the diastereoisomers have identical ring conformations and the same layout of the pendent arms then the observed CPL will be due to contributions from both isomers. However, if the two diastereoisomers have enantiomeric ring conformations and pendent arm helicities then equal and opposite CPL spectra will be observed for each isomer. The CPL from the major isomer would cancel out the contribution to the CPL from the minor isomer so the observed CPL is a result of the diastereoisomer in excess. As the ratio of the major to minor isomer is greater for **(Tb.1e)** (4:1 compared to 2:1 for **(Tb.1d)**) then a larger g_{em} value is expected. The fact that the dissymmetry values are so similar for **(Tb.1d)** and **(Tb.1e)** suggests that the two diastereoisomers in solution have the same macrocyclic ring conformation and pendent arm helicities differing only in the configuration at the remote P centres. This is consistent with the NMR data discussed in Chapter 2.3.

2.6 Resolution

In complexes of **(1d)** and **(1e)**, NMR and luminescence studies suggest that the remote chiral amide pendent arm dictates the handedness of the layout of the phosphinate arms and determines the macrocyclic ring conformation. This results in the formation of 2 diastereoisomers, differing only in the configuration at P, in a ratio which is dependent on the size of the remote chiral group. The larger naphthyl group acts as a better chiral auxiliary than phenyl and therefore has a greater influence on the configuration at the P centre.

Separation of the two diastereoisomers of **(1e)** was attempted using chiral HPLC. Since the diastereoisomers possess aromatic groups, a semi-preparative chiral cyclodextrin column was chosen in the hope that the naphthyl groups would bind into the cyclodextrin cavity to different extents to allow separation. Indeed, the two diastereoisomers were shown to separate analytically and a band ratio of 4:1 was observed (flow rate = 1.4 cm^3 min^{-1}; T = 275 K; t = 0 min, 95% H_2O, 5% MeOH; t = 25 min, 100% MeOH, end time). However, the two bands were very close together and alteration of solvent, temperature and flow rates failed to achieve any preparative separation.

References for Chapter 2

1. S. Aime, M. Botta. D. Parker and J.A.G. Williams, *J. Chem. Soc., Dalton Trans.*, 1995, 2259.
2. K.P. Pulukkody, T.J. Norman, D. Parker, L. Royle and C.J. Broan, *J. Chem. Soc., Perkin Trans. 2*, 1993, 605.
3. J.-J. Yaouanc, N. Le Bris, G. Le Gall, J.-C. Clement, H. Handel and H. des Abbayes, *J. Chem. Soc., Chem. Commun.*, 1991, 206.
4. S. Aime, A. Batsanov, M. Botta, J.A.K. Howard, D. Parker, K. Senanayake and G. Williams, *Inorg. Chem.*, 1994, **33**, 4696.

5. T.J. Swift in 'NMR of Paramagnetic Molecules : Principles and Applications' eds., G.N. LaMar, W.De W. Horrocks, Jr. and T.H. Holm, Academic Press, 1973, London.

6. X. Wang, T. Jin, V. Comblin, A. Lopez-Mut, E. Merciny and J.F. Desreux, *Inorg. Chem.*, 1992, **31**, 1095.

7. S. Aime, M. Botta, D. Parker and J.A.G. Williams, *J. Chem. Soc., Dalton Trans.*, 1996, 17.

8. S. Aime, M. Botta, M. Grandi, M. Panero and F. Uggeri, *Magn. Reson. Chem.*, 1991, **29**, 923.

9. K.A. Connors in ' Comprehensive Supramolecular Chemistry', eds., J.L. Atwood, J.E.D. Davies, D.D. Macnicol, F. Vögtle and J.-M. Lehn, Pergamon, Oxford, 1996, vol. 3, Chapter 6.

10. J.-C.G. Bünzli in 'Lanthanide Probes in Life, Chemical and Earth Sciences', eds., J.-C.G. Bünzli and G.R. Choppin, Elsevier, Amsterdam, 1989, Chapter 7.

11. C.C. Bryden and C.N. Reilly, *Anal. Chem.*, 1982, **54**, 610.

12. D.H. Metcalf, R.G. Ghirardelli and R.A. Palmer, *Inorg. Chem.*, 1985, **24**, 634; 1986, **25**, 2175.

13. D. Parker and J.A.G. Williams, *J. Chem. Soc., Dalton Trans.*, 1996, 3613.

14. Y. Haas and G. Stein, *J. Phys. Chem.*, 1971, **75**, 3668.

15. A. Beeby, D. Parker and J.A.G. Williams, *J. Chem. Soc., Perkin Trans. 2*, 1996, 1565.

16. B. Alpha, R. Ballardini, V. Balzani, J.-M. Lehn, S. Perathonor and N. Sabbatini, *Photochem. Photobiol.*, 1990, **52**, 299.

17. S. Aime, D.A. Voss, W.De W. Horrocks, Jr., C.H. Lake, M.R. Churchill and J.R. Morrow, *Inorg. Chem.*, 1995, **34**, 3294.

18. M. Spirlet, J. Rebizant and J.F. Desreux, *Inorg. Chem.*, 1984, **23**, 359.

19. D. Parker and J.A.G. Williams, *J. Chem. Soc., Perkin Trans. 2*, 1995, 1305.

20. S. Aime, A.S. Batsanov, M. Botta, R.S. Dickins, S. Faulkner, C.E. Foster, J.A.K. Howard, J. Moloney, T.J. Norman, D. Parker, L. Royle and J.A.G. Williams, *J. Chem. Soc., Dalton Trans.*, October, 1997.

21. R.S. Dickins, D. Parker, A.S. de Sousa and J.A.G. Williams, *J. Chem. Soc., Chem. Commun.*, 1996, 697.

22. D.T. Richens,' The Chemistry of Aqua Ions', Wiley, Chichester, 1997, Chapter 3.

23. G.L. Hilmes and J.P. Riehl, *J. Chem. Phys.*, 1983, **87**, 3300.

24. D.H. Metcalf, S.W. Snyder, J.N. DeMar and F.S. Richardson, *J. Am. Chem. Soc.*, 1990, **112**, 469; 1990, **112**, 5681.

25. E. Huskowska, C.L. Maupin, D. Parker, J.P. Riehl and J.A.G. Williams, *Enantiomer*, 1997, **1**, in press.

CHAPTER 3

CATIONIC LANTHANIDE COMPLEXES OF TETRA-, TRI- AND DI-AMIDE TETRAAZAMACROCYLES

CHAPTER 3

CATIONIC LANTHANIDE COMPLEXES OF TETRA-, TRI- AND DI-AMIDE TETRAAZAMACROCYCLES

3.1 Introduction

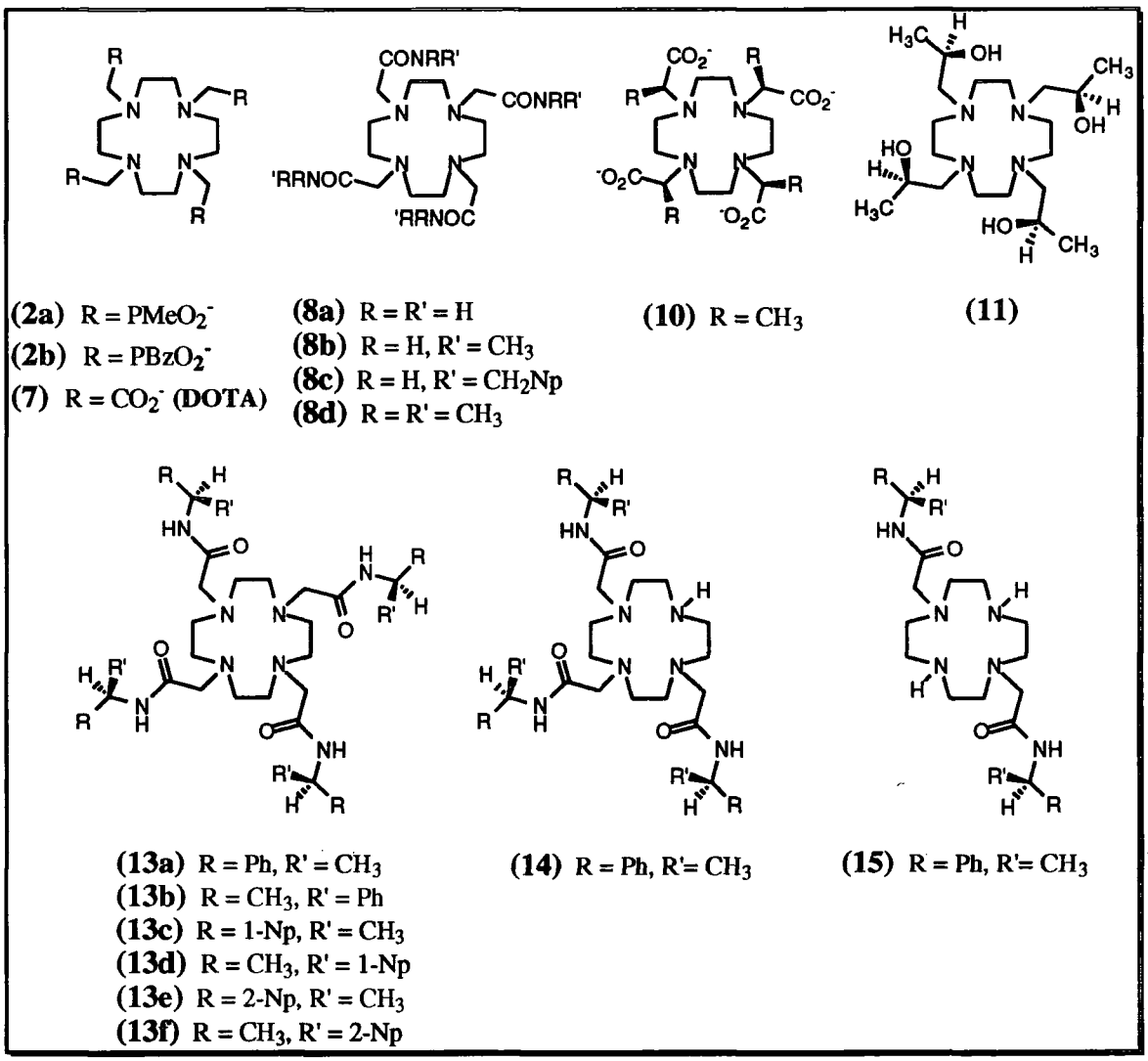

Figure 3.1 *Lanthanide complexes discussed in this chapter.*

As discussed in Chapter 1.2, there are two enantiomeric pairs of diastereoisomers for lanthanide DOTA **(Ln.7)**$^-$ complexes in solution which undergo exchange at room temperature.[1,2] The introduction of a chiral centre α to the macrocyclic ring nitrogen, as in system **(10)** of Desreux and Brittain, will render each of these enantiomeric pairs

diastereomeric, giving rise to four possible isomers in solution, all distinguishable by NMR analysis. Solution state NMR studies reveal the existence of two of these diastereoisomers in a ratio which is dependent on the size of the R group and the nature of the lanthanide ion.[3] The introduction of the chiral centre imparts extra thermodynamic stability and rigidity to the complexes and the isomers are found to be conformationally rigid on the NMR timescale in the range 273-373 K.[3,4]

The introduction of a chiral centre β to the macrocyclic ring nitrogen **(11)**, was shown by Morrow[5] to increase macrocyclic rigidity and resistance to dissociation, resulting in the formation of a single diastereoisomer in solution out of the four possibilities. Similar enhancements in complex rigidity are also demonstrated by the tetraphosphinate complexes of **(2a)** and **(2b)**, as discussed in Chapter 1.2, which have a chiral phosphorus centre β to the macrocyclic ring nitrogen.[6]

The more polarisable amide oxygen is a better donor for lanthanide ions than an alcohol oxygen such as **(11)**. Recent research within the group at Durham has focussed on the use of tetraamide tetraazamacrocycles **(8)**, as ligands for lanthanide ions.[7,8] Such lanthanide complexes are kinetically stable with respect to dissociation and complexes of **(8a)** have been found to be as inert to lanthanide ion dissociation as **(Gd.DOTA)**$^-$ **(Gd.7)**$^-$.[9] As with DOTA complexes, there are two structurally independent elements of chirality associated with such systems. There are two possible ring conformations, related through an inversion axis, and two orientations of the pendent arms, in a clockwise or anticlockwise fashion (**Figure 1.2**, Chapter 1.2). This gives rise to four possible diastereoisomers existing as two enantiomeric pairs. In solution, all four diastereoisomers are present for lanthanide complexes of **(8a)**[9] whereas europium complexes of **(8b)** have been shown to exist in solution as a single chiral diastereoisomer.[8]

In the search for an enantiopure complex that is conformationally rigid on the NMR timescale and lifetime of the metal based emission, lanthanide complexes based on

(13), **(14)** and **(15)** have been synthesised in the expectation that the remote chiral centre will lead to the preferential formation of one rigid diastereoisomer out of the four possibilities. The presence of the chiral centre renders the enantiomeric pairs diastereomeric, therefore all four diastereoisomers in principle, may be distinguished by NMR analysis.

3.2 Synthesis

The complexes were prepared according to **Scheme 3.1.**

Tetraalkylation of $12N_4$ was achieved by reaction with 5 equivalents of the chiral chloroamide, (itself formed by reacting the appropriate chiral amine with chloroacetylchloride at -20 °C), in the presence of 5 equivalents of potassium carbonate in dry *N,N*-dimethylformamide at 60 °C for 48 hours. The product was purified by recrystallisation from acetonitrile following column chromatography on neutral alumina.

Several routes to isolate the triamide derivative were attempted. The first strategy was to use the molybdenum protection of 3 nitrogens on the $12N_4$ ring, discussed in Chapter 2.2, to allow selective functionalisation of one of the ring nitrogens with a moiety that could easily be removed once the 3 amide groups were attached. The allyl group was chosen for such a purpose. However, reaction of allylbromide with the molybdenum tricarbonyl $12N_4$ complex in dry *N,N*-dimethylformamide at a variety of temperatures (-20 °C to 60 °C) yielded only a trans diallyl ring product. Monotosylation of the ring was then attempted by reacting the molybdenum tricarbonyl $12N_4$ complex **(16)** with tosylchloride at room temperature for 24 hours. Decomplexation of the molybdenum moiety in aqueous acid yielded the required product, although in rather poor yield. The three amide groups were then attached by reaction of the monotosylated ring with 4 equivalents of the appropriate chiral chloroamide and potassium carbonate in dry *N,N*-dimethylformamide at 60 °C for 18 h. Purification by column chromatography gave the required product. However, detosylation by Birch reduction using sodium and

liquid ammonia in dry tetrahydrofuran and ethanol at -78 °C resulted in a mixture of di- and trialkylated ring products in very poor yield. The reaction scheme was repeated using the p-methoxy-tosylchloride derivative as this moiety will be more readily cleaved under acidic conditions (eg. HBr / AcOH / PhOH, -50 °C) than the corresponding tosyl group. However, the monotosylation step was very low yielding. The less reactive p-methoxy-tosylimidazole was then chosen for reaction with the molybdenum protected $12N_4$ ring. Only unreacted $12N_4$ was isolated and the route was therefore abandoned.

A successful route to the trialkylated product was achieved by reaction of $12N_4$ with 3 equivalents of the appropriate α-chloroamide, added over 8 hours, in the presence of triethylamine in dry ethanol at 80 °C for 18 hours. Evaporation of the solvent, extraction into aqueous hydrochloric acid and subsequent washing with diethyl ether removed any residual α-chloroamide. Positive ion ESMS revealed the presence of tetra- (5%), tri- (80%) and di- (15%) alkylated products which were carefully separated by column chromatography on neutral alumina.

The trans dialkylated $12N_4$ ring product was isolated in an analagous reaction using 2 equivalents of the chiral chloroamide.

Complexation of tetra-, tri- and di- ligands was achieved by heating the appropriate lanthanide triflate with trimethylorthoformate in dry acetonitrile for 2 hours at reflux temperature followed by the addition of the ligand and further heating for 18 hours. The complexes were purified by recrystallisation from acetonitrile and gave satisfactory NMR and accurate mass data consistent with the proposed structures.

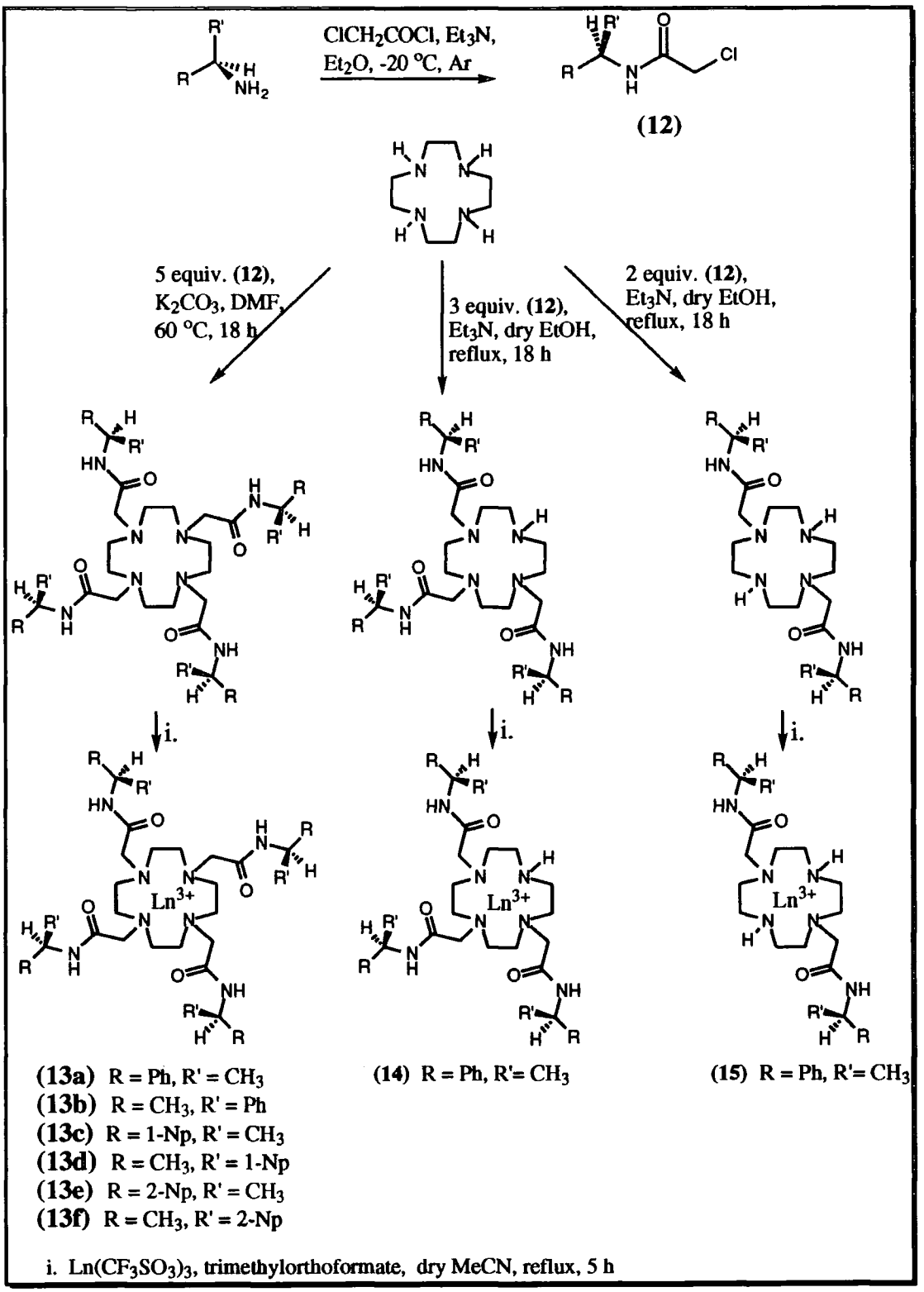

Scheme 3.1 *Procedures for the synthesis of tetra-, tri- and diamide tetraazamacrocyclic complexes.*

3.3 NMR analysis

3.3.1 Tetraamides

Representative ^1H NMR spectra (250 MHz, CD_3OD, 298 K) for various lanthanide complexes of the tetraphenyl derivative **(13a)** are shown in **Figure 3.2**. Immediately obvious is the presence of a single C_4 symmetric complex, suggesting a square antiprismatic geometry. The complex was found to be conformationally rigid on the NMR timescale, showing no exchange broadening in the temperature range 193-320 K (400 MHz, CD_3OD). The spectra observed at low temperatures (233-193 K) do exhibit some degree of line broadening compared to those at higher temperatures but this is due to the temperature dependent paramagnetism of the lanthanide. Better resolved spectra are generally obtained at higher temperature for such paramagnetic complexes.[10]

In the Pr^{3+} and Dy^{3+} complexes of **(13a)** the resonance of the axial proton that is directed towards the lanthanide ion is shifted to lower frequency (δ -43.0 and -387 ppm respectively) whereas in the Eu^{3+} and Yb^{3+} complexes the opposite effect is found, with the resonance shifted to higher frequency (δ 27.5 and 102 ppm respectively). Complexes of Eu^{3+}, Pr^{3+} and Yb^{3+} have minimal line broadening effects on the resonances ($\omega_{1/2}$ ca. 2 Hz), whereas in the complex with Dy^{3+} the resonances were broadened considerably. Such behaviour is consistent with the measured half-height widths for the methyl resonance of 2-picoline in the presence of the appropriate tri(dipivaloylmethane) complex of the lanthanide ion. Linewidths of 5.6, 4.4, 12.0 and 200 ppm were reported for Pr^{3+}, Eu^{3+}, Yb^{3+} and Dy^{3+} respectively.[11]

Analogous spectra were obtained for lanthanide complexes of the tetranaphthyl derivatives **(13c)**, **(13d)**, **(13e)** and **(13f)**, consistent with the formation of a single rigid diastereoisomer in solution.

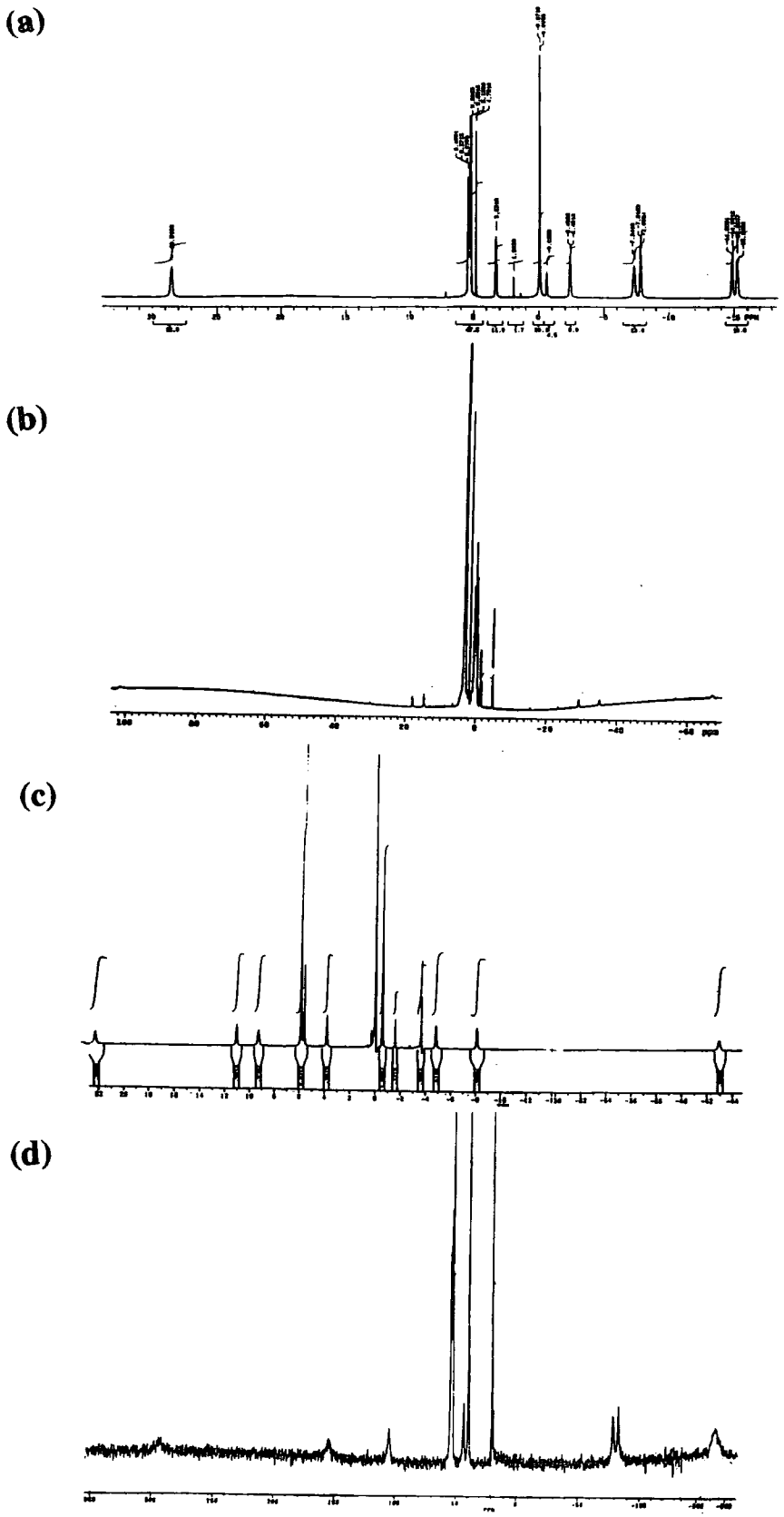

Figure 3.2. ^{1}H spectra for **(a)** $(Eu.13a)^{3+}$, **(b)** $(Yb.13a)^{3+}$, **(c)** $(Pr.13a)^{3+}$ and **(d)** $(Dy.13a)^{3+}$ (250 MHz, CD_3OD, 298 K).

3.3.2 Triamides

The lack of rotational symmetry for complexes of **(14)** means that each ring proton will be in a different chemical environment and will therefore resonate at a different frequency in the ^1H NMR spectrum. Four of the axial ring protons will be directed towards the lanthanide ion, and in the case of Eu^{3+}, will be greatly shifted to higher frequency. Variable temperature ^1H NMR studies in the range 193-333 K on $(\mathbf{Eu.14})^{3+}$ (400 MHz, CD_3OD) suggested that the complex exists as 2 isomers in solution, in a 1:1 ratio. At low temperature (193 K) ten distinct resonances are apparent in the high frequency range (46.5, 44.1, 31.0, 27.5, 27.1, 21.5, 21.4, 13.9, 13.4, 12.7 ppm) corresponding to the four axial ring protons directed towards the metal centre, plus another ring proton in each of the diastereoisomers. As the temperature was increased, the resonances broaded and coalesced with T_c = 273 K. Five distinct resonances (26.4, 16.6, 14.1, 10.1, 9.9 ppm) were observed at temperatures above 293 K. From this coalescence temperature, T_c, it is possible to calculate the free energy of activation, $\Delta G^{\dagger}$, for the exchange process using equation **(3.1)**[12],where δ_ν is the frequency separation of the initially sharp lines.

$$\Delta G^{\dagger} = R\ T_c\ [\ 22.96 + \ln\ (T_c / \delta_\nu)\ ] \qquad \textbf{(3.1)}$$

However, the position of the resonances of $(\mathbf{Eu.14})^{3+}$ are temperature dependent and an average limiting δ_ν value (chosen to be 800 Hz) allows only an estimated value of $\Delta G^{\dagger}$ = 50(±1) kJ mol^{-1} to be determined. The exchange process occurring in the europium complex of DOTA, $(\mathbf{Eu.7})^-$, was shown to have an energy barrier[2] of $\Delta G^{\dagger}$ = 60.7 kJ mol^{-1}.

The two observed isomers are clearly in exchange at room temperature through either a concerted rotation of the pendent arms, a ring inversion or indeed some synchronous motion combining the two. There are four possible diastereoisomers for complexes of **(14)** as discussed in Chapter 3.1 and it is not possible to identify easily from NMR those which are present in solution. The diastereoisomers present in solution will

depend on the nature and relative position of the chiral centre with respect to the macrocyclic ring. In complexes of the tetrasubstituted ligand of **(10)** and the trisubstituted analogue of **(10)**, in which the chiral centre is α to the macrocyclic ring nitrogen, there are two diastereoisomers present. Crystallographic data on the gadolinium complex of the trisubstituted analogue of **(10)**, reported by Tweedle[4], show that the two diastereoisomers have enantiomeric ring conformations whilst the pendent arms are rotated in the same sense. It is tempting to speculate that the chiral triamide complexes reported here will behave analogously, with the pendent arms rotated in the same sense. However, Morrow[5] showed that the chiral europium complex of (SSSS)-**(11)**, formed from reaction of *S*-propylene oxide with $12N_4$, introduced a chiral centre β to the macrocyclic ring nitrogen and led to the formation of one rigid diastereoisomer, as deduced by ^1H NMR. However, X-ray studies on single crystals of the europium complex of **(11)**, (RSSS and SRRR with respect to the chiral C centre), obtained from a synthesis using racemic propylene oxide and $12N_4$, showed the presence of two diastereoisomers in the asymmetric unit cell that have identical macrocyclic ring conformations but differ in the helicity of the pendent arms.

Clearly, X-ray studies on complexes of **(14)** would be invaluable in determining which of the diastereoisomers are present in the solid state, but of course this information can not be correlated directly to solution state structures, although 2D-EXSY solution NMR analysis may reveal the nature of the exchange process.

3.3.3 Diamides

^1H and ^{13}C NMR data for ligand **(15)** were consistent with the formation of only the trans dialkylated ring product. The ^1H NMR spectrum of **(Eu.15)**$^{3+}$ shows that the complex does not possess C_2 symmetry as two peaks were observed for the CH and CH_3 resonances and there were four distinct resonances for the diastereotopic CH_2CO protons. This is also consistent with the presence of 2 carbonyl peaks in the infra-red spectra of complexes of **(15)**. Indeed, by comparison of the chemical shift of the most shifted axial ring proton for **(Eu.15)**$^{3+}$ (δ 16.9) with respect to **(Eu.13a)**$^{3+}$ (δ 28.5) and

(Eu.14)$^{3+}$ (δ 26.6), it is possible that the complex adopts a different structure in solution. As ligand **(15)** only provides six coordination sites for the lanthanide ion, the other three available positions will be occupied by water molecules, and a more open structure will result. In this case, the less compacted tricapped trigonal prismatic geometry may be favoured over the square antiprismatic geometry suggested for complexes of **(13)** and **(14)**. Examples of tricapped trigonal prismatic coordination geometries are well known in lanthanide complexation chemistry, particularly with ligands that are not sterically demanding (eg. DTPA complexes).

3.4. Structural analysis

Crystals suitable for X-ray analysis were obtained from the recrystallisation of the complexes from acetonitrile.

3.4.1 Crystal structures of complexes of the tetraphenylamides (13a) and (13b)

The europium complex **(Eu.13a)**$^{3+}$ crystallises in the chiral space group $P2_12_12_1$ with four molecules in the unit cell. The crystallographic asymmetric unit consists of one europium complex, four trifluoroacetate counterions and a hydronium ion. The corresponding enantiomeric europium complex **(Eu.13b)**$^{3+}$ also crystallises in the $P2_12_12_1$ chiral space group with four molecules in the unit cell but exhibits different packing interactions. The asymmetric unit is also different comprising of one europium complex, three triflate anions, nine waters of recrystallisation and an acetonitrile molecule of solvation. The dysprosium complex **(Dy.13b)**$^{3+}$ is isostructural with the europium complex **(Eu.13b)**$^{3+}$ and displays the same unit cell dimensions and packing interactions. There is one dysprosium complex, three triflate anions, one water molecule and two acetonitrile molecules of solvation in the asymmetric unit cell. A full list of coordinates are provided in **Appendices 4**, **5** and **6** for **(Eu.13a)**$^{3+}$, **(Eu.13b)**$^{3+}$ and **(Dy.13b)**$^{3+}$ respectively.

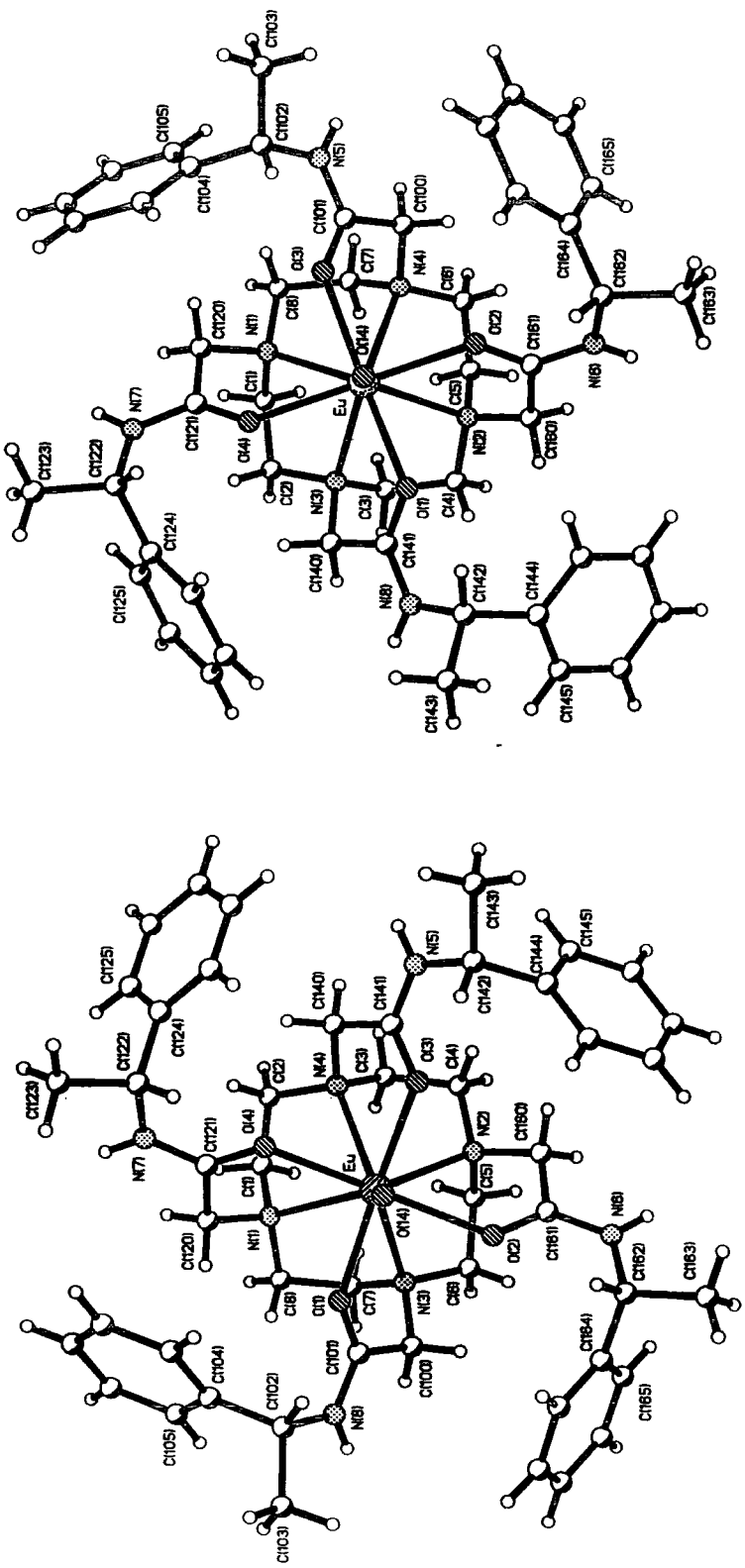

Figure 3.3 *Crystal structures of the enantiomeric complexes* ***(Eu.13a)***$^{3+}$ *and* ***(Eu.13b)***$^{3+}$ *viewed down the* C_4 *axis.*

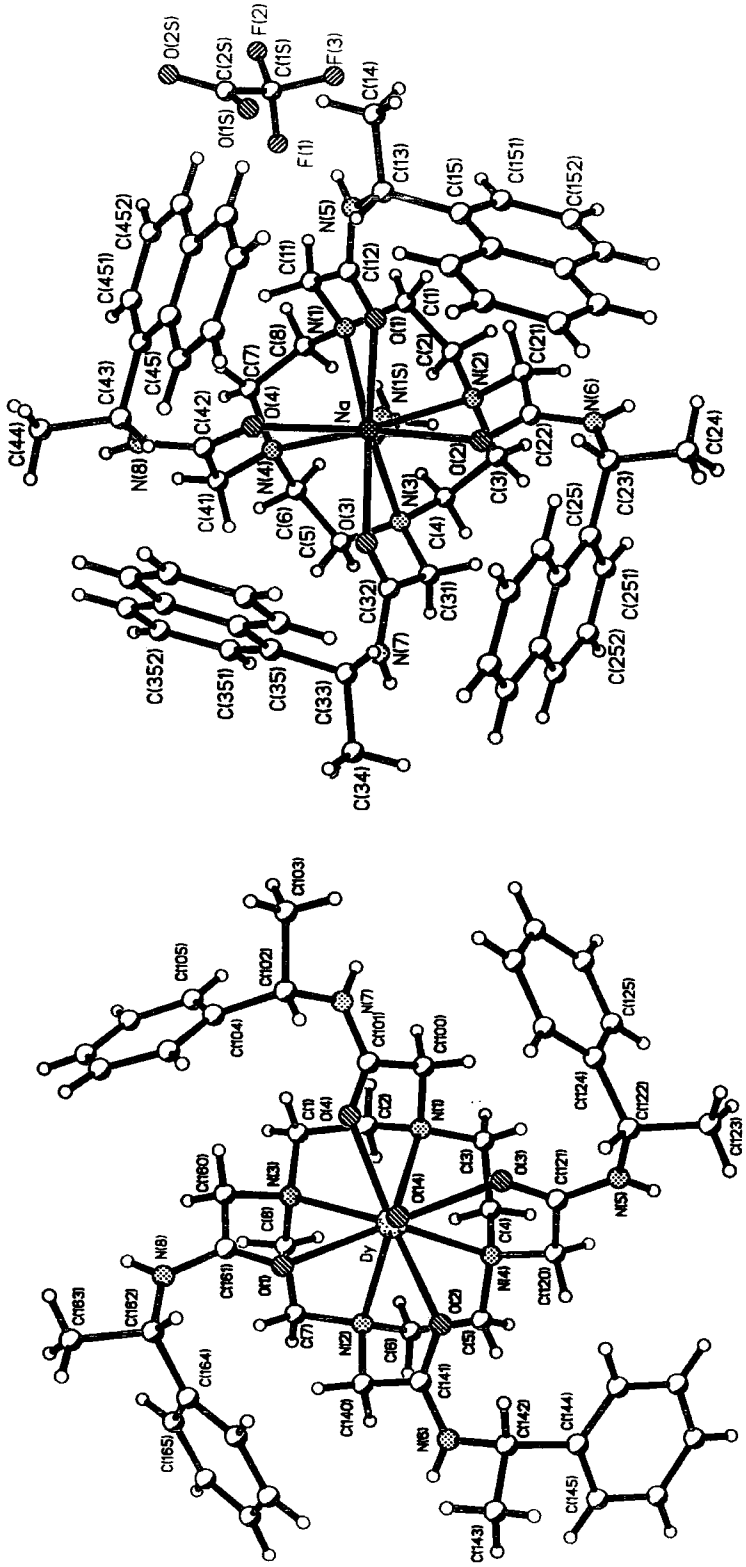

Figure 3.4 *Crystal structures of* $(Dy.13b)^{3+}$ *and* $(Na.13c)^{+}$ *viewed down the* C_4 *axis.*

For all three complexes the environment around the lanthanide ion is a (4:4:1) monocapped square antiprism. The tetraazacyclododecane ring adopts a "square" {3333} conformation[13] in which the four nitrogen atoms are roughly coplanar, on one side of the ring and directed towards the lanthanide ion, occupying four of the coordination sites. The hydrogen atoms of the ethylenediamine groups are staggered. The pendent arms are aligned in a cis fashion, to one side of the tetraazacyclododecane ring. The four oxygen atoms are directed towards the lanthanide ion defining four coordination sites and are approximately in the same plane. The relative rotational orientation of the N_4 and O_4 planes around the four-fold axis determines the twist angle. This angle is $\approx 37^{o}$ which lies short of the idealised twist angle of 45^{o} for the square antiprismatic geometry. The complexes therefore exhibit a slightly distorted square antiprismatic geometry, similar to that found in lanthanide complexes of DOTA (**7**)[14,15,16] ($\Psi = 39^{o}$). The ninth coordination site is occupied by an aqua ligand located in the axial position above the O_4 face. The Eu-O distances for the metal bound water are very similar to those previously reported for nine coordinate europium-aqua complexes.[9,17,18]

	mean bond lengths (Å)			mean bond angles (^{o})	
	M-OH_2	M-O	M-N	N-C-C-N torsion	N-C-C-O dihedral
(Eu.13a)$^{3+}$	2.425	2.367	2.699	58.6	-30.3
(Eu.13b)$^{3+}$	2.437	2.381	2.678	-58.5	31.9
(Dy.13b)$^{3+}$	2.421	2.339	2.648	-58.6	29.7
(Na.13c)$^{+}$	-	2.461	2.718	60.2	-39.2

Table 3.1. *Comparison of selected mean bond lengths (Å) and angles (^{o}) for complexes of* ***(Eu.13a)$^{3+}$, (Eu.13b)$^{3+}$, (Dy.13b)$^{3+}$ and (Na.13c)$^{+}$.***

The lanthanide ion lies closer to the O_4 plane and consequently the mean Ln-O bonds are shorter than the Ln-N bonds by ≈ 0.3 Å (**Table 3.1**). This is consistent with the highly ionic nature of the Ln-O bond compared to the more covalent nature of the Ln-N

bond. The smaller ionic radius of Dy^{3+} gives rise to slightly shorter bond lengths compared to the europium complexes (**Table 3.1**). The mean torsion angle about the N-C-C-N bond in the complexes (± 58.6°) is essentially the same as that found for complexes of DOTA (**7**) (59°).[14,15,16]

The crystal structures of the complexes viewed down the C_4 axis are shown in **Figure 3.3** and **3.4**. The N-C-C-O dihedral angle determines the layout of the pendent arms and is found to be approximately equal and opposite for the enantiomeric europium complexes **(Eu.13a)**$^{3+}$ and **(Eu.13b)**$^{3+}$ (**Table 3.1**). Likewise the N-C-C-N torsion angles are equal and opposite, consistent with the enantiomeric nature of the europium complexes. The crystal structures of **(Eu.13a)**$^{3+}$ and **(Eu.13b)**$^{3+}$ are essentially mirror images of one another (**Figure 3.3**). In the case of the RRRR complex **(Eu.13a)**$^{3+}$ the pendent arms are rotated around in a clockwise fashion, when viewed along the H_2O-Eu bond. In the SSSS complex **(Eu.13b)**$^{3+}$ however, the pendent arms rotate around in a counterclockwise fashion and the conformation of the macrocyclic ring has inverted. Therefore the chirality of the remote amide stereocentre favours both a particular helicity of the pendent arms and a given macrocyclic ring conformation resulting in the preferential formation of one enantiomer. Analogous behaviour is observed for the isostructural dysprosium complex **(Dy.13b)**$^{3+}$ (**Figure 3.4**).

The arrangement of the europium bound water molecule with respect to the position of the trifluoroacetate anions and acetonitrile solvent molecules in the crystal lattice of **(Eu.13a)**$^{3+}$ is shown in (**Figure 3.5**). Stabilisation of the bound water molecule through hydrogen bonding interactions between the hydrogen atoms of the water and the oxygen atoms of the trifluoroacetate anions is evident. The dashed lines indicate the hydrogen bonding between the europium-bound oxygen and the trifluoroacetate counter ion oxygen atoms (O···O distances are 2.831 and 2.832 Å).

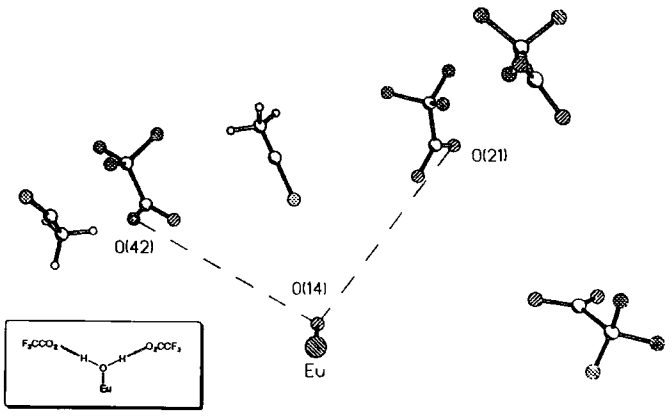

Figure 3.5 *Arrangement of the bound water molecule, trifluoroacetate counter ions and acetonitrile solvent molecules in the crystal lattice of* ***(Eu.13a)***$^{3+}$.

3.4.2 Crystal structure of the sodium complex of the tetranaphthyl amide (Na.13c)$^{+}$

The asymmetric unit cell comprises of one sodium complex, one trifluoroacetate counterion and five acetonitrile molecules of recrystallisation. A full list of coordinates is given in **Appendix 7**.

The crystal structure (**Figure 3.4**) reveals a twisted square antiprismatic geometry with a twist angle of $\Psi = 28^{o}$, well short of the idealised antiprism ($\Psi = 45^{o}$) and very similar to that observed for complexes of the tetraphosphinates **(2a)** and **(2b)** ($\Psi = 29^{o}$).[6] The mean N-C-C-O dihedral angle is -39.2° (**Table 3.1**), larger than that observed for the tetraphenyl complexes described above (≈ 31°), consistent with the 'twisted' square antiprismatic geometry. The mean N-C-C-N torsion angle (60.2°) is silmilar to that observed in the tetraphenyl complexes (58.5°) and in complexes of DOTA **(7)**[14,15,16] (59°), in accordance with a "square" {3333} conformation of the tetraazacyclododecane ring. The mean Na-O (2.46 Å) and Na-N (2.72 Å) bonds are longer than those observed for the corresponding lanthanide complexes of the tetraphenyl complexes consistent with the smaller ionic radius of the sodium ion and the 'twisted' square antiprismatic geometry adopted. The inability of sodium to achieve

a coordination number of nine is evident in the absence of a metal bound water molecule. The four naphthyl groups are aligned in a near orthogonal relationship to one another, the interplanar angles varying from 77.1 to 82.7°, and are steeply inclined to the O_4 plane.

The 'twisted' square antiprism has a more open structure than that of the square antiprism. The small ionic radius of the sodium ion is not ideally suited to the available cavity size in the complex. The 'twisted' square antiprism is favoured for the sodium ion as the less compact structure enables the pendent arms to reach around to allow the coordination to the small ion, with minimised steric interactions.

3.5 Luminescence properties of tetra- tri- and diamide complexes

3.5.1 Fluorescence spectra

The fluorescence spectra (298 K, H_2O + 3 drops TFA) for the 1- and 2-substituted tetranaphthyl ligands **(13c)** ($A^{270\ nm}$ = 0.1) and **(13e)** ($A^{270\ nm}$ = 0.08) are shown in **Figure 3.6**.

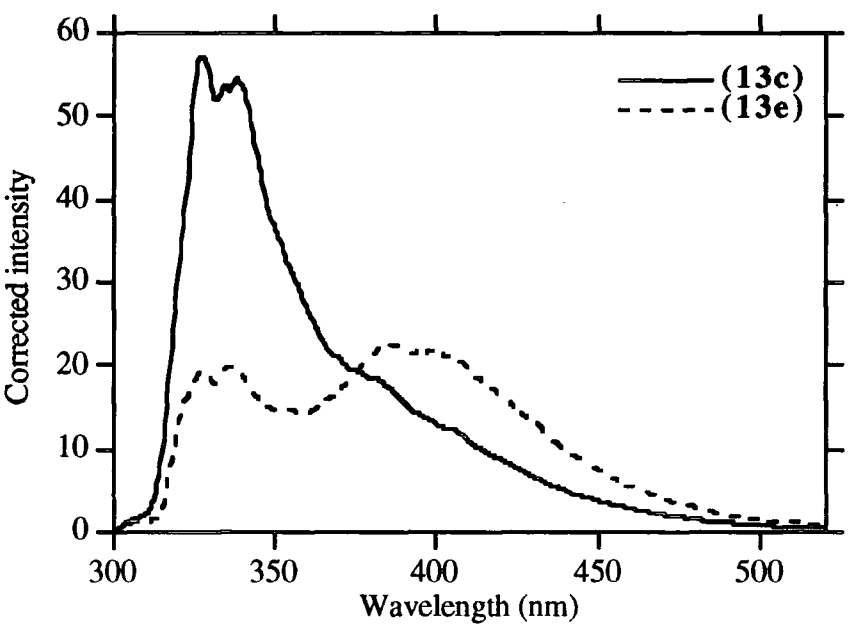

Figure 3.6. *Corrected fluorescence spectra for (13c) ($A^{270\ nm}$ = 0.1) and (13e) ($A^{270\ nm}$ = 0.08) (298 K, H_2O + 3 drops of TFA).*

The ligands exhibit a band at λ_{max} 337 nm, characteristic of naphthyl fluoresence. The presence of a structureless band at longer wavelength (390-410 nm) may be attributed to the formation of a naphthyl excimer.

Excimers are the result of the formation of an **e**xcited d**imer**, produced by the interaction of an excited molecule (M*) with a ground state molecule (M).

M + hv ⟶ M*	absorption
M* ⟶ M + hv	normal fluorescence
M* + M ⟶ MM*	excimer formation
MM* ⟶ M + M + hv	excimer fluorescence

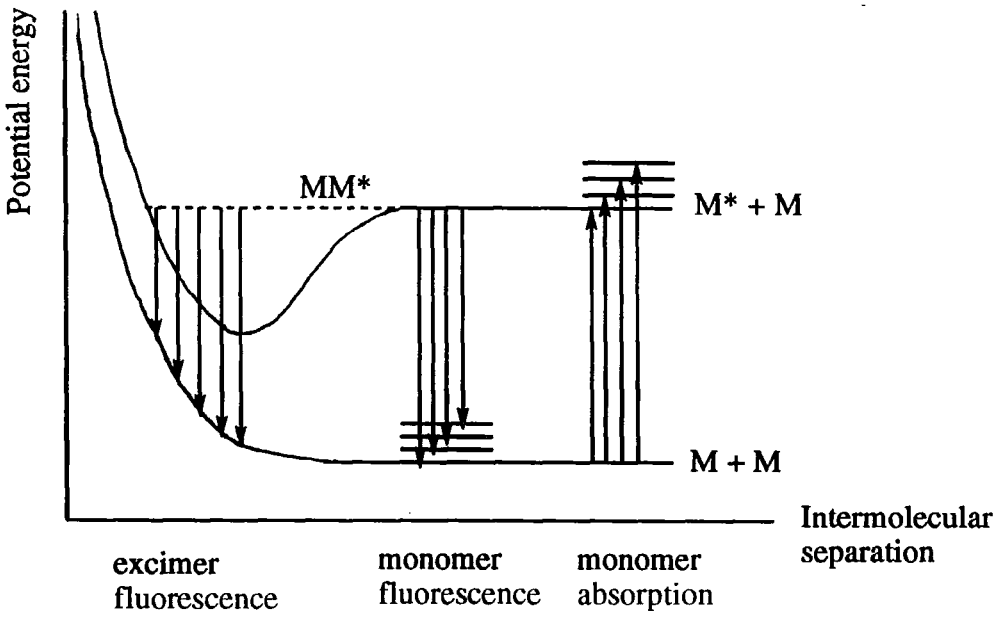

Figure 3.7. *Intermolecular potential energy curves for the interaction of 2 ground state molecules (lower) and that of a ground state molecule with another in its excited state (upper).*

The excited excimer MM* may decay to the ground state excimer radiatively or non-radiatively. However, since there is no attraction between the ground state molecules they immediately separate to regenerate the monomers, M. Excimer emission lies at longer wavelength than normal fluorescence as the excimer is stabilised with respect to

isolated M* molecules. As the lower state of the transition is a repulsive potential energy surface, the excimer emission is structureless (**Figure 3.7**).

Stabilisation of the excimer arises from the promotion of an electron from a filled antibonding orbital in the ground state dimer to an unfilled bonding orbital in the excited excimer, and is determined by the overlap of the orbitals of the interacting groups.

Förster and Kasper first reported that pyrene exhibits excimer formation and fluorescence in cyclohexane.[19] On increasing the concentration of pyrene, the usual structured fluorescence band (λ_{max} 395 nm) decreased in intensity and a new broad, structureless band at longer wavelength (λ_{max} 480 nm) appeared, attributed to the formation of a pyrene excimer. Experimental results suggest that this excimer formation is optimised when the two pyrene groups may align in a plane-parallel orientation, at a distance of 3.3 Å apart.

Excimer formation is not just restricted to intermolecular interactions. Among others, Yanari and Hirayama have reported that polystyrene exhibits intramolecular excimer formation.[20] In this case, the intensity of the normal fluorescence band and the excimer band are independent of concentration. The two interacting groups must be held in the appropriate plane-parallel orientation over the lifetime of the excited state of the dimer and experimental studies have shown this to be maximised when the two groups are separated by 3 methylene or equivalent units.[21]

The excimer fluorescence exhibited by **(13c)** and **(13e)** was found to be independent of concentration (A = 0.5 - 0.05) and so corresponds to the formation of an intramolecular excimer. **Figure 3.6** shows that the relative ratio of naphthyl fluorescence to excimer fluorescence is dependent upon the orientation of the naphthyl groups. Strong excimer formation is evident for the 2-naphthyl ligand **(13e)**, whereas the constitutionally isomeric 1-naphthyl substituted ligand **(13c)**, exhibits very weak excimer fluorescence.

Weak excimer emission occurring from proximate naphthyl chromophores of 2-poly-(naphthyl-Ala) in degassed *N,N*-dimethylformamide has been previously reported, whereas excimer emission was found to be absent in the corresponding poly-1-(naphthyl-Ala) isomer.[22] The naphthyl groups of **(13e)** must be orientated in such a way that the preferred plane-parallel conformation is achieved to a much greater extent than in **(13c)**. The excimer fluorescence for both ligands is absent in methanol and acetonitrile demonstrating the strong solvent dependency of the excimer formation. The ligands **(13d)** and **(13f)** exhibited identical fluorescence behaviour to their enantiomers.

The europium complexes of **(13e)** and **(13f)** also displayed some excimer formation in aqueous solution. The excimer emission intensity was around 40% of the monomer emission intensity, which is less than was observed in the free ligand, suggesting a change in orientation of the naphthyl groups upon metal binding. However, fluorescence spectra revealed no evidence for excimer formation in the europium complexes of **(13c)** and **(13d)**. This pattern of behaviour is consistent with the crystallographic data obtained for the corresponding sodium complex **(Na.13c)$^+$** (**Appendix 7**). The crystal structure shows that the naphthyl chromophores are not in a plane-parallel orientation and therefore are not suitably orientated to undergo excimer formation. Upon metal binding, the naphthyl groups are locked into a particular orientation and the complexes are rigid on the NMR timescale (ms). In the free ligand, the naphthyl groups are not so constrained allowing the two naphthyl groups to orientate themselves in a plane-parallel fashion during the lifetime of the excited state of the dimer (ns), giving rise to excimer fluorescence.

3.5.2 Terbium emission spectra

An intense phosphorescence emission (τ_{H_2O} = 1.74 ms, τ_{D_2O} = 3.45 ms) was observed from the tetraphenyl terbium complexes, **(Tb.13a)$^{3+}$** and **(Tb.13b)$^{3+}$**, following excitation at 254 nm (298 K, H_2O). A representative spectrum for **(Tb.13a)$^{3+}$** is shown in **Figure 3.8** and the $^5D_4 \rightarrow {}^7F_J$ transitions have been assigned. A quantum yield of

0.29 (298 K) was measured in aqueous solution relative to quinine sulphate (in 1 mol dm^{-3} H_2SO_4) as the reference. Emission from terbium tetranaphthyl complexes **(13c)**, **(13d)**, **(13e)** and **(13f)** (λ_{ex} 274 nm, 298 K, H_2O) was only observed following degassing of the sample. The back energy transfer process to the naphthyl triplet state from the $^5D_4$ terbium excited state is a function of molecular oxygen concentration as discussed in Chapter 2.4. The characteristics of the emission spectra for the tetranaphthyl complexes were very similar to those observed with the tetraphenyl complexes.

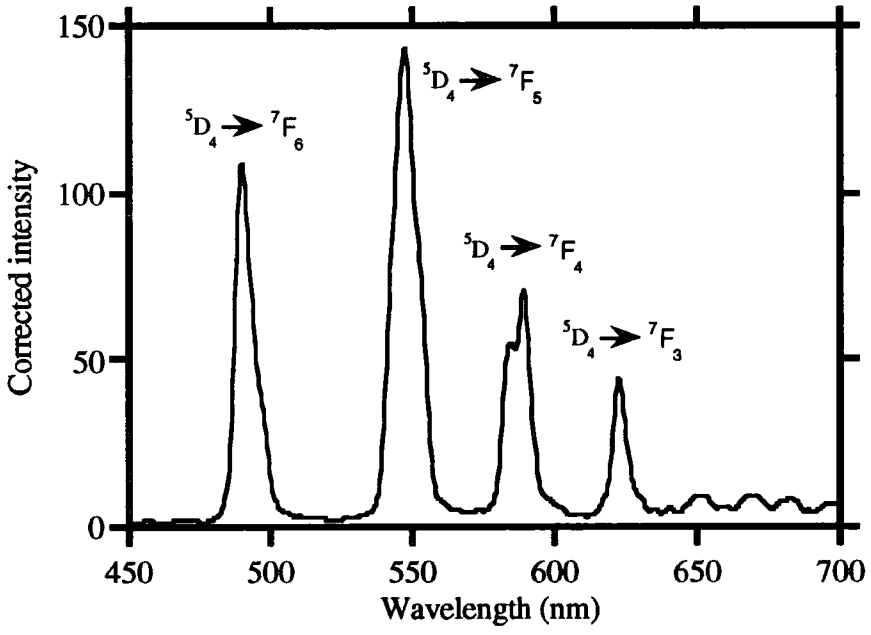

Figure 3.8. *Corrected phosphorescence emission spectrum for* ***(Tb.13a)***$^{3+}$ *(298 K, H_2O) following excitation at 254 nm. The* $^5D_4 \rightarrow {}^7F_J$ *transitions are assigned.*

3.5.3 Europium emission spectra

Phosphorescence emission observed from the corresponding tetraphenyl complexes **(Eu.13a)**$^{3+}$ (τ_{H_2O} = 0.58 ms, τ_{D_2O} = 2.44 ms) and the tetranaphthyl complexes **(Eu.13c)**$^{3+}$ (τ_{H_2O} = 0.53 ms, τ_{D_2O} = 2.7 ms) and **(Eu.13e)**$^{3+}$ (τ_{H_2O} = 0.52 ms, τ_{D_2O} = 2.08 ms) in aqueous solution are much weaker than the terbium analogues due to the competitive charge transfer mechanism of energy capture by the europium ion, discussed in Chapter 2.4.

The phosphorescence emission spectra for the tetra-, tri- and diphenylamide europium complexes, **(Eu.13a)**$^{3+}$, **(Eu.14)**$^{3+}$ and **(Eu.15)**$^{3+}$, are shown in **Figure 3.9**.

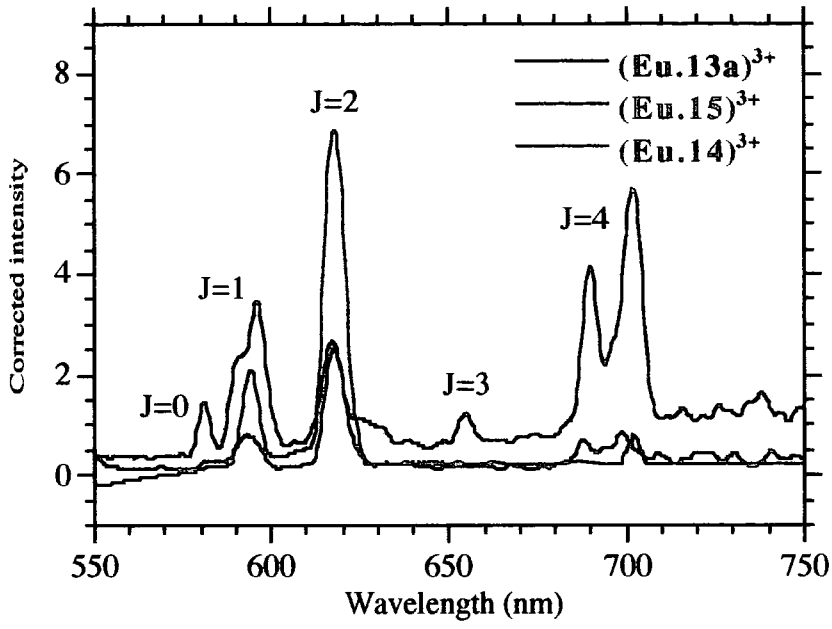

Figure 3.9. *Corrected phosphorescence emission spectra for* ***(Eu.13a)***$^{3+}$ ***(Eu.14)***$^{3+}$ *and* ***(Eu.15)***$^{3+}$ *(298 K, H_2O) following excitation at 254 nm. The $^5D_0 \rightarrow {}^7F_J$ transitions have been assigned and the J values of the bands are labelled.*

The $^5D_0 \rightarrow {}^7F_0$ ($\Delta J = 0$) transition is formally allowed in systems of low symmetry through an electric dipole mechanism[23] and is indeed evident for **(Eu.13a)**$^{3+}$, appearing as a single, weak band at 580 nm. This is consistent with the presence of a single diastereoisomer in solution as the initial and final states of the transition are non-degenerate, therefore the number of components observed is related to the number of chemically distinct environments for the europium ion. The $^5D_0 \rightarrow {}^7F_0$ ($\Delta J = 0$) transition for **(Eu.14)**$^{3+}$ and **(Eu.15)**$^{3+}$ is too weak to be observed under the experimental conditions. However, a highly resolved spectrum using laser excitation and sensitive photon counting equipment may reveal the $\Delta J = 0$ band around 580 nm.

The $^7F_1$ level is split into three non-degenerate states for complexes with low symmetry (C_2 axis or lower), two non-degenerate states in the presence of a 3-fold or higher axis and only one state for icosahedral or cubic symmetry.[23] The complex **(Eu.13a)**$^{3+}$ has a

four-fold symmetry axis, as shown in the X-ray crystal structure (**Appendix 4**). Two components to the $^5D_0 \rightarrow {}^7F_1$ ($\Delta J = 1$) transition are therefore expected and were indeed observed (**Figure 3.9**). The low symmetry exhibited by **(Eu.14)**$^{3+}$ and **(Eu.15)**$^{3+}$ should give rise to three components for the $^5D_0 \rightarrow {}^7F_1$ ($\Delta J = 1$) transition. Due to the weak emission observed from all three europium complexes, the monochromator excitation and emission slit widths were adjusted accordingly to maximise the amount of light getting into the complex and to the detector. Although this allowed the detection of the transition, there is a trade-off in the resolution of the bands and as a result the fine structure of the transitions may not be resolved. This was the case for the $^5D_0 \rightarrow {}^7F_1$ ($\Delta J = 1$) transition for **(Eu.14)**$^{3+}$ and **(Eu.15)**$^{3+}$ (**Figure 3.9**).

The $^5D_0 \rightarrow {}^7F_2$ ($\Delta J = 2$) transition is predicted to exhibit two components for a C_4 symmetric **(Eu.13a)**$^{3+}$ complex, as was observed.[23] The relative intensities of the two components of this hypersensitive transition and the ratio of the relative intensities of the $\Delta J = 1$ / $\Delta J = 2$ band may be related to the coordination geometry of the complex.[24] The $\Delta J = 1$ and $\Delta J = 2$ band components and intensities are very similar to those observed for **(Eu.DOTA)**$^-$ **(Eu.7)**$^-$ suggesting that the complex adopts a square antiprismatic geometry in solution which is consistent with the crystallographic data (**Appendix 4**). For **(Eu.14)**$^{3+}$ and **(Eu.15)**$^{3+}$ the intensity of the $\Delta J = 1$ / $\Delta J = 2$ band ($\approx$0.25) is much smaller than that of **(Eu.13a)**$^{3+}$ (1.7) which is also consistent with a change in coordination geometry.

The $^5D_0 \rightarrow {}^7F_3$ ($\Delta J = 3$) transition is always very weak[25] and was observed for **(Eu.13a)**$^{3+}$, however the transition appears to be absent for **(Eu.14)**$^{3+}$ and **(Eu.15)**$^{3+}$. The $^5D_0 \rightarrow {}^7F_4$ ($\Delta J = 4$) transition was relatively intense for all three complexes and exhibited some degree of fine structure.

3.5.4 Ytterbium luminescence

Emission emanating from Yb^{3+} in the solution state remains relatively unexplored and only a few examples of such near infra-red emission from diketonate complexes[26], Yb^{3+} porphyrins[27] and more recently Yb^{3+} protein complexes[28] have been reported. Ytterbium offers the possibility of long wavelength luminescence (λ_{em} = 980 nm), and as the lowest luminescent level is of relatively low energy (10 200 cm^{-1}), the use of a sensitising chromophore with a low triplet state energy may be employed, avoiding competitive excitation of biological chromophores, thus greatly enhancing the utility of such complexes for *in vivo* applications.

The time resolved luminescence of the Yb^{3+} complexes of **(Yb.13a)$^{3+}$** and **(Yb.13c)$^{3+}$** have been examined[29,30] following excitation by sensitised emission from the aryl chromophores (λ_{ex} = 266 nm). As there is only one excited state, all luminescence is due to the $^2F_{5/2} \rightarrow {}^2F_{7/2}$ transition occurring at 980 nm.

The difference in energies between the triplet state of the chromophore and the excited state of the metal means that the overlap of the emission and absorption bands is poor and subsequently little energy transfer is expected. The excited state of Yb^{3+} could possibly be populated via a process involving an electron transfer mechanism. Recently Horrocks proposed that tryptophan sensitises Yb^{3+} via a long range electron transfer process.[28] Similarly, quenching of indole and related fluorophores tethered to EDTA chelates of lanthanides, with Eu^{3+} and Yb^{3+} complexes being the most effective quenchers, was postulated by Abusaleh and Meares[31] to involve an electron transfer mechanism. However, Yb^{3+} is not readily reduced to Yb^{2+} (E^o = -1.2 V, cf. Eu^{3+} E^o = -0.35) so that photoinduced electron transfer to Yb^{3+} from an excited state of a sensitising chromophore may not occur very readily. An energy transfer mechanism involving overlap of the emission spectrum of the chromophore with a ligand to metal charge transfer band of Yb^{3+} may explain the observed luminescence. However, there was no evidence of a ligand to metal charge transfer band in the absorption spectrum of **(Yb.13a)$^{3+}$**.

Excitation via sensitised emission is preferred over direct excitation for Yb^{3+} ions as the observed emission occurs at the same wavelength as the required excitation (λ_{ex} = 980 nm), therefore the emission intensity will be swamped by scattered light and analysis of the signal is very difficult.

The lifetimes of the excited states for **(Yb.13a)$^{3+}$** (τ_{H_2O} = 0.70 μs, τ_{D_2O} = 6.18 μs) and **(Yb.13c)$^{3+}$** (τ_{H_2O} = 0.83 μs, τ_{D_2O} = 5.00 μs) have been measured and are considerably shorter than that for **(Yb.2b)$^{-}$** (τ_{H_2O} = 4.53 μs, τ_{D_2O} = 8.90 μs).[29,30] The quenching effect of O-H oscillators on the rate constants for ytterbium luminescence may be fitted to equation **(3.3)**[29]

$$q = A\,(k_{H_2O} - k_{D_2O}) - B \qquad \textbf{(3.3)}$$

where q is the number of metal bound water molecules, k_{H_2O} the quenching rate constant in H_2O, k_{D_2O} that in D_2O, A is a constant reflecting the quenching sensitivity (A = 1μs) and B is a term representing the quenching effect of outer sphere water molecules ($0.1 < B < 0.3$). The hydration state of the complexes **(Yb.13a)$^{3+}$** (q = 1.07), **(Yb.13c)$^{3+}$** (q = 0.8) and **(Yb.2b)$^{-}$** (q = 0) has been estimated. The behaviour is in accordance with the presence of one coordinated water molecule for the former complexes compared to none for the latter complex, and is consistent with reported crystallographic studies.[32,33,34] The lifetimes are much shorter than those observed for the corresponding Eu^{3+} and Tb^{3+} complexes which are of the order of milliseconds. The energy gap between the lowest emissive state and the highest non-emissive state is reduced for Yb^{3+} (10 200 cm^{-1}), compared to Eu^{3+} (12 500 cm^{-1}) and Tb^{3+} (14 800 cm^{-1}), resulting in more efficient quenching by OH oscillators for Yb^{3+}. Energy is transferred to lower vibrational levels of the OH manifold where the Franck Condon overlap is greater leading to enhanced sensitivity to OH quenching for Yb^{3+} compared to Eu^{3+} and Tb^{3+}.

3.6 Circular dichroism

3.6.1 Exciton coupling

The interaction of two chromophores in close proximity in a chiral environment gives rise to distinctive circular dichroism (CD) curves with a typical bisignate couplet that characterises exciton coupling. This exciton-coupled circular dichroism enables the configuration of the chiral array to be deduced.[35,36,37] The sign and shape of the CD curve is defined by the absolute skewness of the interacting chromophores and the extent of the chromophoric coupling is proportional to the square of the dipole moment associated with the transition and inversely proportional to the cube of the interchromic distance.[38]

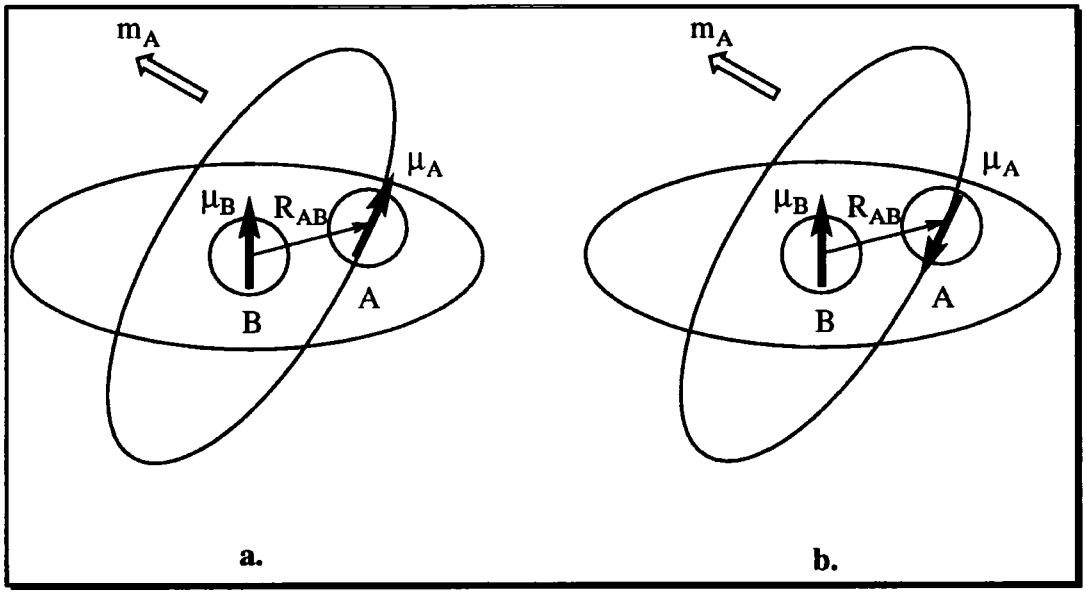

Figure 3.10. *Schematic representation of* ***a.*** *in phase and* ***b.*** *out of phase coupling of the electric dipole transition moment of A and B giving rise to a net helical motion of the electrons in B.*[39]

An electric dipole transition moment, μ_A, occurring in one chromophore, A, will cause the electrons associated with the electric dipole transition moment, μ_B, of chromophore B, to be helically deflected resulting in an induced magnetic character to B. Similarly, μ_B will give rise to magnetic character to μ_A. The two electric dipole transition moments may couple together either in phase or out of phase (**Figure 3.10**) resulting in

two non-degenerate excited states which gives rise to the observed two peaks in the CD spectrum.

For identical chromophores the most significant coupling occurs between transitions of the same energy, E, and this results in helices of electron motion with equal magnitude but opposite CD signs at energies very close to E (**Figure 3.11**).

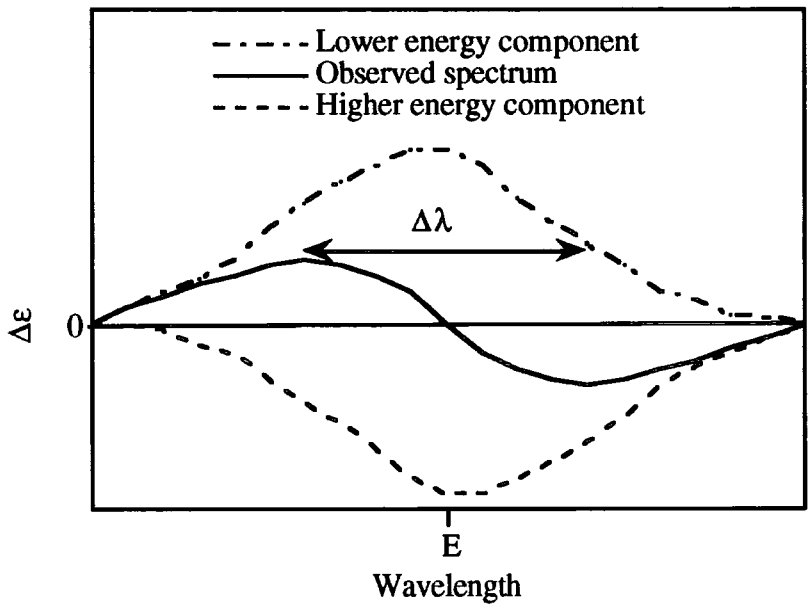

Figure 3.11. *Characteristic bisignate CD profile resulting from the cancellation of overlapping positive and negative bands resulting from the in and out of phase coupling of the electric dipole transition moments of A and B.*

The observed CD spectrum is a combination of the two components and has a bisignate profile with a pair of CD bands, one of shorter wavelength E^-, and one at longer wavelength E^+, relative to the absorption wavelength of the monomeric chromophore, E (equation **(3.1)**).

$$E+/- = E +/- \frac{\mu^2 (\sin\alpha \sin\gamma \cos\tau + 2 \cos\alpha \cos\gamma)}{R_{AB}^3} \qquad (3.1)$$

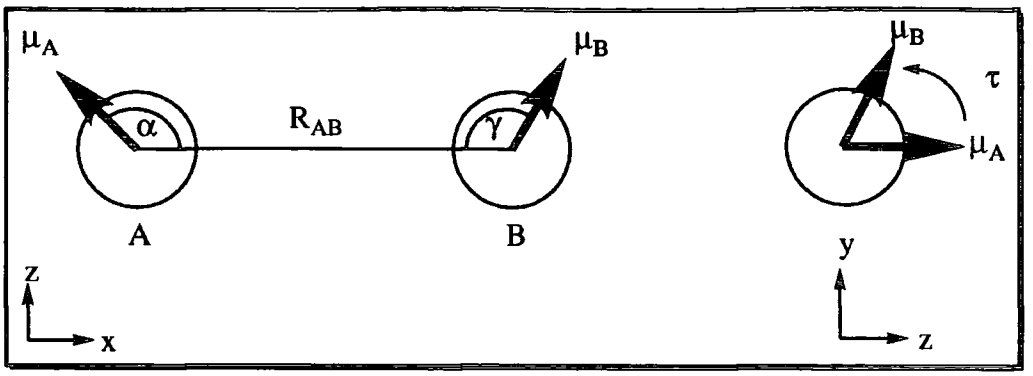

Figure 3.12. *Illustration of the geometry and coordination for the AB system described.*

The bands have approximately equal areas but their intensities, ΔE, are generally unequal.[37] The sign and magnitude of the bands is given by equation **(3.2)**[39], where R^+ refers to the transition occurring at energy E^+ and R^- to the transition at energy E^-.

$$R^{+/-} = \frac{\pi E^{+/-} \mu^2 R_{AB}}{2 h} \sin\alpha \sin\gamma \sin\tau \qquad (3.2)$$

Positive chirality is represented by a CD couplet with a positive band at longer wavelength and a negative band at shorter wavelength. The reverse situation is negative chirality.[39,40]

Exciton coupling has been exhibited by a variety of systems in the solid state[41], in microheterogeneous media[42] and in ordered polymers.[43] Intramolecular exciton coupling of systems in solution has focussed on nonconjugated chromophores possessing large oscillator strengths such as porphyrins[44], phthalocyanines[45], cyanines[46], and squaraines.[47] The orientation dependency of the coupled chromophores has been investigated in such porphyrin systems.[44,48] In conformationally rigid systems such as steroids, biaryls and helicenes[36], the exciton coupled CD method has been used to determine absolute configuration. The method has also been used with coordination complexes of C_3-symmetric tris-chelates of bidentate ligands such as bipyridines and phenanthrolines,[36,49] to elucidate the

stereochemical configuration of a range of isomers. Chiral tetrahedral complexes have also been studied.[50]

3.6.2 Tetraamide circular dichroism

The CD spectra for the 1-naphthyl ligands **(13c)** and **(13d)** and their europium complexes and the 2-naphthyl ligands **(13e)** and **(13f)** and their europium complexes are shown in **Figure 3.13** and **Figure 3.14.** Exact mirror image CD spectra are obtained for pairs of enantiomers, confirming the presence of a single diastereoisomer in solution for such systems, consistent with the NMR analysis discussed in Chapter **3.3.** For the same absolute configuration, the sign of the CD of the 1-naphthyl ligand and its complexes is opposite to that of the 2-naphthyl ligand and its complexes.

Crystallographic studies on the sodium complex of **(13c)** reveal that the dihedral angles between the planes of adjacent pairs of naphthyl chromophores are 81.3, 80.9, 82.7 and 77.1°. Given that the magnitude of the exciton coupling[37] is zero when the dihedral angle between the two chromophores is 0 or 180°, and is maximised when the angle is ≈ 70°, the arrangement of the naphthyl groups in **(Na.13c)$^+$** is such that exciton coupling may be observed. Indeed, strong exciton coupling is observed at room temperature for the sodium complex[33] **(Na.13c)$^+$** **(Figure 3.15)** which displays the characteristic bisignate signal in the CD spectrum centred at 224 nm with $\Delta\lambda$ = 10 nm and disymmetry factors of g_{abs} (219) = -2.2 x 10^{-3} and g_{abs} (229) = +1.4 x 10^{-3}. The absorption bands at longer wavelength arise from a $\pi \longrightarrow \pi^*$ transition with a moment directed along the shorter in-plane axis of the molecule, whereas the bands at shorter wavelength are polarised in the direction of the longer in-plane axis.[36]

The 1-naphthyl (**Figure 3.13**) and 2-naphthyl ligands (**Figure 3.14**) do not exhibit exciton coupling at room temperature. The CD bands for the 2-naphthyl free ligands **(13e)** and **(13f)** in the near u.v. region (250 - 350 nm) at 280 and 310 nm may be attributed to the ^1L_a and ^1L_b naphthyl $\pi \longrightarrow \pi^*$ transition.[51] In the case of the 1-naphthyl ligands, **(13c)** and **(13d)**, the ^1L_a naphthyl transition at 280 nm appeared to

mask the ^1L_b transition at 310 nm. In the far u.v. region (200 - 250 nm) the bisignate CD apparent for **(13e)** and **(13f)** was assigned to the ^1B_b (225 nm) and the ^1C_b (210 nm) transition rather than exciton coupling. The attribution of a bisignate couplet to exciton coupling requires caution and may be tentatively made by considering that $\Sigma\Delta\varepsilon$ within the couplet should have at least twice the usual magnitude obtained with an identical isolated chromophore absorbing in the same region of the spectrum, and if $\Delta\varepsilon > 50$ there is little doubt of the origin of the bands.[40]

The magnitude of the CD of ligands **(13e)** and **(13f)** remains relatively constant irrespective of temperature (**Figure 3.16**) which is consistent with the absence of any exciton coupling. However, on addition of 2 equivalents of KCl to **(13e)**, a large bisignate couplet became apparent with a crossover at 225 nm (**Figure 3.16** and **Figure 3.17**). The intensity of both bands of the bisignate profile was found to change in phase with decreasing temperature (**Figure 3.16**), which is consistent with the coupling of the electric dipole transition moment along the long axis of the naphthyl chromophores, confirming that exciton coupling of negative chirality[37] occurs upon binding of the K^+ ion to the macrocyclic ligand. The CD spectrum in the presence of Ca^{2+} was also shown in **Figure 3.16**. Exciton coupling and hence metal binding was revealed only on decreasing the temperature to -86 °C. The temperature dependence of the observed CD above -86 °C is not consistent with exciton behaviour since the intensity of the band at 215 nm decreases rather than increases on decreasing the temperature, supporting the ^1C_b nature of the transition. The europium complexes **(Eu.13e)**$^{3+}$ and **(Eu.13f)**$^{3+}$ displayed a very small bisignate CD profile which is significantly enhanced on increasing the temperature (**Figure 3.16**). The CD profile of **(13e)** in the presence of Na^+ ions at room temperature is shown in **Figure 3.17** and behaves in the same way as the free ligand, displaying no exciton coupling.

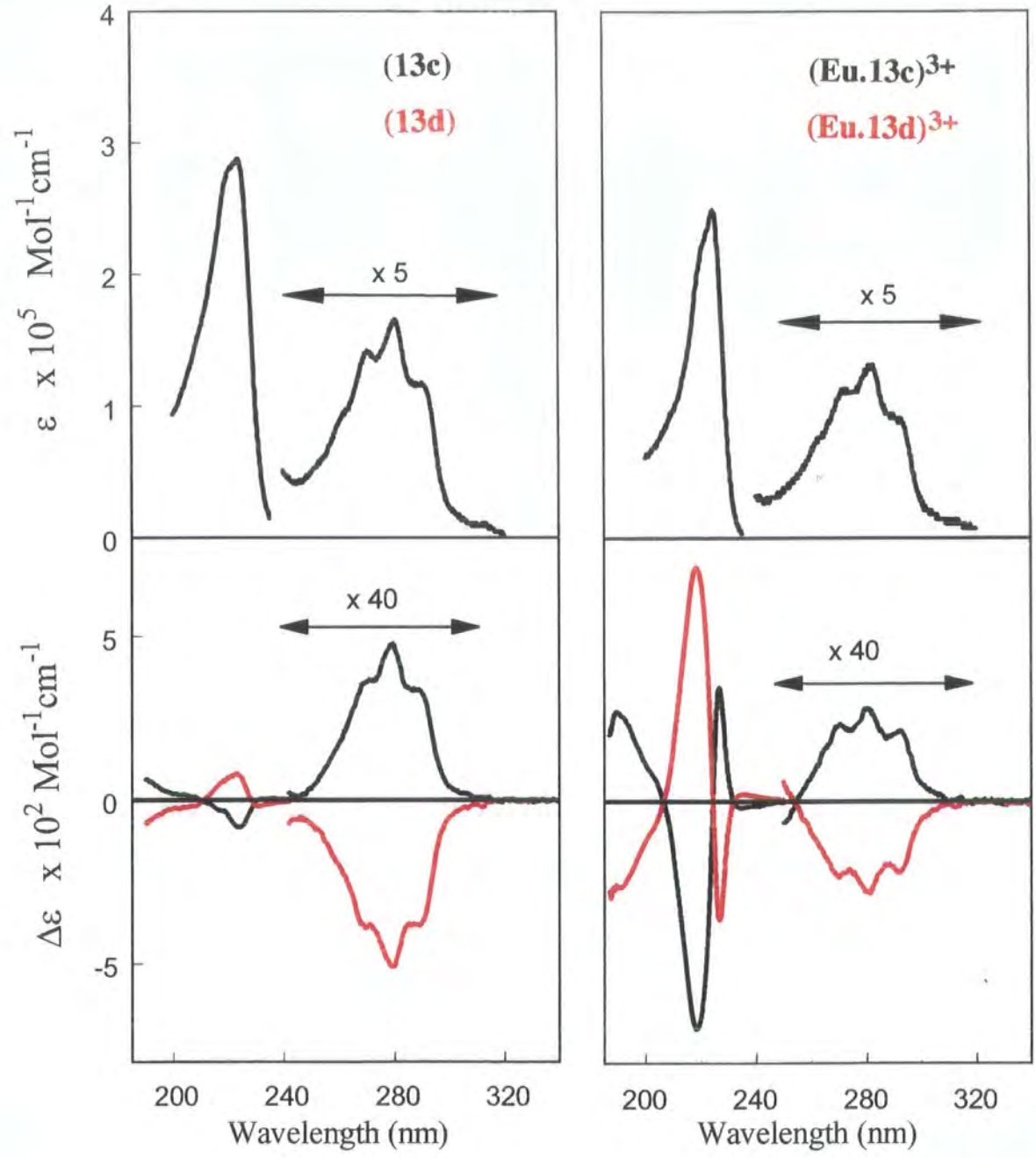

Figure 3.13. Absorbance spectra (upper trace) and circular dichroism spectra (lower trace) for the ligands **(13c)**, **(13d)** and their europium complexes **(Eu.13c)$^{3+}$** and **(Eu.13d)$^{3+}$** (MeOH, 293 K).

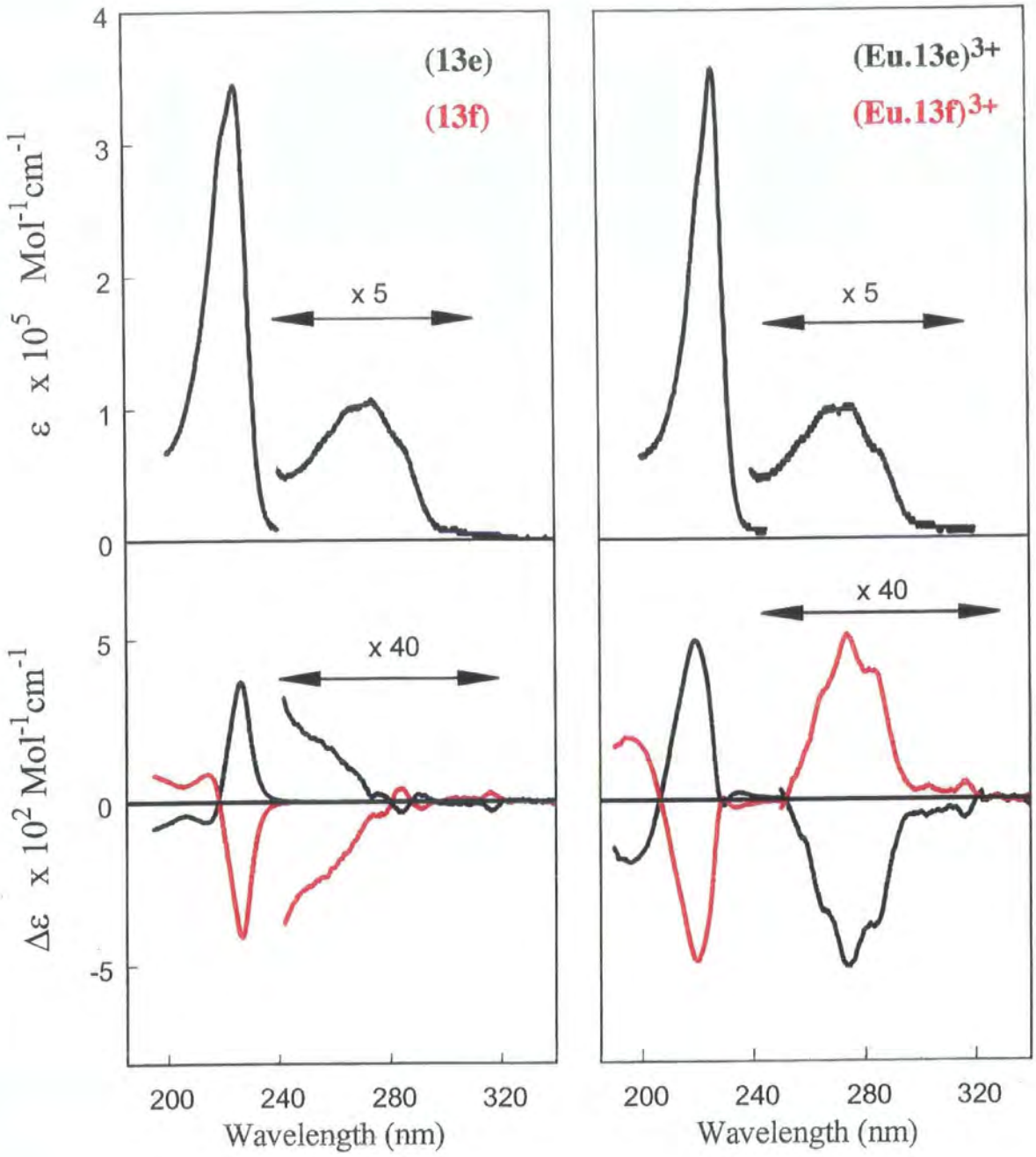

Figure 3.14. *Absorbance spectra (upper trace) and circular dichroism spectra (lower trace) for the ligands* ***(13e)***, ***(13f)*** *and their europium complexes* $(\mathbf{Eu.13e})^{3+}$ *and* $(\mathbf{Eu.13f})^{3+}$ *(MeOH, 293 K).*

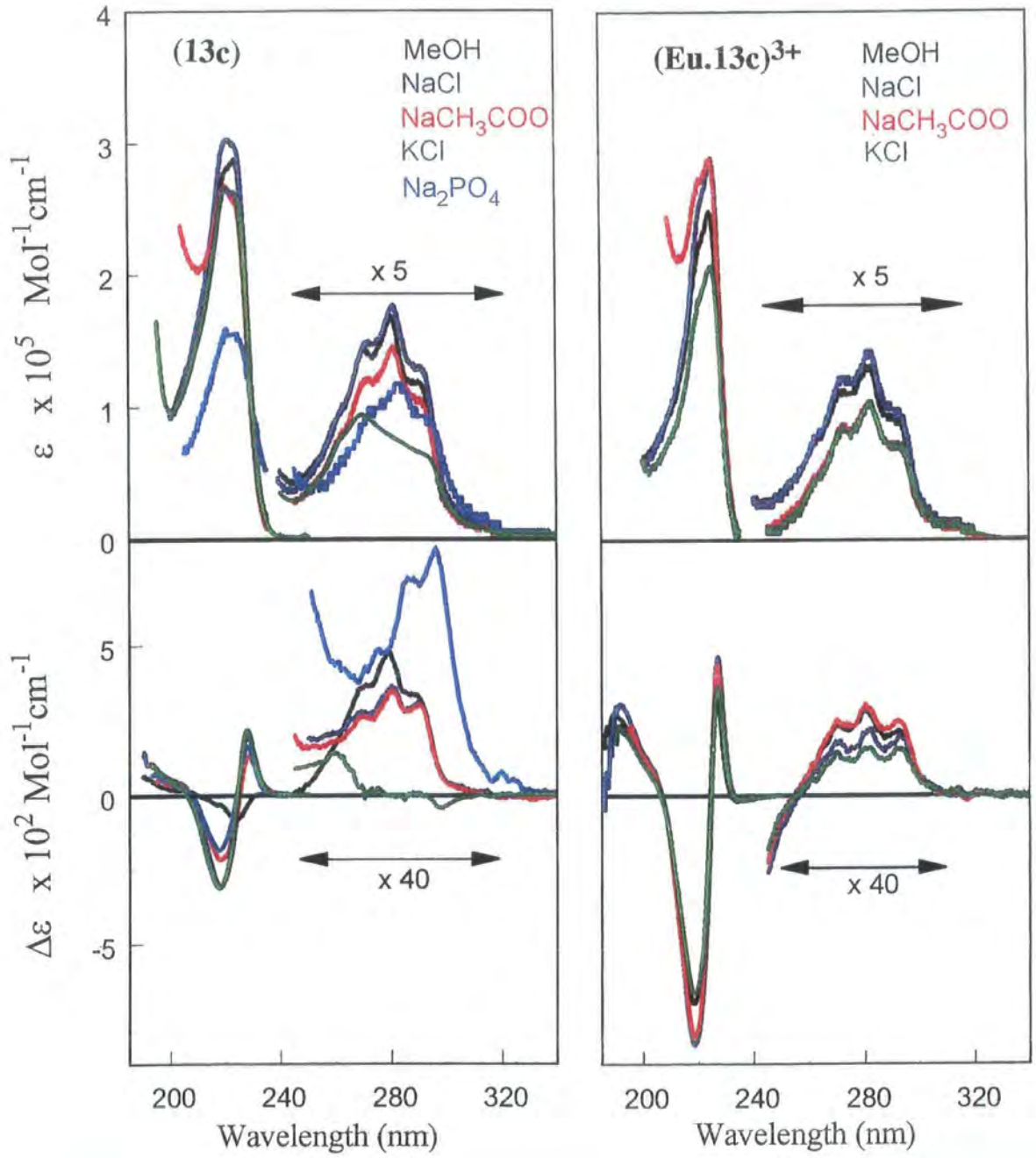

Figure 3.15. *Absorbance spectra (upper trace) and circular dichroism spectra (lower trace) for* ***(13c)*** *and* ***(Eu.13c)$^{3+}$*** *in the presence of a two-fold excess of various salts (MeOH, 293 K).*

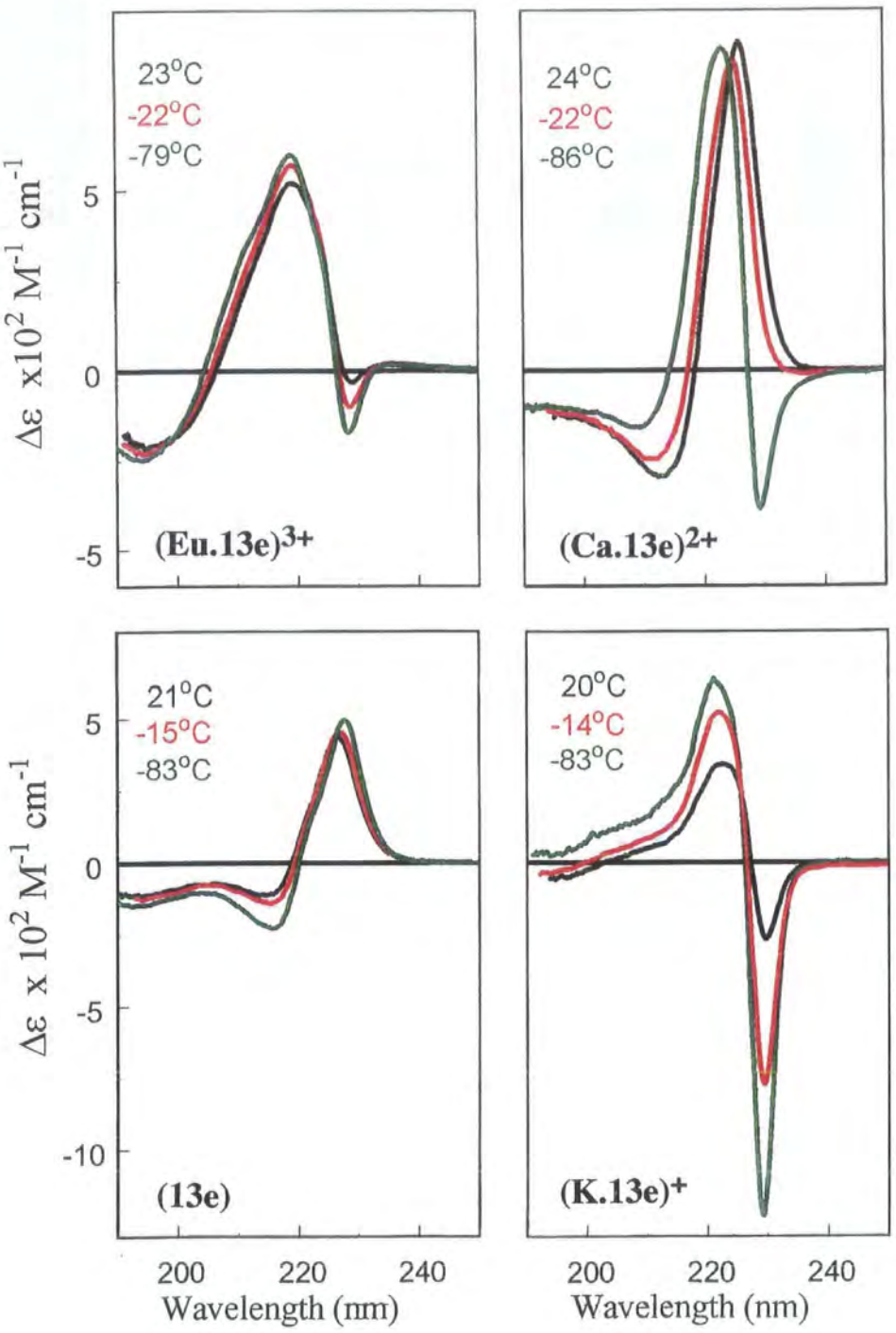

Figure 3.16. *Variable temperature circular dichroism spectra of* ***(Eu.13e)$^{3+}$****,* ***(Ca.13e)$^{2+}$****,* ***(13e)*** *and* ***(K.13e)$^{+}$*** *(MeOH).*

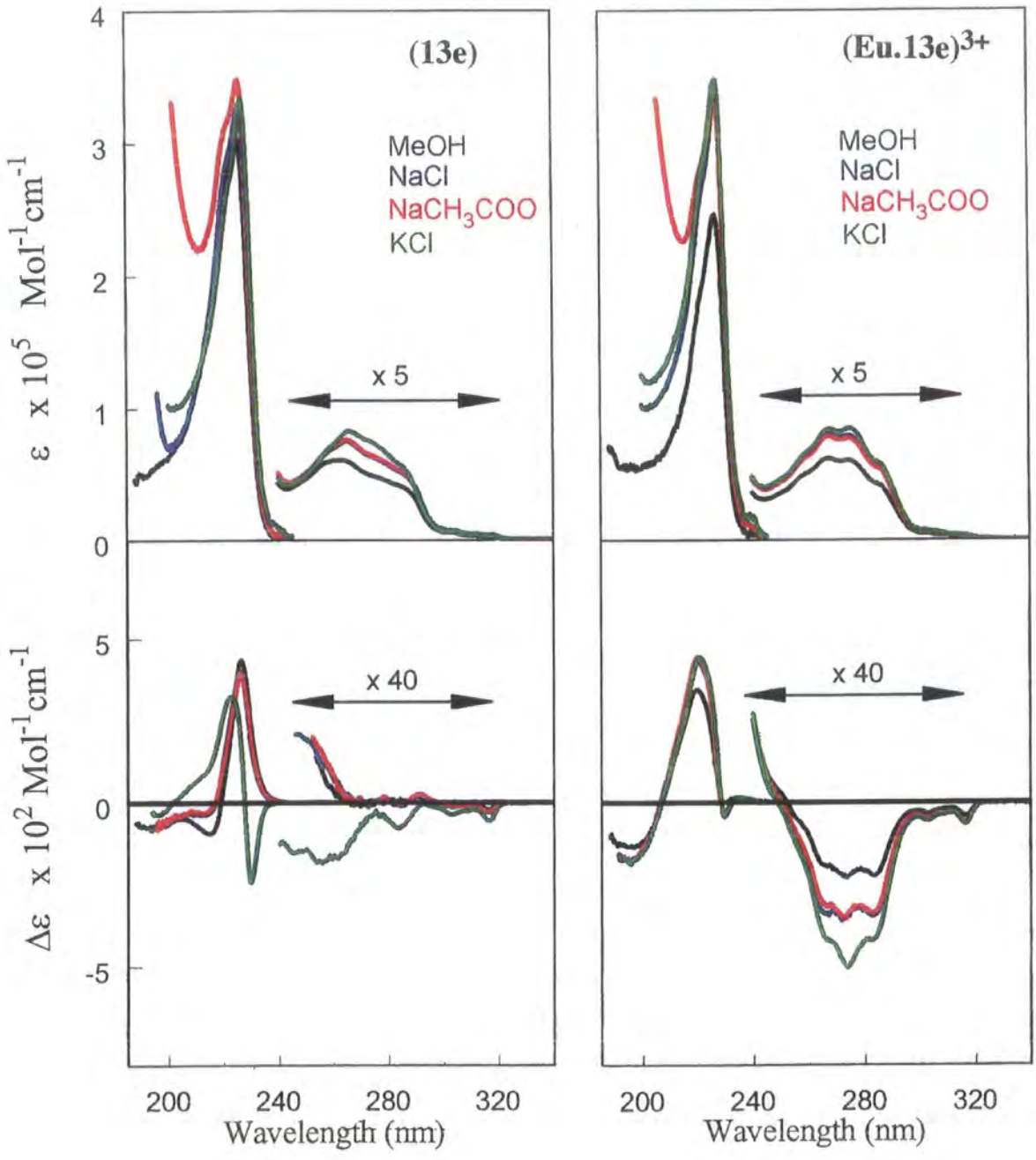

Figure 3.17. *Absorbance spectra (upper trace) and circular dichroism spectra (lower trace) for* ***(13e)*** *and* ***(Eu.13e)*$^{3+}$** *in the presence of a two-fold excess of various salts (MeOH, 293 K).*

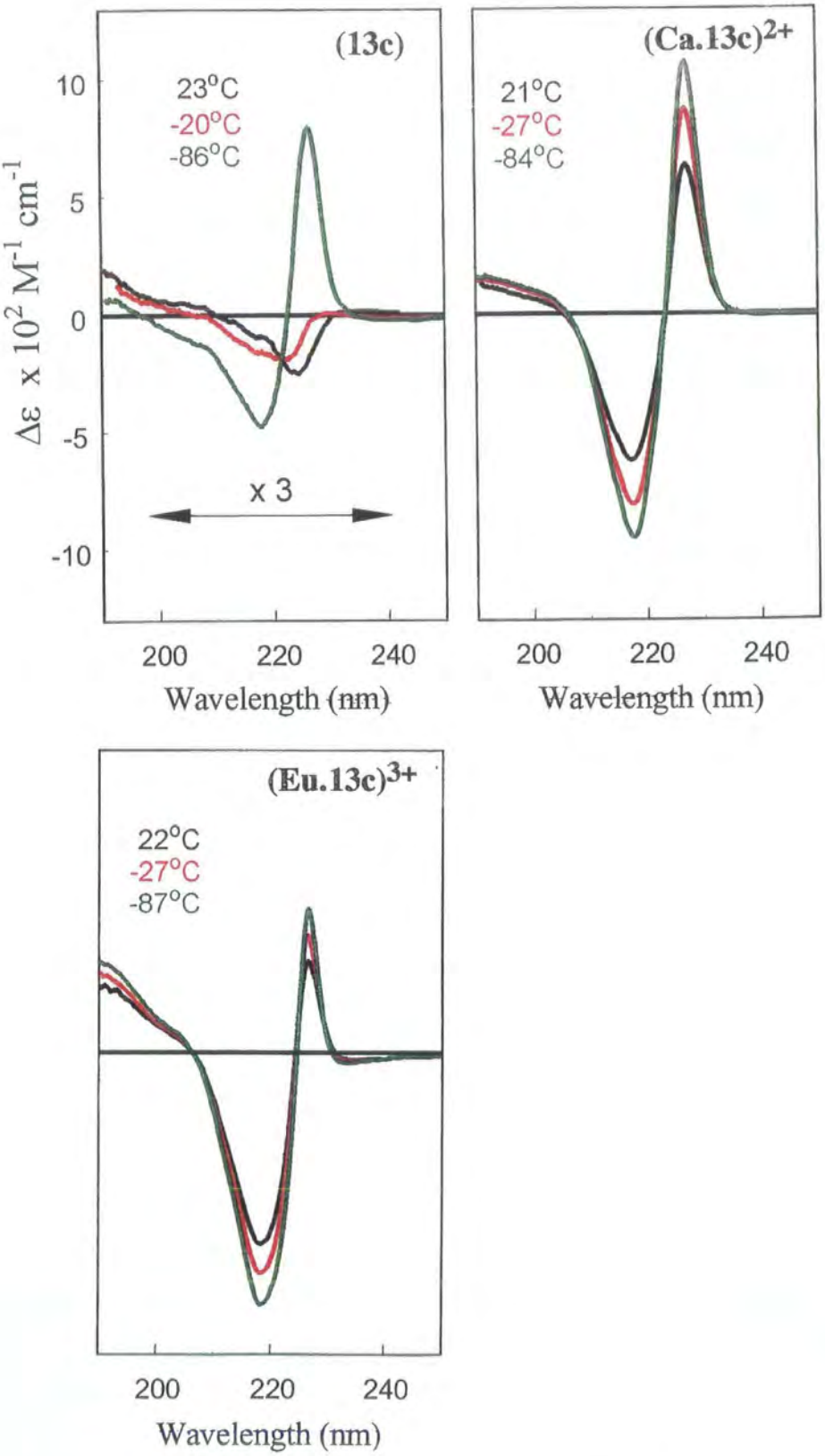

Figure 3.18. *Variable temperature circular dichroism spectra of* ***(13c)***, ***(Ca.13c)$^{2+}$*** *and* ***(Eu.13c)$^{3+}$*** *(MeOH).*

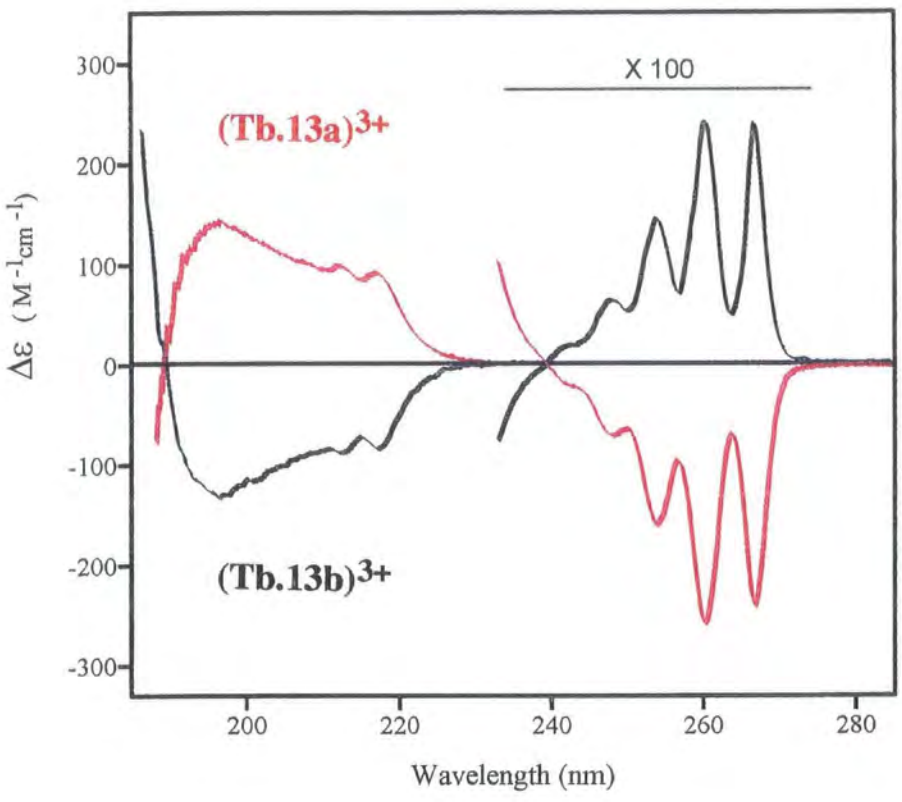

Figure 3.19. *Circular dichroism spectra for the enantiomeric terbium complexes* ***(Tb.13a)***$^{3+}$ *and* ***(Tb.13b)***$^{3+}$ *(MeOH, 293 K).*

In the far u.v. region, no exciton coupling of the free ligand **(13c)** and **(13d)** at room temperature was evident. However, on decreasing the temperature to -86 °C a bisignate profile with crossover at 222 nm was observed (**Figure 3.18**). The europium complexes **(Eu.13c)**$^{3+}$ and **(Eu.13d)**$^{3+}$ display large exciton coupling of positive and negative chirality respectively at room temperature[33] (**Figure 3.13**), with the characteristic bisignate profile centred at 222 nm with $\Delta\lambda$ = 10 nm and dissymmetry factors of g_{abs} (219) = -7.8 x 10^{-3} and g_{abs} (229) = +3.5 x 10^{-3}. Similarly, exciton coupling of positive chirality was induced at room temperature by the addition of 2 equivalents of K^+, Na^+ and Ca^{2+} (**Figure 3.15**) to the free ligands of **(13c)** and was also displayed by the corresponding terbium complexes.

3.6.3 Summary

For ligands and complexes of the 2-naphthyl tetraamides **(13e)** and **(13f)**, exciton coupling at room temperature is largely restricted to the potassium complexes. Upon metal binding of the free ligand to the K^+ ion, the naphthyl groups are aligned in such a way that coupling of the electric dipole moments along the long axis of the naphthyl chromophore may arise, resulting in a bisignate profile centred at 222 nm, typical of exciton coupling. As discussed in Chapter **3.5**, the ligands **(13e)** and **(13f)** display strong intramolecular excimer formation which requires the coplanarity of the two aryl groups and their close juxtaposition (ca. 3.3 to 3.5 Å). The average interchromophoric dihedral angle must therefore be close to zero which is consistent with the absence of any observed exciton coupling. Excimer formation is also evident in the corresponding europium complexes of **(13e)** and **(13f)**. The Ca^{2+} ionic radius in 8 coordinate systems (112 pm) is very similar to that of the Eu^{3+} ion (107 pm). This has been utilised in the isomorphous replacement of Ca^{2+} with lanthanide ions in biological media.[52] Therefore it is not surprising that the Eu^{3+} and Ca^{2+} complexes of **(13e)** and **(13f)** behave very similarly in CD. It has been shown through infra-red, ^{13}C NMR and FABMS studies[53] that the K^+ ion does not bind to the amide CO in such tetraamide systems. The corresponding Ln^{3+}, Na^+ and Ca^{2+} complexes all display strong binding which may also account for the observed differences in the CD spectra.

The situation is reversed for ligands and complexes of 1-naphthyl tetraamides **(13c)** and **(13d)**. The europium complexes do not display any excimer formation but the Eu^{3+}, Ca^{2+}, K^{+} and Na^{+} complexes exhibit a bisignate profile typical of strong exciton coupling occurring between adjacent pairs of naphthyl chromophores which are shown to be aligned in the correct orientation from the related crystal structure of the 8 coordinate Na^{+} complex, (Chapter 3.4). Interestingly, the observed exciton-coupled CD for the Ca^{2+}, K^{+} and Na^{+} complexes of **(13c)** and **(13d)** are relatively symmetrical in comparison to the CD spectra for the corresponding Eu^{3+} complexes (**Figure 3.15** and **3.18**). This observation may tentatively be linked to the formation of 8 coordinate C_4 symmetric complexes for the former and a 9 coordinate but slightly distorted C_4 symmetric complex with Eu^{3+}.

The enantiomeric terbium complexes of the tetraphenylamides **(Tb.13a)$^{3+}$** and **(Tb.13b)$^{3+}$** display equal and opposite optical rotations $[\alpha_D]^{20}$ = +104.2 (c = 2.21 in CH_3OH) and $[\alpha_D]^{20}$ = -104.2 (c = 0.14 in CH_3OH) respectively. The complexes exhibit mirror image CD spectra with no evidence of exciton coupling in the wavelength range 190-250 nm (**Figure 3.19**).[32]

3.6.4 Near infrared circular dichroism

The circular dichroism discussed so far is observed in the u.v. region and is due to transitions occurring in the aryl chromophores of the chiral ligand. The extinction coefficient associated with those π–π^* transitions (ε = 200 - 10 000 M^{-1} cm^{-1}) are much greater than those for the lanthanide ions (ε < 1 M^{-1} cm^{-1}). Any CD occurring from the lanthanide will be more difficult to observe, requiring much more concentrated solutions, and has not been studied in this work. However, near infrared circular dichroism (800 - 2000 nm) associated with f-f magnetic dipole allowed electronic transitions is exhibited by several of the lanthanide ions.[54,55] The nature of the near i.r. CD bands is dependent on the crystal field and chiral environment around the lanthanide ion.

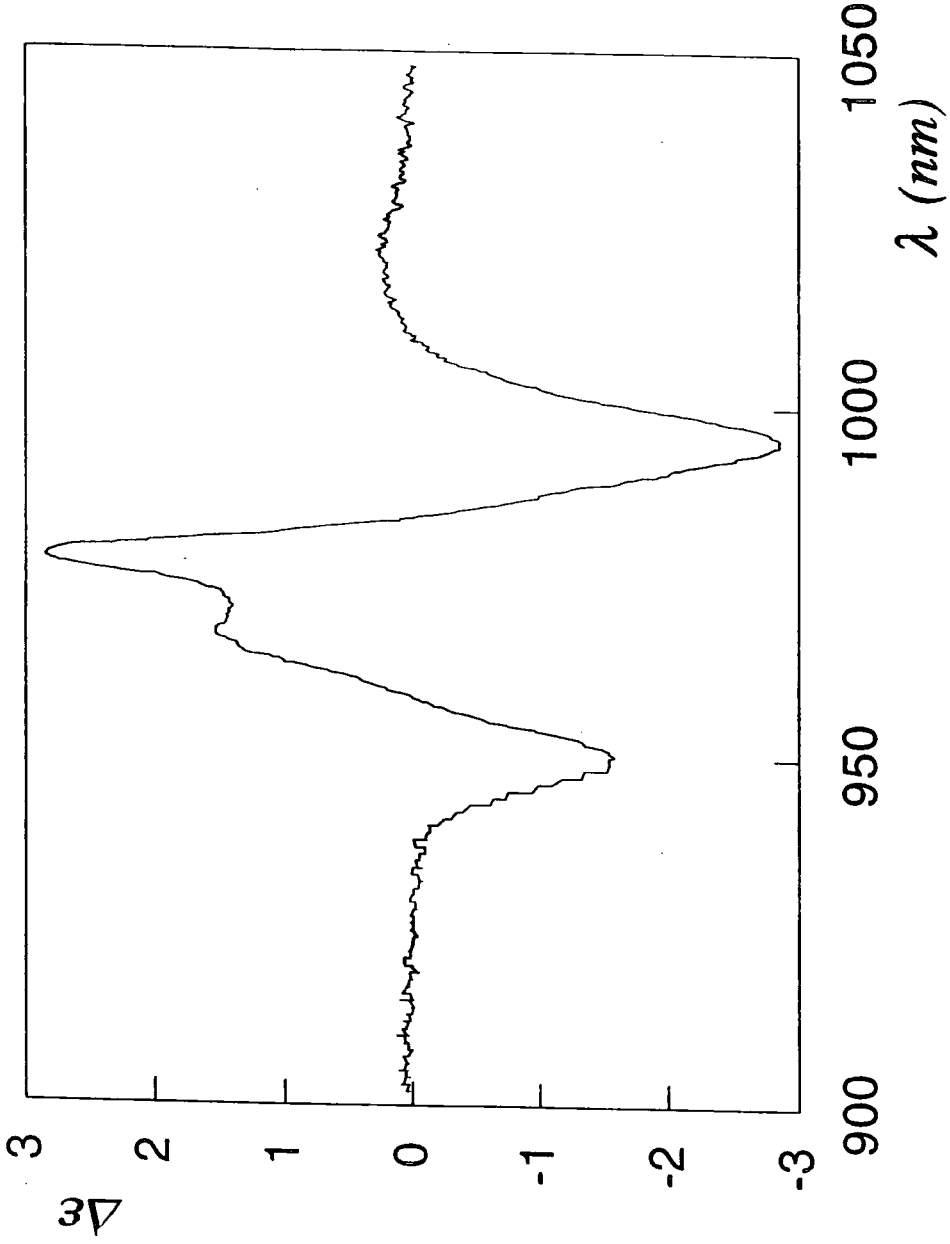

Figure 3.20 *Near infra-red circular dichroism spectrum for* $(Yb.13a)^{3+}$ *(MeOH, 293 K).*

Figure 3.20 shows the near i.r. CD spectrum for **(Yb.13a)$^{3+}$** and is due to the magnetic dipole allowed $^2F_{7/2} \rightarrow {}^2F_{5/2}$ transition occurring around 980 nm. A dissymmetry factor of 0.17 (± 0.08) was calculated for the transition. The transition exhibits rich fine structure which is determined by the ligand crystal field but since little work has been reported to date on C_4 symmetric lanthanide complexes, structural interpretation of the spectra is not yet possible.

3.7 Circularly polarised luminescence

3.7.1 Terbium complexes

Intense circularly polarised emission (**Figure 3.21**) was observed from complexes **(Tb.13a)$^{3+}$** and **(Tb.13b)$^{3+}$** following direct laser excitation of the terbium ion with linearly polarised light (λ_{ex} = 380 nm). The enantiomeric complexes gave rise to mirror image circularly polarised luminescence spectra, and the largest dissymmetry factors were observed for the magnetic dipole transitions $^5D_4 \rightarrow {}^7F_5$ and $^5D_4 \rightarrow {}^7F_3$ where $g_{em}{}^{\lambda\,545} = -0.25$ and $g_{em}{}^{\lambda\,620} = +0.29$ for **(Tb.13a)$^{3+}$**.

Metal based circularly polarised emission was also observed for the complexes **(Tb.13c)$^{3+}$** and **(Tb.13d)$^{3+}$** following indirect sensitisation by u.v. excitation into the proximate naphthyl chromophore (λ_{ex} = 300 nm) (**Figure 3.22**). The solutions were degassed prior to measurement to eliminate the efficient deactivation pathway of the excited state via back energy transfer to the naphthyl triplet state and competitive quenching by molecular oxygen (Chapter 2.4). The strong magnetic dipole character of the $^5D_4 \rightarrow {}^7F_5$ transition gives rise to dissymmetry factors of $g_{em}{}^{\lambda\,544} = +0.17$ and $g_{em}{}^{\lambda\,544} = -0.17$ for **(Tb.13c)$^{3+}$** and **(Tb.13d)$^{3+}$** respectively. Although there have been previous reports of CPL from terbium protein and amino acid complexes following direct excitation[56], the systems described above represent the first examples in which both sets of enantiomers are accessible.

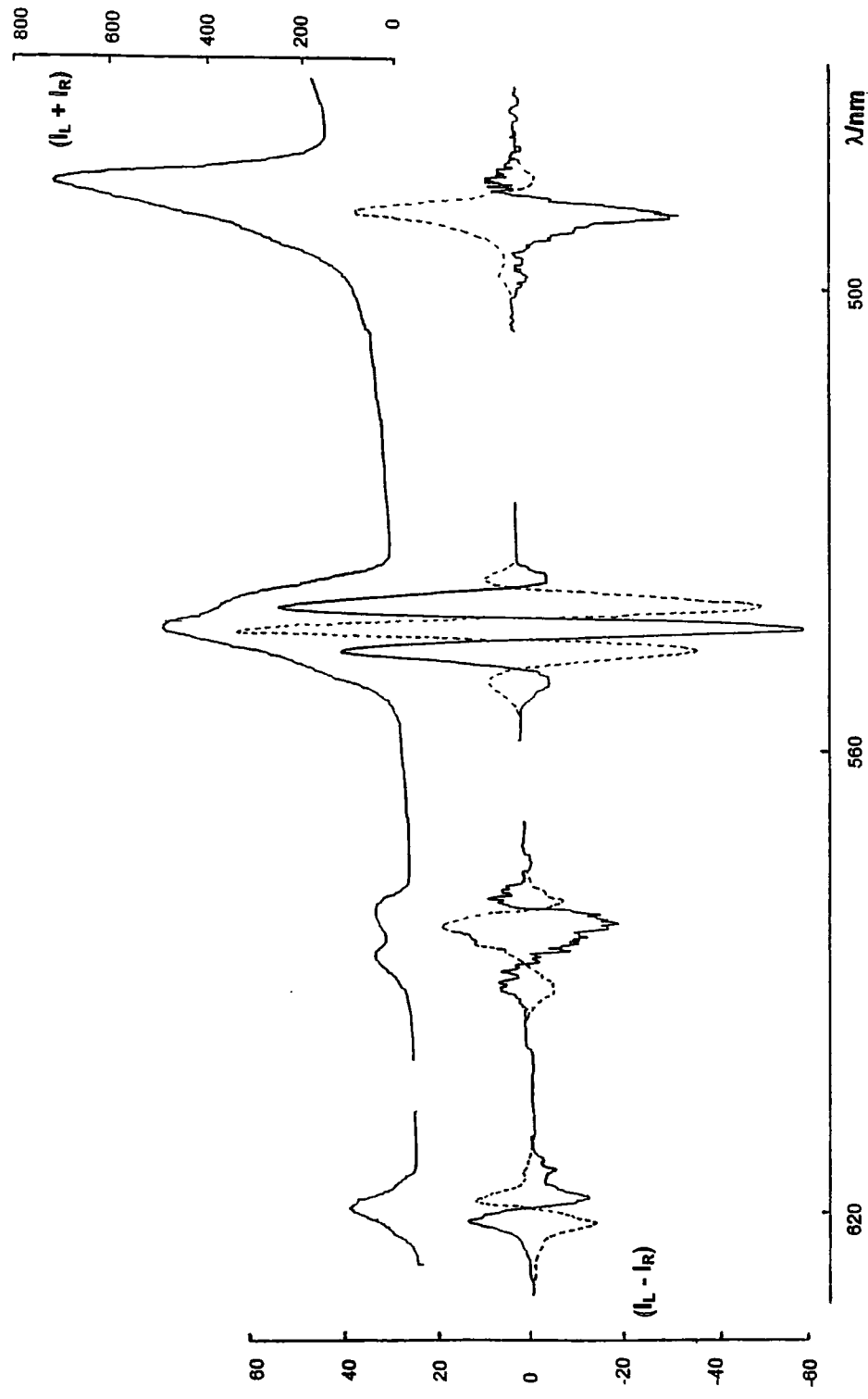

Figure 3.21. *Total emission (upper trace) and circularly polarised emission (lower trace) for* $(Tb.13a)^{3+}$ *(dotted line) and* $(Tb.13b)^{3+}$ *(solid line) following excitation at 380 nm (293 K,* CH_3CN*, 2 x* 10^{-3} *mol* dm^{-3}*).*

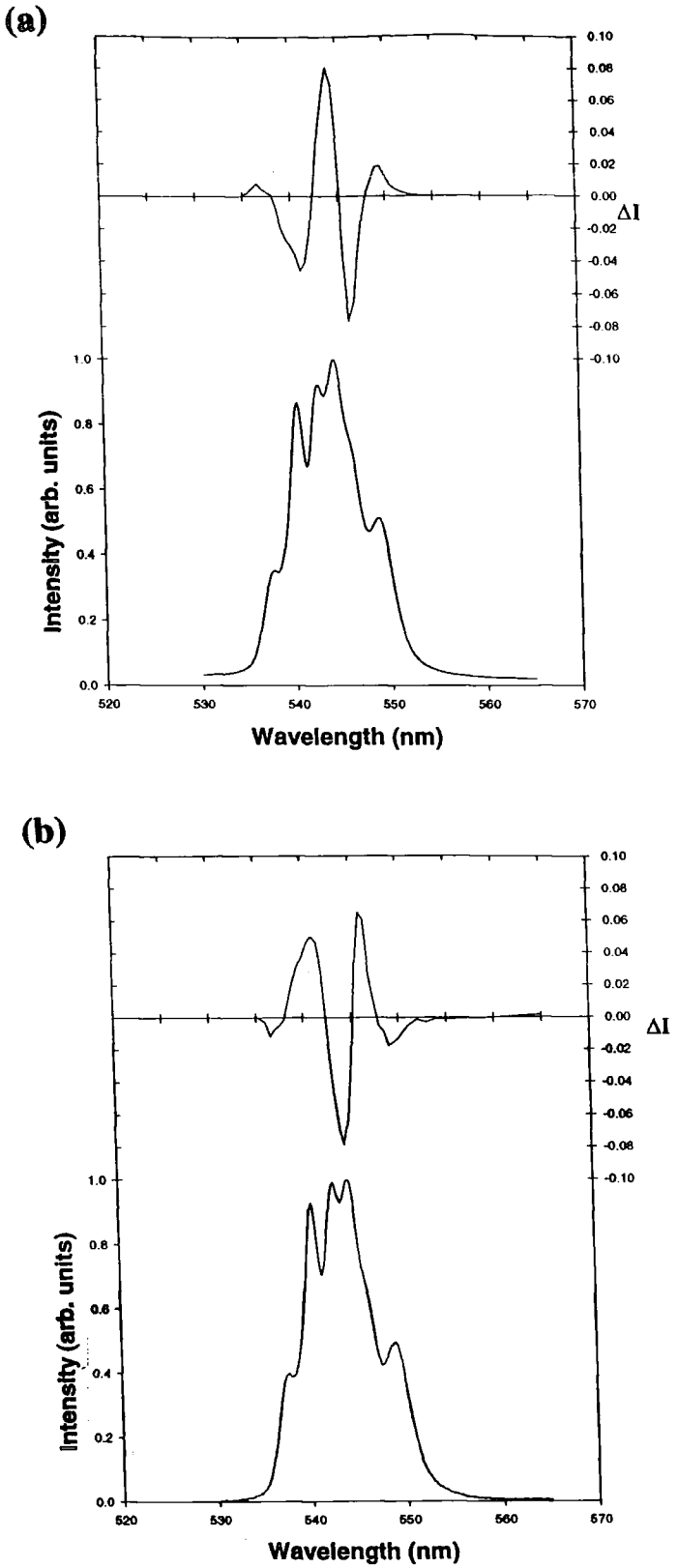

Figure 3.22. *Total emission (lower trace) and circularly polarised emission (upper trace) for* **(a).** $(Tb.13c)^{3+}$ *and* **(b).** $(Tb.13d)^{3+}$ *following excitation at 300 nm (293 K, CH_3CN). The $^5D_4 \rightarrow {}^7F_5$ transitions are shown.*

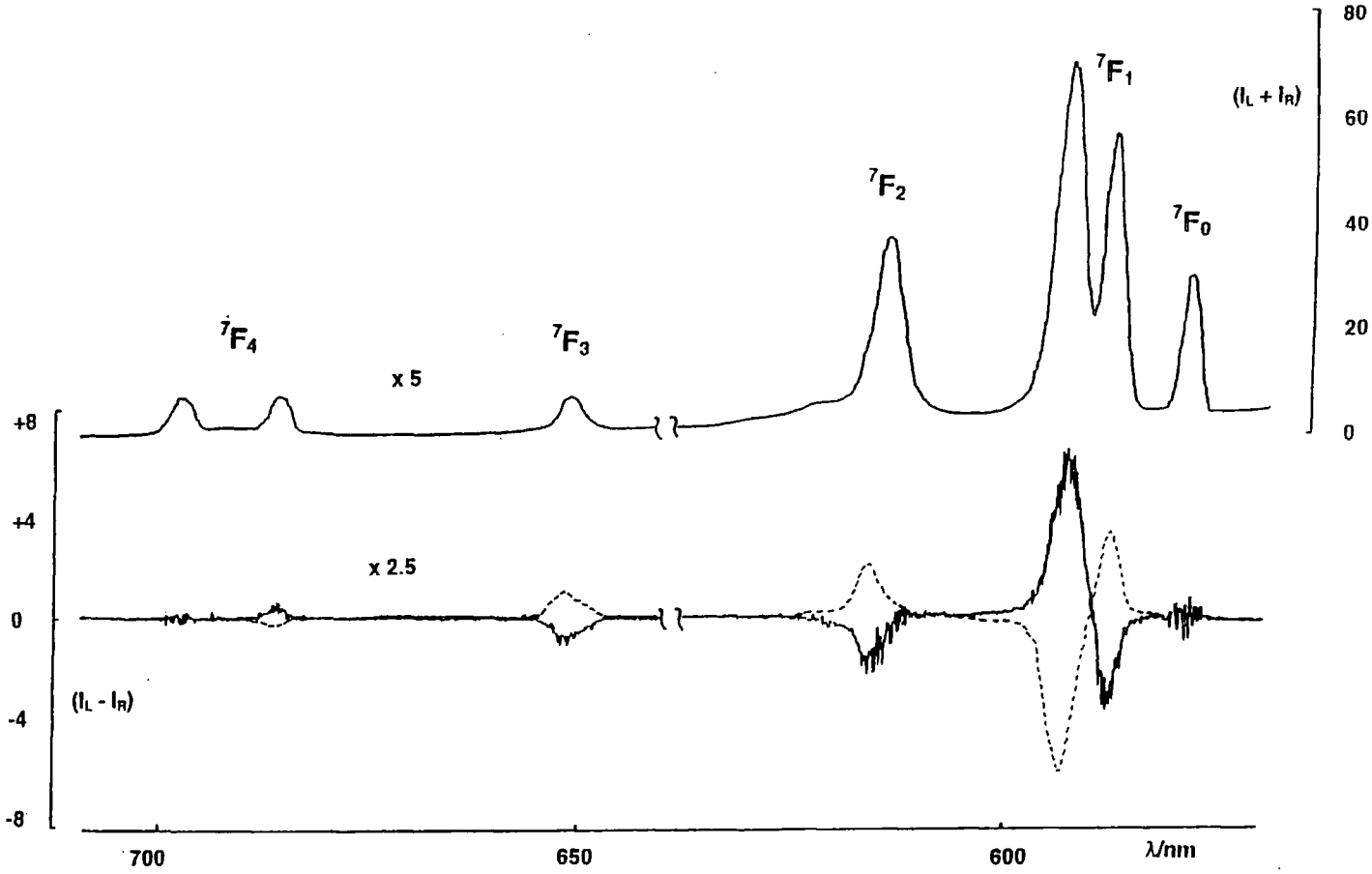

Figure 3.23. *Total emission (upper trace) and circularly polarised emission (lower trace) for* ***(Eu.13c)***$^{3+}$ *(solid line) and* ***(Eu.13d)***$^{3+}$ *(dotted line) following excitation at 395 nm (293 K, CH_3OH, 10^{-2} mol dm^{-3}).*

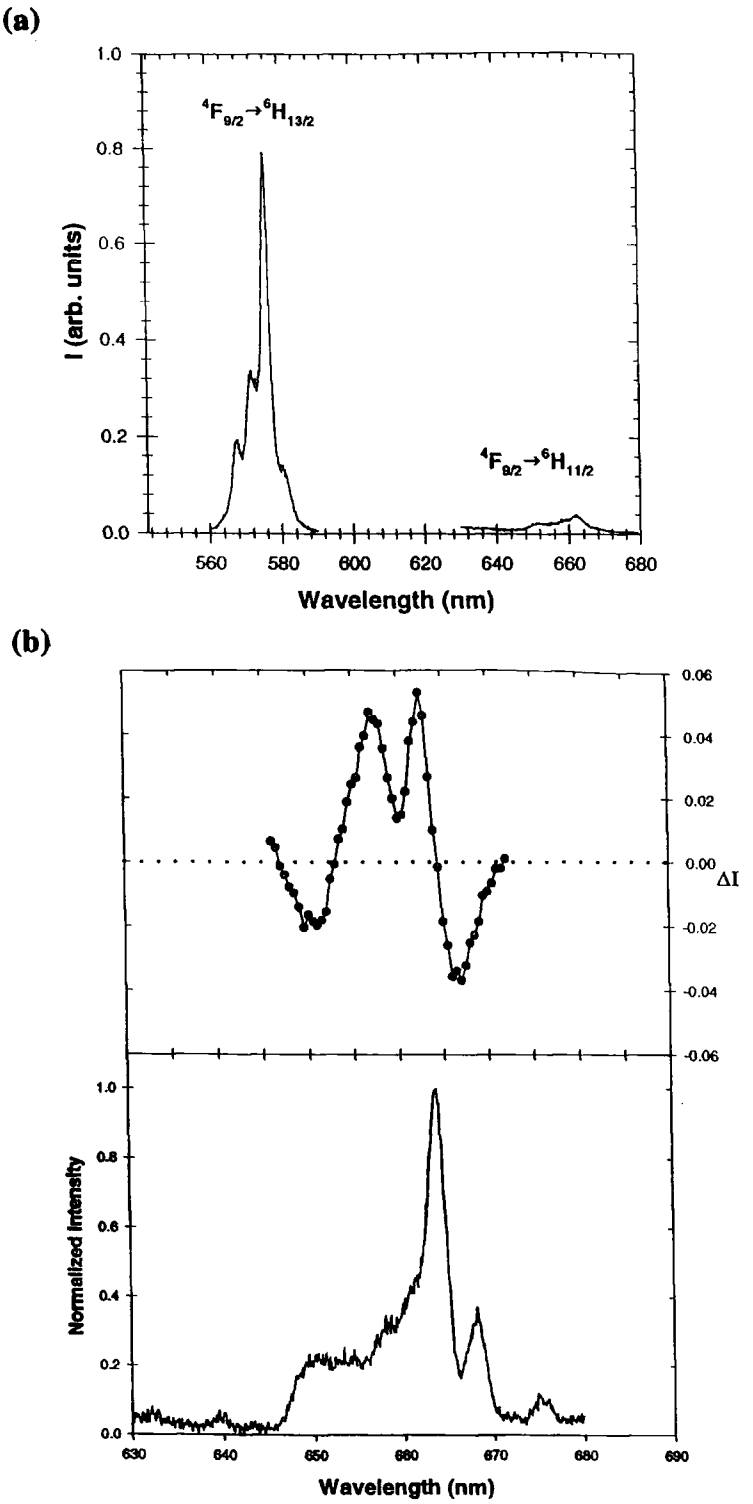

Figure 3.24. **(a).** *Total emission for* $(Dy.13a)^{3+}$ *following excitation at 457.9 nm (293 K).* **(b).** *Total emission (lower trace) and circularly polarised emission (upper trace) for the* $^4F_{9/2} \rightarrow {}^6H_{11/2}$ *transition of* $(Dy.13a)^{3+}$ *following excitation at 457.9 nm (293 K).*

As both the ^7F_J and $^5D_4$ levels are split extensively by ligand crystal fields, a number of components to the transitions arise, resulting in complex circularly polarised emission spectra, the sign and splittings patterns of which are not amenable to detailed interpretation. However, the differential emission intensity generally comprises of several peaks of alternating sign whereas the total emission intensity is often structureless. Therefore terbium CPL spectra may be used to probe the chiral environment around the metal ion and to monitor structural changes.

The observed sign and magnitude of the CPL of the $^5D_4 \rightarrow {}^7F_5$ transition of the tetraphenyl **(Tb.13a)**$^{3+}$ and tetranaphthyl **(Tb.13c)**$^{3+}$ complexes at 545 nm are very similar suggesting that the chiral environment around the terbium ion is not significantly affected by the change in the remote chiral centre, but is determined primarily by the helicity of the pendent arms and/or the configuration of the macrocyclic chelate rings.

3.7.2 Europium complexes

Circularly polarised luminescence from europium complexes is generally much weaker than that observed from corresponding terbium analogues.[57] Indeed, Brittain and Desreux reported that weak CPL is exhibited by the chiral europium complex of **(10)**[58], although no quantitative information was given. Direct excitation of the europium ion at λ_{ex} = 395 nm of the complexes **(Eu.13c)**$^{3+}$ and **(Eu.13d)**$^{3+}$ gave rise to weak CPL spectra which displayed enantiomeric behaviour as expected (**Figure 3.23**).

The degeneracies of the ^7F_J and $^5D_0$ levels of Eu^{3+} ions, caused by the ligand crystal fields, are much reduced compared to Tb^{3+} complexes therefore much simpler spectra are obtained which can be interpreted to yield structural information. The $^5D_0 \rightarrow {}^7F_0$ transition is non-degenerate and a single component is observed in the total emission spectrum. However, for the complexes **(Eu.13c)**$^{3+}$ and **(Eu.13d)**$^{3+}$ there was no observed CPL corresponding to this transition. There are very few examples of CPL corresponding to the forbidden $^5D_0 \rightarrow {}^7F_0$ transition. In general, very weak CPL

($g_{em} < 10^{-4}$) is observed in systems where Eu^{3+} is involved in a dimeric or oligomeric species, possibly undergoing strong metal-metal interactions.[57] The $^5D_0 \rightarrow {}^7F_1$ transition being predominantly magnetic dipole in character, produces the largest dissymmetry factor for europium complexes. The transition displayed two components consistent with a C_4 symmetric complex[48], with relatively large dissymmetry factors of $g_{em}^{\lambda\,593} = +0.18$ and $g_{em}^{\lambda\,588} = -0.12$ for **(Eu.13c)$^{3+}$**. Two components are also predicted for the $^5D_0 \rightarrow {}^7F_2$ transition. However, only one component was observed in both the total emission and circularly polarised emission. These bands were not symmetrical with respect to one another, suggesting that there are indeed two components to the total emission, which are closely spaced, and only one component in the circularly polarised emission. The remaining $^5D_0 \rightarrow {}^7F_3$ and $^5D_0 \rightarrow {}^7F_4$ transitions exhibited weak total emission intensity but did display relatively intense circularly polarised emission with dissymmetry factors $g_{em}^{\lambda\,650} = -0.3$ and $g_{em}^{\lambda\,690} = +0.11$ for **(Eu.13c)$^{3+}$** respectively.

The isomeric 2-naphthyl complexes **(Eu.13e)$^{3+}$** and **(Eu.13f)$^{3+}$** showed essentially identical emission and CPL to the 1-naphthyl analogues **(13c)** and **(13d)** although the quantum yields were lower. This is consistent with the competitive formation of an excimer, as discussed in Chapter 3.5, which provides an alternative deactivation pathway for the excited state through excimer fluorescence, thereby subsequently decreasing the overall metal phosphorescence quantum yield.

3.7.3 Dysprosium complexes

Luminescence arising from Dy^{3+} complexes is generally much weaker than that from corresponding Eu^{3+} and Tb^{3+} complexes.[59] The smaller energy gap of Dy^{3+} (7850 cm^{-1}) compared to Eu^{3+} (12 500 cm^{-1}) and Tb^{3+} (14 800 cm^{-1}) means that deactivation by high energy vibrations of solvent molecules is much more efficient, as discussed in Chapter 1.4. Indeed, Stein and Würzberg[60] reported that efficient energy transfer from the excited state of Dy^{3+} to the $\nu = 3$ vibrational level of H_2O occurs, whereas for Eu^{3+} and Tb^{3+} this energy transfer occurs to $\nu = 4$ and $\nu = 5$ vibrational levels respectively

where the Franck Condon overlap is poorer and therefore energy transfer is less efficient. The smaller energy gap exhibited by Dy^{3+} may also be bridged by other vibrations which accounts for the very short excited state lifetime (τ_{H_2O} = 2.35 μs) reported for the free ion in aqueous solution[60] compared to that of Eu^{3+} (τ_{H_2O} = 110 μs) and Tb^{3+} (τ_{H_2O} = 400 μs).

Weak metal based emission was observed following direct excitation at λ_{ex} = 457.9 nm (**Figure 3.24 (a)**). The strongest emission arose from the $^4F_{9/2} \rightarrow {}^6H_{13/2}$ transition at 576 nm which was shown to be very weakly circularly polarised. The weak $^4F_{9/2} \rightarrow {}^6H_{11/2}$ transition was also apparent at approximately 660 nm but displayed strong circularly polarised emission (**Figure 3.24 (b)**) with dissymmetry factors of $g_{em}{}^{\lambda\,657}$ = +0.35 and $g_{em}{}^{\lambda\,667}$ = -0.41

3.8 Conclusion

In the tetraamide complexes described above, the remote chiral stereocentre determines the layout of the pendent arms and the macrocyclic ring conformation leading to the formation of a single, conformationally rigid enantiomer. The europium and terbium complexes gave rise to striking, well-defined metal-based circularly polarised emission. Strong exciton coupling was observed between adjacent pairs of naphthyl chromophores in the 1-naphthyl complexes of europium whereas the constitutionally isomeric 2-naphthyl complexes underwent excimer formation.

The well defined chiral lanthanide complexes described may be used as a basis for a more rigorous CD and CPL study of the intra- and intermolecular energy transfer processes occurring in related systems. Variation of the substituent around the stereogenic carbon centre (eg. Me vs CO_2R) will enable additional functionalisation and coupling strategies to be employed. For example, coupling to an acridine moiety may provide a method of signalling the binding of the intercalator to DNA, via monitoring the changes in the CD or CPL. Variation of the chiral organic chromophore, with due consideration to the triplet energy and the nature of the bound

lanthanide, will allow excitation at a more favourable longer wavelength to be employed.

References for Chapter 3

1. S. Aime, M. Botta, M. Fasano, M.P.M. Marques, C.F.G.C. Geraldes, D. Pubanz and A.E. Merbach, *Inorg. Chem.*, 1997, **36**, 2059.
2. S. Hoeft and K. Roth, *Chem. Ber.*, 1993, **126**, 869.
3. H.G. Brittain and J.F. Desreux, *Inorg. Chem.*, 1984, **23**, 4459.
4. S.I. Kang, R.S. Ranganathan, J.E. Emswiler, K. Kumar, J.Z. Gougoutas, M.F. Malley and M.F. Tweedle, *Inorg. Chem.*, 1993, **32**, 2912.
5. K.O.A. Chin, J.R. Morrow, C.H. Lake, M.R. Churchill, *Inorg. Chem.*, 1994, **33**, 656.
6. S. Aime, A.S. Batsanov, M. Botta, J.A.K. Howard, D. Parker, K. Senanayake and J.A.G. Williams, *Inorg. Chem.*, 1994, **33**, 4696.
7. A. Beeby, D. Parker and J.A.G. Williams, J. *Chem. Soc., Perkin Trans. 2*, 1996, 1565; D. Parker and J.A.G. Williams, *J. Chem. Soc., Perkin Trans. 2*, 1995, 1305.
8. S. Aime, A. Barge. M. Botta, D. Parker, A.S. de Sousa, J. *Am. Chem. Soc.*, 1997, **119**, 4767.
9. S. Amin, D.A. Voss, W.De W. Horrocks, Jr., C.H. Lake, M.R. Churchill and J.R. Morrow, *Inorg. Chem.*, 1995, **34**, 3294; S. Amin, J.R. Morrow, C.H. Lake and M.R. Churchill, *Angew. Chem., Int. Ed. Engl.*, 1994, **33**, 773.
10. T.J. Swift in 'NMR of Paramagnetic Molecules : Principles and Applications', eds., G.N. LaMar, W.De W. Horrocks, Jr. and R.H. Holm, Academic Press, London, 1973, Chapter 2.
11. W.De W. Horrocks, Jr. and J.P. Sipe III, *Science*, 1972, **177**, 994.
12. D.H. Williams and I. Fleming, 'Spectroscopic Methods in Organic Chemistry', Mc-Graw-Hill Book Company (UK) Limited, 1980, Chapter 3.
13. J. Dale, *Isr. J. Chem.*, 1980, **20**, 3.
14. M. Spirlet, J. Rebizant and J.F. Desreux, *Inorg. Chem.*, 1984, **23**, 359.

15. J.-P. Dubost, M. Leger, M.-H. Langlois, D. Meyer and M. Schaefer, *C.R. Acad. Sci. Paris Ser. 2,* 1991, **312**, 349.

16. D. Parker, K. Pulukkody, A. Batsanov, F. Smith and J.A.K. Howard, *J. Chem. Soc., Dalton Trans,* 1994, 689.

17. D. Parker and J.A.G. Williams, *J. Chem. Soc., Perkin Trans. 2,* 1995, 1305 and 1996, 1581.

18. R.D. Rodgers, A.N. Rollins and M.M. Benning, *Inorg. Chem.,* 1988, **27**, 3826.

19. T. Förster and K. Kasper, *Z. Phys. Chem. (Munich),* 1954, **1**, 275; T. Förster, *Pure Appl. Chem.*, 1962, **4**, 121.

20. S.S. Yanari. F.A. Bovey and R. Lumry, *Nature*, 1963, **200**, 242; F. Hirayama, *J. Chem. Phys.,* 1965, **42**, 3163.

21. S. Ito, M. Yarnamoto and Y. Nishijima, *Bull. Chem. Soc. Jpn.*, 1981, **54**, 35.

22. M. Sisido, S. Egusa, A. Okamoto and Y. Imanishi, *J. Am. Chem. Soc.,* 1983, **105**, 3351 and 4077.

23. J.-C.G. Bünzli in 'Lanthanide Probes in Life, Chemical and Earth Sciences', eds., J.-C.G. Bünzli and G.R. Choppin, Elsevier, Amsterdam, 1989, Chapter 7.

24. S. Aime, M. Botta, D. Parker and J.A.G. Wiliams, *J. Chem. Soc., Dalton Trans.*, 1996, 17.

25. F.S. Richardson, *Chem. Rev.*, 1982, **82**, 541.

26. W.G. Perkins and G.A. Crosby, *J. Chem. Phys.*, 1965, **42**, 407.

27. M.I. Gaiduh, V.V. Grigoryants, A.F. Mironov, V.D. Rumyantseva, V.I. Chissov and G.M. Sukhin, *J. Photochem. Photobiol. B*, 1990, **7**, 15.

28. W. De W. Horrocks, Jr., J.P. Bolender, W.D. Smith and R.M. Supkowski, *J. Am. Chem. Soc.*, 1997, **119**, 5972.

29. A. Beeby, R.S. Dickins, S. Faulkner, D. Parker and J.A.G. Williams, *Chem. Commun.*, 1997, 1401.

30. S. Faulkner, A. Beeby, R.S. Dickins, D. Parker and J.A.G. Williams, *J. Fluorescence,* submitted September 1997.

31. A. Abusaleh and C.F. Meares, *Photochem. Photobiol.*, 1984, **39**, 763.

32. R.S. Dickins, J.A.K. Howard, C.H. Lehmann, J. Moloney, D. Parker and R.D. Peacock, *Angew. Chem., Int. Ed. Engl.*, 1997, **36**, 521.

33. R.S. Dickins, J.A.K. Howard, J. Moloney, D. Parker and R.D. Peacock and G. Siligardi, *Chem. Commun.*, 1997, 1747.

34. S. Aime, A.S. Batsanov, M. Botta, R.S. Dickins, S. Faulkner, C.E. Foster, A. Harrison, J.A.K. Howard, J. Moloney, T.J. Norman, D. Parker, L. Royle and J.A.G. Williams, *J. Chem., Soc., Dalton Trans.*, October 1997.

35. N. Harada, K. Nakanishi, *Acc. Chem. Res.*, 1972, **5**, 257.

36. S.F. Mason, 'Molecular Optical Activity and the Chiral Discrimination', Cambridge University Press, Cambridge, 1982.

37. N. Harada, K. Nakanishi, 'Circular Dichoism Spectroscopy - Exciton Coupling in Organic Stereochemisty', University Science Books, Mill Valley, C.A. 1983.

38. N. Harada, S.L. Chen and K. Nakanishi, *J. Am. Chem. Soc.*, 1975, **97**, 5345.

39. A. Rodger and B. Nordén, 'Circular Dichroism and Linear Dichroism', Oxford University Press, Oxford, 1997, Chapter 5.

40. E.L. Eliel and S.H. Wilen, 'Stereochemistry of Organic Compounds', 1994, Wiley. London, Chapter 13.

41. A.E. Rosenoff, V.K. Walworth and G.R. Bird, *Photogr. Sci. Eng.*, 1970, **14**, 328; G.E. Fischen, J. *Photogr. Sci.*, 1973, **21**, 11.

42. D.G. Whitten, *Acc. Chem. Res.*, 1993, **26**, 502.

43. J.H. Perlstein, 'Electrical Properties of Polymers', ed., D. Seaner, Academic Press, New York, 1982, 59.

44. S. Matile, N. Berova and K. Nakanishi, *J. Am. Chem. Soc.*, 1995, **117**, 7021; A. Harriman, V. Heitz and J.-P. Sauvage, *J. Phys. Chem.*, 1993, **97**, 5940; S. Matile, N. Berova, K. Nakanishi, J. Fleischhauer and R.W. Woody, *J. Am. Chem. Soc.*, 1996, **118**, 5798.

45. H. Lam, S.M. Marcuccio, P.I. Svirskaya, S. Greenberg, A.B.P. Lever, C.C. Leznoff and R.L. Cerny, *Can. J. Chem.*, 1989, **67**, 1087.

46. A.K. Chibisov, G.V. Zakharova, H. Gorner, Y.A. Sogulyaev, I.L. Mushkalo and A.I. Tolmachev, *J. Phys. Chem.*, 1995, **99**, 886.

47. K. Liang, M.S. Farakat, J. Perlstein, K.-Y. Law and D.G. Whitten, *J. Am. Chem. Soc.*, 1997, **119**, 830.

48. A. Osuka and K. Maruyama, *J. Am. Chem. Soc.*, 1988, **110**, 4454.

49. S.F. Mason and B.J. Peart, *J. Chem. Soc., Dalton Trans.*, 1973, 949.

50. A.F. Drake, S.J. Hirst, R. Kuroda and S.F. Mason, *Inorg. Chem.*, 1982, **21**, 533.

51. J.R. Platt, *J. Chem. Phys.*, 1949, **17**, 484.

52. A.D. Sherry and C.F.G.C. Geraldes in 'Lanthanide Probes in Life, Chemical and Earth Sciences', eds. J.-C.G. Bünzli and G.R. Choppin, Elsevier, Amsterdam, 1989, Chapter 4.

53. R. Kataky, K.E. Matthes, P.E. Nicholson, D. Parker and H.J. Buschmann, *J. Chem. Soc., Perkin 2*, 1990, 1425.

54. G. Stein and E.J. Würzberg, *J. Chem. Phys.*, 1975, **62**, 211.

55. R.D. Peacock, *Struct. Bonding (Berlin)*, 1975, **22**, 83.

56. N. Coruh, J.P. Riehl, *Biochemistry*, 1991, **31**, 7970.

57. F.S. Richardson and J.P. Riehl, *Chem. Rev.*, 1977, **77**, 773; 1986, **86**, 1.

58. H.G. Brittain and J.F. Desreux, *Inorg. Chem.*, 1984, **23**, 4459.

59. A. Heller, *J. Mol. Spectrosc.*, 1969, **28**, 208.

60. G. Stein and E. Würzberg, *J. Chem. Phys.*, 1975, **62**, 208.

CHAPTER 4

EFFECT OF ANIONS ON CATIONIC LANTHANIDE COMPLEXES OF TETRA-, TRI- AND DI-AMINE TETRAAZAMACROCYCLES

CHAPTER 4

EFFECT OF ANIONS ON CATIONIC LANTHANIDE COMPLEXES OF TETRA-, TRI- AND DI-AMIDE TETRAAZAMACROCYCLES

4.1 Introduction

There is a great deal of current research interest in the design and synthesis of positively charged or electron deficient, neutral abiotic molecules for the selective reversible binding of anions.[1] Anions play numerous fundamental roles in chemical and biological processes as nucleophiles, bases, redox agents and phase transfer catalysts.[1,2] Exploration of anion complexation abilities may help to understand many phenomena such as the role of anions in membrane transport and phase transfer catalysis, the mechanism of ATP hydrolysis, the genetically engineered exchange of amino acids in a protein, the interaction mechanism of DNA with biologically important polyamines and histones[3] and other reactions of enzymes among which at least two-thirds are mediated by anions.[4]

Anions generally possess varying stoichiometries, geometries and pH dependencies, factors which must be considered in the design of suitable receptors. Selectivity in anion binding is governed by such factors. In particular anion recognition will involve electrostatic and hydrogen bonding interactions and structural aspects such as the shape, size and nucleophilicity of the anions are very important. Since it is difficult to design a receptor system with a positively charged dipole surface (compare, for example, the negative surface of the cation binding cyclic polyethers[5]) a number of recognition features, such as hydrogen bonding sites, must be incorporated along with positively charged or electron deficient binding sites.

4.1.1 Neutral receptors

Neutral anion receptors have been designed that incorporate Lewis acidic binding sites such as boron[6] **(29)**, silicon[7] **(30)**, tin[8] **(31)** and mercury[9] **(32)** but they bind anions only weakly in competitive protic solvents. These molecules lack the possibility of structural variation which is usually the basis for achieving selectivity in complexation. A number of research groups have followed Nature's lead and designed and synthesised neutral anion receptors based on hydrogen bonding interactions alone[10]. Examples include the porphyrinogen systems **(33)**, and when in concert with electrostatic interactions, as found with the functionalised uranyl salene derivatives **(34)**[11], highly specific $H_2PO_4^-$ recognition may be displayed in aprotic media ($K_d < 10^{-5}$ mol dm^{-3} in CH_3CN-DMSO; 99:1).

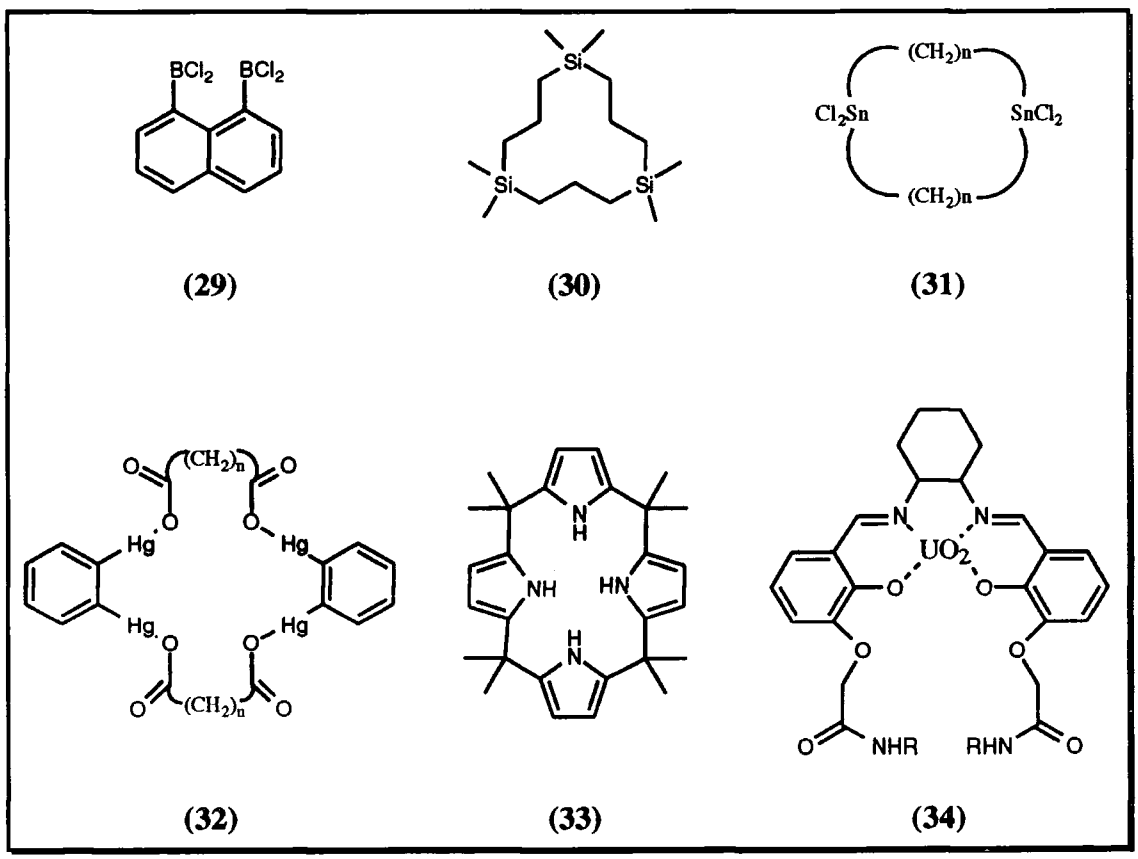

4.1.2 Cationic receptors

Cationic receptors based on quaternary ammonium groups[4,12] **(35)**, guanidinium fragments[13,14] **(36)** and protonated polyamines[15,16,17] **(37)** have been reported and display relatively strong binding but modest selectivity. The chiral guanidinium based

receptor (**36**), represented the first example of enantioselective recognition of an anionic species by an abiotic receptor, exhibiting stability constants of $K_d = 9.5 \times 10^{-4}$ mol dm^{-3} and 1.87×10^{-3} mol dm^{-3} for the L- and D-enantiomers of the triethylammonium salts of *N*-acetyltryptophan.[14] Mono-, bis- and tris-cobaltocenium receptors containing aryl, biaryl and pyridine amide substituents (**38**), have also been shown to exhibit contrasting Cl^- and $H_2PO_4^-$ anion selectivity trends.[18] The relative position of the transition metal Lewis acid centre and CONH-anion binding interactions dictates the receptor-anion thermodynamic stability and selectivity.

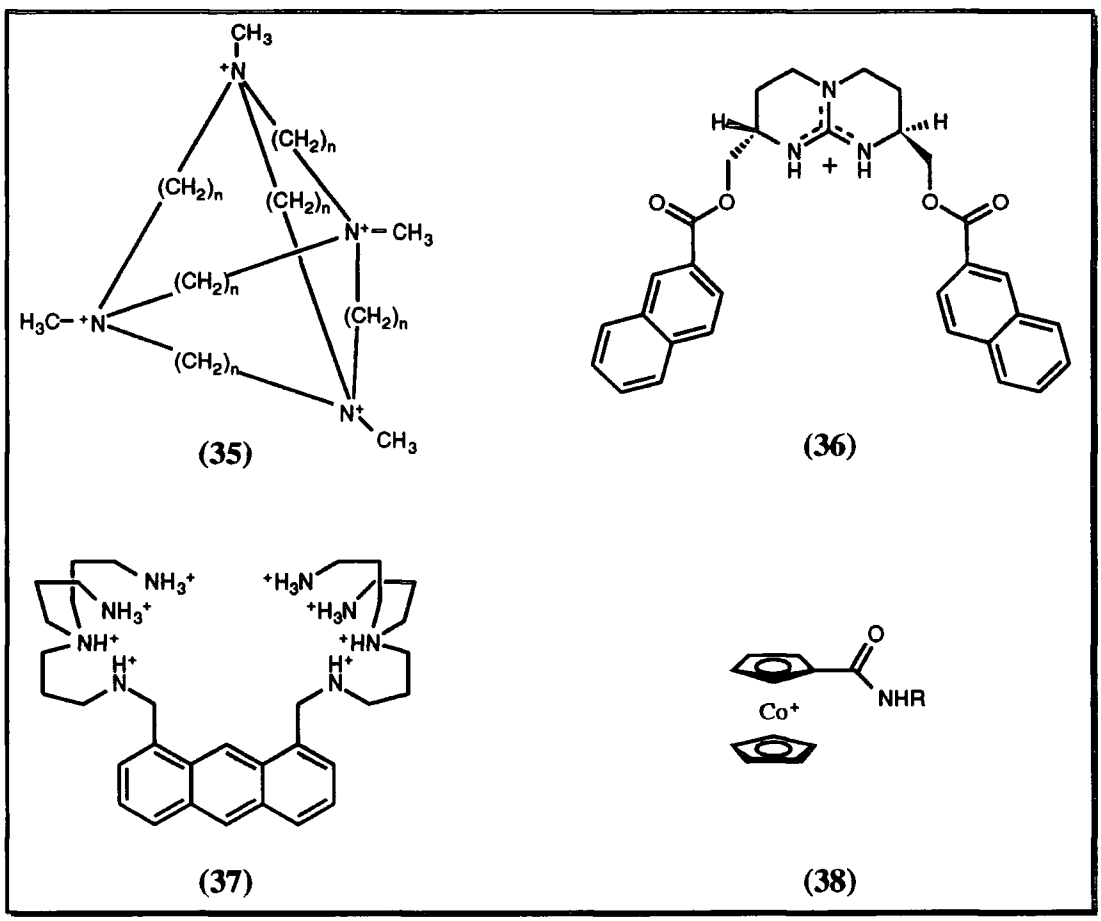

4.1.3 Sensing of anion binding

There are relatively few reported examples of the above systems that have the capability of sensing anions via physical signalling methodologies such as optical[19] and electrochemical techniques.[9] Vance and Czarnik[15,16] reported the use of a fluorescent chemosensor for anions based on an acyclic anthracene appended polyammonium receptor (**37**). Complexation of anions such as phosphate and sulphate resulted in an

enhancement of the fluorescence signal. Lehn has demonstrated that the luminescence lifetime of Eu^{3+} and Tb^{3+} cryptates is increased upon phosphate binding[21]. Ion-pair formation was accomplished by removal of one water molecule from the first coordination sphere of the metal ion, as determined using the Horrock's equation (Chapter 1.4). The first redox responsive class of anion receptors reported were the positively charged cobaltocenium systems described by Beer[22] that were used to 'sense' the bromide ion electrochemically, but only in aprotic media. Binding of anions to chiral systems may be monitored by observing changes in circular dichroism. For example, the metal-centred CD of chiral tris diamine cobalt complexes is perturbed upon ion pairing with oxy-anions such as phosphates.[23]

The concentration of some selected anions in different body fluids are given in **Table 4.1**.[24]

Anion	Serum			Intracellular fluid			Urine		
	max	mean	min	max	mean	min	max	mean	min
Cl^-	110	103	95	76.9	-	-	240	-	120
Br^-	≈0.17	≈0.03	$\approx 9\times10^{-3}$	-	-	-	≈0.11	-	≈0.04
HCO_3^-	26.5	24	21.3	11.9	-	10.9	-	-	-
HPO_4^{2-}	≈1	≈0.5	≈0.3	-	-	-	-	≈18	-
SO_4^{2-}	≈0.5	≈0.3	0.15	-	-	-	-	≈25	-

Table 4.1 *Representative concentrations (mmol dm^{-3}) of selected anions in body fluids.*[24]

The analysis of chloride and bicarbonate ions are most interesting biochemically. Chloride ion channels are involved in the exchange of Cl^- for HCO_3^- anions in erythrocytes. Chloride receptors are of biological interest as the genetic disease cystic fibrosis is implicated when the Cl^- ion channels fail to function properly.[25] There are a number of examples from the literature of selective chloride receptors.[18,26] A selective

bicarbonate sensor that may discriminate from chloride would be advantageous. In clinical practice, the calculation of bicarbonate concentration employs the Henderson-Hasselbach equation[24] (equation (**4.1**)) which requires the measurement of pH and pCO_2. However, this method is rather inaccurate and slow.

$$pH = pK + \frac{\log [HCO_3^-]}{[CO_2]_{dissolved}} \qquad \text{(with pK = 6.35)} \qquad \textbf{(4.1)}$$

4.2 NMR analysis

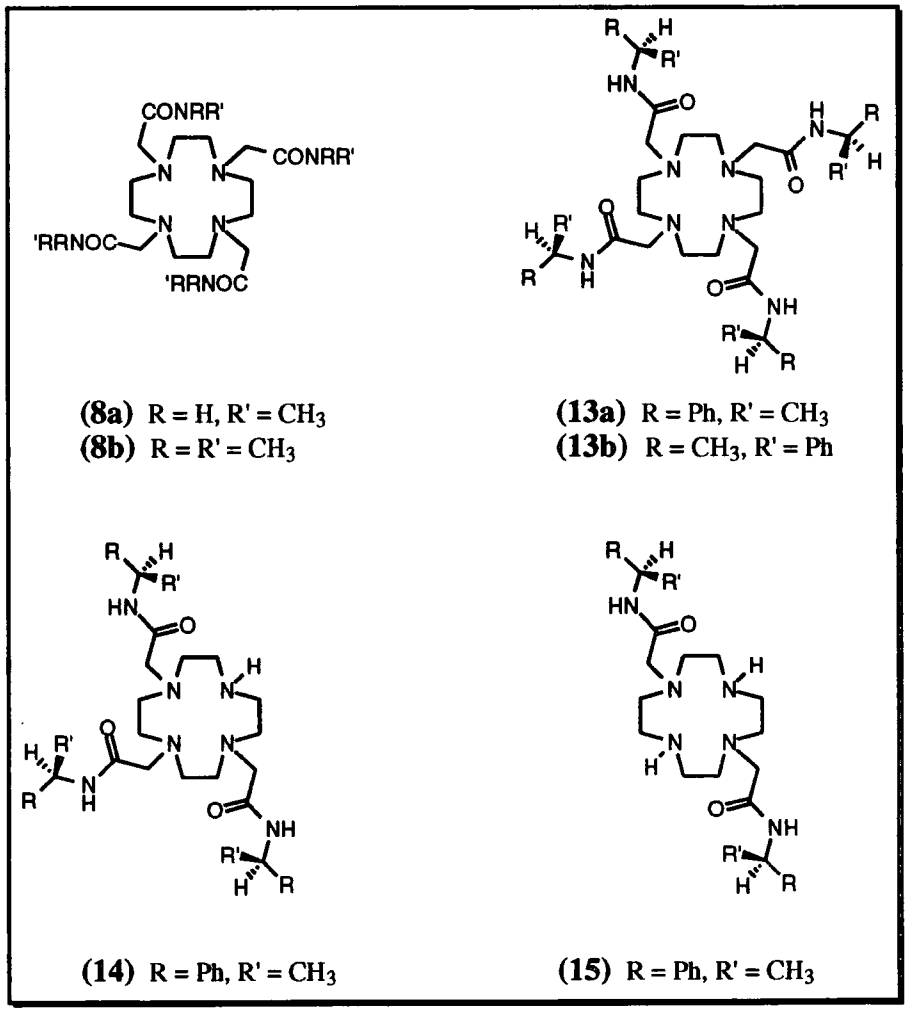

Figure 4.1. *Lanthanide complexes discussed in this chapter.*

The lanthanide complexes of (**8b**) (6 mmol dm^{-3}) have been shown to act as extracellular ^{31}P NMR shift reagents for inorganic phosphate in serum (ca. 1 mmol dm^{-3}), allowing the intra- versus extra-cellular phosphate concentration to be

monitored.[27] The ability of lanthanide complexes of **(13a)**, **(14)** and **(15)** to cause a shift in the appropriate NMR resonances of the anions phosphate, bicarbonate and fluoride upon binding has been studied.

The complexes chosen, possessing one, two or three displaceable water molecules, may afford different ligation possibilities to a given anion. The tetraamide complexes of **(13a)**, may interact with an anion electrostatically, by stabilising hydrogen-bonding interactions or by displacement of the single water molecule. The triamide lanthanide complexes, **(14)**, offer the additional possibility of anion chelation, with the loss of two bound water molecules. Such a tendency might intuitively be expected to be even more pronounced with the lanthanide complexes of the diamide, **(15)**.

The observed chemical shift of an anion bound to a paramagnetic system will be due to diamagnetic, pseudocontact and contact contributions as discussed in Chapter 1.3. For lanthanide ions, the pseudocontact contribution largely predominates as the unpaired electron spin density largely resides on the lanthanide ion. Therefore the electrons in the 4f orbitals are largely shielded from valence orbitals involved in bonding between the metal and ligand. The anion chemical shifts are due mainly to through space interactions which have an inverse dependence on the cube of the distance between the paramagnetic ion and the anion NMR active nucleus.

4.2.1 Effect of phosphate

The effect of incremental addition of the europium complexes of **(Eu.13a)**$^{3+}$, **(Eu.14)**$^{3+}$ and **(Eu.15)**$^{3+}$ on the ^{31}P resonance of the phosphate anion upon binding was monitored and the results are is shown in **Figure 4.2**. In each case the counter anion for the complex was the trifluoromethanesulfonate (triflate) anion, which is weakly nucleophilic compared to the anions under investigation.

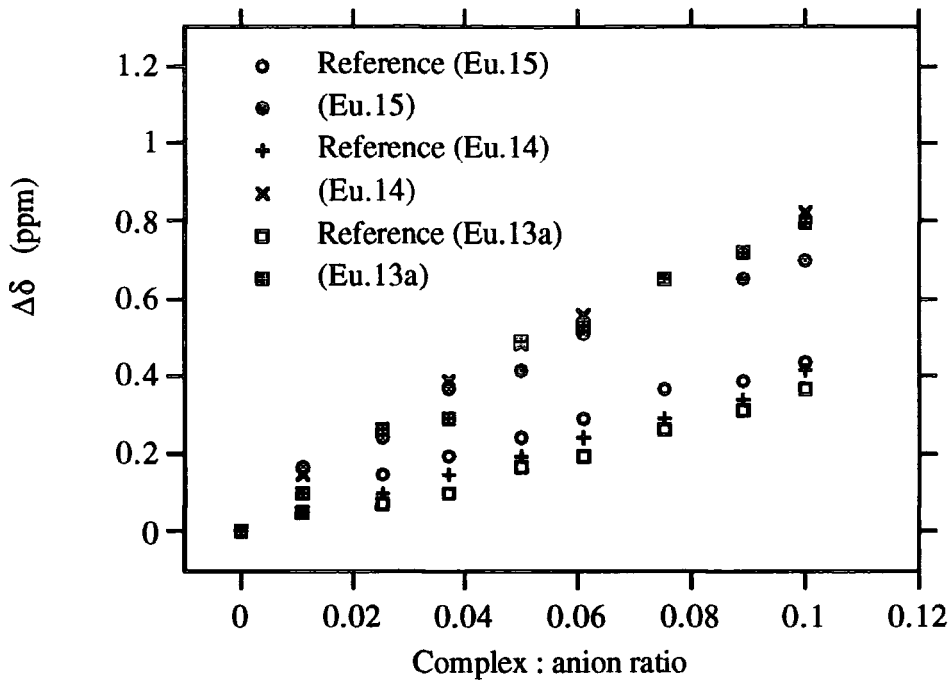

Figure 4.2. *The observed change in the ^{31}P chemical shifts for the phosphate resonance and that of the internal reference Ph_3MePCl (10^{-3} mol dm^{-3}) on addition of complexes* ***(Eu13a)***$^{3+}$, ***(Eu.14)***$^{3+}$ *and* ***(Eu.15)***$^{3+}$ *(H_2O, 293 K).*

The cationic phosphorus internal reference, $Ph_3MeP^+Cl^-$ (10^{-3} mol dm^{-3}) was added to each solution. It served to assess the change in chemical shift due to the variation of the paramagnetic susceptibilty of the solution upon addition of increasing amounts of the lanthanide complex.

Small shifts in the ^{31}P resonance of phosphate were observed on addition of each of the complexes. The complexes **(Eu.13a)**$^{3+}$ and **(Eu.14)**$^{3+}$, with one and two available coordination sites respectively, exhibited very similar shifting abilities, whereas **(Eu.15)**$^{3+}$, with three available coordination sites, appeared to shift the ^{31}P resonance to a slightly lesser extent. Clearly the observed shifts do not depend upon the number of available coordination sites. It was suggested in Chapter 3.3 that complexes of the diamide ligand **(15)** may adopt a tricapped trigonal prismatic geometry whereas complexes of **(13a)** and **(14)** exist in the more compact square antiprismatic form. In the latter complexes, the phosphate anion may approach more closely to the metal

centre thereby reducing the metal-anion distance, which is in accordance with a larger pseudocontact contribution to the observed anion shift, and accounts for the slightly greater shifting abilities observed for **(Eu.13a)**$^{3+}$ and **(Eu.14)**$^{3+}$ compared to **(Eu.15)**$^{3+}$.

Although the corresponding praseodymium complexes behaved similarly, the corresponding dysprosium complexes were also examined but gave rise to a high degree of signal broadening of the anion resonance, which prevented the shifting abilities of the complexes from being analysed accurately.

4.2.2 Effect of bicarbonate

The addition of increasing amounts of **(Eu.14)**$^{3+}$ to a solution containing $NaH^{13}CO_3$ (10 mmol dm^{-3}) was monitored by ^{13}C NMR. No observed effect on the position of the ^{13}C resonance was noted at a complex / anion ratio of 1:10. The bicarbonate anion, with only one negative charge may display a smaller ion-pairing effect than the doubly charged hydrogenphosphate anion. The anion-metal distance will therefore be longer for bicarbonate and hence the pseudocontact contribution will be much smaller, which may account for the lack of any significant shift in the resonance.

4.2.3 Effect of fluoride

Analogous experiments were carried out with F^- and the europium complex, **(Eu.14)**$^{3+}$. The shifting ability of **(Eu.14)**$^{3+}$ on the ^{19}F resonance of fluoride is shown in **Figure 4.3**.

A large change in the chemical shift of fluoride, relative to the internal triflate reference resonance, was observed on addition of the paramagnetic complex **(Eu.14)**$^{3+}$. In this case the resonance under observation is actually due to the nucleus that may be directly bound to the metal centre. Therefore the distance between the metal and the NMR active nucleus is short (ca. 2.4 Å) and a large pseudocontact contribution to the chemical shift may be expected, resulting in a large perturbation to the position of the ^{19}F resonance. In the case of phosphate and bicarbonate, the nucleus under observation

is not directly bound to the metal, and the distance between the NMR active nucleus and the paramagnetic centre is longer (ca. 3.3 Å). The pseudocontact contribution to the observed chemical shift will therefore be smaller than in the case of the directly bound fluoride ion which may account for the much reduced and negligible shifts observed in the presence of phosphate and bicarbonate respectively.

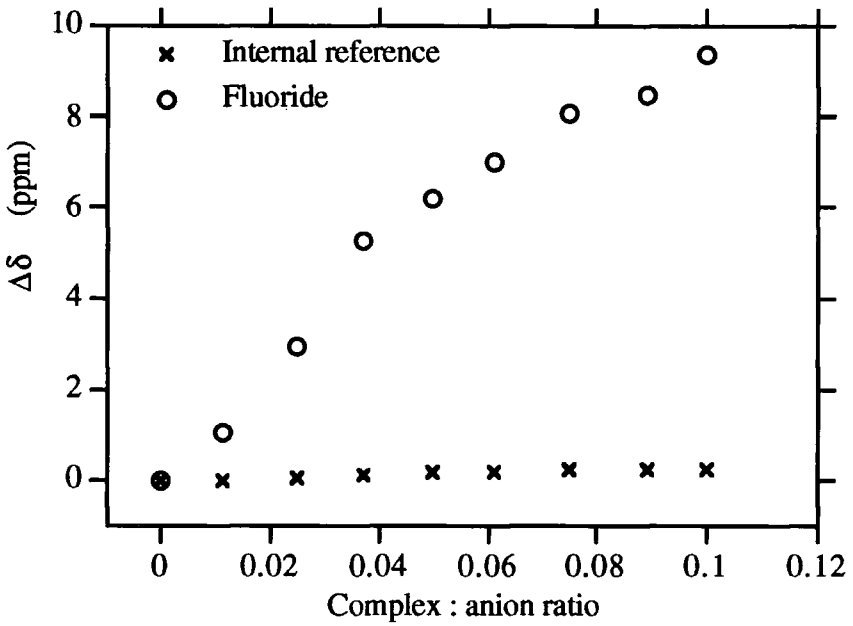

Figure 4.3. *The observed change in the ^{19}F shifts of fluoride and the internal triflate reference in the presence of* ***(Eu.14)***$^{3+}$.

4.3 Lanthanide luminescence

4.3.1 Lifetimes

The luminescence intensity and lifetime of lanthanide complexes may be influenced by solvent molecules and other species that are able to enter into the first coordination sphere of the metal ion. For example, an increase in the luminescence lifetime has been observed upon the addition of fluoride[28] and phosphate[21] anions to europium and terbium [2.2.1] cryptates, caused by the displacement of some coordinated water molecules.

The luminescence lifetimes of europium and terbium complexes of **(13a)**, **(14)** and **(15)** have been measured in H_2O and D_2O in the absence and presence of a ten-fold excess of selected halide and oxy-anions (**Table 4.2** and **4.3**). As discussed in Chapter 1.4, the lifetime of the excited state in H_2O is significantly reduced by the presence of XH oscillators which provide additional deactivation pathways.

$$k_{obs}^{H2O} = k_{nat} + k_{nr} + \Sigma k_{XH} \qquad (4.2)$$

where k_{nat} is the radiative rate constant, k_{nr} is the rate constant for non-radiative deactivation and Σk_{XH} is the sum of the rate constants for energy transfer to proximate energy matched XH oscillators.

The corresponding XD oscillators are much less efficient at deactivation and their contribution to the observed rate constant in D_2O may be neglected.

$$k_{obs}^{D2O} = k_{nat} + k_{nr} \qquad (4.3)$$

Therefore $$\Delta k = k_{obs}^{H2O} - k_{obs}^{D2O} = \Sigma k_{XH} \qquad (4.4)$$

The corresponding number of coordinated water molecules, q, has been estimated using the Horrock's equation[29] (equation **(4.5)**).

$$q = A_{Ln} \Delta k \qquad (4.5)$$

A_{Ln} is a proportionality constant specific to the Ln ion where $A_{Eu} = 1.05$ and $A_{Tb} = 4.2$.

A correction has been made to the data presented in **Tables 4.2** and **4.3** to allow for the contribution due to closely diffusing water OH and amide NH oscillators[30], q_{corr}.

complex / anion	pH	τ_{H_2O} ms	τ_{D_2O} ms	k_{H_2O} $(ms)^{-1}$	k_{D_2O} $(ms)^{-1}$	Δk $(ms)^{-1}$	ΣOH s^{-1}	ΣNH s^{-1}	$\Delta k'$ $(ms)^{-1}$	Δk_{corr} $(ms)^{-1}$	q_{corr}
(Eu.8d)$^{3+}$	5.5	0.63	1.85	1.60	0.54	1.06	1060	-	1.06	0.99	1.0
(Eu.8b)$^{3+}$	5.5	0.55	2.13	1.82	0.47	1.35	1060	292	1.06	0.99	1.0
(Eu.13a)$^{3+}$	5.5	0.58	2.44	1.72	0.41	1.31	1018	292	1.02	0.95	1.0
(Eu.14)$^{3+}$	5.5	0.26	0.65	3.85	1.54	2.31	2091	219	2.09	1.90	2.0
CO_3^{2-}	11	0.43	0.61	2.33	1.64	0.69	471	219	0.47	0.28	0.29
HCO_3^-	6.5	0.41	0.60	2.44	1.67	0.77	551	219	0.55	0.36	0.38
HPO_4^{2-}	7.5	0.38	0.65	2.63	1.54	1.09	871	219	0.87	0.68	0.71
SO_4^{2-}	5.5	0.34	0.60	2.94	1.67	1.27	1051	219	1.05	0.86	0.90
F^-	5.5	0.37	0.72	2.70	1.39	1.31	1091	219	1.09	0.90	0.95
$CH_3CO_2^-$	5.5	0.29	0.59	3.45	1.69	1.76	1541	219	1.54	1.35	1.42
(Eu.15)$^{3+}$	5.5	0.17	0.35	5.88	2.86	3.02	2874	146	2.87	2.85	3.0
SO_4^{2-}	5.5	0.22	0.34	4.47	2.94	1.53	1384	146	1.38	1.36	1.42
HCO_3^-	6.5	0.24	0.38	4.17	2.63	1.54	1374	146	1.39	1.37	1.44
HPO_4^{2-}	7.5	0.24	0.41	4.22	2.44	1.78	1584	146	1.63	1.61	1.64
F^-	7.5	0.25	0.44	4.07	2.26	1.81	1664	146	1.66	1.64	1.72
$CH_3CO_2^-$	5.5	0.21	0.34	5.12	2.95	2.17	2.24	146	2.02	2.0	2.10

Table 4.2 *Effect of added anions (10 mmol dm^{-3}) on the lifetime of the excited state of europium complexes of (13a), (14) and (15) (1 mmol dm^{-3} in complex, 293 K) and the corrected hydration numbers, q_{corr}. Errors on k values are ≤5%.*

Balzani and coworkers[31] previously showed that the europium bound amine NH group of a tetraazacyclododecane ring does not undergo H/D exchange under ambient conditions. NH/ND Exchange did occur on heating a sealed D_2O solution of the complex at 70 °C for 5 days. By comparison of the rate constants in D_2O for the deactivation of the excited state, k_{D_2O}, for **(Eu.13a)$^{3+}$** (k_{D_2O} = 0.41 $(ms)^{-1}$), **(Eu.14)$^{3+}$** (k_{D_2O} = 1.54 $(ms)^{-1}$) and **(Eu.15)$^{3+}$** (k_{D_2O} = 2.86 $(ms)^{-1}$), where deactivation pathways due to exchangeable XH oscillators are eliminated, the quenching contribution due to

coupling via the macrocyclic ring NH vibrations (≈ 3300 cm^{-1}) can be assessed. The ring NH contribution to Δk is estimated to be approximately 1000 s^{-1} for europium complexes which is consistent with the value predicted by Balzani[31]. This is approximately double that for the estimated contribution to Δk due to the quenching effect of bound OH oscillators (≈ 475 s^{-1}). Quenching by the amine NH oscillator in the corresponding terbium complexes is much smaller, of the order of 100 s^{-1}, which is consistent with the less efficient deactivation for Tb^{3+} compared to Eu^{3+} complexes due to the larger energy gap for the former, as discussed in Chapter 1.4.

Europium complexes

The excited state lifetimes in H_2O and D_2O for the europium complexes of **(13a)**, **(14)** and **(15)** are reported in **Table 4.2** along with an estimate of the number of coordinated water molecules, q. As discussed in Chapter 2.4, closely diffusing OH and NH oscillators provide efficient deactivation pathways for the Eu^{3+} and Tb^{3+} ions which are absent in D_2O. Therefore Δk values represent a sum of the contributions from XH oscillators and, as a result, the apparent q values will be higher than expected. By comparison of the Δk value for the complex **(Eu.8d)**$^{3+}$, possessing no amide NH, to that for **(Eu.8b)**$^{3+}$, possessing four, the contribution due to each amide NH oscillator may be estimated to be ≈ 73 s^{-1}. Assuming that this amide quenching contribution remains the same in the europium complexes **(Eu.13a)**$^{3+}$, **(Eu.14)**$^{3+}$ and **(Eu.15)**$^{3+}$, the effect of amide oscillator quenching to the measured Δk may be partitioned to give Δk', and hence allowed for in the subsequent determination of the hydration state, q'. The q' values for the tetra- **(Eu.13a)**$^{3+}$ (q' = 1.07), tri- **(Eu.14)**$^{3+}$ (q' = 2.20) and diamide **(Eu.15)**$^{3+}$ (q' = 3.02) complexes suggest that the complexes have one, two and three bound water molecules respectively. The observed q' values are a little higher than expected due to contributions from closely diffusing water molecules. These contributions may also be partitioned out by assuming that each bound water molecule contributes ≈ 950 s^{-1} to Δk, thereby giving rise to contributions of 68, 191 and 24 s^{-1} for **(Eu.13a)**$^{3+}$, **(Eu.14)**$^{3+}$ and **(Eu.15)**$^{3+}$ respectively, and the corrected Δk_{corr} value which allows the determination of the corrected hydration state, q_{corr}.

The lifetime of the excited state of the chiral tetraamide complex **(Eu.13a)$^{3+}$** (10^{-3} mol dm^{-3} in H_2O, 293 K) was not affected by the addition of a ten-fold excess of anions such as phosphate, fluoride and hydroxide. However, as shown in **Table 4.2**, the lifetimes of the excited states of **(Eu.14)$^{3+}$** and **(Eu.15)$^{3+}$** were greatly affected by the presence of a variety of oxy-anions and halides. Assuming the contribution to Δk due to amide NH and closely diffusing OH oscillators to be $3 \times 73 + 191 = 410$ s^{-1} for **(Eu.14)$^{3+}$** , an estimation of the number of bound water molecules, q_{corr}, in the presence of anions may be made. At a concentration of 10^{-2} mol dm^{-3}, acetate, sulphate and fluoride appeared to displace one of the quenching water molecules in the europium complex (10^{-3} mol dm^{-3}) whereas bicarbonate and carbonate replaced both of the bound water molecules leading to a large observed change in the measured lifetime.

For the complex **(Eu.15)$^{3+}$**, the Δk contributions due to amide NH and closely diffusing water OH oscillators are essentially $\approx 2 \times 73 + 24 = 170$ s^{-1}. Displacement of one bound water molecule was observed on addition of all the anions.

Terbium complexes

The excited state lifetimes in H_2O and D_2O for the terbium complexes of **(13a)**, **(14)** and **(15)**, reported in **Table 4.3**, suggest that there are one, two and three water molecules bound to the Tb^{3+} ion respectively. The quenching effect of unbound XH oscillators in the deactivation of the excited state is much less pronounced for Tb^{3+} compared to Eu^{3+} (as discussed in Chapter 1.4) and is estimated to account for ≈ 40 s^{-1} to Δk. The corrected Δk_{corr} values and subsequent determination of the corrected hydration number, q_{corr}, are given in **Table 4.3**.

The excited state lifetime of the tetraamide complex **(Tb.13a)** was not affected by the addition of a ten-fold excess of anions such as phosphate, fluoride and hydroxide, consistent with the behaviour of the europium complexes. The effect of the addition of oxy-anions and halides to **(Tb.14)$^{3+}$** also mirrored that of the corresponding europium

complexes, with displacement of one bound water molecule observed in the presence of phosphate, fluoride, sulphate and acetate. The lifetime of **(Tb.14)$^{3+}$** was not affected by the presence of iodide and nitrate whereas on addition of carbonate and bicarbonate displacement of both bound water molecules was observed.

complex / anion	pH	τ_{H_2O} ms	τ_{D_2O} ms	k_{H_2O} $(ms)^{-1}$	k_{D_2O} $(ms)^{-1}$	Δk $(ms)^{-1}$	Δk_{corr} $(ms)^{-1}$	q_{corr}
(Tb.13a)$^{3+}$	5.5	1.74	3.45	0.57	0.29	0.28	0.24	1.0
(Tb.14)$^{3+}$	5.5	1.19	2.59	0.84	0.39	0.45	0.41	1.7
CO_3^{2-}	11	1.88	2.17	0.53	0.46	0.07	0.03	0.13
HCO_3^-	6.5	1.84	2.21	0.54	0.45	0.09	0.05	0.21
OH^-	12	1.76	2.16	0.57	0.43	0.14	0.10	0.42
citrate	5.5	1.81	2.41	0.55	0.41	0.14	0.10	0.42
HPO_4^{2-}	7.5	1.74	2.68	0.57	0.37	0.2	0.16	0.67
F^-	5.5	1.64	2.76	0.61	0.36	0.25	0.21	0.88
SO_4^{2-}	5.5	1.51	2.70	0.66	0.37	0.29	0.25	1.05
$CH_3CO_2^-$	5.5	1.36	2.41	0.74	0.41	0.33	0.29	1.22
NO_3^-	5.5	1.19	2.40	0.84	0.42	0.42	0.38	1.60
I^-	5.5	1.15	2.56	0.87	0.39	0.48	0.44	1.85
(Tb.15)$^{3+}$	5.5	0.89	2.13	1.12	0.47	0.65	0.61	2.6
HPO_4^{2-}	7.5	1.44	2.28	0.69	0.44	0.25	0.21	0.88
HCO_3^-	6.5	1.24	1.93	0.81	0.52	0.29	0.25	1.05
F^-	5.5	1.28	2.28	0.78	0.44	0.34	0.30	1.26
SO_4^{2-}	5.5	1.09	2.23	0.92	0.45	0.47	0.43	1.81
$CH_3CO_2^-$	5.5	1.02	2.02	0.98	0.50	0.48	0.44	1.85
I^-	5.5	0.91	2.05	1.10	0.49	0.61	0.57	2.40

Figure 4.3. *Effect of added anions (10 mmol dm^{-3}) on the lifetime of the excited state of terbium complexes of* ***(13a)***, ***(14)*** *and* ***(15)*** *(1 mmol dm^{-3}, 293 K) and the hydration number, q. Errors on k values are ≤5%.*

The complexes used in the measurement were the triflate salts and a control experiment was undertaken to assess the effect of the triflate counter ion by preparing the corresponding chloride salt by anion exchange. Chloride was chosen as the anion does not affect the excited state lifetime of the complex. Addition of a ten fold excess of the triflate anion to the chloride salt of **(Tb.14)**$^{3+}$ resulted in no measurable change in the excited state lifetimes.

For **(Tb.15)**$^{3+}$, addition of fluoride and bicarbonate appeared to displace two bound water molecules whereas sulphate and acetate displaced just one, and iodide had no observed effect.

Tetraamide summary

The lifetimes of the excited states of europium and terbium complexes of the tetraamide **(13a)** were not affected by the presence of added anions. The crystal structure of **(Eu.13a)**$^{3+}$ (Chapter 3.4) reveals that the hydrogen atoms of the lanthanide bound water molecule are engaged in hydrogen bonding interactions with the oxygen atoms of the proximate triflate counterions. This stabilising interaction coupled with the steric demand at the metal centre may account for the lack of displacement of the bound water molecule upon addition of anions, and subsequently no apparent change in the lifetime of the excited state.

Triamide summary

The size and geometry of the anion will determine its binding capabilities. For example, urea appended porphyrins bind spherical chloride anions strongly ($K_d < 10^{-5}$ mol dm^{-3}, DMSO, 293 K) and selectively over trigonal nitrate and tetrahedral phosphate anions (10^{-3}-10^{-2} : 1).[26] The coordinative unsaturated europium and terbium complexes of **(14)** have 2 available sites for anion coordination. Bicarbonate and carbonate appeared to displace both of the metal bound water molecules. The formation of a bidentate adduct, as depicted in **Scheme 4.1**, where chelation involves attack by a lanthanide bound OH group at the trigonal carbonyl centre, may account for

this observation. The mechanism closely resembles that of the mode of action of the zinc enzyme carbonic anhydrase in the hydrolysis of carbon dioxide to bicarbonate.[32] The excited state lifetimes in the presence of bicarbonate and carbonate are very similar suggesting the formation of the same chelated species upon binding. The slightly higher k value observed for HCO_3^- in H_2O may be accounted for by the presence of the proximate OH oscillator.

Support for a such a mechanism may be obtained from isotope incorporation experiments. The incorporation of ^{18}O into HCO_3^-, from an $^{18}OH_2$ solution of the europium complex in the presence of bicarbonate was studied by ESMS. Unfortunately, the peak due to $[MLOH]^{2+}$ species dominated the spectrum and no conclusive evidence for the incorporation of ^{18}O into the bicarbonate could be obtained. The ESMS experiment requires a sample of concentration of $\leq 10^{-4}$ mol dm^{-3}, and at this dilution, there is not expected to be a significant concentration of the anion-ligated species unless the effective binding constant for anion association is $\geq 10^3$.

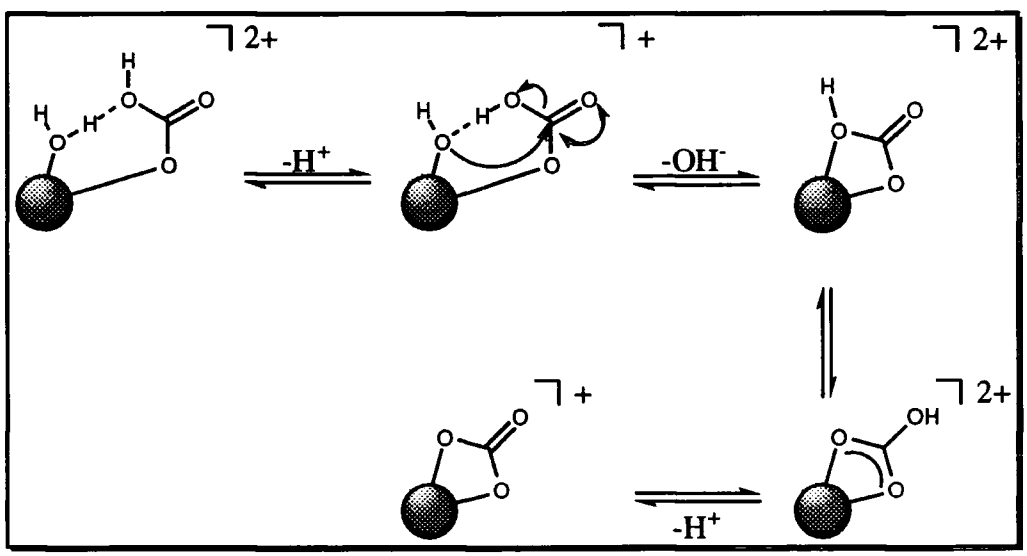

Scheme 4.1. *Possible mechanism for the bidentate chelation of bicarbonate.*

It appears that a trigonal anion is favoured for this bidentate binding. However, trigonal nitrate and acetate anions displaced only one of the bound water molecules. These anions cannot participate in the suggested mechanism for bidentate binding shown in **Scheme 4.1** due to the absence of a leaving group at the trigonal centre.

In general, the binding ability of an anion at a metal centre depends on a number of factors. The free energy of anion hydration (Hofmeister series)[33],

$$CF_3SO_3^- < I^- < NO_3^- < CH_3CO_2^- < SO_4^{2-} < HPO_4^{2-}$$

is important and complex formation will be energetically unfavourable for species such as HPO_4^{2-} because of loss of this hydration energy. Nucleophilicity or σ-donor ability plays an important role. This may be semi-quantitatively related to the pKa of the conjugate acid so that nitrate and sulphate are poor σ-donors, whereas phosphate and carbonate are much better. Hydrogen bonding may stabilise the binding interactions with the anion acting either as a H-bonding donor (eg. HPO_4^{2-}) or acceptor (eg. Cl^-) to proximate ligand based acceptors and donors (eg. amide CONH groups).

Further support for the distinctive nature of the carbonate adducts is provided from the europium emission spectra. As discussed in Chapter 1.4 and 2.4, the $\Delta J = 2$ transition occurring at 620 nm is highly sensitive to the coordination environment around the metal.[35] The europium emission spectra of **(Eu.14)$^{3+}$** is shown in **Figure 4.4** in the absence and presence of a ten-fold excess of phosphate, fluoride and bicarbonate anions.

The concentrations of the individual solutions were different for each anion, therefore comparison of the absolute intensities of the observed bands may not be performed. However, the relative intensities of the $\Delta J = 2 : \Delta J = 1$ band in the presence of different anions are independent of concentration and may be assessed to yield information on the environment around the lanthanide ion. The intensity ratios of the $\Delta J = 2 : \Delta J = 1$ bands were 4:1 for bicarbonate, 4:3 for fluoride and 2:1 for phosphate suggesting that the europium ion in the bicarbonate adduct does indeed have a different coordination environment compared to the situation in the presence of the other anions.

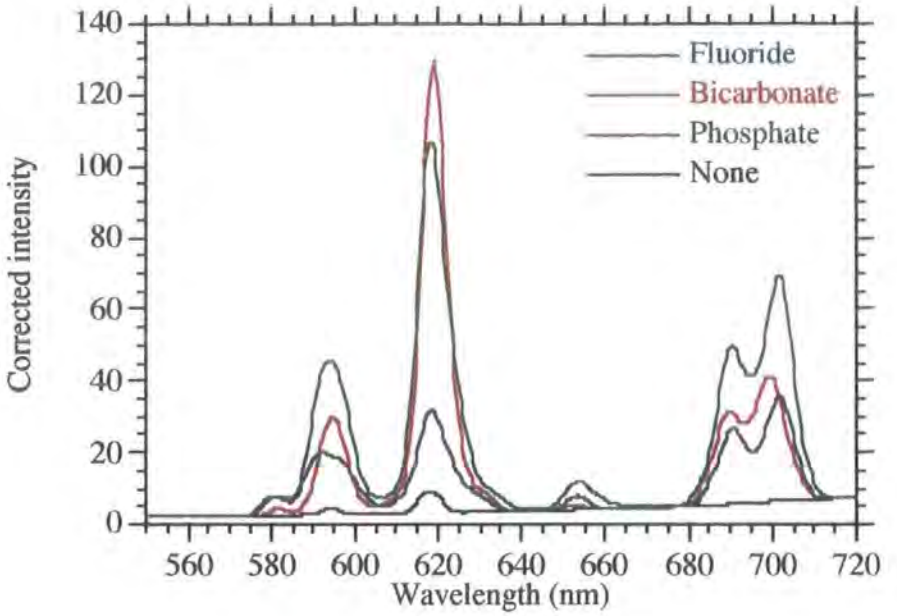

Figure 4.4. *Corrected phosphorescence emission spectra for* $(\mathbf{Eu.14})^{3+}$ *(1 mmol dm*$^{-3}$*, 293 K) in the absence and presence of a ten-fold excess of fluoride, bicarbonate and phosphate, following excitation at 254 nm.*

Diamide summary

There are three available sites for coordination in the diamide complexes of **(15)**. For $(\mathbf{Eu.15})^{3+}$, the addition of bicarbonate and sulphate anions apparently resulted in displacement of 1.5 of the bound water molecules whereas phosphate, fluoride and acetate displaced only one. However, in the corresponding terbium complexes $(\mathbf{Tb.15})^{3+}$, two of the bound water molecules were displaced by bicarbonate, fluoride and phosphate and sulphate and acetate displaced only one. The observed inconsistencies between the europium and terbium complexes of **(15)** may be attributed to different solution state structures. NMR analysis of $(\mathbf{Eu.15})^{3+}$ (Chapter 4.3) suggests that the complex exists in a tricapped trigonal prismatic geometry. The smaller terbium ion however may prefer to adopt the more compact square antiprismatic structure. The two geometries will display different coordination preferences and may therefore account for the observed anion effects on the excited state lifetimes. Further studies are warranted with these systems, investigating the concentration dependence of the anion effects, preferably using a passive buffer system (eg. MOPS or MES).

4.3.2 Effect of pH

The effect of pH on the lifetimes of the europium and terbium complexes of **(13a)**, **(14)** and **(15)** has been investigated. Although the lifetimes of both of the europium complexes appeared to be insensitive to pH in the range 2-10, the lifetimes of the terbium diamide $(\mathbf{Tb.15})^{3+}$ and triamide $(\mathbf{Tb.14})^{3+}$ complexes exhibited a strong pH dependency, as depicted in **Figure 4.5.**

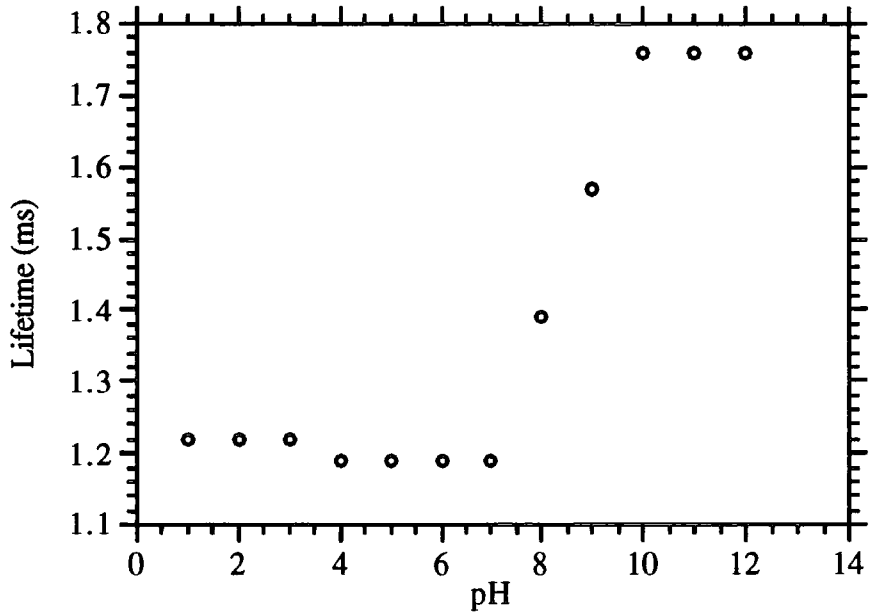

Figure 4.5. *pH Dependency of the excited state lifetime of* $(\mathbf{Tb.14})^{3+}$ *(1 mmol* dm^{-3} *solution in water, 0.1 mol* dm^{-3} *in NaCl,* λ_{ex} *= 254 nm, 293 K).*

There was no observed effect on the lifetime of the excited state of the terbium tetraamide complex $(\mathbf{Tb.13a})^{3+}$ following addition of hydroxide and examining the range 5.5-11. This is slightly surprising, given that the pKa for the equilibrium $MLOH_2 \rightleftharpoons MLOH$ has been measured to be 7.9 for the gadolinium complex[34] of the tetraamide analogue, $(\mathbf{Gd.8b})^{3+}$.

The lifetime of the excited state of the triamide complex $(\mathbf{Tb.14})^{3+}$ remained relatively constant at low pH and increased sharply between pH = 7 to pH = 10 where it approached a value of 1.74 ms. As the pH is increased, one of the bound water molecules may be deprotonated giving an $[MLOH]^{2+}$ complex. The number of OH

oscillators available for deactivation of the excited state is thereby reduced, resulting in an increase of the excited state lifetime. The observed q value for **(Tb.14)$^{3+}$** in the presence of hydroxide (**Table 4.3**), suggests the presence of only one bound OH oscillator which is consistent with the formation of an MLOH species in which the ninth coordination site is occupied by a Cl^- anion. It is well known that the metal bound water of di- and polyaquo species becomes labile following deprotonation.[36] As the pH titration was recorded in the presence of chloride (I = 0.1, NaCl), chloride anions present in solution may bind to the other coordination site (**Scheme 4.2**) via a dissociative exchange mechanism.

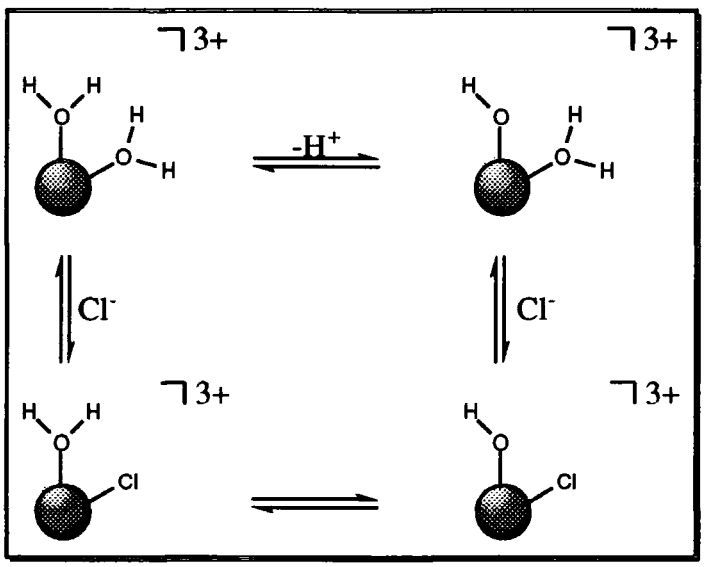

Scheme 4.2

The diamide terbium complex **(Tb.15)$^{3+}$** also exhibited a similar pH dependency with the lifetime increasing with increasing pH, τ_{H_2O} = 0.89 ms (pH = 2), τ_{H_2O} = 0.91 ms (pH = 5), τ_{H_2O} = 1.25 ms (pH = 12).

For the corresponding europium complexes of the triamide **(Eu.14)$^{3+}$** and the diamide **(Eu.15)$^{3+}$** the lifetimes of the excited state remained constant throughout the pH range 2-12. This pH insensitivity is curious and not readily explained but may be related to the ease of reduction of $Eu^{3+} \rightarrow Eu^{2+}$ (E^o = -0.35 V). An equilibrium may be set up between a bound aquo species and a bound hydroxide, as depicted in **Scheme 4.3,** with

the europium ion serving as a charge sink and a hydrogen-bonded water molecule being involved.

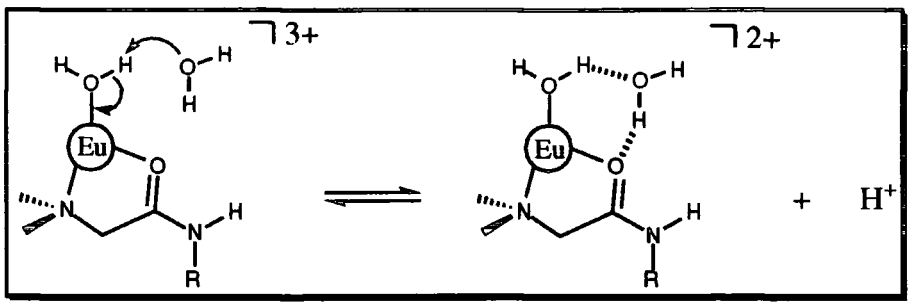

Scheme 4.3

Thus the europium centre may experience both bound water and hydroxide independent of the pH which may account for the constant lifetime observed. Such a mechanism will be unfavourable for terbium as the reduction potential for $Tb^{3+} \rightarrow Tb^{2+}$ is -2.3 V.

In the analysis of the q values observed upon anion addition to the terbium complexes, the pH dependency must be considered. For the majority of the anion-complex solutions studied, the measured pH was between 5.5 and 6, the same as that for the free complex, therefore a direct comparison of the q values may be made. However, care must be taken in considering phosphate, bicarbonate and carbonate in which the measured pH was 7.5, 6.5 and 11 respectively.

The low q value observed for **(Tb.14)**$^{3+}$ in the presence of carbonate, consistent with the displacement of two bound water molecules, could therefore be attributed to replacement of one of the water molecules with a hydroxide molecule. However, the observed q value for **(Tb.14)**$^{3+}$ in the presence of carbonate (0.29) is lower than than expected for such a $[ML.HCO_3.OH]^+$ species. Such a postulate does not readily account for the lack of formation of a similar species with the corresponding trigonal nitrate and acetate anions. Although ESMS (positive ion mode) showed the presence of an $[MLOH]^+$ species there was no evidence for such a $[ML.HCO_3.OH]^+$ species. The observations are consistent with a series of equilibria combining the formation of the

bidentate adduct described in **Scheme 4.1** for bicarbonate and carbonate binding, in competition with formation of a hydroxide bound species.

4.3.3 Effect of concentration

The variation in the radiative lifetimes of $(\mathbf{Tb.14})^{3+}$ as a function of the concentration of added sodium bicarbonate was measured and is shown in **Figure 4.6**. A change in pH from 5.5 - 7.0 was observed.

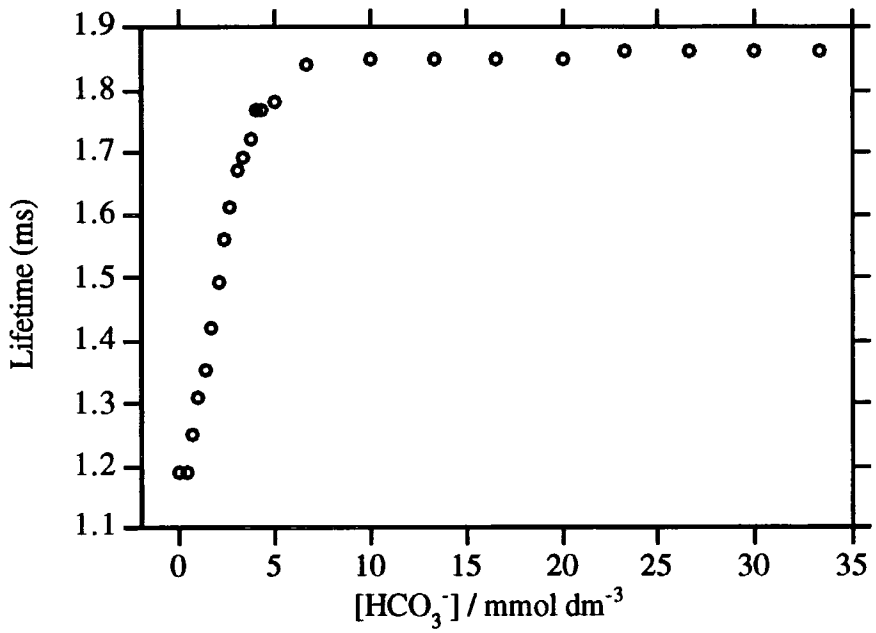

Figure 4.6. *Variation of the excited state lifetime of* $(\mathbf{Tb.14})^{3+}$ *(1 mmol* dm^{-3} *293K) with added sodium bicarbonate.*

Such a titration allows an estimate of the dissociation constant for the associated binding. However, in the case of bicarbonate binding to $(\mathbf{Tb.14})^{3+}$, the equilibria involved are likely to be rather complex, combining those depicted in **Scheme 4.1** and **4.2**. Therefore only an estimate of the dissociation constant for bicarbonate binding may be made. A value of $K_d = 2.5$ mmol dm^{-3} may be derived.

Further support for the involvement of several species in the bicarbonate binding equilibria was provided by electrospray mass spectrometry. Electrospray mass spectrometry (positive ion mode) revealed the formation of a predominant $[MLOH]^+$ species at 831.3, with less intense peaks at 875.2 and 876.2 whose relative abundance was in agreement with the isotope pattern calculated for $[ML+ HCO_3]^+$ (875.34 (100%) and 876.34 (51%)). Weak half mass peaks at 437.6 and 438.2, corresponding to doubly charged $[ML + HCO_3]^{2+}$, and at 416.1 corresponding to $[MLOH]^{2+}$ were also apparent.

4.4 Chiroptical studies

4.4.1 Circular dichroism

Since the luminescence of europium and terbium complexes of **(14)** is perturbed upon addition of anions such as phosphate and bicarbonate, the effect of such anions on the circular dichroism exhibited by the complexes was examined. The addition of phosphate and bicarbonate to $\mathbf{(Eu.14)^{3+}}$ does not significantly change the observed circular dichroism as shown in **Figure 4.7**. This is hardly surprising since the observable bands are due to $\pi \rightarrow \pi^*$ transitions occurring in the aromatic rings of the chiral ligand. The molar absorptivities of the lanthanide ions are very low ($\varepsilon < 1$ M^{-1} cm^{-1}) compared to the phenyl ring ($\varepsilon \approx 200$ M^{-1} cm^{-1}) and therefore the phenyl absorbance will dominate the CD spectra. Since the anions bind directly to the lanthanide ion, the chiral environment around the metal will be perturbed. However, the anions will have very little effect on the chiral environment of the phenyl as was revealed by the CD spectra.

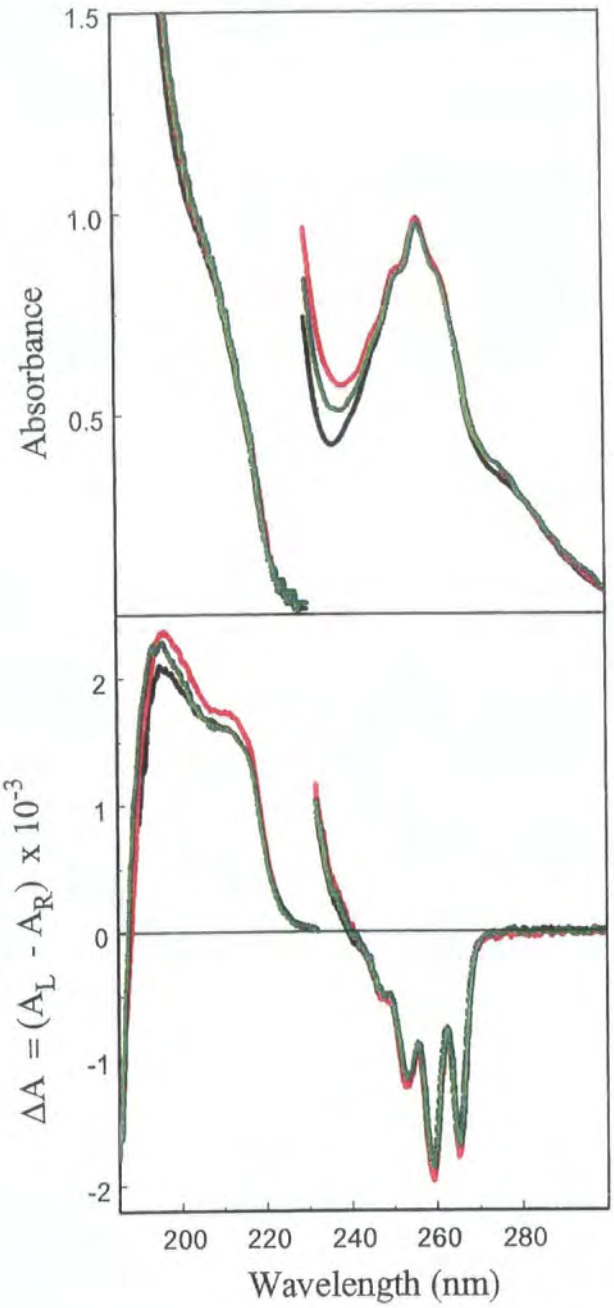

Figure 4.7. *Absorbance spectra (top trace) and circular dichroism spectra (lower trace) of* ***(Eu.14a)***$^{3+}$ *in the absence (black) and presence of bicarbonate (red) and phosphate (green) (MeOH, 293 K).*

In order to probe the changes in the chiral environment around the lanthanide ion in the presence of anions, the near infrared CD spectra of the corresponding ytterbium complex could be analysed. Ytterbium displays near i.r. CD bands around 980 nm due to f-f magnetic dipole allowed transitions occurring in the metal ion.[37,38] The observed bands will be dependent on the crystal field and chiral environment around the lanthanide ion and may therefore be used to elucidate structural information. Such work has not been carried out to date, but is worthy of further investigation.

4.4.2 Circularly Polarised Luminescence

Effect of added anions

As circularly polarised luminescence probes the chirality associated with the excited state of the lanthanide ion, the sign and magnitude of the observed CPL will be highly sensitive to changes in the lanthanide ion environment. The effect of the addition of a ten-fold excess of phosphate and carbonate anions on the CPL of the terbium complex **(Tb.14)$^{3+}$** is shown in **Figure 4.8**.

Examination of the most intense CPL band at 545 nm reveals relatively similar CPL for the terbium complex in the absence (**Figure 4.8a**) and presence (**Figure 4.8b**) of phosphate. The components to the $^5D_4 \rightarrow {}^7F_5$ transition have slightly different intensities and one of the components is split for the former, consistent with the formation of a di- and mono-aquo species for **(Tb.14)$^{3+}$** and **(Tb.14.H_2PO_4)$^{2+}$** respectively. The components of the $^5D_4 \rightarrow {}^7F_5$ transition are clearly very different in the presence of carbonate (**Figure 4.8c**). This is consistent with a pronounced change in the chiral environment of the terbium excited state under these conditions (pH = 11).

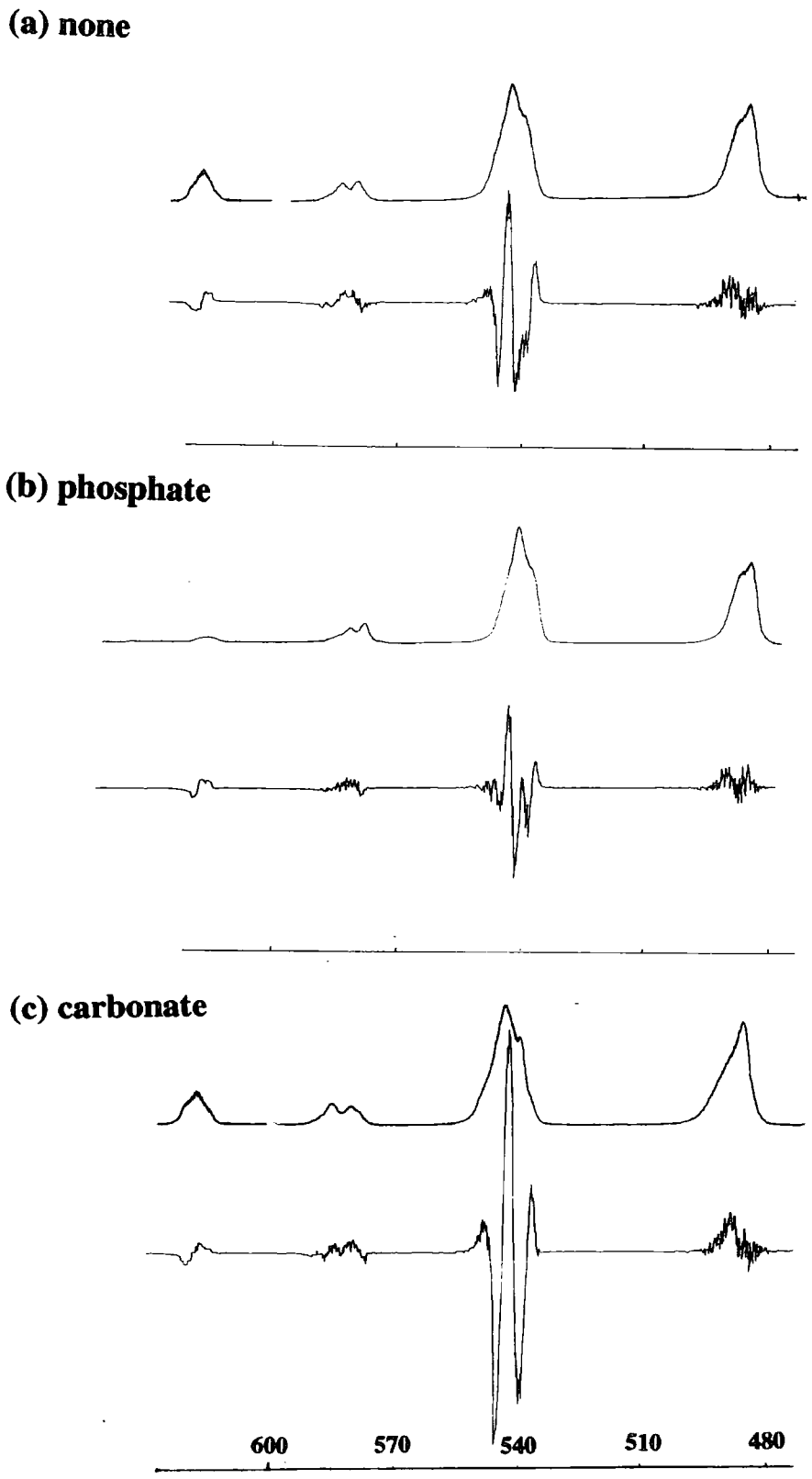

Figure 4.8. *CPL (lower trace) and total emission (upper trace) spectra of* $(Tb.14)^{3+}$ *in the absence* ***(a)*** *and presence of phosphate* ***(b)*** *and carbonate* ***(c)*** *anions, following excitation at 260 nm (MeOH, 293 K).*

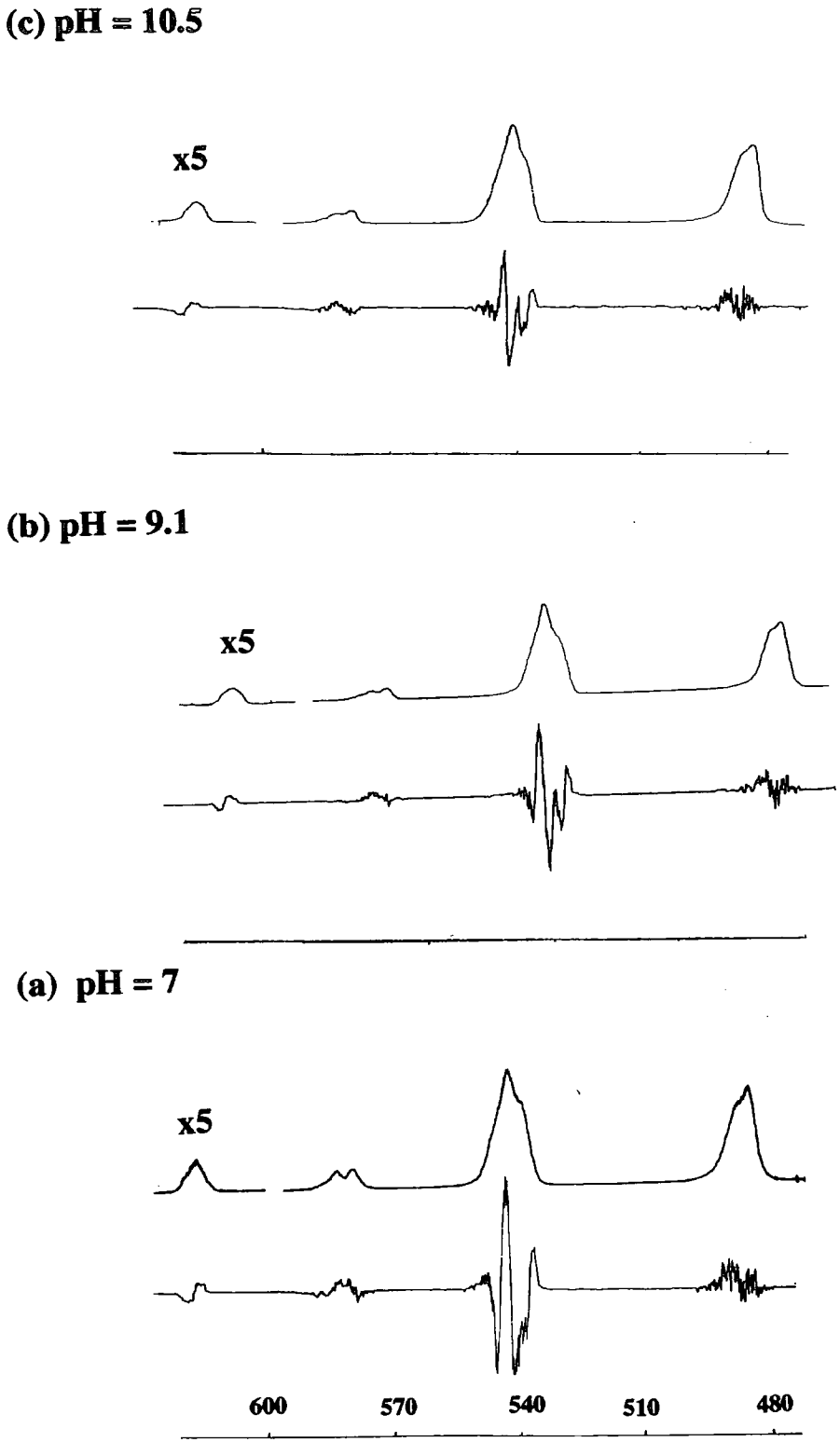

Figure 4.9. *CPL (lower trace) and total emission (upper trace) spectra of* ***(Tb.14)***$^{3+}$ *following excitation at 260 nm, at* ***(a)*** *pH = 7,* ***(b)*** *pH = 9.1 and* ***(c)*** *pH = 10.5 (MeOH, 293 K).*

Effect of pH

The effect of pH on the CPL of **(Tb.14)$^{3+}$** is shown in **Figure 4.9**. The q value observed for **(Tb.14)$^{3+}$** at pH = 12 was consistent with the displacement of two bound water molecules and formation of an aquo species with one bound hydroxide and one bound chloride anion. The change in the CPL at pH = 10.5 compared to that at pH = 7 is consistent with this modulation of the environment about the lanthanide terbium ion in the excited state. The CPL spectrum for **(Tb.14)$^{3+}$** at pH = 10.5 was identical to that of the carbonate adduct. Electrospray mass spectrometry (positive ion mode) revealed the presence of an $[MLOH]^+$ species for **(Tb.14)$^{3+}$** in the presence of carbonate and it was suggested that an equilibrium exists between the bidentate carbonate species and this MLOH species. The observed similaries in the CPL spectra could therefore be attributed to the presence of an $[MLOH]^+$ species for both. Displacement of the two bound water molecules was observed for both species, which dramatically changes the chiral environment around the terbium ion, compared to the di-aquo species of **(Tb.14)$^{3+}$** (pH = 7) and the mono-aquo species of **(Tb.14)$^{3+}$** in the presence of phosphate.

It would be advantageous to study the CPL exhibited from the corresponding europium complexes as although the spectra are weaker, fewer crystal field components are associated with each band which allows a detailed structural analysis to be made. Furthermore, CPL spectra need to be acquired at pH=7 (eg. using MOPS or MES buffer), and the effect of added HCO_3^-, CO_3^{2-} and HPO_4^{2-} determined under these conditions.

4.5 Conclusion

The coordinately unsaturated europium and terbium complexes of **(14)** may offer a unique way of signalling the presence of selected anions in aqueous media. The presence of carbonate and bicarbonate in particular may be deduced through measurement of the luminesence lifetime of the excited state and observation of the associated circularly polarised emission. The CPL exhibited by such complexes is

highly sensitive to the chiral environment about the lanthanide ion in its excited state and may be used to ascertain detailed structural information and the detection of changes in the helicity of the complex incurred upon anion binding. Further work is required to assess the concentration dependent effect of individual anions, under controlled pH conditions. In addition, using the analogous highly paramagnetic gadolinium or dysprosium complexes, pH and concentration dependent measurements of the relaxation rate of the ^{13}C, ^{31}P or ^{19}F resonance of the added anion (eg. $H^{13}CO_3^-$, HPO_4^{2-}, F^-) should reveal the variation in the proximity of the anion to the paramagnetic centre.

References for Chapter 4

1. F.P. Schmidtchen, *Nachr. Chem. Tech. Lab.*, 1988, **30**, 8; H.E. Katz in 'Inclusion Compounds', eds., J.L. Atwood, E.D. Davies and D.D. MacNicol, Oxford University Press, New York, vol. 4, 391; R.M. Izatt, K. Pawlak and J.S. Bradshaw, *Chem. Rev.*, 1995, **95**, 2529.
2. J.J.R.F. da Silva and R.J.P. Williams, *Struct. Bonding (Berlin)*, 1976, **29**, 67.
3. H.J. Schneider, T. Blatter, B. Palm, U. Pfingstag, V. Rüdiger and I. Theis, *J. Am. Chem. Soc.*, 1992, **114**, 7704.
4. F.P. Schmidtchen, *Angew. Chem., Int. Ed. Engl.*, 1977, **16**, 720.
5. L.F. Lindoy, 'The Chemistry of Macrocyclic Ligand Complexes', Cambridge University Press, Cambridge, 1989.
6. H.E. Katz, *Organometallics*, 1987, **6**, 1134.
7. M.E. Jung and H. Xia, *Tet. Lett.*, 1988, **29**, 297.
8. M. Newcomb, A. Modonill, M.T. Blanda and J.K. Judia, *Organometallics*, 1987, **6**, 145.
9. A.L. Beauchamp, M.J. Olivier, J.P. Wuest and B.J. Zacharie, *J. Am. Chem. Soc.*, 1986, **108**, 73.
10. P.A. Gale, J.L. Sessler, V. Král and V. Lynch, *J. Am. Chem. Soc.*, 1996, **128**, 5140.

11. D.M. Rudkevich, W. Verboom, Z. Brzozka, M.J. Palys, W.P.R.V. Stauthamer, G.J. van Hummel, S.M. Franken, S. Harkema, J.F.J. Engbersen and D.N. Reinhoudt, *J. Am. Chem. Soc.*, 1994, **116**, 4341.

12. F.P. Schmidtchen, A. Gleich and A. Schummer, *Pure Appl. Chem.*, 1989, **61**, 1535.

13. B. Dietrich, T.M. Fyles, J.-M. Lehn, L.G. Pease and D.L. Fyles, *J. Chem. Soc., Chem. Commun.*, 1978, 934; F.P. Schmidtchen, *Tet. Lett.*, 1989, **30**, 4493.

14. A. Echararren, A. Gatan, J.-M. Lehn and J. de Mendoza, *J. Am. Chem. Soc.*, 1989, **111**, 4994.

15. D.H. Vance and A.W. Czarnik, *J. Am. Chem. Soc.*, 1994, **116**, 9397.

16. M.E. Huston, E.U. Akhaya and A.W. Czarnik, *J. Am. Chem. Soc.*, 1989, **111**, 8735.

17. C.H. Park and H.E. Simmons, *J. Am. Chem. Soc.*, 1968, **90**, 2431; B. Dietrich, M.W. Hosseini and J.-M. Lehn, *J. Am. Chem. Soc.*, 1981, **103**, 1282.

18. P.D. Beer, M.G.B. Drew and A.R. Graydon, *J. Chem. Soc., Dalton Trans.*, 1996, 4129; P.D. Beer, *Chem. Commun.*, 1996, 689; P.D. Beer, D. Hesek, J. Hodacova and S.T. Stokes, *J. Chem. Soc., Chem. Commun.*, 1992, 270; P.D. Beer, C. Hazelwood, D. Hesek, J. Hodacova and S.T. Stokes, *J. Chem. Soc., Dalton Trans.*, 1993, 1327.

19. A.W. Czarnik, *Acc. Chem. Res.*, 1994, **27**, 302.

20. P.D. Beer, *Adv. Mater.*, 1994, **6**, 607.

21. M. Guardigli, J.-M. Lehn, G. Mathis and N. Sabbatini, *J. Alloys and Compounds*, 1992, **180**, 363.

22. P.D. Beer and A.D. Keefe, *J. Organomet. Chem.*, 1989, **375**, C40.

23. J.E. Sarneski and F.L. Urbach, *J. Am. Chem. Soc.*, 1971, **93**, 887.

24. D. Parker in 'Crown Compounds, Towards Future Aplications', ed., S.R. Cooper, V.C.H. Publishers, New York, 1994, Chapter 4.

25. L. Stryer in 'Biochemistry', ed., W.H. Freeman, New York, 1988; J.W. Hanrahan, J.A. Tabcharani, F. Becq, C.J. Mathews, O. Augustinas, T.J. Jensen,

X.-B. Chang and J.R. Riordan in 'Ion Channels and Genetic Diseases', eds., D.C. Dawson and R.A. Frizzel, Rockefeller University Press, New York, 1995.

26. R.C. Jagessar and D.H. Burns, *Chem. Commun.*, 1997, 1685.
27. S. Aime, M. Botta, D. Parker and A.S. de Sousa, unpublished work.
28. N. Sabbatini, S. Perathoner, G. Laltanzi, S. Dellonte and V. Balzani, J. *Phys. Chem.*, 1987, **91**, 6136.
29. W.De W. Horrocks, Jr. and D.R. Sudnick, *J. Am. Chem. Soc.*, 1979, **101**, 334.
30. R.S. Dickins, D. Parker, A.S. de Sousa and J.A.G. Williams, *Chem. Commun.*, 1996, 697.
31. P.L. Anelli, V. Balzani, L. Prodi and F. Uggeri, *Gazz. Chim. Ital.*, 1991, **121**, 359.
32. D.W. Christianson and C.A. Fierke, *Acc. Chem. Res.*, 1996, **29**, 331; I. Bertini and C. Luchinat in 'Bioinorganic Chemistry', eds., I. Bertini H.B. Gray, S.J. Lippard and I.S. Valentine, University Science Books, Mill Valley, 1994.
33. J.J.R.F. da Silva and R.J.P. Williams, 'The Biological Chemistry of the Elements', Oxford University Press, New York, 1993.
34. S. Aime, A. Barge, M. Botta, D. Parker and A.S. de Sousa, *J. Am. Chem. Soc.*, 1997, **119**, 4767.
35. S. Aime, M. Botta, D. Parker and J.A.G. Williams, *J. Chem. Soc., Dalton Trans.*, 1996, 17.
36. D.T. Richens, 'The Chemistry of Aqua Ions', Wiley, Chichester, 1997.
37. G. Stein and E.J. Würzberg, *J. Chem. Phys.*, 1975, **62**, 211.
38. R.D. Peacock, *Struct. Bonding (Berlin)*, 1975, **22**, 83.

CHAPTER 5

EXPERIMENTAL DETAILS

CHAPTER 5

EXPERIMENTAL DETAILS

5.1 General synthetic procedures and characterisation techniques

5.1.1 Reaction conditions

Reactions requiring anhydrous or inert conditions were carried out using Schlenk-line techniques under an atmosphere of dry argon. Anhydrous solvents when required were freshly distilled over the appropriate drying agent. Water was purified by the 'Purite$_{STILL}$ plus' system.

5.1.2 Purification procedures

Thin layer chromatography was carried out on neutral alumina plates (Merck Art 5550) or silica plates (Merck 5554) and detection was made following irradiation at 254 nm or by staining with iodine. Column chromatography was carried out using neutral alumina (Merck Aluminium Oxide 90, activity II-III, 70-230 mesh) pre-soaked in ethyl acetate, or silica (Merck Silica Gel 60, 230-400 mesh). Analytical and semi-preparative HPLC were performed on a Varian 9010/9065 Polychrom system using a chiral cyclodextrin column (Shodex OR pak CDB - 853 HQ series, β-cyclodextrin) and a flow rate of 1.4 $cm^3\ min^{-1}$ (T = 2 °C; t = 0 min, 95% H_2O, 5% MeOH; t = 25 min, 100% MeOH, end time).

5.1.3 Characterisation techniques

Melting points were measured with a Köfter block and are uncorrected.

Infra-red spectra were recorded on a Perkin-Elmer 1600 FT spectrometer with GRAMS Analyst software, oils examined as thin films and solids incorporated into KBr discs as stated; and a Graseby-Specac "Golden Gate" Diamond ATR accessory spectrometer.

NMR spectra were acquired using a Brüker AC250 spectrometer operating at 250.13, 62.9, 101.1 and 235.3 MHz for ^{1}H, $^{13}C\{^{1}H\}$, $^{31}P\{^{1}H\}$ and $^{19}F\{^{1}H\}$ measurements respectively; a Varian VXR 200 operating at 200 MHz for ^{1}H; a Joel EX-90 operating at 90 and 36 MHz for ^{1}H and $^{31}P\{^{1}H\}$ respectively; a Joel EX-400 operating at 400, 100.6 and 161.8 MHz for ^{1}H, $^{13}C\{^{1}H\}$ and $^{31}P\{^{1}H\}$ respectively and a Varian VXR400 operating at 400 MHz for ^{1}H. Two-dimensional spectra were run on a Joel EX-90 and a Varian VXR 200. ^{1}H variable temperature studies were carried out on a Varian VXR 400; a Joel EX-90 and a Joel EX-400 instruments. Proton relaxivities were measured at 25 °C on a 20 MHz Spin-Master Spectrometer (Stelar) by means of the inversion recovery technique. ^{1}H and $^{13}C\{^{1}H\}$ spectra were referenced internally relative to *tert*-butanol (1 drop; δ_H 0; δ_C 31.3) for paramagnetic complexes or to the residual protio-solvent resonances which are reported relative to TMS (δ 0). $^{31}P\{^{1}H\}$ spectra were referenced externally relative to H_3PO_4 in D_2O (δ 0). $^{19}F\{^{1}H\}$ spectra were referenced internally relative to $CFCl_3$ (1 drop; δ_H 0). All chemical shifts are given in ppm and coupling constants are in Hz.

Mass spectra were recorded on a VG 7070E spectrometer operating in DCI (ammonia) or FAB (glycerol matrix) mode. Electrospray mass spectra were recorded on a VG Platform II (Fisons instrument) operating in positive or negative ion mode as stated. FAB and accurate mass spectra were recorded at the EPSRC Mass Spectrometry Service at Swansea.

Optical rotations were measured at the EPSRC National Chiroptical Spectroscopy Centre at Kings College, London on a Perkin-Elmer 141 polarimeter, calibrated with sucrose solutions, 10 mg cm^{-3} ($[\alpha_D]$ 66.6 °).

5.2 General luminescence procedures

5.2.1 Luminescence spectra

Ultraviolet absorbance spectra were recorded on a Unicam u.v./visible spectrometer UV2-100 with Unicam Vision Software Version 2.11.

Fluorescence spectra were recorded on a Perkin-Elmer LS50B spectrofluorimeter using FL Winlab Version 1.10 software, equipped with a Hamamatsu R928 photomultiplier tube using quartz fluorescence cuvettes of pathlength 1 cm.

Phosphorescence emission and excitation spectra were recorded on the same instrument operating in time-resolved mode with a delay time of 0.1 ms and a gate time of 10 ms. Emission spectra were corrected for the wavelength dependence of the photomultiplier tube and the most highly resolved spectra were obtained with slit widths (half-height bandwidth) of 10 nm (excitation) and 2.5 nm (emission). The spectrometer automatically corrects the phosphorescence excitation spectra through a reference photomultiplier tube and the spectra were obtained by monitoring the emission at 590 or 619 nm for Eu^{3+} and 545 nm for Tb^{3+} complexes.

5.2.2 Quantum yields

Luminescence quantum yields, ϕ, were measured according to the procedure described by Haas and Stein[1], summarised below, using $[Ru(2,2'\text{-bipyridyl})]^{2+}$ ($\phi = 0.028$ in H_2O)[2] and quinine sulfate ($\phi = 0.546$ in 0.5 mol dm^{-3} H_2SO_4)[3] as standards for Eu^{3+} and Tb^{3+} complexes respectively.

$$\phi = \frac{\text{number of photons emitted}}{\text{number of photons absorbed}} \alpha \frac{E}{A}$$

where E is the combined area under the emission bands and A is the area under the absorbance curve in the excitation band.

Hence

$$\frac{\phi_u}{\phi_s} = \frac{E_u/A_u}{E_s/A_s}$$

where u and s denote values for the sample and standard respectively. E_s and E_u were obtained under the same conditions using minimum excitation slit widths for a number of solutions having absorbance in the range 0.01-0.1. The uncertainty in the absorbance was minimised by choosing excitation wavelengths in a relatively flat portion of the absorption spectra.

The observed phosphorescence (E) was related to the total phosphorescence (E_T) through **equation 5.1.**[4]

$$\frac{E_T}{E} = \frac{1 - \exp(-20/\tau)}{\exp(-t_D/\tau) - \exp[-(t_d + t_g)\tau]} \qquad \textbf{(5.1)}$$

where τ is the phosphorescence lifetime, t_d the delay time and t_g the gate time (values in ms and for a cycle time of 20 ms).

The relative quantum yield was obtained from the ratio of gradients of plots of E/A for sample and standard and are reproducible to within 10%.

5.2.3 Excited state lifetimes

Lifetimes were measured on a Perkin-Elmer LS50B spectrofluorimeter using phlemming software, written by Dr. A. Beeby, University of Durham. Reported lifetimes, τ, are the average of at least 3 separate measurements calculated by monitoring the emission intensity at 590 or 619 nm for Eu^{3+} and 545 nm for Tb^{3+} complexes after at least 20 different delay times covering 2 or more lifetimes. The gate time was 0.1 ms and slit widths of 15 nm and 5 nm or less were employed for Eu^{3+} and Tb^{3+} complexes respectively. The phosphorescence decay curves were fitted by an equation of the form $I(t) = I(0) \exp(-t / \tau)$ using a curve fitting program (Kaleidagraph software on an Apple Macintosh or Grafit software on a PC), where I(t) is the intensity at time t after the excitation flash, I(0) the initial intensity at $t = 0$ and τ is the phosphorescence lifetime. High correlation coefficients were observed, τ is

reproducible to at least ± 0.06 ms and independent of concentration over the range examined (0.05-0.5).

5.2.4 Chiroptical techniques

Circular dichroism spectra were recorded on a Jasco J720 CD spectropolarimeter, calibrated with ammonium-*d*-camphor-10-sulfonate. All data were corrected for baseline, concentration and pathlength.

Circularly polarised luminescence spectra were recorded by Dr. R.D. Peacock, University of Glasgow and Prof. J. Riehl, Michigan Technological University, U.S.A. Excitation of the $^7F_6 \longrightarrow {}^5D_4$ transition of Tb^{3+} was accomplished with the 488 nm line of a Coherent Innova 70 argon-ion laser. Excitation of the Eu^{3+} (560-581 nm) was accomplished by using a Coherent-599 tunable dye laser (0.03 nm resolution) using the argon-ion laser as a pump source. The laser dye used in the measurement was Rhodamine 110 in ethylene glycol. Calibration of the emission monochromator (and subsequently the dye laser) was accomplished by passing scattered light from a low power He-Ne laser through the detection system. The error in the dye laser wavelength was assumed to be equal to the resolution of the emission detection. The optical detection system consisted of a photoelastic modulator (PEM, Hinds, Int.) operating at 50 kHz, and a linear polariser which together act as a circular analyser, followed by a long pass filter, focusing lens, and a 0.22 nm monochromator. The emitted light was detected by a cooled EM1-9558QB photomultiplier tube operating in photon counting mode. The output pulses from the photomultiplier tube were passed through a variable gain amplifier / discriminator and input into a specially built differential photon counter. The 50 kHz reference signal from the photoelastic modulator was used to direct the incoming pulses into two separate counters, an up-counter which counts every photon pulse and thus is a measure of the total luminescence signal $I = I_{left} + I_{right}$, and an up/down counter which adds pulses when the analyser is transmitting left circularly polarised light and subtracts when the analyser is transmitting right circularly polarised light. This second counter provides a measure of the differential emission

intensity $\Delta I = I_{left} - I_{right}$. The differential photon counter allows for the selection of a time window for counting which is centred around the maximum in the modulation cycle. For the measurements reported here, the window was set to 50%.

5.3 Synthetic procedures and characterisation data for Chapter 2

2-*Chloro*-N-[(S)-*methylbenzyl*]*ethanamide* **(12b)**

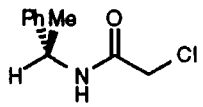

Chloroacetylchloride (0.78 cm^3, 9.9 mmol) in dry diethyl ether (20 cm^3) was added dropwise to a stirred solution of (*S*)-α-methylbenzylamine (1.1 cm^3, 8.3 mmol) and triethylamine (1.4 cm^3, 9.9 mmol) in dry diethyl ether (30 cm^3) at -20 °C. The reaction mixture was allowed to warm to room temperature and stirred for 1 h. The resulting white precipitate was dissolved in water (60 cm^3) and the organic layer washed with hydrochloric acid (0.1 mol dm^{-3}, 50 cm^3), water (3 x 30 cm^3), dried (K_2CO_3) and the solvent removed *in vacuo* to yield a white solid. Recrystallisation from diethyl ether yielded white needles (0.95 g, 60%), m.p. 95-96 °C; ν_{max} (KBr)/cm^{-1} 3265 (N-H), 1652 (C=O); δ_H (250 MHz; $CDCl_3$) 7.41-7.34 (5 H, m, Ar), 6.82 (1 H, br s, NH), 5.18 (1 H, m, CH), 4.11 (1 H, d, ^2J 15.1, CH_2), 4.08 (1 H, d, ^2J 15.1, CH_2), 1.58 (3 H, d, ^3J 6.7, CH_3); $\delta_C\{^1H\}$ (62.9 MHz; $CDCl_3$) 165.0 (CO), 142.4 (q-Ar), 128.8 (m-Ar), 127.6 (p-Ar), 126.1 (o-Ar), 49.2 (CHN), 42.6 (CH_2), 21.7 (CH_3); m/z (DCI) 198 (100%, M^+) (Found: C, 60.6; H, 6.15; N, 6.90. $C_{10}H_{12}ClNO$ requires C, 60.8; H, 6.12; N, 7.08%).

2-*Chloro*-N-[(R)- 1-*naphthyl*]*ethylethanamide* **(12c)**

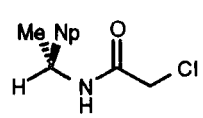

The title compound was prepared following a method similar to that for **(12b)** using (*R*)-1-(1-naphthyl)ethylamine (0.94 cm^3, 5.8 mmol) and triethylamine (0.98 cm^3, 7 mmol) in dry diethyl ether (30 cm^3) and reacting with a solution of chloroacetylchloride (0.56 cm^3, 7 mmol) in dry diethyl ether (30 cm^3). The product was recrystallised from

diethyl ether and was isolated as white needles (1.1 g, 76%), m.p. 144-145 °C; ν_{max} (KBr)/cm^{-1} 3296 (N-H), 1648 (C=O); δ_H (250 MHz; $CDCl_3$) 8.12-7.48 (7 H, m, Ar), 6.84 (1 H, br s, NH), 5.99 (1 H, m, CH), 4.13 (1 H, d, ^2J 15.3, CH_2), 4.11 (1 H, d, ^2J 15.3, CH_2), 1.75 (3 H, d, ^3J 7.0, CH_3); $\delta_C\{^1H\}$ (62.9 MHz; $CDCl_3$) 165.0 (CO), 137.5 (Ar), 133.9 (Ar), 130.9 (Ar), 128.9 (Ar), 128.6 (Ar), 126.8 (Ar), 126.0 (Ar), 125.3 (Ar), 123.1 (Ar), 122.6 (Ar), 45.2 (CH), 42.6 (CH_2), 20.9 (CH_3); m/z (DCI) 248 (100%, MH^+), 212 (18%, M^+ - Cl), 155 (70%, M^+ - NHCOCl) (Found: C, 68.1; H, 5.64; N, 5.59. $C_{14}H_{14}ClON$ requires C, 67.8; H, 5.69; N, 5.65%).

2-*Chloro*-N-[(S)- 1-*naphthyl*]*ethylethanamide* **(12d)**

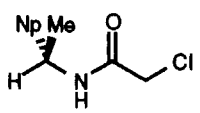

The title compound was prepared following a method similar to that for **(12b)** using (*S*)-1-(1-naphthyl)ethylamine (4.72 cm^3, 29.2 mmol) and triethylamine (4.9 cm^3, 35.1 mmol) in dry diethyl ether (100 cm^3) and reacting with a solution of chloroacetylchloride (2.79 cm^3, 35.1 mmol) in dry diethyl ether (50 cm^3). The product was recrystallised from diethyl ether and was isolated as white needles (3.5 g, 48%). Characterisation data are the same as those reported for **(12c)**. (Found: C, 68.0; H, 5.60; N, 5.54. $C_{14}H_{14}ClON$ requires C, 67.8; H, 5.69; N, 5.65%).

1-[(S)-1-(1-*phenyl*)*ethylcarbamoylmethyl*]-1,4,7,10-*tetraazacyclododecane* **(17d)**

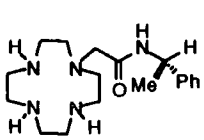

1,4,7,10-Tetraazacyclododecane (0.4 g, 2.3 mmol) and molybdenum hexacarbonyl (0.6 g, 2.3 mmol) in dry dibutyl ether (20 cm^3) were heated at reflux under argon for 2 h to give a bright yellow precipitate of the 1,4,7,10-tetraazacyclododecane-molybdenum tricarbonyl complex **(16)** which was filtered under argon and dried *in vacuo*. The complex **(16)** (0.8 g, 2.3 mmol) and fine mesh anhydrous potassium carbonate (0.4 g, 2.8 mmol) were taken into degassed *N,N*-dimethylformamide (30 cm^3) and a solution

of 2-chloro-*N*-[(*S*)-methylbenzyl]ethanamide **(12b)** (0.45 g, 2.3 mmol) in dry *N,N*-dimethylformamide (1 cm^3) was added under argon by steel cannula. The reaction mixture was heated at 60 °C for 4 h under an argon atmosphere. The solvent was removed by distillation *in vacuo* and the brown residue was taken into hydrochloric acid (1 mol dm^{-3}, 13 cm^3) and the resulting acidic brown suspension was stirred open to air for 18 h. Molybdenum residues were removed by centrifugation and filtration and the aqueous layer was washed with dichloromethane (30 cm^3) and chloroform (30 cm^3). The pH of the solution was raised to 14 by addition of sodium hydroxide pellets, with cooling. The product was extracted into dichloromethane (3 x 30 cm^3), washed with water (3 x 30 cm^3), dried (K_2CO_3) and the solvent removed *in vacuo* to yield a yellow-brown oil (620 mg, 81%), R_f (Al_2O_3; 10% CH_3OH-CH_2Cl_2; I_2 and u.v. detection) 0.44-0.1; ν_{max} (film)/cm^{-1} 3285 (N-H), 1666 (C=O); δ_H (250 MHz; $CDCl_3$) 8.23 (1 H, d, ^3J 7.7, NHCO), 7.45-7.28 (5 H, m, Ar), 5.21 (1 H, m, CH), 3.20 (2 H, s, CH_2), 2.92-2.54 (16 H, m, ring-CH_2), 2.00-1.90 (3 H, m, ring-NH), 1.56 (3 H, d, ^3J 5.0, CH_3); $\delta_C\{^1H\}$ (62.9 MHz; $CDCl_3$) 170.3 (CO), 143.3 (q-Ar), 128.2 (m-Ar), 126.8 (p-Ar), 126.1 (o-Ar), 58.8 ($\underline{C}H_2CO$), 52.9 (ring-CH_2), 48.0 (CHN), 46.7 (ring-CH_2), 46.4 (ring-CH_2), 45.3 (ring-CH_2), 21.3 (CH_3); m/z (DCI) 334 (100%, M^+).

1-[(R)-1-(1-*naphthyl)ethylcarbamoylmethyl*]-1,4,7,10-*tetraazacyclododecane* **(17e)**

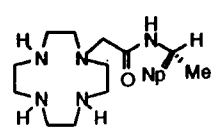

The title compound was prepared following a similar method to that for **(17d)** using 1,4,7,10-tetraazacyclododecane-molybdenum tricarbonyl complex **(16)** (1 g, 2.86 mmol), 2-chloro-*N*-[(*R*)-1-naphthyl]ethylethanamide **(12c)** (0.71 g, 2.86 mmol) and potassium carbonate (0.55 g, 4.0 mmol) in degassed, dry *N,N*-dimethylformamide (30 cm^3) to yield a brown oil (0.55 g, 50%) after purification, ν_{max} (film)/cm^{-1} 3421 (N-H), 1643 (C=O); δ_H (250 MHz; $CDCl_3$) 8.52 (1 H, d, ^3J 8.0, NHCO), 8.12-7.49 (7 H, m, Ar), 5.95 (1 H, m, CH), 3.25 (1 H, d, ^2J 17.5, CH_2CO), 3.19 (1 H, d, ^2J 17.5, CH_2CO), 2.59-2.20 (19 H, m, ring-CH_2, ring-NH), 1.71 (3 H, d, ^3J 6.9, CH_3); $\delta_C\{^1H\}$ (62.9

MHz; $CDCl_3$), 170.6 (CO), 138.2 (q-Ar), 133.6, (q-Ar), 131.2 (q-Ar), 128.6 (Ar), 128.0 (Ar), 126.4 (Ar), 125.8 (Ar), 125.2 (Ar), 123.5 (Ar), 122.9 (Ar), 58.9 ($\underline{C}H_2CO$), 53.4 (ring-CH_2), 46.8 (ring-CH_2), 45.6 (ring-CH_2), 44.5 (ring-CH_2), 43.9 (CHN), 20.0 (CH_3); m/z (DCI) 384 (100%, MH^+).

1-[(S)-1-(1-*naphthyl*)*ethylcarbamoylmethyl*]-1,4,7,10-*tetraazacyclododecane* **(17f)**

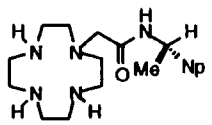

The title compound was prepared following a similar method to that for **(17d)** using 1,4,7,10-tetraazacyclododecane-molybdenum tricarbonyl complex **(16)** (4.2 g, 12.1 mmol), 2-chloro-*N*-[(*S*)-1-naphthyl]ethylethanamide **(12d)** (3.0 g, 12.1 mmol) and potassium carbonate (2.34 g, 17 mmol) in degassed, *N*,*N*-dry dimethylformamide (60 cm^3) to yield a brown oil (2.3 g, 50%) after purification. Characterisation data are the same as those reported for **(17e).**

1-[(1-*Naphthyl*)*methylcarbamoylmethyl*]-1,4,7,10-*tetraazacyclododecane* **(17c)**

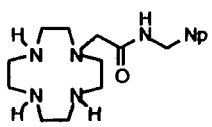

The title compound was prepared following a method similar to that for **(17d)** using 1,4,7,10-tetraazacyclododecane-molybdenum tricarbonyl complex **(16)** (0.75 g, 2.14 mmol), 2-chloro-*N*-(naphthylmethyl)ethanamide[5] (0.5 g, 2.14 mmol) and potassium carbonate (0.35 g, 2.57 mmol) in degassed, dry *N*,*N*-dimethylformamide (30 cm^3) to yield a yellow oil (0.2 g, 25%) after purification, ν_{max} (film)/cm^{-1} 3365 (N-H), 1652 (C=O); δ_H (250 MHz; $CDCl_3$) 8.50-8.40 (1 H, br m, NHCO), 7.82-7.76 (4 H, m, Ar), 7.48-7.41 (3 H, m, Ar), 4.61 (2 H, d, ^3J 5.0, CH_2Ar), 3.24 (2 H, s, CH_2CO), 2.69-2.39 (19 H, m, ring-CH_2, ring-NH); $\delta_C\{^1H\}$ (62.9 MHz; $CDCl_3$) 171.3 (CO), 135.9 (Ar), 133.0 (Ar), 132.3 (Ar), 128.1 (Ar), 127.5 (Ar), 127.4 (Ar), 126.4 (Ar), 126.2 (Ar), 126.1 (Ar), 125.7 (Ar), 59.1 ($\underline{C}H_2CO$), 53.1 (ring-CH_2), 46.9 (ring-CH_2), 46.3 (ring-CH_2), 45.6 (ring-CH_2), 43.1 (CH_2Ar); m/z (DCI) 370 (100%, MH^+).

Methyldiethoxyphosphine **(18)**

Diethylchlorophosphite (14.3 cm^3, 0.1 mol) was added dropwise, over 1 h, to a cooled solution of methylmagnesium bromide (33.3 cm^3 of a 3 mol dm^{-3} solution in diethyl ether, 0.1 mol) under argon at 20 °C. The mixture was allowed to warm to room temperature and stirred for a further 1 h. The resulting precipitate was removed by filtration off under argon by cannula transfer. Distillation under reduced pressure yielded methyldiethoxyphosphine as a solution in diethyl ether whose molarity was established by addition of a known mass of diethylphenylphosphonite followed by ^{31}P nmr integration of the two distinct singlets, $\delta_P\{^1H\}$ (101.3 MHz) 176.4.

Triethyl-10-[(*S*)-1-(1-*phenyl*)*ethylcarbamoylmethyl*]-1,4,7,10-*tetraazacyclododecane*-1,4,7-*triyltrimethylenetri*(*methylphosphinate*) **(19d)**

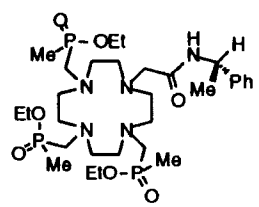

The monosubstituted macrocycle **(17d)** (0.56 g, 1.68 mmol) was allowed to heat at reflux temperature in dry tetrahydrofuran (40 cm^3), under argon over 4Å molecular sieves for 30 min. Methyldiethoxyphosphine **(18)** (26.3 cm^3 of a 1.1 mol dm^{-3} solution in diethyl ether, 7.56 mmol) was added to the cooled solution. After heating for 10 min at reflux, paraformaldehyde (0.25 g, 8.4 mmol) was added and the solution was heated at reflux for a further 18 h. The solvent was removed *in vacuo* to yield a brown oil. The product was purified by alumina column chromatography (gradient elution from dichloromethane to 2% methanol-dichloromethane) giving a yellow oil (0.6 g, 55%), R_f (Al_2O_3; 10% MeOH-CH_2Cl_2; I_2 and u.v. detection) 0.61; ν_{max} (film)/cm-1 3384 (br) (N-H), 1665 (C=O); δ_H (250 MHz; $CDCl_3$) 8.15 (1 H, ^3J 8.2, NH), 7.32-7.18 (5 H, m, Ar), 5.12 (1 H, m, CH), 4.03-3.94 (6 H, m, $C\underline{H}_2CH_3$), 3.11-2.48 (24 H, br m, CH_2CO, CH_2P, ring-CH_2), 1.50-1.36 (12 H, m, PCH_3, CH_3), 1.25 (9H, t, ^3J 7.0, $CH_2C\underline{H}_3$); $\delta_C\{^1H\}$ (62.9 MHz; $CDCl_3$) 170.2 (CO), 143.5 (q-Ar), 128.2 (m-Ar), 126.9 (p-Ar),

126.4 (o-Ar), 59.9 ($\underline{C}H_2CH_3$), 55.4 (ring-CH_2), 53.9 (d, ^3J 88, CH_2P), 47.9 (CHN), 21.3 (CH_3), 16.5 ($CH_2\underline{C}H_3$), 13.6 (d, ^1J 89, PCH_3); $\delta_P\{^1H\}$ (101.3 MHz; $CDCl_3$) 52.0 (3 P, br); m/z (DCI) 694 (100%, M^+) (A satisfactory accurate mass spectrum could not be obtained for this product).

Triethyl-10-[(R)-1-(1-*naphthyl*)*ethylcarbamoylmethyl*]-1,4,7,10-*tetraazacyclododecane*-1,4,7-*triyltrimethylenetri*(*methylphosphinate*) (**19e**)

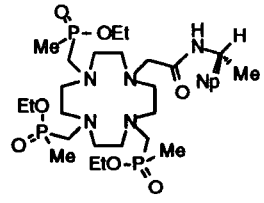

The title compound was prepared following a method similar to that for (**19d**) using the monosubstituted macrocycle (**17e**) (0.16 g, 0.42 mmol), methyldiethoxyphosphine (**18**) (6.5 cm^3 of a 1.1 mol dm^{-3} solution in diethyl ether, 1.9 mmol), paraformaldehyde (0.06 g, 2.1 mmol) in dry tetrahydrofuran (20 cm^3) to yield a yellow oil (0.17 g, 54%) after purification, R_f (Al_2O_3; 10% CH_3OH-CH_2Cl_2; I_2 and u.v. detection) 0.68; ν_{max} (film)/cm^{-1} 3397 (br) (N-H), 1652 (C=O); δ_H (250 MHz; $CDCl_3$) 8.45-7.47 (7 H, m, Ar), 5.93 (1 H, m, CH), 3.99 (6 H, m, $C\underline{H}_2CH_3$), 3.19-2.32 (24 H, br m, ring-CH_2, CH_2P, CH_2CO), 1.54 (9 H, d, ^2J 13.0, PCH_3), 1.37-1.28 (12 H, m, $CH_2C\underline{H}_3$, CH_3); $\delta_C\{^1H\}$ (62.9 MHz; $CDCl_3$) 170.3 (CO), 138.5 (q-Ar), 133.7 (q-Ar), 131.5 (q-Ar), 128.5 (Ar), 128.1 (Ar), 126.4 (Ar), 125.8 (Ar), 125.0 (Ar), 123.7 (Ar), 123.0 (Ar), 60.0 ($\underline{C}H_2CH_3$), 55.7-53.0 (ring-CH_2, $\underline{C}H_2CO$), 43.6 (CHN), 20.1 (CH_3), 16.6 ($CH_2\underline{C}H_3$), 13.7 (d, ^1J 89, PCH_3); $\delta_P\{^1H\}$ (101.3 MHz; $CDCl_3$) 53.3-51.4 (3 P, br m); m/z (DCI) 744 (100%, MH^+) (A satisfactory accurate mass spectrum could not be obtained for this product).

Triethyl-10-[(S)-1-(1-*naphthyl*)*ethylcarbamoylmethyl*]-1,4,7,10-*tetraazacyclododecane*-1,4,7-*triyltrimethylenetri*(*methylphosphinate*) **(19f)**

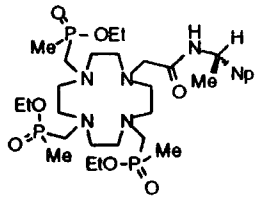

The title compound was prepared following a method similar to that for **(19d)** using the monosubstituted macrocycle **(17f)** (2.0 g, 5.2 mmol), methyldiethoxyphosphine **(18)** (77 cm^3 of a 0.3 mol dm^{-3} solution in diethyl ether, 23.6 mmol), paraformaldehyde (0.8 g, 26.2 mmol) in dry tetrahydrofuran (100 cm^3) to yield a yellow oil (2 g, 52%) after purification. Characterisation data are the same as those reported for **(19e)**.

Triethyl-10-[(1-*naphthyl*)*methylcarbamoylmethyl*]-1,4,7,10-*tetraazacyclododecane*-1,4,7-*triyltrimethylenetri*(*methylphosphinate*) **(19c)**

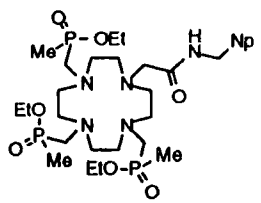

The title compound was prepared following a method similar to that for **(19d)** using the monosubstituted macrocycle **(17c)** (0.2 g, 0.55 mmol), methyldiethoxyphosphine **(18)** (26.7 cm^3 of a 0.09 mol dm^{-3} solution in diethyl ether, 2.46 mmol), paraformaldehyde (0.08 g, 2.73 mmol) in dry tetrahydrofuran (30 cm^3) to yield a yellow oil (0.1 g, 29%) after purification, R_f (Al_2O_3; 10% CH_3OH-CH_2Cl_2; I_2 and u.v. detection) 0.57; δ_H (250 MHz; $CDCl_3$) 8.70 (1 H, s, NH), 7.89-7.86 (4 H, m, Ar), 7.55-7.52 (3 H, m, Ar), 4.73 (2 H, d, ^3J 6.8, CH_2Ar), 4.04 (6 H, m, $C\underline{H}_2CH_3$), 3.29 (2 H, s, CH_2CO), 3.10-2.46 (22 H, ring-CH_2, CH_2P), 1.50-1.30 (18 H, m, PCH_3, $CH_2\underline{C}H_3$); $\delta_C\{^1H\}$ (62.9 MHz; $CDCl_3$) 171.5 (CO), 136.7 (q-Ar), 133.3 (q-Ar), 132.6 (q-Ar), 128.2 (Ar), 127.6 (Ar), 126.6 (Ar), 126.3 (Ar), 125.8 (Ar), 60.1 ($\underline{C}H_2CH_3$), 55.5-53.3 (ring-CH_2, CH_2P, $\underline{C}H_2CO$), 43.2 (CH_2N), 16.7 ($CH_2\underline{C}H_3$), 13.9 (d, ^1J 88, PCH_3); $\delta_P\{^1H\}$ (101.3 MHz;

$CDCl_3$) 52.5, (1 P), 52.2 (1 P), 52.1 (1 P). (A satisfactory accurate mass spectrum could not be obtained for this product).

10-[(S)-1-(1-*Phenyl*)*ethylcarbamoylmethyl*]-1,4,7,10-*tetraazacyclododecane*-1,4,7-*triyltrimethylenetri*(*methylphosphinic acid*) **(1d)**

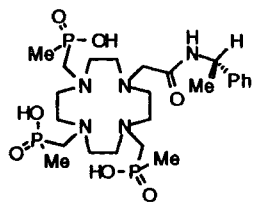

The monoamide triphosphinate ester **(19d)** (0.3 g, 0.4 mmol) was stirred in a solution of potassium hydroxide (10 cm^3 of a 10% solution in water) at room temperature for 18 h. The solution was neutralised to pH 6.5 with hydrochloric acid (0.1 mol dm^{-3} solution) and the solvent removed by lyophilization. The resulting solid was dissolved in hot ethanol (5 cm^3) and the remaining salts removed by centrifugation followed by filtration. The solvent was removed *in vacuo* to give a pale yellow solid (0.2 g, 82%), m.p. >200 °C; ν_{max} (solid)/cm^{-1} 3288 (br) (N-H), 1639 (C=O); δ_H (250 MHz; D_2O) 8.09 (1 H, s, NH), 7.07-6.97 (5 H, m, Ar), 4.58 (1 H, m, CH), 3.33-2.14 (24 H, br m, ring-CH_2, CH_2P, CH_2CO), 1.11 (3 H, d, ^3J 6.8, CH_3), 0.95 (9 H, d, ^2J 13.0, PCH_3); $\delta_C\{^1H\}$ (62.9 MHz; D_2O) 171.1 (CO), 143.5 (q-Ar), 128.7 (m-Ar), 127.3 (p-Ar), 125.7 (o-Ar), 55.0-47.0 (ring-CH_2, $\underline{C}H_2CO$, CH_2P, CHN), 21.2 (CH_3), 16.6 (d, ^1J 91, PCH_3); $\delta_P\{^1H\}$ (101.3 MHz; D_2O) 40.0-28.6 (3 P, br); m/z (FAB) 610 (100%, MH^+) (Found: MH^+, 610.2699. $C_{24}H_{47}N_5O_7P_3$ requires MH^+, 610.2688).

10-[(R)-1-(1-*Naphthyl*)*ethylcarbamoylmethyl*]-1,4,7,10-*tetraazacyclododecane*-1,4,7-*triyltrimethylenetri*(*methylphosphinic acid*) **(1e)**

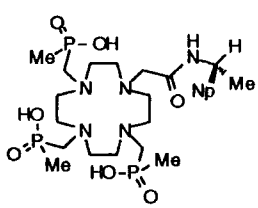

The title compound was prepared following a method similar to that for **(1d)** using monoamide triphosphinate ester **(19e)** (0.16 g, 0.2 mmol) in a solution of potassium hydroxide (10 cm^3 of a 10% solution in water) to give a pale yellow solid (0.13 g, 92%), m.p. >200 °C; ν_{max} (solid)/cm^{-1} 3243 (N-H), 1652 (C=O); δ_H (250 MHz; D_2O) 7.80-7.10 (7 H, m, Ar), 5.36 (1 H, m, CH), 3.30-2.00 (24 H, br m, ring-CH_2, CH_2P, CH_2CO), 1.20 (3 H, d, ^3J 6.7, CH_3), 0.93-0.79 (9 H, br m, PCH_3); $\delta_C\{^1H\}$ (62.9 MHz; D_2O) 170.1 (CO), 138.6 (q-Ar), 133.4 (q-Ar), 130.0 (q-Ar), 127.3-123.8 (Ar), 121.3, (Ar), 53.7-45.0 (br m, CH_2P, ring-CH_2, CHN, $\underline{C}H_2CO$), 20.0-15.0 (br m, CH_3, PCH_3); $\delta_P\{^1H\}$ (101.3 MHz; D_2O) 39.6-27.0 (3 P, br m); m/z (FAB) 660 (100%, MH^+) (Found: MH^+, 660.2858. $C_{28}H_{49}N_5O_7P_3$ requires MH^+, 660.2844).

10-[(S)-1-(1-*Naphthyl)ethylcarbamoylmethyl*]-1,4,7,10-*tetraazacyclododecane*-1,4,7-*triyltrimethylenetri(methylphosphinic acid)* **(1f)**

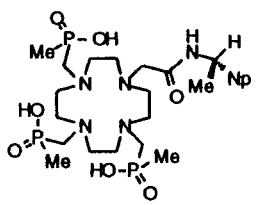

The title compound was prepared following a method similar to that for **(1d)** using monoamide triphosphinate ester **(19f)** (0.65 g, 0.87 mmol) in a solution of potassium hydroxide (10 cm^3 of a 10% solution in water) to give a pale yellow solid (0.53 g, 92%). Characterisation data are the same as those reported for **(1e)**. (Found: MNa^+, 682.2682. $C_{28}H_{48}N_5NaO_7P_3$ requires MNa^+, 682.2664).

10-[(1-*Naphthyl)methylcarbamoylmethyl*]-1,4,7,10-*tetraazacyclododecane*-1,4,7-*triyltrimethylenetri(methylphosphinic acid)* **(1c)**

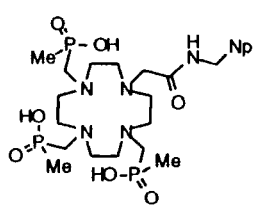

The title compound was prepared following a method similar to that for **(1d)** using monoamide triphospinate ester **(19c)** (0.1 g, 0.16 mmol) in a solution of potassium hydroxide (10 cm^3 of a 10% solution in water) to give a pale yellow solid (0.07 g, 67%), m.p. >200 ^oC; ν_{max} (solid)/cm^{-1} 3291 (br) (N-H), 1644 (C=O); δ_H (250 MHz; D_2O) 7.60-7.16 (7 H, br m, Ar), 4.22 (2 H, s, CH_2Ar), 3.23-2.59 (24 H, br m, ring-CH_2, CH_2CO, CH_2P), 0.88 (9 H, d, ^2J 13.4, PCH_3); $\delta_C\{^1H\}$ (62.9 MHz; D_2O) 172.1 (CO), 135.5 (q-Ar), 132.8, (q-Ar) 132.2 (q-Ar), 128.3 (Ar), 127.5 (Ar), 126.5 (Ar), 126.1 (Ar), 125.7 (Ar), 56.4 ($\underline{C}H_2CO$), 54.2-50.5 (ring-CH_2, CH_2P), 43.0 (CH_2N), 16.9 (d, ^1J 96, PCH_3); $\delta_P\{^1H\}$ (101.3 MHz; D_2O) 39.4 (2 P), 33.0 (1 P); m/z (ES-) 645 (100%, M)
(A satisfactory accurate mass spectrum could not be obtained for this product).

Lanthanide complexes of **(1c)-(1f)**

[Eu.1d] (20d)

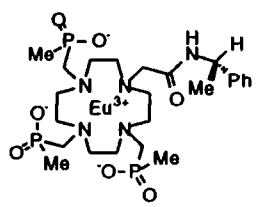

Europium (III) acetate (0.05 g, 0.14 mmol) was added to a stirred solution of compound **(1d)** (0.07 g, 0.12 mmol) in water (3 cm^3) and the solution was heated at reflux for 18 h. The solvent was removed by lyophilisation and the resulting solid extracted into hot ethanol (4 cm^3). The remaining salts were removed by centrifugation followed by filtration and the solvent removed in vacuo to give a yellow-brown solid. Purification by column chromatography through a plug of alumina (5% MeOH-CH_2Cl_2) yielded a pale yellow solid (0.02 g, 22%), m.p. >250 ^oC; R_f (Al_2O_3; 15% MeOH-CH_2Cl_2; I_2 detection) 0.4 (br); ν_{max} (solid)/cm^{-1} 3314 (br) (N-H), 1620 (C=O); m/z (ES-) 758.05 (100%, M) (Found: MH^+, 760.1663. $C_{24}H_{44}EuN_5O_7P_3$ requires MH^+, 760.1666).
Major isomer δ_H (90 MHz; D_2O; 291 K) [Partial assignment] 28.2 (1 H, br, ring-H_{ax}), 25.1 (1 H, br, ring-H_{ax}), 17.2 (1 H, br, ring-H_{ax}), 13.7 (1 H, br, ring-H_{ax}), 9.5 (1 H, br, ring-H_{ax}), 6.8-5.9 (5 H, m, Ar), 2.1 (3 H, d, ^3J 6.2, CH_3), 1.6-(-0.7) (3 H, br, ring-H_{eq}), -1.5 (3 H, d, ^2J 16, PCH_3), -3.8 (3 H, d, ^2J 14, PCH_3), -4.5-(-5.9) (2 H, br, ring-H_{ax}),

-6.4 (3 H, d, ^{2}J 14, PCH_3), -6.9-(-7.8) (2 H, br, ring-H_{eq}), -10.8-(-11.5) (2 H, br, ring-H_{ax}, ring-H_{eq}), -14.5-(-15.3) (2 H, br, ring-H_{eq}); $\delta_C\{^1H\}$ (62.9 MHz; D_2O) 200.9 (CO), 146.3 (q-Ar), 128.7 (m-Ar), 127.0 (p-Ar), 125.5 (o-Ar), 107.4-60.0 (ring-CH_2, CH_2P, $\underline{C}H_2CO$), 52.6 (CHN), 24.8 (CH_3), 6.8-2.1 (PCH_3); $\delta_P\{^1H\}$ (101.3 MHz; D_2O) 95.5 (1 P), 83.3 (1 P), 68.2 (1 P).

Minor isomer δ_H (90 MHz; D_2O; 18 K) [Partial assignment] 27.6 (1 H, br, ring-H_{ax}), 25.1 (1 H, br, ring-H_{ax}), 17.2 (1 H, br, ring-H_{ax}), 13.7 (1 H, br, ring-H_{ax}), 11.0 (1 H, br, ring-H_{ax}), 6.8-5.9 (5 H, m, Ar), 1.8-(-0.5) (3 H, br, ring-H_{eq}), 1.3 (3 H, d, ^{3}J 6.3, CH_3), -0.3 (3 H, d, ^{2}J 14, PCH_3), -4.4 (3 H, d, ^{2}J 14, PCH_3), -5.9 (3 H, d, ^{2}J 16, PCH_3), -7.6-(-15.5) (8 H, br, 3 ring-H_{ax}, 5 ring-H_{eq}); $\delta_C\{^1H\}$ (62.9 MHz; D_2O) 202.6 (CO), 134-125 (Ar), 107.4-60.0 (ring-CH_2, CH_2P, $\underline{C}H_2CO$), 53.7 (CHN), 23.3 (CH_3), 6.8-2.1 (PCH_3); $\delta_P\{^1H\}$ (101.3 MHz; D_2O) 97.3 (1 P), 79.0 (1 P), 64.6 (1 P).

[Eu.1e] (20e)

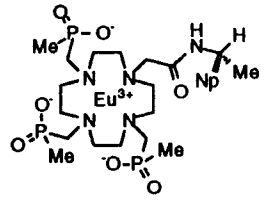

The title compound was prepared following a method similar to that for **(20d)** using europium (III) acetate (0.012 g, 0.13 mmol), compound **(1e)** (0.06 g, 0.09 mmol) in water (3 cm^3) to yield a pale yellow solid (0.034 g, 46%), m.p. >250 ^oC; R_f (Al_2O_3; 15% CH_3OH-CH_2Cl_2; I_2 detection) 0.35 (br); ν_{max} (solid)/cm^{-1} 3256 (br) (N-H), 1620 (C=O); m/z (ES-) 808 (100%, M) (Found: MH^+, 810.1983. $C_{28}H_{45}EuN_5O_7P_3$ requires MH^+, 810.1822).

Major isomer δ_H (90 MHz; D_2O; 278 K) [Partial assignment] 28.7 (1 H, br, ring-H_{ax}), 25.7 (1 H, br, ring-H_{ax}), 17.6 (1 H, br, ring-H_{ax}), 2.2 (3 H, d, ^{3}J 6.6, CH_3), -2.3 (3 H, d, ^{2}J 14.7, PCH_3), -4.0 (3 H, d, ^{2}J 15.5, PCH_3), -6.6 (3 H. d, ^{2}J 15.5, PCH_3); $\delta_C\{^1H\}$ (400 MHz; D_2O; 278K) 227 (CO), 145 (q-Ar), 136 (q-Ar), 135 (q-Ar), 131 (Ar), 130 (Ar), 129 (Ar), 128 (Ar), 127 (Ar), 125 (Ar), 122 (Ar), 134-127 (ring-CH_2, CH_2P, $\underline{C}H_2CO$),

52 (CHN), 25 (CH_3), 8-4 (PCH_3); $\delta_P\{^1H\}$ (101.3 MHz; D_2O) 96.0 (1 P), 82.3 (1 P), 66.8 (1 P).

Minor isomer δ_H (90 MHz; D_2O; 278K) [Partial assignment] 29.1 (1 H, br, ring-H_{ax}), 27.5 (1 H, br, ring-H_{ax}), 15.1 (1 H, br, ring-H_{ax}), 1.77 (1 H, d, ^3J 5.9, CH_3), -3.4 (3 H, d, ^2J 15.5, PCH_3), -5.1 (3 H, d, ^2J 15.5, PCH_3), -6.4 (1 H, d, ^2J 15.5, PCH_3); $\delta_C\{^1H\}$ (400 MHz; D_2O; 298K) 250 (CO), 147 (q-Ar), 141 (q-Ar), 138 (q-Ar), 134-127 (Ar), 110-65 (ring-CH_2, CH_2P, $\underline{C}H_2CO$), 53 (CHN), 24 (CH_3), 8-4 (PCH_3); $\delta_P\{^1H\}$ (101.3 MHz; D_2O) 97.9 (1 P), 80.3 (1 P), 66.0 (1 P).

[Eu.1f] (20f)

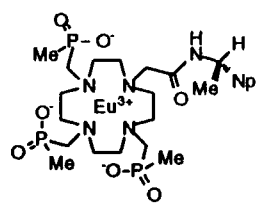

The title compound was prepared following a method similar to that for **(20d)** using europium (III) acetate (0.2 g, 0.3 mmol), compound **(1f)** (0.2 g, 0.3 mmol) in water (3 cm^3) to yield a pale yellow solid (0.13 g, 53%). Characterisation data are the same as those reported for **(20e).** (Found: MH^+, 810.1943. $C_{28}H_{45}EuN_5O_7P_3$ requires MH^+, 810.1822).

[Eu.1c] (20c)

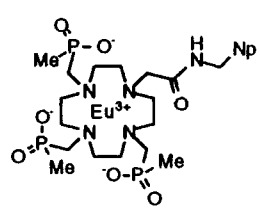

The title compound was prepared using a method similar to that for **(20d)** using europium (III) acetate (0.047 g, 0.14 mmol), compound **(1c)** (0.055 g, 0.1 mmol) in water (3 cm^3) to yield a pale yellow solid (0.028 g, 41%), m.p. >250 ^oC; R_f (Al_2O_3; 10% CH_3OH-CH_2Cl_2; I_2 detection) 0.74-0.34; δ_H (90 MHz; D_2O; 301K) [Partial assignment] 27.7 (1 H, br, ring-H_{ax}), 24.6 (1 H, br, ring-H_{ax}), 17.1 (1 H, br, ring-H_{ax}),

12.9 (1 H, br, ring-H_{ax}), 9.41 (1 H, br, ring-H_{ax}), 8.44-6.58 (5 H, m, Ar), 1.71-(-0.51) (3 H, br, ring-H_{eq}), -1.20 (3 H, d, ^{2}J 14, PCH_3), -3.62 (3 H, d, ^{2}J 14, PCH_3), -4.42 (1 H, br, ring-H_{ax}), -5.93 (3 H, d, ^{2}J 14, PCH_3), -6.01-(-7.4) (3 H, br, ring-H_{ax}, 2 ring-H_{eq}), -10.0-(-14.1) (4 H, br, ring-H_{ax}, 3 ring-H_{eq}); $\delta_C\{^1H\}$ (400 MHz; D_2O; 298K), 203.5 (CO), 140.5 (q-Ar), 137.0 (q-Ar), 135.0 (q-Ar), 131.5 (Ar), 130.5 (Ar), 130.0 (Ar), 129.0 (Ar), 128.5 (Ar), 128.0 (Ar), 127.5 (Ar), 108.0 (ring-CH_2), 106.0 (ring-CH_2), 104.0 (ring-CH_2), 86.0 (ring-CH_2), 85.0 (d, ^{1}J 90, CH_2P), 82.0 (ring-CH_2), 72.5 (ring-CH_2), 69.5 (d, ^{1}J 90, PCH_2), 68.5 (ring-CH_2, $\underline{C}H_2CO$), 63.0 (d, ^{1}J 90, PCH_2), 48.0 (CH_2Np), 7.5 (d, ^{1}J 90, PCH_3), 6.5 (d, ^{1}J 90, PCH_3), 4.5 (d, ^{1}J 90, PCH_3); $\delta_P\{^1H\}$ (101.3 MHz; D_2O) 96.6 (1 P), 84.4 (1 P), 67.4 (1 P); m/z (ES-) 794 (100%, M) (A satisfactory accurate mass could not be obtained for this product).

[Gd.1d] (21d)

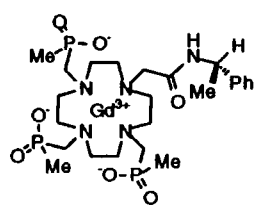

The title compound was prepared following a method similar to that for **(20d)** using gadolinium (III) acetate (0.046 g, 0.14 mmol), compound **(1d)** (0.06 g, 0.1 mmol) in water (3 cm^3) to yield a colourless solid (0.02 g, 26%), m.p. >250 °C; R_f (Al_2O_3; 15% CH_3OH-CH_2Cl_2; I_2 detection) 0.60 (br); ν_{max} (solid)/cm^{-1} 3300 (br) (N-H), 1620 (C=O); m/z (ES-) 762 (100%, M) (Found: M, 764.1631. $C_{24}H_{43}GdN_5O_7P_3$ requires M, 764.1616).

[Gd.(1f)] (21f)

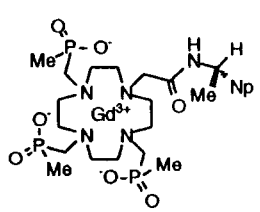

The title compound was prepared following a method similar to that for **(20d)** using gadolinium (III) acetate (0.049 g, 0.15 mmol), compound **(1f)** (0.07 g, 0.1 mmol) in water (3 cm^3) to yield a colourless solid (0.02 g, 25%), m.p. >250 °C; R_f (Al_2O_3; 15% CH_3OH-CH_2Cl_2; I_2 detection) 0.42 (br); m/z (ES-) 812 (100%, M). (A satisfactory accurate mass spectrum could not be obtained for this product).

[Tb.1d] (22d)

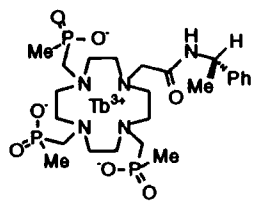

The title compound was prepared following a method similar to that for **(20d)** using terbium (III) acetate (0.05 g, 0.14 mmol), compound **(1d)** (0.06 g, 0.1 mmol) in water (3 cm^3) to yield a pale yellow solid (0.03 g, 40%), m.p. >250 °C; R_f (Al_2O_3; 15% CH_3OH-CH_2Cl_2; I_2 detection) 0.4 (br); ν_{max} (solid)/cm^{-1} 3333 (br) (N-H), 1620 (C=O); $\delta_P\{^1H\}$ (101.3 MHz; D_2O) 631, (br), 607 (br), 599 (br), 495 (br), 455, (br); m/z (ES-) 764 (100%, M) (Found: MH^+, 766.1737. $C_{24}H_{44}N_5O_7P_3Tb$ requires MH^+, 766.1707).

[Tb.1e] (22e)

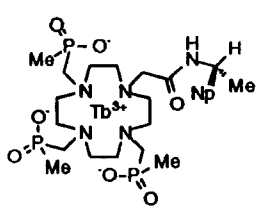

The title compound was prepared following a method similar to that for **(20d)** using terbium (III) acetate (0.043 g, 0.13 mmol), compound **(1e)** (0.06 g, 0.09 mmol) in water (3 cm^3) to yield a pale yellow solid (0.03 g, 40%), m.p. >250 °C; R_f (Al_2O_3; 15% CH_3OH-CH_2Cl_2; I_2 detection) 0.51 (br); ν_{max} (solid)/cm^{-1} 3333 (br) (N-H), 1614 (C=O); $\delta_P\{^1H\}$ (101.3 MHz; D_2O) 663 (br), 619 (br), 609 (br), 487 (br), 450 (br); m/z

(ES-) 814 (100%, M) (Found: MH^+, 816.1862. $C_{28}H_{46}N_5O_7P_3Tb$ requires MH^+, 816.1863).

[Tb.1f] (22f)

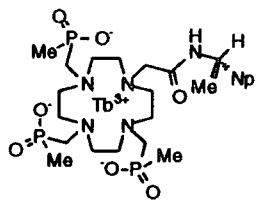

The title compound was prepared following a method similar to that for **(20d)** using terbium (III) acetate (0.071 g, 0.21 mmol), compound **(1f)** (0.1 g, 0.15 mmol) in water (3 cm^3) to yield a yellow solid (0.08 g, 65%). Characterisation data are the same as those reported for **(22e)**. (Found: MH^+, 816.1880. $C_{28}H_{46}N_5O_7P_3Tb$ requires MH^+, 816.1863).

5.4 Synthetic procedures and characterisation data for Chapter 3

5.4.1 Tetraphenylamide ligands and complexes

2-*Chloro*-N-[(R)-*methylbenzyl*]*ethanamide* **(12a)**

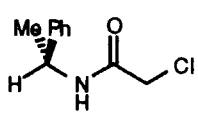

The title compound was prepared following a method similar to that for **(12b)** using (*R*)-α-methylbenzylamine (6 cm^3, 46.2 mmol) and triethylamine (7.7 cm^3, 55.5 mmol) in dry diethyl ether (60 cm^3) and reacting with a solution of chloroacetylchloride (4.4 cm^3, 55.5 mmol) in dry diethyl ether (40 cm^3). The product was recrystallised from diethyl ether and was isolated as white needles (5.6 g, 61%). Characterisation data are the same as those reported for **(12b)**. (Found: C, 60.7; H, 6.14; N, 6.91. $C_{10}H_{12}ClNO$ requires C, 60.8; H, 6.12; N, 7.08%).

1,4,7,10-*Tetrakis*-[(R)-1-(1-*phenyl*)*ethylcarbamoylmethyl*]-1,4,7,10-*tetraazacyclododecane* (**13a**)

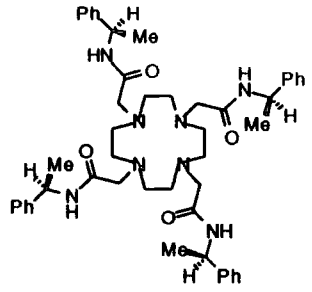

2-Chloro-*N*-[(*R*)-methylbenzyl]ethanamide (**12a**) (5.5 g, 27.8 mmol) in dry *N*,*N*-dimethylformamide (5 cm^3) was added to a stirred solution of 1,4,7,10-tetraazacyclododecane (0.96 g, 5.6 mmol) and fine mesh anhydrous potassium carbonate (3.8 g, 27.8 mmol) in dry *N*,*N*-dimethylformamide (60 cm^3) under an argon atmosphere. The reaction mixture was heated at 60 °C for 48 h. The solvent was removed by distillation *in vacuo* and the resulting brown oil was extracted into dichloromethane (40 cm^3), washed with water (3 x 40 cm^3) and brine (40 cm^3), dried (K_2CO_3) and the solvent removed *in vacuo* to yield a yellow oil. The product was purified by alumina column chromatography (gradient elution from dichloromethane to 2% methanol-dichloromethane). Recrystallisation from acetonitrile adding hexane yielded white needles (1.4 g, 31%), m.p. 120-122 °C (dec.); R_f (Al_2O_3; 10% CH_3OH-CH_2Cl_2; I_2 and u.v. detection) 0.34 (br); ν_{max} (thin film)/cm^{-1} 3293 (N-H), 1659 (C=O); δ_H (250 MHz; $CDCl_3$) 7.38-7.33 (20 H, m, Ar), 7.13 (4 H, d, ^3J 8.2, NH), 5.20 (4 H, m, CH), 2.97 (8 H, br s, CH_2CO), 2.60 (16 H, br s, ring-CH_2), 1.56 (12 H, d, ^3J 7, CH_3); $\delta_C\{^1H\}$ (62.9 MHz; $CDCl_3$) 170.2 (CO), 143.6 (q-Ar), 129.1 (m-Ar), 127.8 (p-Ar), 126.7 (o-Ar), 59.3 ($\underline{C}H_2CO$), 53.5 (ring-CH_2), 48.7 (CHN), 21.9 (CH_3); m/z (ES+) 839 (100%, MNa^+), 817 (63%, M^+) (Found: C, 70.1; H, 7.88 N, 13.9 $C_{48}H_{64}N_8O_4$ requires C, 70.6; H, 7.89; N, 13.7%).

1,4,7,10-*Tetrakis*-[(S)-1-(1-*phenyl*)*ethylcarbamoylmethyl*]-1,4,7,10-*tetraazacyclododecane* **(13b)**

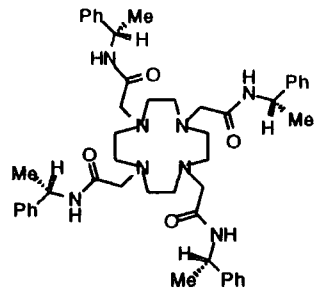

The title compound was prepared following a method similar to that for **(13a)** using 1,4,7,10-tetraazacyclododecane (0.96 g, 5.6 mmol) and fine mesh anhydrous potassium carbonate (3.8 g, 27.8 mmol) in dry *N,N*-dimethylformamide (60 cm^3) and 2-chloro-*N*-[(*S*)-methylbenzyl]ethanamide **(12b)** (5.6 g, 27.8 mmol) in dry *N,N*-dimethylformamide (10 cm^3). The product was recrystallised from acetonitrile and isolated as white needles (1.46g, 37%). Characterisation data are the same as those reported for **(13a)**. (Found: C, 70.6; H, 8.01; N, 14.0. $C_{48}H_{64}N_8O_4$ requires C, 70.6; H, 7.90; N, 13.7%).

Lanthanide Metal Triflates

Ytterbium (III) *triflate*

Prepared by a procedure similar to that described for lanthanum triflate.[6] Trifluoromethanesulphonic acid (10 g) was added to a suspension of ytterbium oxide (2.4 g) in water (5 cm^3) and the solution was stirred for 1 h. The water was removed *in vacuo* and the resulting white solid dried *in vacuo* (3.2 g, 85%) (Found: C, 5.28; H, 1.15; N, 0. $C_3F_9S_3O_9Yb.4H_2O$ requires C, 5.20; H, 1.16; N, 0%).

Praseodymium (III) *triflate*

Trifluoromethanesulphonic acid (10 g) was added to praseodymium chloride (1 g) and the mixture was heated at 60 °C for 1 h. Anhydrous acetonitrile (20 cm^3) was added and the resulting precipitate was removed by filtration, washed with more acetonitrile (4 x 20 cm^3) and dried *in vacuo* to give a pale green solid (0.5 g, 21 %) (Found: C, 4.80; H, 2.18; N, 0. $C_3F_9S_3O_9Pr.8H_2O$ requires C, 4.92; H, 2.20; N, 0%).

Lanthanide complexes of **(13a)** *and* **(13b)**

$[Dy.13a]^{3+}$ (23a)

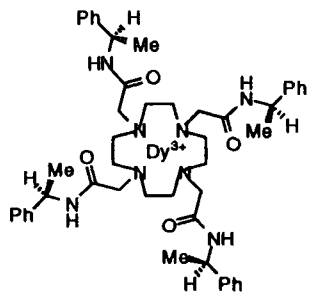

Dysprosium (III) triflate (0.116 g, 0.19 mmol) and trimethylorthoformate (2 cm^3) were heated at reflux in dry acetonitrile (2 cm^3) for 2 h. A solution of ligand **(13a)** (0.155 g, 0.19 mmol) in dry acetonitrile (1 cm^3) was added and the solution heated at reflux for a further 18 h. The solution was concentrated and added dropwise with stirring to diethyl ether (100 cm^3). The resulting white solid was filtered, dried *in vacuo* and recrystallised from acetonitrile to give white needles (0.18 g, 65%), m.p. >250 °C; R_f (SiO_2; 30% CH_3OH-$CH_3CO_2NH_4$) 0.15 (br); ν_{max} (solid)/cm^{-1} 3256 (br) (N-H), 1626 (C=O); δ_H (250 MHz; CD_3OD) 246.6 (4 H, br s, ring-H_{eq}), 108.6 (4 H, br s, ring-H_{ax}), 58.3 (4 H, br s, ring-H_{eq}), 8.4-6.7 (20 H, m, Ar), -3.1 (4 H, br s, CH), -7.1 (12 H, s, CH_3), -125.0 (4 H, br s, CH_2CO), -129.2 (4 H, br s, CH_2CO), -386.6 (4 H, br s, ring-H_{ax}); m/z (ES+) 1276 (15%, $[M^{3+} + 2(CF_3SO_3^-)]^+$), 564 (100%, $[M^{3+} + (CF_3SO_3^-)]^{2+}$), 326 (15%, M^{3+}) (Found: C, 42.8; H, 4.52; N, 7.56. $C_{51}H_{64}DyF_9N_8O_{13}S_3$ requires C, 42.9; H, 4.52; N, 7.85%).

$[Dy.13b]^{3+}$ (23b)

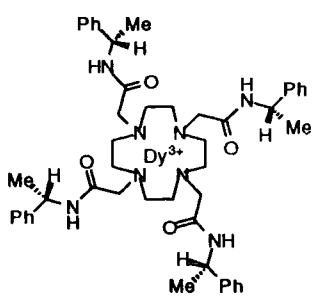

The title compound was prepared following a method similar to that for **(23a)** using dysprosium (III) triflate (0.373 g, 0.61 mmol) and trimethylorthoformate (5 cm^3) in dry acetonitrile (2 cm^3) and the ligand **(13b)** (0.5 g, 0.61 mmol) in dry acetonitrile (1 cm^3). Recrystallisation from acetonitrile yielded white needles (0.54 g, 62%). Characterisation data are the same as those reported for **(23a)**. (Found: C, 42.6; H, 4.47; N, 7.85. $C_{51}H_{64}DyF_9N_8O_{13}S_3.H_2O$ requires C, 42.4; H, 4.60; N, 7.76%).

$[Eu.13a]^{3+}$ (24a)

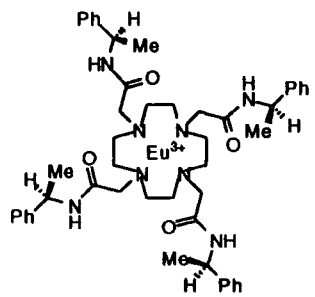

The title compound was prepared following a method similar to that for **(23a)** using europium (III) triflate (0.17 g, 0.28 mmol) and trimethylorthoformate (2 cm^3) in dry acetonitrile (1 cm^3) and the ligand **(13a)** (0.225 g, 0.28 mmol) in dry acetonitrile (1 cm^3). Recrystallisation from acetonitrile yielded white needles (0.27 g, 68%), m.p. >250 °C; R_f (SiO_2; 30% CH_3OH-$CH_3CO_2NH_4$) 0.2 (br); ν_{max} (solid)/cm^{-1} 3249 (br) (N-H), 1620 (C=O); δ_H (200 MHz; CD_3OD) 27.5 (4 H, s, ring-H_{ax}), 4.32-4.26 (20 H, m, Ar), 2.14 (4 H, br s, CH), -1.17 (12 H, d, ^3J 6.3, CH_3), -3.50 (4 H, d, ^2J 12.5, ring-H_{eq}), -8.44 (4 H, br s, ring-H'_{ax}), -8.93 (4 H, d, ^2J 13.0, ring-H'_{eq}), -16.0 (4 H, d, ^2J 15.5, CH_2CO), -16.4 (4 H, d, ^2J 15.6, CH_2CO); $\delta_C\{^1H\}$ (62.9 MHz; CD_3OD) 189.0 (CO), 142.3 (q-Ar), 127.9 (m-Ar), 127.2 (p-Ar), 124.3 (o-Ar), 110-107 (br, ring-CH_2), 90.0 (br, $\underline{C}H_2CO$), 85-83 (br, ring-CH_2), 47.1 (CHN), 21.7 (CH_3); m/z (ES+) 1267 (20%, $[M^{3+} + 2(CF_3SO_3^-)]^+$), 559 (100%, $[M^{3+} + (CF_3SO_3^-)]^{2+}$), 323 (20%, M^{3+}) (Found: C, 42.3; H, 4.64; N, 7.64. $C_{51}H_{64}EuF_9N_8O_{13}S_3.2H_2O$ requires C, 42.2; H, 4.72; N, 7.72%).

[Eu.13b]$^{3+}$ (24b)

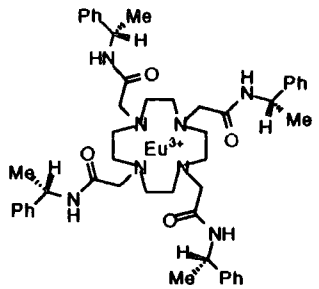

The title compound was prepared following a method similar to that for **(23a)** using europium (III) triflate (0.37 g, 0.61 mmol) and trimethylorthoformate (5 cm^3) in dry acetonitrile (2 cm^3) and the ligand **(13b)** (0.5 g, 0.61 mmol) in dry acetonitrile (1 cm^3). Recrystallisation from acetonitrile yielded white needles (0.61 g, 69%). Characterisation data are the same as those reported for **(24a)** (Found: C, 43.0; H, 4.52; N, 7.95. $C_{51}H_{64}EuF_9N_8O_{13}S_3$ requires C, 43.3; H, 4.55; N, 7.91%).

[Pr.13a]$^{3+}$ (25a)

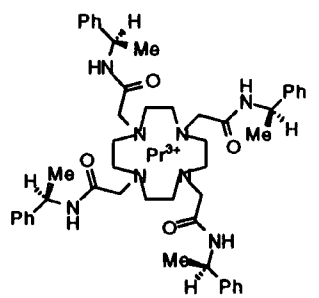

The title compound was prepared following a method similar to that for **(23a)** using praseodymium (III) triflate (0.3 g, 0.51 mmol) and trimethylorthoformate (1 cm^3) in dry acetonitrile (2 cm^3) and the ligand **(13a)** (0.42 g, 0.51 mmol) in dry acetonitrile (1 cm^3). Recrystallisation from acetonitrile yielded white needles (0.4 g, 56%), m.p. >250 ^oC; ν_{max} (solid)/cm^{-1} 3230 (br) (N-H), 1620 (C=O); δ_H (250 MHz; CD_3OD) 22.25 (4 H, br s, ring-H_{eq}), 11.05 (4 H, br s, ring-H_{ax}), 9.28 (4 H, br s, ring-H_{eq}), 5.86-5.62 (20 H, m, Ar), 3.82 (4 H, br s, CH), -0.57 (12 H, s, CH_3), -4.83 (4 H, br s, CH_2CO), -8.10 (4 H, d, ^2J 9.1, CH_2CO), -42.98 (4 H, br s, ring-H_{ax}); m/z (ES+) 553.5 (100%, $[M^{3+} + (CF_3SO_3^-)]^{2+}$); (Found: C, 42.7; H, 4.61; N, 7.64. $C_{51}H_{64}F_9N_8O_{13}PrS_3$ requires C, 42.5; H, 4.76; N, 7.77%).

[Tb.13a]$^{3+}$ (26a)

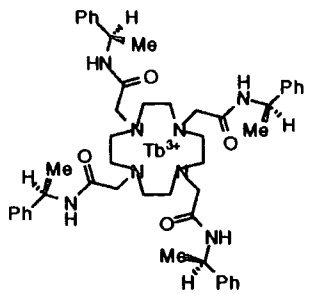

The title compound was prepared following a method similar to that for **(23a)** using terbium (III) triflate (0.15 g, 0.24 mmol) and trimethylorthoformate (1 cm^3) in dry acetonitrile (2 cm^3) and the ligand **(13a)** (0.20 g, 0.24 mmol) in dry acetonitrile (1 cm^3). Recrystallisation from acetonitrile yielded white needles (0.178 g, 52%), m.p. >250 °C; ν_{max} (solid)/cm^{-1} 3269 (br) (N-H), 1620 (C=O); m/z (ES+) 1274 (10%, $[M^{3+} + 2(CF_3SO_3^-)]^+$), 563 (100%, $[M^{3+} + (CF_3SO_3^-)]^{2+}$), 325 (30%, M^{3+}); $[\alpha]_D$ +104.2 (c. 2.211 in CH_3OH) (Found: C, 41.9; H, 4.48; N, 7.60. $C_{51}H_{64}F_9N_8O_{13}S_3Tb.H_2O$ requires C, 42.0; H, 4.70; N, 7.68%).

[Tb.13b]$^{3+}$ (26b)

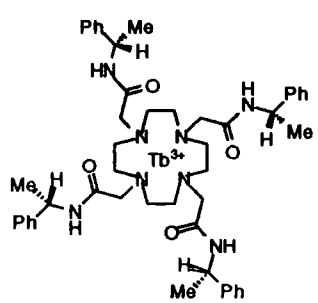

The title compound was prepared following a method similar to that for **(23a)** using terbium triflate (0.22 g, 0.37 mmol) and trimethylorthoformate (2 cm^3) in dry acetonitrile (2 cm^3) and the ligand **(13b)** (0.30 g, 0.37 mmol) in dry acetonitrile (1 cm^3). Recrystallisation from acetonitrile yielded white needles (0.284 g, 54%). Characterisation data are the same as those reported for **(26a)**, $[\alpha]_D$ -104.2 (c. 0.144 in CH_3OH) (Found: C, 43.4; H, 4.58; N, 7.78. $C_{51}H_{64}F_9N_8O_{13}S_3Tb$ requires C, 43.0; H, 4.53; N, 7.87%).

$[Yb.13a]^{3+}$ (27a)

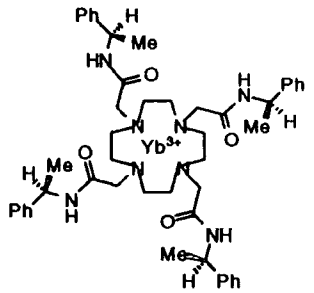

The title compound was prepared following a method similar to that for **(23a)** using ytterbium (III) triflate (0.15 g, 0.24 mmol) and trimethylorthoformate (1 cm^3) in dry acetonitrile (2 cm^3) and the ligand **(13a)** (0.2 g, 0.24 mmol) in dry acetonitrile (1 cm^3). Recrystallisation from acetonitrile yielded white needles (0.21 g, 61%), m.p. >250 °C; ν_{max} (solid)/cm^{-1} 3249 (br) (N-H), 1620 (C=O); δ_H (250 MHz; CD_3OD) 102 (4 H, br s, ring-H_{ax}), 18.2 (4 H, br s, ring-H_{eq}), 14.8 (4 H, br s, ring-H_{eq}), 4.80-1.83 (20 H, m, Ar), -1.42 (4 H, s, CH), -4.73 (12 H, s, CH_3), -28.8 (4 H, s, CH_2CO), -34.5 (4 H, s, CH_2CO), -66.5 (4 H, br s, ring-H_{ax}); m/z (ES+) 568 (100%, $[M^{3+} + (CF_3SO_3^-)]^{2+}$), 494 (50%, M^{3+}) (Found: C, 41.6; H, 4.41; N, 7.30. $C_{51}H_{64}F_9N_8O_{13}S_3Yb$ requires C, 41.6; H, 4.65; N, 7.61%).

5.4.2 Triphenylamide ligands and complexes

1,4,7-*Tris*-[(R)-1-(1-*phenyl*)*ethylcarbamoylmethyl*]-1,4,7,10-*tetraazacyclododecane* **(14)**

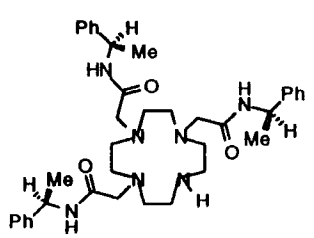

2-Chloro-*N*-[(*R*)-methylbenzyl]ethanamide **(12a)** (1.17 g, 5.9 mmol) in dry ethanol (10 cm^3) was added dropwise over 8 h to a heated solution of 1,4,7,10-tetraazacyclododecane (0.34 g, 2.0 mmol) and triethylamine (0.83 cm^3, 5.9 mmol) in dry ethanol (30 cm^3) at 60 °C. The reaction mixture was heated at reflux temperature

for a further 18 h, concentrated *in vacuo,* poured into aqueous hydrochloric acid (0.1 mol dm^{-3}, 40 cm^3) and washed with diethylether (3 x 30 cm^3). The aqueous phase was neutralised by the addition of sodium hydroxide solution (0.1 mol dm^{-3}) and extracted into dichloromethane (3 x 30 cm^3). The extract was dried (K_2CO_3) and the solvent removed i*n vacuo* to yield a yellow oil. The product was purified by alumina column chromatography (gradient elution from dichloromethane to 2% methanol-dichloromethane) giving a pale yellow solid (380 mg, 29%), m.p. 63-65 °C; R_f (Al_2O_3; 10% MeOH-CH_2Cl_2; I_2 and u.v. detection) 0.5 (br); ν_{max} (thin film)/cm^{-1} 3363 (N-H), 1643 (C=O); δ_H (250MHz; $CDCl_3$) 7.30 (3 H, s, NHCO), 7.29-7.21 (15 H, m, Ar), 5.12 (3 H, m, CH), 2.97 (4 H, br s, CH_2CO), 2.93 (2 H, br s , CH_2CO), 2.58 (16 H, br m, ring-CH_2), 1.8 (1 H, br s, ring-NH), 1.48 (6 H, d, ^3J 7.1, CH_3), 1.45 (3 H, d, ^3J 7.6, CH_3); $\delta_C\{^1H\}$ (62.9 MHz; $CDCl_3$) 170.8 (2 C, CO), 170.6 (CO), 143.7 (q-Ar), 129.1 (m-Ar), 127.8 (p-Ar), 127.0 (o-Ar), 59.9 (2 C, $\underline{C}H_2CO$), 58.0 ($\underline{C}H_2CO$), 54.5 (ring-CH_2), 53.6 (ring-CH_2), 48.9 (2 C, CHN), 48.6 (CHN), 47.6 (ring-CH_2), 22.1 (CH_3), 21.9 (CH_3); m/z (ES+) 656 (100%, MH^+) (Found: 656.4287. $C_{38}H_{54}N_7O_3$ requires MH^+, 656.4288).

Lanthanide complexes of **(14)**

$[Dy.14]^{3+}$

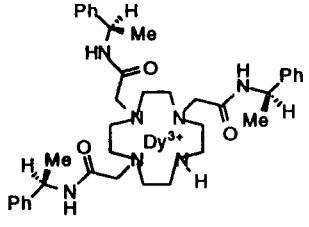

The title compound was prepared following a method similar to that for **(23a)** using dysprosium (III) triflate (0.09 g, 0.15 mmol) and trimethylorthoformate (2 cm^3) in dry acetonitrile (1 cm^3) and the ligand **(14)** (0.10 g, 0.15 mmol) in dry acetonitrile (1 cm^3) to yield a pale brown solid (0.13 g, 68%), m.p. 161-165 °C; ν_{max} (solid)/cm^{-1} 3262 (br) (N-H), 1620 (C=O); m/z (ES+) 1115 (30%, $[M^{3+} + 2(CF_3SO_3^-)]^+$), 484 (100%, $[M^{3+} + (CF_3SO_3^-)]^{2+}$).

[Eu.14]$^{3+}$

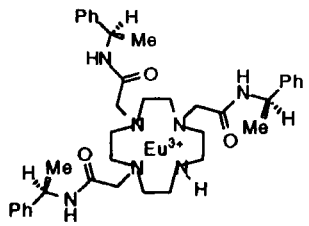

The title compound was prepared following a method similar to that for **(23a)** using europium (III) triflate (0.09 g, 0.15 mmol) and trimethylorthoformate (2 cm^3) in dry acetonitrile (1 cm^3) and the ligand **(14)** (0.10 g, 0.15 mmol) in dry acetonitrile (1 cm^3) to yield a pale brown solid (0.12 g, 65%), m.p. 174-177 °C; ν_{max} (solid)/cm^{-1} 3288 (br) (N-H), 1620 (C=O); m/z (ES+) 1107 (15%, $[M^{3+} + 2(CF_3SO_3^-)]^+$), 478 (100%, $[M^{3+} + (CF_3SO_3^-)]^{2+}$) (Found: 957.2971. $C_{39}H_{53}EuF_3N_7O_6S$ requires M, 957.2959).

[Tb.14]$^{3+}$

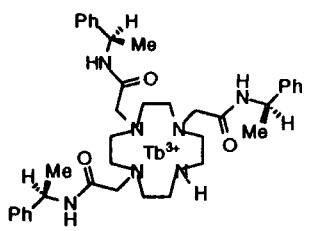

The title compound was prepared following a method similar to that for **(23a)** using terbium (III) triflate (0.12 g, 0.2 mmol) and trimethylorthoformate (1 cm^3) in dry acetonitrile (2 cm^3) and the ligand **(14)** (0.13 g, 0.2 mmol) in dry acetonitrile (1 cm^3) to yield a pale brown solid (0.15 g, 58%), m.p. 160-163 °C; ν_{max} (solid)/cm^{-1} 3294 (br) (N-H), 1620 (C=O); m/z (ES+) 1113 (10%, $[M^{3+} + 2(CF_3SO_3^-)]^+$), 482 (100%, $[M^{3+} + (CF_3SO_3^-)]^{2+}$) (Found: 963.3025. $C_{39}H_{53}F_3N_7O_6STb$ requires M, 963.3000).

5.4.3 Diphenylamide ligands and complexes

1,7-*Bis*-[(R)-1-(1-*phenyl*)*ethylcarbamoylmethyl*]-1,4,7,10-*tetraazacyclododecane* **(15)**

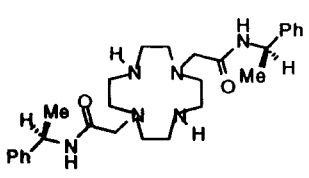

The title compound was prepared following a method similar to that for **(14)** using 1,4,7,10-tetraazacyclododecane (0.34 g, 2.0 mmol) and triethylamine (0.83 cm^3, 5.9 mmol) in dry ethanol (30 cm^3) and 2-chloro-*N*-[(*R*)-methylbenzyl]ethanamide **(12a)** (1.17 g, 5.9 mmol) in dry ethanol (10 cm^3). The product was purified by flash silica chromatography (gradient elution from dichloromethane to 3% isopropylamine-dichloromethane) giving a pale yellow solid (300 mg, 11%), m.p. 53-55 °C; R_f (SiO_2; 8% $(CH_3)_2CHNH_2$-CH_2Cl_2; I_2 and u.v. detection) 0.39; ν_{max} (thin film)/cm^{-1} 3366 (N-H), 1652 (C=O); δ_H (250MHz; $CDCl_3$) 7.78 (2 H, d, ^3J 7.5, NHCO), 7.34-7.23 (10 H, m, Ar), 5.11 (2 H, m, CH), 3.07 (4 H, m, CH_2CO), 2.90-2.50 (16 H, br m, ring-CH_2), 2.10 (2 H, br s, ring-NH), 1.49 (4 H, d, ^3J 6.8, CH_3); $\delta_C\{^1H\}$ (62.9 MHz; $CDCl_3$) 170.8 (CO), 144.0 (q-Ar), 129.3 (m-Ar), 128.0 (p-Ar), 127.2 (o-Ar), 57.6 ($\underline{C}H_2CO$), 53.4 (ring-CH_2), 52.7 (ring-CH_2), 49.0 (CHN), 45.9 (ring-CH_2), 45.5 (ring-CH_2), 22.0 (CH_3); m/z (ES+) 495 (100%, MH^+) (Found: 495.3427. $C_{28}H_{42}N_6O_2$ requires MH^+, 495.3447).

Lanthanide complexes of **(15)**

$[Dy.15]^{3+}$

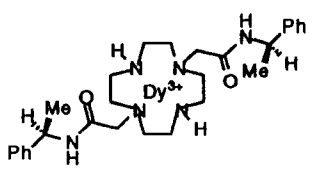

The title compound was prepared following a method similar to that for **(23a)** using dysprosium (III) triflate (0.12 g, 0.2 mmol) and trimethylorthoformate (2 cm^3) in dry acetonitrile (1 cm^3) and the ligand **(15)** (0.10 g, 0.2 mmol) in dry acetonitrile (1 cm^3) to yield a pale brown solid (0.14 g, 63%), m.p. 151-154 °C; ν_{max} (solid)/cm^{-1} 3307 (br) (N-H), 1639 (C=O), 1614 (C=O); m/z (ES+) 954 (15%, $[M^{3+} + 2(CF_3SO_3^-)]^+$), 404 (100%, $[M^{3+} + (CF_3SO_3^-)]^{2+}$).

[Eu.15]$^{3+}$

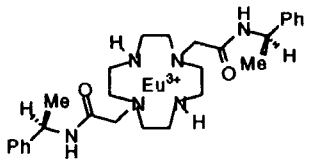

The title compound was prepared following a method similar to that for **(23a)** using europium (III) triflate (0.12 g, 0.2 mmol) and trimethylorthoformate (2 cm^3) in dry acetonitrile (1 cm^3) and the ligand **(15)** (0.10 g, 0.2 mmol) in dry acetonitrile (1 cm^3) to yield a pale brown solid (0.14 g, 62%), m.p. 171-175 °C; ν_{max} (solid)/cm^{-1} 3300 (br) (N-H), 1639 (C=O), 1614 (C=O); m/z (ES+) 942 (80%, $[M^{3+} + 2(CF_3SO_3^-)]^+$), 398 (100%, $[M^{3+} + (CF_3SO_3^-)]^{2+}$) (Found: 945.1633. $C_{30}H_{42}EuF_6N_6O_8S_2$ requires M, 945.1656).

[Tb.15]$^{3+}$

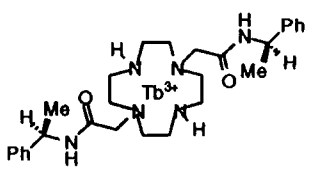

The title compound was prepared following a method similar to that for **(23a)** using terbium (III) triflate (0.12 g, 0.2 mmol) and trimethylorthoformate (1 cm^3) in dry acetonitrile (2 cm^3) and the ligand **(15)** (0.10 g, 0.2 mmol) in dry acetonitrile (1 cm^3) to yield a pale brown solid (0.11 g, 51%), m.p. 158-161 °C; ν_{max} (solid)/cm^{-1} 3300 (br) (N-H), 1639 (C=O), 1614 (C=O); m/z (ES+) 951 (75%, $[M^{3+} + 2(CF_3SO_3^-)]^+$), 401 (100%, $[M^{3+} + (CF_3SO_3^-)]^{2+}$) (Found: 951.1705. $C_{30}H_{42}F_6N_6O_8S_2Tb$ requires M, 951.1697).

5.4.4 Tetranaphthylamide ligands and complexes

2-*Chloro*-N-[(R)- 2-*naphthyl*]*ethylethanamide* **(12e)**

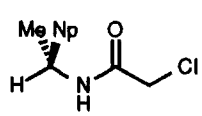

The title compound was prepared following a method similar to that for **(12a)** using (*R*)-1-(2-naphthyl)ethylamine (5 g, 29.2 mmol) and triethylamine (4.88 cm^3, 35.0 mmol) in dry diethyl ether (60 cm^3) and reacting with a solution of chloroacetylchloride (2.79 cm^3, 35.0 mmol) in dry diethyl ether (30 cm^3). The product was recrystallised from diethyl ether and isolated as white needles (5.57 g, 77%), m.p. 114-115 ^oC; ν_{max} (solid)/cm^{-1} 3256 (N-H), 1646 (C=O); δ_H (250 MHz; $CDCl_3$) 7.88-7.75 (4 H, m, Ar), 7.52-7.43 (3 H, m, Ar), 6.94 (1 H, br s, NH), 5.32 (1 H, m, CH), 4.12 (1 H, d, ^2J 15.1, CH_2), 4.04 (1 H, d, ^2J 15.0, CH_2), 1.64 (3 H, d, ^3J 7.0, CH_3); $\delta_C\{^1H\}$ (62.9 MHz; $CDCl_3$) 165.7 (CO), 140.3 (Ar), 133.7 (Ar), 133.4 (Ar), 129.3 (Ar), 128.5 (Ar), 128.2 (Ar), 127.0 (Ar), 126.7 (Ar), 125.2 (Ar), 125.0 (Ar), 49.9 (CH), 43.3 (CH_2), 22.2 (CH_3); m/z (DCI) 248 (100%, MH^+) (Found: C, 67.8; H, 5.67; N, 5.66%. $C_{14}H_{14}ClON$ requires C, 67.8; H, 5.69; N, 5.65%).

2-*Chloro*-N-[(S)- 2-*naphthyl*]*ethylethanamide* **(12f)**

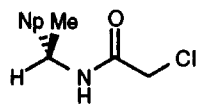

The title compound was prepared following a method similar to that for **(12a)** using (*S*)-1-(2-naphthyl)ethylamine (5 g, 29.2 mmol) and triethylamine (4.9 cm^3, 35.1 mmol) in dry diethyl ether (100 cm^3) and reacting with a solution of chloroacetylchloride (2.79 cm^3, 35.1 mmol) in dry diethyl ether (50 cm^3). The product was recrystallised from diethyl ether and isolated as white needles (4.7 g, 65%). Characterisation data are the same as those reported for **(12e)**. (Found: C, 67.9; H, 5.76; N, 5.67. $C_{14}H_{14}ClON$ requires C, 67.8; H, 5.69; N, 5.65%).

1,4,7,10-*Tetrakis*-[(R)-1-(1-*naphthyl*)*ethylcarbamoylmethyl*]-1,4,7,10-*tetraazacyclododecane* (**13c**)

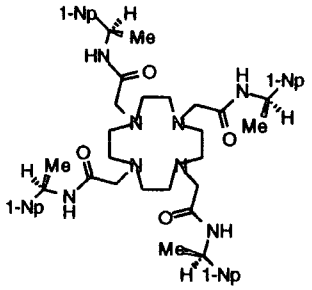

The title compound was prepared following a method similar to that for (**13a**) using 1,4,7,10-tetraazacyclododecane (0.39 g, 2.3 mmol) and fine mesh anhydrous potassium carbonate (1.6 g, 11.3 mmol) in dry *N*,*N*-dimethylformamide (30 cm^3) and 2-chloro-*N*-[(*R*)-1-*naphthyl*]*ethylethanamide* (**12c**) (2.8 g, 11.3 mmol) in dry *N*,*N*-dimethylformamide (10 cm^3). The product was recrystallised from acetonitrile and isolated as white needles (1.1 g, 45%), m.p. 195-196 °C; R_f (Al_2O_3; 10% CH_3OH-CH_2Cl_2; I_2 and u.v. detection) 0.57; ν_{max} (thin film)/cm^{-1} 3281 (N-H), 1656 (C=O); δ_H (250 MHz; $CDCl_3$) 7.97-7.68 (4 H, m, Ar), 7.75-7.68 (8 H, m, Ar), 7.51-7.29 (16 H, m, Ar), 6.65 (4 H, d, ^3J 8, NH), 5.86 (4 H, m, CH), 2.44 (8 H, br s, CH_2CO), 1.82-1.60 (16 H, m, ring-CH_2), 1.62 (12 H, d, ^3J 6.7, CH_3); $\delta_C\{^1H\}$ (62.9 MHz; $CDCl_3$) 169.8 (CO), 138.5 (q-Ar) 134.4 (q-Ar), 131.8 (q-Ar), 129.4 (Ar) , 129.1 (Ar) , 127.1 (Ar) , 126.5 (Ar) , 125.8 (Ar) , 124.0 (Ar), 123.4 (Ar), 58.5 ($\underline{C}H_2CO$), 53.7 (ring-CH_2), 44.4 (CHN), 20.8 (CH_3); m/z (ES+) 1040 (15%, MNa^+), 1018 (100%, MH^+); α_D +27.4° (c. 0.767 in MeOH) (Found: C, 74.5 H, 7.00; N, 10.5. $C_{64}H_{72}N_8O_4.H_2O$ requires C, 74.3 H, 7.20; N, 10.8%).

1,4,7,10-*Tetrakis*-[(S)-1-(1-*naphthyl*)*ethylcarbamoylmethyl*]-1,4,7,10-*tetraazacyclododecane* (**13d**)

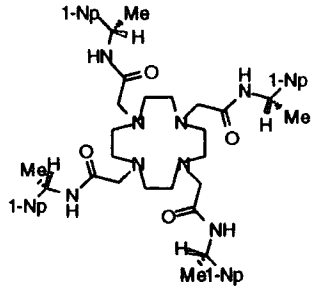

The title compound was prepared following a method similar to that for **(13a)** using 1,4,7,10-tetraazacyclododecane (0.77 g, 4.4 mmol) and fine mesh anhydrous potassium carbonate (3.0 g, 22.2 mmol) in dry *N*,*N*-dimethylformamide (30 cm^3) and 2-chloro-*N*-[(*S*)-1-*naphthyl*]*ethylethanamide* (**12d**) (5.5 g, 22.2 mmol) in dry *N*,*N*-dimethylformamide (10 cm^3). The product was recrystallised from acetonitrile and isolated as white needles (3.0 g, 67%). Characterisation data are the same as those reported for **(13c)**, α_D -28.4° (c. 0.668 in MeOH) (Found: C, 74.7; H, 7.30 N, 11.0. $C_{64}H_{72}N_8O_4.H_2O$ requires C, 74.3; H, 7.20; N, 10.8%).

1,4,7,10-*Tetrakis*-[(R)-1-(2-*naphthyl*)*ethylcarbamoylmethyl*]-1,4,7,10-*tetraazacyclododecane* (**13e**)

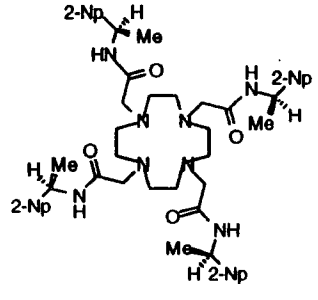

The title compound was prepared following a method similar to that for **(13a)** using 1,4,7,10-tetraazacyclododecane (0.765 g, 4.4 mmol) and fine mesh anhydrous potassium carbonate (3.0 g, 22.2 mmol) in dry *N*,*N*-dimethylformamide (30 cm^3) and 2-chloro-*N*-((*R*)-1-naphthyl)ethylethanamide (**12e**) (5.5 g, 22.2 mmol) in dry *N*,*N*-dimethylformamide (10 cm^3). The product was recrystallised from acetonitrile and isolated as white needles (1.1 g, 24%), m.p. 182-183 °C; R_f (Al_2O_3; 10% CH_3OH-

CH_2Cl_2; I_2 and u.v. detection) 0.43; ν_{max} (thin film)/cm^{-1} 3281 (N-H), 1656 (C=O); δ_H (250 MHz; $CDCl_3$) 7.84-7.75 (16 H, m, Ar), 7.51-7.40 (12 H, m, Ar), 7.00 (4 H, d, ^3J 7.6, NH), 5.32 (4 H, m, CH), 2.83 (8 H, br s, CH_2CO), 2.52 (16 H, br s, ring-CH_2), 1.59 (12 H, d, ^3J 6.8, CH_3); $\delta_C\{^1H\}$ (62.9 MHz; $CDCl_3$) 170.3 (CO), 141.1 (q-Ar) 133.7 (q-Ar), 133.0 (q-Ar), 128.8 (Ar) , 128.2 (Ar) , 128.0 (Ar) , 126.7 (Ar) , 126.4 (Ar) , 125.4 (Ar), 125.1 (Ar) , 59.0 ($\underline{C}H_2CO$), 53.8 (ring-CH_2), 48.6 (CHN), 21.7 (CH_3); m/z (ES+) 1040 (60%, MNa^+), 529 (100%, MK^+H^+) (Found: C, 74.1; H, 7.06 N, 11.0. $C_{64}H_{72}N_8O_4$ .H_2O requires C, 74.3; H, 7.20; N, 10.8%).

1,4,7,10-*Tetrakis*-[(S)-1-(2-*naphthyl*)*ethylcarbamoylmethyl*]-1,4,7,10-*tetraazacyclododecane* **(13f)**

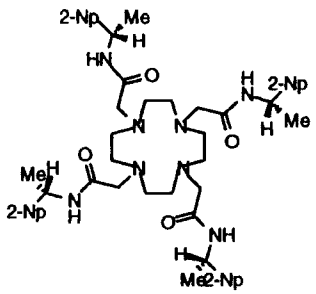

The title compound was prepared following a method similar to that for **(13a)** using 1,4,7,10-tetraazacyclododecane (0.65 g, 3.8 mmol) and fine mesh anhydrous potassium carbonate (2.6 g, 18.9 mmol) in dry *N*,*N*-dimethylformamide (30 cm^3) and 2-chloro-*N*-[(*S*)-2-naphthyl]ethylethanamide **(12f)** (4.7 g, 18.9 mmol) in dry *N*,*N*-dimethylformamide (10 cm^3). The product was recrystallised from acetonitrile and isolated as white needles (1.23 g, 32%). Characterisation data are the same as those reported for **(13e)** (Found: C, 73.5; H, 7.08 N, 10.8. $C_{64}H_{72}N_8O_4.2H_2O$ requires C, 73.0; H, 7.27; N, 10.6%).

Lanthanide complexes of **(13c) - (13f)**

$[Eu.13c]^{3+}$ (24c)

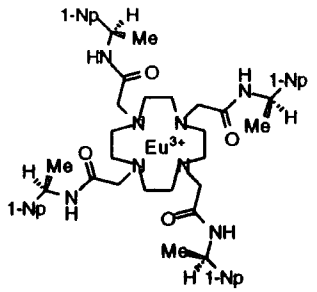

The title compound was prepared following a method similar to that for **(23a)** using europium (III) triflate (0.058 g, 0.98 mmol) and trimethylorthoformate (1 cm^3) in dry acetonitrile (2 cm^3) and the ligand **(13c)** (0.1 g, 0.98 mmol) in dry acetonitrile (1 cm^3). The product was recrystallised from acetonitrile and isolated as white needles (0.05 g, 31%), m.p. >250 °C; ν_{max} (thin film)/cm^{-1} 3261 (N-H), 1619 (C=O); δ_H (250 MHz; CD_3OD) 26.2 (4 H, s, ring-H_{ax}), 7.49 (8 H, s, Ar), 6.07 (4 H, s, Ar), 5.53 (4 H, s, Ar), 4.88 (4 H, s, Ar), 4.48 (4 H, s, Ar), 3.10 (4 H, s, Ar), 2.23 (4 H, br s, CH), -1.24 (12 H, br s, CH_3), -4.11 (4 H, br s, ring-H_{eq}), -8.36 (4 H, br s, ring-H_{ax}), -9.58 (4 H, br s, ring-H_{eq}), -16.3 (4 H, br s, CH_2CO), -16.7 (4 H, br s, CH_2CO); $\delta_C\{^1H\}$ (62.9 MHz; CD_3OD) 188.1 (CO), 138.2 (Ar), 133.2 (Ar), 129.4 (Ar), 128.3 (Ar), 127.8 (Ar), 127.2 (Ar), 124.4 (Ar), 123.1 (Ar), 121.0 (Ar), 107.4-105.6 (br, ring-CH_2), 89.4 ($\underline{C}H_2CO$), 73.9 (br, ring-CH_2), 42.8 (CHN), 21.2 (CH_3); m/z (ES+) 1467 (100%, $[M^{3+} + 2(CF_3SO_3^-)]^+$) (Found: C, 49.2; H, 4.54; N, 6.72. $C_{67}H_{72}EuF_9N_8O_{13}S_3.H_2O$ requires C, 49.2; H, 4.56; N, 6.85%).

$[Eu.13d]^{3+}$ (24d)

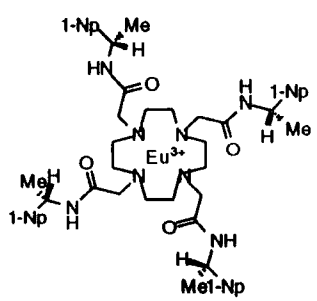

The title compound was prepared following a method similar to that for **(23a)** using europium (III) triflate (0.118 g, 0.2 mmol) and trimethylorthoformate (2 cm^3) in dry acetonitrile (2 cm^3) and the ligand **(13d)** (0.2 g, 0.2 mmol) in dry acetonitrile (2 cm^3). The product was recrystallised from acetonitrile and isolated as white needles (0.5 g, 31%). Characterisation data are the same as those reported for **(24c)** (Found: C, 49.6; H, 4.61; N, 6.69. $C_{67}H_{72}EuF_9N_8O_{13}S_3.H_2O$ requires C, 49.2; H, 4.56; N, 6.85%).

$[Eu.13e]^{3+}$ (24e)

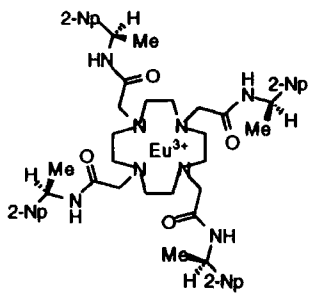

The title compound was prepared following a method similar to that for **(23e)** using europium (III) triflate (0.12 g, 0.2 mmol) and trimethylorthoformate (1 cm^3) in dry acetonitrile (2 cm^3) and the ligand **(13e)** (0.2 g, 0.2 mmol) in dry acetonitrile (2 cm^3). The product was recrystallised from acetonitrile and isolated as white needles (0.13 g, 40%), m.p. >250 °C; ν_{max} (solid)/cm^{-1} 3260 (br) (N-H), 1620 (C=O); δ_H (250 MHz; CD_3OD) 25.6 (4 H, s, ring-H_{ax}), 5.86 (4 H, s, Ar), 5.66 (4 H, s, Ar), 5.49 (8 H, s, Ar), 5.00 (4 H, s, Ar), 4.88 (4 H, s, Ar), 3.89 (4 H, s, Ar), 2.09 (4 H, br s, CH), -1.16 (12 H, br s, CH_3), -4.19 (4 H, br s, ring-H_{eq}), -7.83 (4 H, br s, ring-H_{ax}), -9.33 (4 H, br s, ring-H_{eq}), -15.5 (4 H, br s, CH_2CO), -16.0 (4 H, br s, CH_2CO); $\delta_C\{^1H\}$ (62.9 MHz; CD_3OD) 188.8 (CO), 139.5 (q-Ar), 132.8 (q-Ar), 132.3 (q-Ar), 128.2 (Ar), 128.0 (Ar), 127.7 (Ar), 127.0, (Ar), 123.3 (Ar), 121.8 (Ar), 121.0 (Ar), 106.4 (br, ring-CH_2), 89.7 ($\underline{C}H_2CO$), 74.6 (br, ring-CH_2), 47.3 (CHN), 22.3 (CH_3); m/z (ES+) 1467 (10%, $[M^{3+} + 2(CF_3SO_3^-)]^+$), 659 (100%, $[M^{3+} + CF_3SO_3^-]^{2+}$) (Found: C, 47.8; H, 4.70; N, 6.29. $C_{67}H_{72}EuF_9N_8O_{13}S_3.4H_2O$ requires C, 47.7; H, 4.78; N, 6.64%).

[Eu.13f]$^{3+}$ (24f)

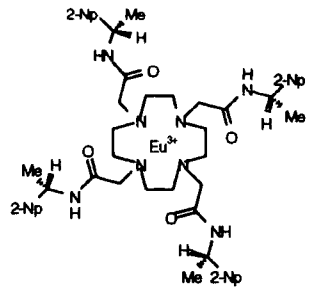

The title compound was prepared following a method similar to that for **(23a)** using europium triflate (0.058 g, 0.1 mmol) and trimethylorthoformate (1 cm^3) in dry acetonitrile (2 cm^3) and the ligand **(13f)** (0.1 g, 0.1 mmol) in dry acetonitrile (2 cm^3). The product was recrystallised from acetonitrile and isolated as white needles (0.15 g, 47%). Characterisation data are the same as those reported for **(24e)** (Found: C, 49.0; H, 4.49; N, 6.63. $C_{67}H_{72}EuF_9N_8O_{13}S_3.H_2O$ requires C, 49.2; H, 4.56; N, 6.85%).

[Gd.13c]$^{3+}$ (28)

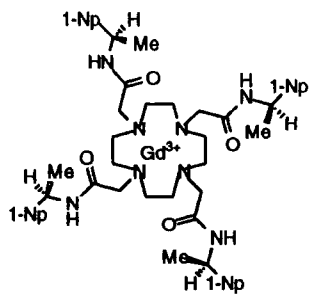

The title compound was prepared following a method similar to that for **(23a)** using gadolinium (III) triflate (0.13 g, 0.21 mmol) and trimethylorthoformate (2 cm^3) in dry acetonitrile (3 cm^3) and the ligand **(13c)** (0.21 g, 0.21 mmol) in dry acetonitrile (2 cm^3). The product was recrystallised from acetonitrile and isolated as white needles (0.17 g, 51%), m.p. >250 ^oC; ν_{max} (solid)/cm^{-1} 3256 (br) (N-H), 1620 (C=O); m/z (ES+) 661 (100%, $[M^{3+} + CF_3SO_3^-]^{2+}$) (Found: C, 49.0; H, 4.50; N, 6.37. $C_{67}H_{72}F_9GdN_8O_{13}S_3.H_2O$ requires C, 49.0; H, 4.55; N, 6.83%).

[Tb.13c]$^{3+}$ (26c)

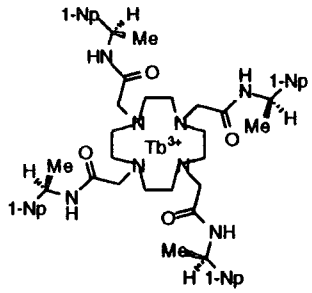

The title compound was prepared following a method similar to that for **(23a)** using terbium (III) triflate (0.03 g, 0.05 mmol) and trimethylorthoformate (1 cm^3) in dry acetonitrile (2 cm^3) and the ligand **(13c)** (0.05 g, 0.05 mmol) in dry acetonitrile (2 cm^3). The product was recrystallised from acetonitrile and isolated as white needles (0.04 g, 49%), m.p. >250 ^oC; ν_{max} (solid)/cm^{-1} 3262 (br) (N-H), 1614 (C=O); m/z (ES+) 1474 (10%, $[M^{3+} + 2(CF_3SO_3^-)]^+$), 662 (100%, $[M^{3+} + CF_3SO_3^-]^{2+}$) (Found: C, 47.4; H, 4.58; N, 6.53. $C_{67}H_{72}F_9N_8O_{13}S_3Tb.4H_2O$ requires C, 47.5; H, 4.76; N, 6.61%).

[Tb.13d]$^{3+}$ (26d)

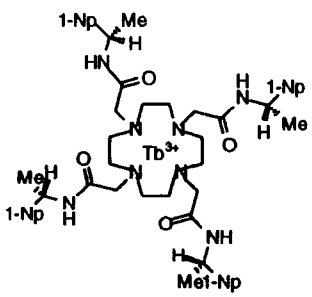

The title compound was prepared following a method similar to that for **(23a)** using terbium (III) triflate (0.03 g, 0.05 mmol) and trimethylorthoformate (1 cm^3) in dry acetonitrile (2 cm^3) and the ligand **(13d)** (0.05 g, 0.05 mmol) in dry acetonitrile (2 cm^3). The product was recrystallised from acetonitrile and isolated as white needles (0.04 g, 47%). Characterisation data are the same as those reported for **(26c)** (Found: C, 46.7; H, 4.63; N, 6.34. $C_{67}H_{72}F_9N_8O_{13}S_3Tb.5H_2O$ requires C, 47.0; H, 4.82; N, 6.54%).

$[Yb.13d]^{3+}$ (27d)

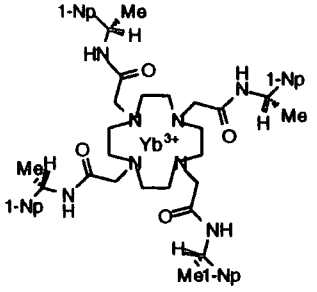

The title compound was prepared following a method similar to that for **(23a)** using ytterbium (III) triflate (0.09 g, 0.15 mmol) and trimethylorthoformate (1 cm^3) in dry acetonitrile (2 cm^3) and the ligand **(13d)** (0.15 g, 0.15 mmol) in dry acetonitrile (2 cm^3). The product was recrystallised from acetonitrile and isolated as white needles (0.11 g, 44%), m.p. >250 °C; ν_{max} (solid)/cm^{-1} 3262 (br) (N-H), 1620 (C=O); δ_H (250 MHz; CD_3OD) 102 (4 H, br s, ring-H_{ax}), 17.8 (4 H, br s, ring-H_{eq}), 14.7 (4 H, br s, ring-H_{eq}), 3.80-1.62 (28 H, m, Ar), -1.15 (4 H, s, CH), -4.97 (12 H, s, CH_3), -29.1 (4 H, s, CH_2CO), -34.7 (4 H, s, CH_2CO), -66.6 (4 H, br s, ring-H_{ax}); m/z (ES+) 1487 (15%, $[M^{3+} + 2(CF_3SO_3^-)]^+$), 669 (100%, $[M^{3+} + CF_3SO_3^-]^{2+}$) (Found: C, 48.0; H, 4.39; N, 6.50. $C_{67}H_{72}F_9N_8O_{13}S_3Yb.2H_2O$ requires C, 48.1; H, 4.58; N, 6.70%).

5.5 Experimental details for Chapter 4

5.5.1 Solution nmr

The following procedure was adopted to investigate the effect of adding Eu^{3+} and Dy^{3+} complexes of the phenylamide series to the resonance positions of interacting anions containing nmr active nuclei (All measurements were made on a Brüker AC250 instrument).

50 µl aliquots of a solution of the complex in methanol (10^{-2} mol dm^{-3}, metal : ligand ratio ranging from 0.01 to 0.1) were added successively to a 400 µl solution of the anion (10^{-1} mol dm^{-3}) in a 5 mm nmr tube containing 1 drop of an internal reference. The change in the chemical shift of the anion and the reference upon addition of the complex were monitored. The instrument was referenced to a suitable external reference between each run being H_3PO_4 in D_2O (δ_P 0) for ^{31}P, $^{13}CH_3OH$ (δ_C 49.3) for ^{13}C and $CFCl_3$ in $CHCl_3$ (δ_F 0) for ^{19}F. On addition of the complex, the

paramagnetic susceptibility of the whole sample is affected. The presence of an internal reference, that does not interact with the complex, is required in order to monitor the change in chemical shift caused by this change in the paramagnetic susceptibility of the sample, therefore allowing the 'true' shifting ability of the complex towards the interacting anion to be assessed. Suitable non-interacting internal references were chosen being $MePh_3PCl$ in MeOH (δ_P 21.6) for ^{31}P, $^{13}CH_3OH$ (δ_C 49.3) for ^{13}C and CH_3CHFOH (δ_F -222.3) for ^{19}F.

5.5.2 Luminescence

Effect of added anions

The following procedure was adopted for the investigation of the effect of added anions on the excited state lifetimes of Eu^{3+} and Tb^{3+} complexes of the phenylamide series.

A solution of the appropriate sodium salt (1.5 cm^3, 10^{-2} mol dm^{-3}, in H_2O) was added to a solution of the complex (1.5 cm^3, 10^{-3} mol dm^{-3}, in H_2O) and the lifetime was measured. For Eu^{3+}: λ_{ex} = 254 nm, λ_{em} = 590 nm, slit $width_{ex}$ = 15 nm, slit $width_{em}$ = 20 nm, t_d = 100-1000 μs, t_g = 100 μs. For Tb^{3+}: λ_{ex} = 254 nm, λ_{em} = 545 nm, slit $width_{ex}$ = 5 nm, slit $width_{em}$ = 5 nm, t_d = 100-4000 μs, t_g = 100 μs.

pH Dependence

The following procedure was adopted for the investigation of the pH dependence of the excited state lifetimes of Eu^{3+} and Tb^{3+} complexes of the phenylamide series.

Hydrochloric acid was added carefully to a solution of the complex (20 cm^3, 10^{-3} mol dm^{-3}, in water) to pH = 1 and the lifetime was measured (HCl was chosen as the chloride anion was found not to affect the lifetime of the excited state). The pH was increased by careful addition of sodium hydroxide solution and the lifetime was measured at every pH unit to pH = 13.

Anion concentration dependence

The following procedure was adopted for the investigation of the effect of the concentration of sodium bicarbonate added on the lifetime of the excited state of the complex **(Tb.13a)**.

Suitable aliquots of a concentrated solution of sodium bicarbonate (such that the concentration of bicarbonate ranged from 3 x 10-4 mol dm-3 to 33 x 10-3 mol dm-3) were added successively to a solution of the complex (3 cm3, 10-3 mol dm-3) and the lifetimes were measured. The small dilution factor (of only 6.6%) was ignored as lifetimes are independent of concentration.

5.5.3 Chiroptical studies

Effect of added anions on CD

The following procedure was adopted for the investigation of the effect of added anions on the CD of complexes of the phenylamide series.

A solution of the appropriate sodium salt (1.5 cm^3, 10^{-2} mol dm^{-3}, in H_2O) was added to a solution of the complex (1.5 cm^3, 10^{-3} mol dm^{-3}, in H_2O) and the CD was measured.

Effect of added anions on CPL

The following procedure was adopted for the investigation of the effect of added anions on the CPL of complexes of the phenylamide series.

A solution of the appropriate sodium salt (1.5 cm^3, 10^{-2} mol dm^{-3}, in H_2O) was added to a solution of the complex (1.5 cm^3, 10^{-3} mol dm^{-3}, in H_2O) and the CPL was measured following direct excitation at 260 nm. The slit widths were adjusted accordingly to give approximately equal emission intensities in the 540 nm band.

References for Chapter 5

1. Y. Haas and G. Stein, *J. Phys. Chem.*, 1971, **75**, 3668.
2. K. Nakamaru, *Bull. Chem. Soc. Jpn.*, 1982, **55**, 2697.
3. S.R. Meech and D. Phillips, *J. Photochem.*, 1983, **23**, 193.

4. A.T.R. Williams, S.A. Winfield and J.N. Miller, *Analyst (London)*, 1983, **108**, 1471.

5. J.A.G. Williams, Ph.D. Thesis, University of Durham, 1994.

6. P.H. Smith and K.N. Raymond, *Inorg. Chem.*, 1985, **24**, 3469.

APPENDICES

Appendix 1 Courses, lectures and seminars attended

First year courses

New Methods of Polymer Synthesis

Practical NMR

Synthetic Methods in Organometallic and Coordination Chemistry

Research colloquia, seminars and lectures

The following were attended, organised by the Department of Chemistry (October 1994-July 1997).

1994

October 5 Prof. N. L. Owen, Brigham Young University, Utah, USA
Determining Molecular Structure - the INADEQUATE NMR way

November 3 Prof. B. F. G. Johnson, Edinburgh University
Arene-metal Clusters

November 9 Dr G. Hogarth, University College, London
New Vistas in Metal-imido Chemistry

November 10 Dr M. Block, Zeneca Pharmaceuticals, Macclesfield
Large-scale Manufacture of ZD 1542, a Thromboxane Antagonist Synthase Inhibitor

November 16 Prof. M. Page, University of Huddersfield
Four-membered Rings and β-Lactamase

November 23 Dr J. M. J. Williams, University of Loughborough
New Approaches to Asymmetric Catalysis

December 7 Prof. D. Briggs, ICI and University of Durham

Surface Mass Spectrometry

1995

January 11 Prof. P. Parsons, University of Reading

Applications of Tandem Reactions in Organic Synthesis

January 25 Dr D. A. Roberts, Zeneca Pharmaceuticals

The Design and Synthesis of Inhibitors of the Renin-angiotensin System

February 8 Dr D. O'Hare, Oxford University

Synthesis and Solid-state Properties of Poly-, Oligo- and Multidecker Metallocenes

February 22 Prof. E. Schaumann, University of Clausthal

Silicon- and Sulphur-mediated Ring-opening Reactions of Epoxide

March 1 Dr M. Rosseinsky, Oxford University

Fullerene Intercalation Chemistry

April 26 Dr M. Schroder, University of Edinburgh

Redox-active Macrocyclic Complexes : Rings, Stacks and Liquid Crystals

May 4 Prof. A. J. Kresge, University of Toronto

The Ingold Lecture Reactive Intermediates : Carboxylic-acid Enols and Other Unstable Species

October 13 Prof. R. Schmutzler, Univ Braunschweig, FRG.
Calixarene-Phosphorus Chemistry: A New Dimension in Phosphorus Chemistry

October 18 Prof. A. Alexakis, Univ. Pierre et Marie Curie, Paris,
Synthetic and Analytical Uses of Chiral Diamines

October 25 Dr.D.Martin Davies, University of Northumbria
Chemical reactions in organised systems.

November 1 Prof. W. Motherwell, UCL London
New Reactions for Organic Synthesis

November 8 Dr. D. Craig, Imperial College, London
New Stategies for the Assembly of Heterocyclic Systems

November 9 Prof. Williams, University of Oxford
Metals in Medicine

November 15 Dr Andrea Sella, UCL, London
Chemistry of Lanthanides with Polypyrazoylborate Ligands

November 22 Prof. I Soutar, Lancaster University
A Water of Glass? Luminescence Studies of Water-Soluble Polymers.

1996

January 10 Dr Bill Henderson, Waikato University, NZ
Electrospray Mass Spectrometry - a new sporting technique

January 10 Dr T. O'Brien, St Thomas' Hospital, London
The Changing Face of Critical Care

January 24 Dr Alan Armstrong, Nottingham Univesity
Alkene Oxidation and Natural Product Synthesis

February 7 Dr R.B. Moody, Exeter University
Nitrosations, Nitrations and Oxidations with Nitrous Acid

February 14 Prof. Nolte, Netherlands
Design Strategies For Supramolecular Assemblies

February 28 Prof. E. W. Randall, Queen Mary & Westfield College
New Perspectives in NMR Imaging

March 6 Dr Richard Whitby, Univ of Southampton
New approaches to chiral catalysts: Induction of planar and metal centred asymmetry

March 12 RSC Endowed Lecture - Prof. V. Balzani, Univ of Bologna
Supramolecular Photochemistry

March 27 Prof. A.S. de Silva, Belfast
Luminescent Sensors

October 14 Professor A. R. Katritzky, University of Gainesville,University of Florida, USA
Recent Advances in Benzotriazole Mediated Synthetic Methodology

October 22 Professor B. J. Tighe, Department of Molecular Sciences and Chemistry, University of Aston
Making Polymers for Biomedical Application - can we meet Nature's Challenge?
Joint lecture with the Institute of Materials

October 23 Professor H. Ringsdorf (Perkin Centenary Lecture), Johannes Gutenberg-Universitat, Mainz, Germany
Function Based on Organisation

October 30 Dr Phillip Mountford, Nottingham University
Recent Developments in Group IV Imido Chemistry

November 18 Professor G. A. Olah, University of Southern California, USA
Crossing Conventional Lines in my Chemistry of the Elements

November 19 Professor R. E. Grigg, University of Leeds
Assembly of Complex Molecules by Palladium-Catalysed Queueing Processes

November 27 Dr Richard Templer, Imperial College, London
Molecular Tubes and Sponges

December 3 Professor D. Phillips, Imperial College, London
"A Little Light Relief" -

December 11 Dr Chris Richards, Cardiff University
Stereochemical Games with Metallocenes

1997

January 15 Dr V. K. Aggarwal, University of Sheffield
Sulfur Mediated Asymmetric Synthesis

January 16 Dr Sally Brooker, University of Otago, NZ
Macrocycles: Exciting yet Controlled Thiolate Coordination Chemistry

February 18 Professor Sir James Black, Foundation/King's College London
My Dialogues with Medicinal Chemists

February 26 Dr Tony Ryan, UMIST
Making Hairpins from Rings and Chains

March 4 Professor C. W. Rees, Imperial College
Some Very Heterocyclic Chemistry

March 5 Dr J. Staunton FRS, Cambridge University
Tinkering with biosynthesis: towards a new generation of antibiotics

March 10 Prof. J. Riehl, Michigan Technologival University, USA.
Enantioselctive Quenching of Lanthanide Ions

Graduate Colloquia, comprising research talks by third-year graduate students, have been attended each year.

Conferences and courses attended

December 20 1994 Stereochemistry at Sheffield
University of Sheffield

January 3-4 1995	R.S.C. U.K. Macrocyclic Conference University of Newcastle
March 26-April 1 1995	Inorganic and Organomettalic NMR, European Initiative for Training in NMR University of Torino, Italy
December 19 1995	Stereochemistry at Sheffield University of Sheffield
January 4-5 1996	R.S.C. U.K. Macrocyclic Conference* University of Sheffield
August 18-23 1996	31st International Conference on Coordination Chemistry* University of British Columbia, Vancouver, Canada
December 17 1996	Stereochemistry at Sheffield University of Sheffield
December 18-19 1996	R.S.C. U.K. Macrocyclic Conference** University of Cardiff
May 7 1997	21st Century Heterocyclic Chemistry University of Sunderland

* indicates poster presentation

** indicates oral presentation

Appendix 2 Publications

R.S. Dickins, D. Parker, A. de Sousa and J.A.G. Wiliams, 'Closely Diffusing O-H, Amide N-H and Methylene C-H Quench the Excited State of Europium Complexes in Solution', *Chem. Commun.*, 1996, 697.

R.S. Dickins, J.A.K. Howard, C.W. Lehmann, J. Moloney, D. Parker and R.D. Peacock, 'Structural Rigidity and Luminescence of Chiral Lanthanide Complexes Based on 1,4,7,10-Tetraazacyclododecane', *Angew. Chem., Int. Ed. Engl.*, 1997, **36**, 521.

A. Beeby, R.S. Dickins, S. Faulkner, D. Parker and J.A.G. Williams, 'Luminescence from Ytterbium (III) and its Complexes in Solution', *Chem. Commun.*, 1997, 1401.

R.S. Dickins, J.A.K. Howard, J. Moloney, D. Parker, R.D. Peacock and G. Siligardi, 'Strong Exciton Coupling and Circularly Polarised Luminescence in Rigid Complexes of Chiral Macrocyclic Tetranaphthylamides', *Chem. Commun.*, 1997, 1747.

S. Aime, A.S. Batsanov, M. Botta, R.S. Dickins, S. Faulkner, C.E. Foster, A. Harrison, J.A.K. Howard, J. Moloney, T.J. Norman, D. Parker, L. Royle and J.A.G. Wiliams, 'Nuclear Magnetic Resonance, Luminescence and Structural Studies of Lanthanide Complexes with Octadentate Macrocyclic Ligands Bearing Benzylphosphinate Groups', *J. Chem. Soc., Dalton Trans.*, October 1997.

Appendix 3 Crystal data for (Eu.2b)$^{-}$

Table 1. Crystal data and structure refinement for 1.

Identification code	96srv059
Empirical formula	C40 H84.5 Eu N4 Na0.50 O24 P4
Formula weight	1292.95
Temperature	150(2) K
Wavelength	0.71073 A
Crystal system	Orthorhombic
Space group	Pbcn
Unit cell dimensions	a = 22.842(2) A alpha = 90 deg. b = 22.620(2) A beta = 90 deg. c = 21.178(2) A gamma = 90 deg.
Volume	10942(2) A^3
Z	8
Density (calculated)	1.569 g/cm^3
Absorption coefficient	1.350 mm^-1
F(000)	5380
Crystal size	0.4 x 0.3 x 0.2 mm
Theta range for data collection	1.27 to 25.88 deg.
Index ranges	-27<=h<=16, -27<=k<=26, -25<=l<=24
Reflections collected	48208
Independent reflections	9766 [R(int) = 0.1660]
Observed reflections, I>2sigma(I)	7102
Absorption correction	Semiempirical
Max. and min. transmission	0.8196 and 0.4370
Refinement method	Full-matrix least-squares on F^2
Data / restraints / parameters	9643 / 0 / 695
Goodness-of-fit on F^2	2.098
Final R indices [I>2sigma(I)]	R1 = 0.1059, wR2 = 0.2526
R indices (all data)	R1 = 0.1427, wR2 = 0.2834

Extinction coefficient	0.0006(1)
Largest shift/e.s.d. ratio	-0.020
Largest diff. peak and hole	2.313 and -2.790 e.A^-3

Table 2. Atomic coordinates (x 10^4) and equivalent isotropic displacement parameters (A^2 x 10^3) for 1. U(eq) is defined as one third of the trace of the orthogonalized Uij tensor.

	x	y	z	U(eq)
Eu	2748(1)	2372(1)	5388(1)	25(1)
P(1)	3526(1)	2620(2)	4022(2)	35(1)
P(2)	3905(1)	2937(1)	6239(2)	31(1)
P(3)	2363(1)	1613(1)	6730(2)	29(1)
P(4)	2010(1)	1312(1)	4550(2)	32(1)
N(1)	2509(4)	3135(4)	4458(6)	34(3)
N(2)	2924(4)	3484(4)	5736(6)	35(3)
N(3)	2017(4)	2725(4)	6314(6)	35(3)
N(4)	1601(4)	2366(4)	5035(6)	30(3)
O(11)	3562(3)	2505(4)	4726(5)	34(2)
O(12)	3962(3)	3058(4)	3764(6)	50(3)
O(21)	3480(3)	2425(3)	6146(4)	27(2)
O(22)	4026(4)	3131(4)	6904(5)	41(3)
O(31)	2499(3)	1576(4)	6032(5)	33(2)
O(32)	1862(4)	1231(4)	6947(5)	46(3)
O(41)	2566(3)	1687(3)	4606(5)	28(2)
O(42)	1808(3)	1194(4)	3881(5)	40(2)
C(1)	2792(6)	3706(6)	4591(8)	45(4)
C(2)	2697(7)	3908(6)	5252(9)	52(5)
C(3)	2662(5)	3601(5)	6363(7)	34(4)
C(4)	2045(6)	3361(6)	6416(9)	48(4)
C(5)	1415(5)	2530(6)	6173(8)	43(4)
C(6)	1229(5)	2668(6)	5513(7)	38(3)
C(7)	1530(5)	2645(5)	4415(8)	35(3)
C(8)	1858(5)	3225(6)	4370(9)	42(4)
C(10)	2779(4)	2884(5)	3860(7)	30(3)
C(11)	3577(5)	1930(6)	3590(8)	39(4)
C(12)	4156(5)	1613(6)	3696(8)	41(4)
C(13)	4626(6)	1722(7)	3294(9)	53(5)
C(14)	5149(6)	1424(8)	3389(11)	67(6)
C(15)	5211(6)	1038(8)	3870(11)	66(6)
C(16)	4756(7)	931(8)	4286(10)	66(5)
C(17)	4220(7)	1223(7)	4171(9)	58(5)
C(20)	3585(6)	3548(6)	5797(8)	39(4)
C(21)	4593(5)	2773(6)	5836(8)	43(4)
C(22)	4868(5)	2197(7)	6097(7)	39(4)
C(23)	4750(6)	1658(8)	5830(9)	53(5)
C(24)	5007(8)	1149(8)	6078(11)	72(6)
C(25)	5368(8)	1157(11)	6531(13)	82(7)
C(26)	5509(6)	1690(13)	6828(11)	88(8)
C(27)	5261(5)	2228(9)	6613(8)	59(5)
C(30)	2215(5)	2396(6)	6901(8)	41(4)
C(31)	3009(5)	1470(5)	7217(7)	27(3)
C(32)	3234(5)	847(6)	7224(8)	36(3)
C(33)	3793(5)	708(6)	7007(9)	47(4)
C(34)	4022(6)	146(7)	7078(10)	60(5)
C(35)	3712(8)	-299(7)	7327(10)	64(5)
C(36)	3134(8)	-177(7)	7550(9)	61(5)
C(37)	2905(6)	391(6)	7494(8)	47(4)
C(40)	1450(5)	1713(5)	4983(7)	32(3)

C(41)	2116(5)	618(6)	4965(9)	48(5)
C(42)	2709(5)	346(5)	4876(9)	42(4)
C(43)	2888(5)	111(6)	4296(9)	45(4)
C(44)	3423(6)	-170(7)	4260(11)	63(5)
C(45)	3786(6)	-222(7)	4781(11)	62(6)
C(46)	3638(6)	24(7)	5341(10)	59(5)
C(47)	3090(6)	315(6)	5383(9)	51(4)
Na	5037(8)	4476(4)	7318(6)	41(4)
O(1W)	5571(4)	4002(5)	6325(8)	77(4)
O(2W)	5829(5)	5033(6)	4754(8)	88(5)
O(3W)	6717(5)	4754(5)	6881(6)	62(3)
O(4W)	5056(5)	4164(5)	5181(7)	63(3)
O(5W)	3176(4)	2967(4)	7884(6)	55(3)
O(6W)	4675(5)	5898(5)	6943(7)	69(4)
O(7W)	3987(4)	4359(4)	7169(5)	44(3)
O(8W)	5034(10)	3310(11)	4355(13)	69(6)
O(9W)	5139(6)	3518(7)	7277(10)	63(6)
O(10W)	5088(10)	3510(10)	3997(14)	76(7)
O(11W)	6381(8)	5924(8)	6900(11)	79(6)
O(12W)	6089(8)	5607(8)	6086(11)	80(7)
O(13W)	5337(8)	3024(10)	2359(15)	108(9)
O(14W)	5844(7)	3298(8)	2489(11)	74(6)
O(15W)	6556(10)	4903(9)	3757(12)	88(6)
O(16W)	6162(8)	4590(10)	3489(14)	101(8)
O(17W)	4332(8)	6252(8)	6684(12)	81(7)
O(18W)	5214(8)	5429(9)	6976(13)	49(6)
O(19W)	5322(10)	5110(11)	6742(14)	66(8)

Table 3. Bond lengths [A] and angles [deg] for 1.

Eu-O(41)	2.304(8)
Eu-O(21)	2.321(8)
Eu-O(31)	2.328(9)
Eu-O(11)	2.349(9)
Eu-N(2)	2.652(10)
Eu-N(1)	2.675(11)
Eu-N(3)	2.696(12)
Eu-N(4)	2.725(9)
Eu-P(4)	3.424(3)
Eu-P(3)	3.435(4)
Eu-P(1)	3.441(4)
Eu-P(2)	3.446(3)
P(1)-O(12)	1.507(9)
P(1)-O(11)	1.516(10)
P(1)-C(11)	1.81(2)
P(1)-C(10)	1.839(11)
P(2)-O(22)	1.501(11)
P(2)-O(21)	1.524(8)
P(2)-C(20)	1.824(14)
P(2)-C(21)	1.826(14)
P(3)-O(32)	1.507(9)
P(3)-O(31)	1.513(11)
P(3)-C(31)	1.829(12)
P(3)-C(30)	1.839(14)
P(4)-O(42)	1.516(11)
P(4)-O(41)	1.531(7)
P(4)-C(40)	1.816(13)
P(4)-C(41)	1.816(14)
N(1)-C(1)	1.47(2)
N(1)-C(8)	1.51(2)
N(1)-C(10)	1.52(2)
N(2)-C(3)	1.48(2)
N(2)-C(2)	1.50(2)
N(2)-C(20)	1.52(2)
N(3)-C(4)	1.46(2)
N(3)-C(5)	1.48(2)
N(3)-C(30)	1.52(2)
N(4)-C(7)	1.47(2)
N(4)-C(6)	1.49(2)
N(4)-C(40)	1.52(2)
C(1)-C(2)	1.49(2)
C(3)-C(4)	1.52(2)
C(5)-C(6)	1.49(2)
C(7)-C(8)	1.51(2)
C(11)-C(12)	1.52(2)
C(12)-C(17)	1.35(2)
C(12)-C(13)	1.39(2)
C(13)-C(14)	1.39(2)
C(14)-C(15)	1.35(3)
C(15)-C(16)	1.38(2)
C(16)-C(17)	1.41(2)
C(21)-C(22)	1.55(2)
C(22)-C(23)	1.37(2)
C(22)-C(27)	1.42(2)
C(23)-C(24)	1.40(2)
C(24)-C(25)	1.26(3)

C(25)-C(26)	1.40(3)
C(26)-C(27)	1.42(3)
C(31)-C(32)	1.50(2)
C(32)-C(33)	1.39(2)
C(32)-C(37)	1.40(2)
C(33)-C(34)	1.38(2)
C(34)-C(35)	1.34(2)
C(35)-C(36)	1.43(2)
C(36)-C(37)	1.39(2)
C(41)-C(42)	1.50(2)
C(42)-C(47)	1.38(2)
C(42)-C(43)	1.40(2)
C(43)-C(44)	1.38(2)
C(44)-C(45)	1.38(3)
C(45)-C(46)	1.35(3)
C(46)-C(47)	1.42(2)
Na-Na#1	0.79(2)
Na-O(19W)	1.99(3)
Na-O(9W)	2.18(2)
Na-O(18W)	2.31(2)
Na-O(9W)#1	2.37(2)
Na-O(7W)	2.43(2)
Na-O(7W)#1	2.49(2)
Na-O(19W)#1	2.59(3)
Na-O(1W)	2.66(2)
Na-O(18W)#1	2.68(2)
O(6W)-O(17W)	1.25(2)
O(6W)-O(18W)	1.63(2)
O(7W)-Na#1	2.49(2)
O(8W)-O(10W)	0.89(3)
O(9W)-O(9W)#1	1.14(4)
O(9W)-Na#1	2.37(2)
O(13W)-O(14W)	1.34(2)
O(13W)-O(13W)#2	1.65(4)
O(15W)-O(16W)	1.28(3)
O(18W)-O(19W)	0.91(3)
O(18W)-Na#1	2.68(2)
O(19W)-Na#1	2.59(3)

O(41)-Eu-O(21)	131.5(3)
O(41)-Eu-O(31)	81.8(3)
O(21)-Eu-O(31)	79.1(3)
O(41)-Eu-O(11)	78.5(3)
O(21)-Eu-O(11)	80.5(3)
O(31)-Eu-O(11)	130.0(3)
O(41)-Eu-N(2)	149.8(4)
O(21)-Eu-N(2)	69.4(3)
O(31)-Eu-N(2)	127.3(4)
O(11)-Eu-N(2)	85.7(3)
O(41)-Eu-N(1)	82.4(3)
O(21)-Eu-N(1)	128.5(3)
O(31)-Eu-N(1)	151.7(3)
O(11)-Eu-N(1)	68.9(3)
N(2)-Eu-N(1)	67.9(3)
O(41)-Eu-N(3)	127.5(3)
O(21)-Eu-N(3)	85.8(3)
O(31)-Eu-N(3)	69.6(3)
O(11)-Eu-N(3)	152.4(3)
N(2)-Eu-N(3)	67.1(3)
N(1)-Eu-N(3)	102.6(3)

O(41)-Eu-N(4)	68.0(3)
O(21)-Eu-N(4)	151.9(3)
O(31)-Eu-N(4)	85.5(3)
O(11)-Eu-N(4)	126.8(3)
N(2)-Eu-N(4)	103.1(3)
N(1)-Eu-N(4)	66.8(3)
N(3)-Eu-N(4)	66.7(3)
O(41)-Eu-P(4)	21.4(2)
O(21)-Eu-P(4)	138.5(2)
O(31)-Eu-P(4)	69.1(2)
O(11)-Eu-P(4)	99.8(2)
N(2)-Eu-P(4)	151.9(2)
N(1)-Eu-P(4)	88.3(2)
N(3)-Eu-P(4)	106.2(2)
N(4)-Eu-P(4)	51.8(2)
O(41)-Eu-P(3)	102.3(2)
O(21)-Eu-P(3)	68.8(2)
O(31)-Eu-P(3)	21.0(2)
O(11)-Eu-P(3)	139.5(2)
N(2)-Eu-P(3)	106.4(3)
N(1)-Eu-P(3)	151.6(2)
N(3)-Eu-P(3)	52.2(2)
N(4)-Eu-P(3)	88.8(3)
P(4)-Eu-P(3)	87.32(9)
O(41)-Eu-P(1)	66.4(2)
O(21)-Eu-P(1)	101.6(2)
O(31)-Eu-P(1)	138.2(2)
O(11)-Eu-P(1)	21.3(2)
N(2)-Eu-P(1)	90.0(3)
N(1)-Eu-P(1)	51.8(3)
N(3)-Eu-P(1)	152.0(2)
N(4)-Eu-P(1)	105.5(3)
P(4)-Eu-P(1)	86.17(9)
P(3)-Eu-P(1)	155.46(8)
O(41)-Eu-P(2)	139.8(2)
O(21)-Eu-P(2)	20.9(2)
O(31)-Eu-P(2)	99.6(2)
O(11)-Eu-P(2)	69.9(2)
N(2)-Eu-P(2)	52.1(2)
N(1)-Eu-P(2)	107.6(2)
N(3)-Eu-P(2)	89.1(2)
N(4)-Eu-P(2)	152.0(2)
P(4)-Eu-P(2)	155.25(8)
P(3)-Eu-P(2)	87.05(8)
P(1)-Eu-P(2)	89.04(9)
O(12)-P(1)-O(11)	115.6(6)
O(12)-P(1)-C(11)	110.0(7)
O(11)-P(1)-C(11)	110.1(6)
O(12)-P(1)-C(10)	109.4(5)
O(11)-P(1)-C(10)	106.9(6)
C(11)-P(1)-C(10)	104.2(6)
O(12)-P(1)-Eu	138.8(5)
O(11)-P(1)-Eu	34.3(3)
C(11)-P(1)-Eu	108.4(5)
C(10)-P(1)-Eu	74.4(5)
O(22)-P(2)-O(21)	117.4(5)
O(22)-P(2)-C(20)	109.5(6)
O(21)-P(2)-C(20)	104.7(5)
O(22)-P(2)-C(21)	109.9(6)
O(21)-P(2)-C(21)	109.6(6)

C(20)-P(2)-C(21)	105.0(7)
O(22)-P(2)-Eu	137.8(4)
O(21)-P(2)-Eu	33.0(3)
C(20)-P(2)-Eu	72.8(4)
C(21)-P(2)-Eu	109.9(5)
O(32)-P(3)-O(31)	115.0(6)
O(32)-P(3)-C(31)	109.9(5)
O(31)-P(3)-C(31)	112.0(5)
O(32)-P(3)-C(30)	110.7(6)
O(31)-P(3)-C(30)	106.4(6)
C(31)-P(3)-C(30)	102.0(6)
O(32)-P(3)-Eu	137.2(4)
O(31)-P(3)-Eu	33.5(3)
C(31)-P(3)-Eu	110.4(4)
C(30)-P(3)-Eu	74.3(5)
O(42)-P(4)-O(41)	115.0(5)
O(42)-P(4)-C(40)	110.2(6)
O(41)-P(4)-C(40)	105.6(5)
O(42)-P(4)-C(41)	109.9(7)
O(41)-P(4)-C(41)	109.4(5)
C(40)-P(4)-C(41)	106.3(7)
O(42)-P(4)-Eu	139.3(4)
O(41)-P(4)-Eu	33.3(3)
C(40)-P(4)-Eu	74.7(4)
C(41)-P(4)-Eu	106.8(5)
C(1)-N(1)-C(8)	109.7(10)
C(1)-N(1)-C(10)	108.0(11)
C(8)-N(1)-C(10)	110.2(11)
C(1)-N(1)-Eu	109.7(8)
C(8)-N(1)-Eu	112.2(8)
C(10)-N(1)-Eu	106.9(7)
C(3)-N(2)-C(2)	111.1(11)
C(3)-N(2)-C(20)	107.9(11)
C(2)-N(2)-C(20)	109.8(11)
C(3)-N(2)-Eu	111.0(7)
C(2)-N(2)-Eu	111.4(8)
C(20)-N(2)-Eu	105.3(7)
C(4)-N(3)-C(5)	111.4(10)
C(4)-N(3)-C(30)	110.5(12)
C(5)-N(3)-C(30)	107.3(11)
C(4)-N(3)-Eu	112.0(9)
C(5)-N(3)-Eu	110.0(9)
C(30)-N(3)-Eu	105.5(7)
C(7)-N(4)-C(6)	110.5(10)
C(7)-N(4)-C(40)	109.1(11)
C(6)-N(4)-C(40)	111.5(10)
C(7)-N(4)-Eu	110.4(7)
C(6)-N(4)-Eu	111.1(7)
C(40)-N(4)-Eu	104.0(6)
P(1)-O(11)-Eu	124.4(5)
P(2)-O(21)-Eu	126.1(5)
P(3)-O(31)-Eu	125.5(5)
P(4)-O(41)-Eu	125.3(5)
N(1)-C(1)-C(2)	112.7(13)
C(1)-C(2)-N(2)	113.4(12)
N(2)-C(3)-C(4)	112.2(11)
N(3)-C(4)-C(3)	112.5(10)
N(3)-C(5)-C(6)	113.1(12)
N(4)-C(6)-C(5)	112.2(10)
N(4)-C(7)-C(8)	112.0(12)

N(1)-C(8)-C(7)	111.2(10)
N(1)-C(10)-P(1)	110.0(9)
C(12)-C(11)-P(1)	112.8(10)
C(17)-C(12)-C(13)	119.3(13)
C(17)-C(12)-C(11)	120.9(13)
C(13)-C(12)-C(11)	119.8(13)
C(14)-C(13)-C(12)	119(2)
C(15)-C(14)-C(13)	121(2)
C(14)-C(15)-C(16)	121.0(14)
C(15)-C(16)-C(17)	117(2)
C(12)-C(17)-C(16)	122(2)
N(2)-C(20)-P(2)	111.6(9)
C(22)-C(21)-P(2)	110.6(10)
C(23)-C(22)-C(27)	119(2)
C(23)-C(22)-C(21)	121.3(14)
C(27)-C(22)-C(21)	119(2)
C(22)-C(23)-C(24)	120(2)
C(25)-C(24)-C(23)	123(2)
C(24)-C(25)-C(26)	120(2)
C(25)-C(26)-C(27)	120(2)
C(22)-C(27)-C(26)	117(2)
N(3)-C(30)-P(3)	111.4(10)
C(32)-C(31)-P(3)	116.6(9)
C(33)-C(32)-C(37)	117.5(13)
C(33)-C(32)-C(31)	121.4(12)
C(37)-C(32)-C(31)	120.9(11)
C(34)-C(33)-C(32)	121(2)
C(35)-C(34)-C(33)	122.2(14)
C(34)-C(35)-C(36)	118.3(14)
C(37)-C(36)-C(35)	120(2)
C(36)-C(37)-C(32)	120.9(14)
N(4)-C(40)-P(4)	111.2(8)
C(42)-C(41)-P(4)	114.4(11)
C(47)-C(42)-C(43)	118.5(13)
C(47)-C(42)-C(41)	119(2)
C(43)-C(42)-C(41)	122.1(14)
C(44)-C(43)-C(42)	119(2)
C(43)-C(44)-C(45)	122(2)
C(46)-C(45)-C(44)	120.9(14)
C(45)-C(46)-C(47)	118(2)
C(42)-C(47)-C(46)	122(2)
Na#1-Na-O(19W)	131.9(12)
Na#1-Na-O(9W)	93.5(7)
O(19W)-Na-O(9W)	130.9(11)
Na#1-Na-O(18W)	110.1(8)
O(19W)-Na-O(18W)	22.9(9)
O(9W)-Na-O(18W)	153.6(10)
Na#1-Na-O(9W)#1	67.0(6)
O(19W)-Na-O(9W)#1	159.5(11)
O(9W)-Na-O(9W)#1	28.6(9)
O(18W)-Na-O(9W)#1	177.1(10)
Na#1-Na-O(7W)	85(3)
O(19W)-Na-O(7W)	108.8(10)
O(9W)-Na-O(7W)	89.6(7)
O(18W)-Na-O(7W)	103.5(8)
O(9W)#1-Na-O(7W)	77.3(6)
Na#1-Na-O(7W)#1	76(3)
O(19W)-Na-O(7W)#1	92.9(10)
O(9W)-Na-O(7W)#1	79.4(7)
O(18W)-Na-O(7W)#1	94.5(8)

O(9W)#1-Na-O(7W)#1	84.1(7)
O(7W)-Na-O(7W)#1	157.8(6)
Na#1-Na-O(19W)#1	35.0(9)
O(19W)-Na-O(19W)#1	100(2)
O(9W)-Na-O(19W)#1	128.0(10)
O(18W)-Na-O(19W)#1	77.3(11)
O(9W)#1-Na-O(19W)#1	100.1(9)
O(7W)-Na-O(19W)#1	81.2(7)
O(7W)#1-Na-O(19W)#1	90.4(8)
Na#1-Na-O(1W)	151(2)
O(19W)-Na-O(1W)	69.9(9)
O(9W)-Na-O(1W)	61.2(6)
O(18W)-Na-O(1W)	92.7(8)
O(9W)#1-Na-O(1W)	89.7(6)
O(7W)-Na-O(1W)	107.8(6)
O(7W)#1-Na-O(1W)	83.7(6)
O(19W)#1-Na-O(1W)	168.1(8)
Na#1-Na-O(18W)#1	53.9(7)
O(19W)-Na-O(18W)#1	80.4(12)
O(9W)-Na-O(18W)#1	147.4(10)
O(18W)-Na-O(18W)#1	57.6(13)
O(9W)#1-Na-O(18W)#1	119.8(9)
O(7W)-Na-O(18W)#1	87.1(7)
O(7W)#1-Na-O(18W)#1	91.9(7)
O(19W)#1-Na-O(18W)#1	19.7(6)
O(1W)-Na-O(18W)#1	149.7(8)
O(17W)-O(6W)-O(18W)	156(2)
Na-O(7W)-Na#1	18.3(5)
O(9W)#1-O(9W)-Na	84.7(5)
O(9W)#1-O(9W)-Na#1	66.7(6)
Na-O(9W)-Na#1	19.4(6)
O(14W)-O(13W)-O(13W)#2	137(3)
O(19W)-O(18W)-O(6W)	134(3)
O(19W)-O(18W)-Na	59(2)
O(6W)-O(18W)-Na	119.2(12)
O(19W)-O(18W)-Na#1	74(2)
O(6W)-O(18W)-Na#1	112.7(12)
Na-O(18W)-Na#1	16.0(5)
O(18W)-O(19W)-Na	99(3)
O(18W)-O(19W)-Na#1	86(3)
Na-O(19W)-Na#1	13.1(5)

Symmetry transformations used to generate equivalent atoms:
#1 -x+1,y,-z+3/2 #2 -x+1,y,-z+1/2

Table 4. Anisotropic displacement parameters (A^2 x 10^3) for 1.
The anisotropic displacement factor exponent takes the form:
-2 pi^2 [h^2 a*^2 U11 + ... + 2 h k a* b* U12]

	U11	U22	U33	U23	U13	U12
Eu	15(1)	18(1)	43(1)	-1(1)	-2(1)	0(1)
P(1)	16(2)	40(2)	49(2)	11(2)	-2(2)	-4(1)
P(2)	19(2)	26(2)	48(2)	2(2)	-5(2)	-7(1)
P(3)	9(1)	30(2)	47(2)	3(2)	0(1)	0(1)
P(4)	14(1)	22(2)	58(3)	-2(2)	-3(2)	-3(1)
N(1)	23(5)	25(6)	54(8)	-2(5)	-14(6)	-5(4)
N(2)	23(5)	24(6)	59(9)	-1(5)	-26(6)	0(4)
N(3)	27(5)	25(6)	52(8)	-10(5)	-10(5)	7(4)
N(4)	17(5)	24(5)	50(8)	-9(5)	-3(5)	3(4)
O(11)	21(4)	34(5)	47(6)	1(4)	-4(4)	-10(3)
O(12)	15(4)	54(6)	80(9)	36(6)	-8(5)	-9(4)
O(21)	17(4)	24(4)	39(6)	5(4)	-2(4)	-5(3)
O(22)	30(5)	31(5)	62(8)	-1(5)	-10(5)	-16(4)
O(31)	13(4)	29(5)	57(7)	4(4)	-9(4)	-5(3)
O(32)	18(4)	53(6)	65(8)	21(5)	-3(5)	-5(4)
O(41)	9(3)	20(4)	56(6)	-7(4)	-1(4)	-5(3)
O(42)	20(4)	32(5)	67(8)	-5(5)	-3(5)	-1(4)
C(1)	41(8)	25(7)	69(12)	16(7)	-32(8)	-10(6)
C(2)	59(9)	14(6)	83(14)	10(7)	-41(9)	4(6)
C(3)	16(6)	25(7)	60(11)	-15(6)	-17(6)	9(5)
C(4)	25(7)	35(8)	85(14)	-28(8)	-1(8)	12(6)
C(5)	16(6)	49(9)	64(11)	-8(8)	2(7)	0(5)
C(6)	14(6)	39(8)	59(10)	-5(7)	0(6)	5(5)
C(7)	15(5)	27(7)	63(10)	-9(7)	-4(6)	8(5)
C(8)	25(7)	26(7)	75(12)	8(7)	-10(7)	-5(5)
C(10)	7(5)	27(6)	57(9)	1(7)	0(6)	-5(5)
C(11)	13(6)	58(9)	45(10)	-2(7)	-4(6)	-1(6)
C(12)	20(6)	44(8)	57(11)	8(8)	3(7)	7(6)
C(13)	31(8)	63(11)	64(12)	16(9)	1(8)	21(7)
C(14)	25(8)	69(12)	107(18)	22(12)	22(9)	14(7)
C(15)	20(7)	84(13)	95(17)	-10(12)	-3(9)	20(8)
C(16)	62(11)	55(11)	80(15)	24(10)	9(11)	16(8)
C(17)	33(8)	64(11)	76(14)	6(10)	-3(8)	7(7)
C(20)	36(7)	29(7)	53(10)	2(7)	-10(7)	-12(6)
C(21)	25(7)	50(9)	54(11)	13(8)	-3(7)	-7(6)
C(22)	19(6)	59(9)	41(9)	12(7)	5(6)	-6(6)
C(23)	23(7)	72(12)	64(13)	9(9)	5(8)	7(7)
C(24)	50(10)	72(12)	92(17)	1(12)	10(11)	31(9)
C(25)	39(11)	104(18)	102(20)	42(15)	27(12)	28(11)
C(26)	11(7)	178(24)	75(16)	58(17)	10(8)	35(11)
C(27)	15(6)	114(15)	47(11)	16(10)	3(7)	-7(8)
C(30)	24(6)	36(7)	63(11)	-8(7)	6(7)	-8(6)
C(31)	14(5)	24(6)	43(9)	9(6)	11(6)	-7(5)
C(32)	17(6)	34(7)	57(10)	-2(7)	-7(6)	-1(5)
C(33)	21(7)	40(8)	80(13)	-11(8)	-5(7)	3(6)
C(34)	30(7)	48(10)	101(16)	-23(10)	-3(9)	20(7)

C(35)	73(12)	32(9)	88(16)	-8(9)	-7(11)	17(8)
C(36)	77(12)	37(9)	70(14)	11(9)	8(10)	4(8)
C(37)	43(8)	35(8)	63(12)	0(8)	9(8)	3(6)
C(40)	12(5)	30(7)	53(10)	7(6)	-6(6)	-4(5)
C(41)	24(7)	25(7)	94(15)	2(8)	-19(8)	-8(5)
C(42)	23(6)	20(7)	84(13)	-2(7)	-12(7)	-8(5)
C(43)	26(7)	30(8)	78(13)	9(8)	-13(8)	-2(5)
C(44)	39(8)	43(10)	106(17)	-12(10)	-6(10)	6(7)
C(45)	27(7)	41(9)	118(18)	-3(10)	-31(10)	7(6)
C(46)	39(8)	40(9)	99(16)	-17(10)	-35(10)	18(7)
C(47)	37(8)	36(8)	79(13)	-2(8)	-20(8)	5(6)
Na	22(6)	36(5)	64(14)	-4(5)	-8(10)	-2(5)
O(1W)	29(5)	70(8)	133(14)	-3(8)	-11(7)	-7(5)
O(2W)	41(6)	69(8)	153(15)	35(9)	34(8)	21(6)
O(3W)	63(7)	49(7)	74(9)	-3(6)	-4(7)	-21(5)
O(4W)	60(7)	45(6)	83(10)	9(6)	9(7)	10(5)
O(5W)	44(6)	50(6)	71(9)	2(6)	0(6)	-30(5)
O(6W)	44(6)	66(8)	98(12)	7(8)	-1(7)	-1(6)
O(7W)	29(5)	38(5)	66(8)	1(5)	-8(5)	-2(4)
O(8W)	49(11)	80(17)	79(19)	16(13)	6(12)	3(11)
O(9W)	34(10)	66(10)	91(18)	-2(10)	0(9)	-12(7)
O(10W)	54(12)	72(15)	101(23)	13(14)	1(14)	-14(10)
O(11W)	74(12)	56(11)	105(19)	16(11)	-2(12)	-3(9)
O(12W)	59(11)	64(12)	118(20)	6(12)	30(12)	-11(9)
O(13W)	56(12)	103(18)	164(28)	-21(17)	3(15)	-16(11)
O(14W)	51(10)	74(12)	98(18)	7(12)	-6(11)	-21(9)
O(15W)	88(14)	84(15)	91(18)	-11(13)	-4(14)	2(12)
O(16W)	51(11)	102(17)	150(26)	4(16)	-29(14)	9(11)
O(17W)	67(12)	51(11)	126(21)	21(12)	-8(13)	20(9)
O(18W)	29(11)	24(11)	93(21)	2(12)	-1(12)	-1(9)
O(19W)	68(16)	46(16)	82(22)	20(14)	19(15)	33(13)

Table 5. Hydrogen coordinates (x 10^4) and isotropic displacement parameters (A^2 x 10^3) for 1.

	x	y	z	U(eq)
H(1A)	2629(6)	4004(6)	4297(8)	54
H(1B)	3216(6)	3670(6)	4505(8)	54
H(2A)	2895(7)	4294(6)	5308(9)	63
H(2B)	2274(7)	3969(6)	5324(9)	63
H(3A)	2661(5)	4033(5)	6440(7)	41
H(3B)	2904(5)	3414(5)	6696(7)	41
H(4A)	1881(6)	3459(6)	6836(9)	58
H(4B)	1799(6)	3556(6)	6091(9)	58
H(5A)	1393(5)	2097(6)	6237(8)	51
H(5B)	1137(5)	2718(6)	6469(8)	51
H(6A)	1253(5)	3101(6)	5450(7)	45
H(6B)	815(5)	2550(6)	5454(7)	45
H(7A)	1110(5)	2704(5)	4319(8)	42
H(7B)	1693(5)	2375(5)	4091(8)	42
H(8A)	1790(5)	3403(6)	3949(9)	50
H(8B)	1703(5)	3499(6)	4694(9)	50
H(10A)	2789(4)	3190(5)	3525(7)	37
H(10B)	2536(4)	2551(5)	3708(7)	37
H(11A)	3247(5)	1668(6)	3708(8)	46
H(11B)	3544(5)	2017(6)	3133(8)	46
H(13)	4585(6)	1990(7)	2951(9)	63
H(14)	5473(6)	1500(8)	3120(11)	80
H(15)	5574(6)	839(8)	3927(11)	79
H(16)	4806(7)	664(8)	4629(10)	79
H(17)	3897(7)	1132(7)	4437(9)	69
H(20A)	3679(6)	3927(6)	6007(8)	47
H(20B)	3757(6)	3558(6)	5368(8)	47
H(21A)	4531(5)	2747(6)	5374(8)	51
H(21B)	4873(5)	3099(6)	5919(8)	51
H(23)	4497(6)	1629(8)	5475(9)	64
H(24)	4903(8)	785(8)	5886(11)	86
H(25)	5534(8)	788(11)	6650(13)	98
H(26)	5766(6)	1681(13)	7180(11)	105
H(27)	5355(5)	2598(9)	6800(8)	71
H(30A)	1912(5)	2426(6)	7234(8)	49
H(30B)	2577(5)	2582(6)	7064(8)	49
H(31A)	3330(5)	1727(5)	7063(7)	32
H(31B)	2921(5)	1591(5)	7656(7)	32
H(33)	4015(5)	1010(6)	6808(9)	56
H(34)	4410(6)	69(7)	6940(10)	72
H(35)	3865(8)	-687(7)	7370(10)	77
H(36)	2897(8)	-481(7)	7724(9)	73
H(37)	2522(6)	469(6)	7647(8)	56
H(40A)	1066(5)	1661(5)	4773(7)	38
H(40B)	1420(5)	1548(5)	5415(7)	38
H(41A)	2052(5)	681(6)	5423(9)	57
H(41B)	1817(5)	333(6)	4817(9)	57
H(43)	2647(5)	143(6)	3933(9)	54
H(44)	3538(6)	-346(7)	3873(11)	75
H(45)	4150(6)	-421(7)	4742(11)	74
H(46)	3889(6)	-14(7)	5697(10)	71

H(47)	2992(6)	506(6)	5768(9)	61

Appendix 4 Crystal data for $(Eu.13a)^{3+}$

$C_{60}H_{73}EuF_{12}N_{10}O_{13}$, M = 1522.24, orthorhombic, space group $P2_12_12_1$, a = 14.9659(1), b = 18.4202(1), c = 24.9210(1) Å, U = 6870.2(1)Å^3, Z = 4, $\rho_{calcd.}$ = 1.472 g cm^{-3}, F (000) = 3112, μ = 10.11 cm^{-1}, crystal dimensions 0.3×0.3×0.4 mm, MoK-α radiation (λ=0.71073 Å), measurement at 150(2) K. Final R (on F) and wR_2 (on F^2) were 0.030 and 0.090 respectively for all 11760 unique data. Final GOF = 0.95, and the final difference Fourier map showed no feature > +0.89 and < -0.63 e Å^{-3}. A Flack x parameter of -0.009(8) showed the refinement had been carried out with the correct polarity.

Intensity data were collected on a *Siemens* SMART automated 3-circle diffractometer equipped with a CCD (512 x 512 pixels) area detector for all four complexes. The structures were solved using Patterson and Fourier methods (SHELXS86)[1] and refined on F^2 using all unique data by full - matrix least - squares (SHELXL93)[2]. All non-hydrogen atoms were refined with anisotropic displacement parameters. Hydrogen atoms were generated in calculated positions and refined using a riding model.

Table 1. Crystal data and structure refinement for 1.

Empirical formula	C60 H73 Eu F12 N10 O13
Formula weight	1522.24
Temperature	150(2) K
Wavelength	.71073 A
Crystal system	Orthorhombic
Space group	P2(1)2(1)2(1)
Unit cell dimensions	a = 14.9659(1) A alpha = 90 deg. b = 18.4204(1) A beta = 90 deg. c = 24.9210(3) A gamma = 90 deg.
Volume	6870.2(1) A^3
Z	4
Number of reflexions used	8192
Crystal description	block
Crystal colour	colourless
Density (calculated)	1.472 Mg/m^3
Absorption coefficient	1.011 mm^-1
F(000)	3112
Crystal size	0.4 x 0.3 x 0.3 mm
Theta range for data collection	1.37 to 25.72 deg.
Index ranges	-17<=h<=16, -22<=k<=21, -29<=l<=26
Experiment device	Siemens SMART-CCD
Experiment methods	Omega scans
Reflections collected	36069
Independent reflections	11766 [R(int) = 0.0299]
Absorption correction	Semi-empirical from psi-scans
Refinement method	Full-matrix least-squares on F^2
Data / restraints / parameters	11760 / 0 / 839
Goodness-of-fit on F^2	0.950
Final R indices [I>2sigma(I)]	R1 = 0.030, wR2 = 0.090
R indices (all data)	R1 = 0.0311, wR2 = 0.0898

Absolute structure parameter	-.009(8)
Largest diff. peak and hole	0.891 and -0.629 e.A^-3

Table 2. Atomic coordinates (x 10^4) and equivalent isotropic displacement parameters (A^2 x 10^3) for 1. U(eq) is defined as one third of the trace of the orthogonalized Uij tensor.

	x	y	z	U(eq)
O(11)	2208(2)	5656(2)	2019(2)	59(1)
O(12)	3393(2)	4940(2)	2054(2)	64(1)
O(21)	4105(3)	7802(2)	-793(2)	62(1)
O(22)	4986(4)	7114(3)	-283(2)	85(2)
O(31)	2327(3)	2502(2)	742(1)	61(1)
O(32)	2879(4)	1517(2)	382(2)	81(1)
O(41)	10177(3)	6964(2)	-407(2)	67(1)
O(42)	11201(3)	7702(2)	-762(2)	67(1)
C(12S)	2642(3)	5143(2)	2190(2)	39(1)
C(22S)	4495(4)	7241(3)	-686(2)	51(1)
C(32S)	2649(3)	2158(2)	375(2)	44(1)
C(42S)	10760(4)	7145(3)	-747(2)	56(1)
C(11S)	2226(3)	4683(3)	2651(2)	53(1)
C(21S)	4416(5)	6589(3)	-1055(3)	70(2)
C(31S)	2705(6)	2572(4)	-152(2)	84(2)
C(41S)	10898(6)	6593(4)	-1191(4)	90(3)
F(11)	2726(3)	4585(4)	3046(2)	134(2)
F(12)	1994(4)	4036(2)	2459(3)	144(3)
F(13)	1447(3)	4954(3)	2826(2)	91(1)
F(21)	4163(5)	5998(3)	-812(2)	126(2)
F(22)	3877(4)	6705(3)	-1468(2)	107(2)
F(23)	5216(5)	6427(3)	-1272(2)	128(2)
F(31)	1937(6)	2570(3)	-405(2)	163(3)
F(32)	3259(5)	2233(3)	-502(2)	142(3)
F(33)	2967(4)	3246(2)	-104(2)	126(2)
F(41)	11465(4)	6789(3)	-1557(2)	113(2)
F(42)	10134(6)	6461(6)	-1442(3)	206(5)
F(43)	11076(7)	5942(3)	-1014(3)	183(4)
N(1S)	7631(7)	6992(5)	-320(4)	139(3)
N(2S)	12653(11)	4912(7)	-528(5)	215(5)
C(1S)	8001(5)	6700(4)	-1322(3)	79(2)
C(2S)	7831(5)	6807(4)	-882(3)	80(2)
C(3S)	12374(13)	6453(9)	-401(7)	225(5)
C(4S)	12370(12)	5739(10)	-487(7)	243(6)
Eu(1)	7596(1)	5597(1)	1902(1)	23(1)
O(1)	7608(2)	6716(1)	1389(1)	33(1)
O(4)	6997(2)	6491(1)	2493(1)	31(1)
O(5)	6186(2)	5698(2)	1487(1)	32(1)
N(8)	4691(2)	5608(2)	1449(1)	39(1)
C(141)	9744(2)	5837(2)	1970(2)	27(1)
C(5)	7368(3)	4933(2)	3206(1)	33(1)
N(2)	8966(2)	4649(2)	2043(1)	28(1)
C(101)	5455(2)	5566(2)	1710(2)	31(1)
N(3)	8034(2)	5411(2)	2939(1)	29(1)
C(6)	6399(3)	5075(2)	3051(2)	34(1)
C(2)	8830(3)	3975(2)	1719(2)	31(1)
C(4)	8938(3)	5086(2)	3000(2)	31(1)
C(161)	7279(3)	6607(2)	2955(1)	30(1)
C(144)	10215(3)	7162(2)	2674(2)	37(1)
C(3)	9079(3)	4448(2)	2617(1)	31(1)

N(7)	6976(2)	7145(2)	3257(1)	37(1)
N(4)	6256(2)	4979(2)	2463(1)	30(1)
C(160)	8025(3)	6142(2)	3185(2)	32(1)
C(102)	4661(3)	5843(3)	882(2)	43(1)
C(145)	10663(3)	6851(3)	3101(2)	48(1)
C(149)	9505(3)	7622(2)	2779(2)	40(1)
C(162)	6280(3)	7638(2)	3061(2)	45(1)
C(146)	10409(4)	6997(3)	3634(2)	55(1)
O(3)	8998(2)	6153(1)	2016(1)	27(1)
C(129)	10442(3)	5535(3)	534(2)	37(1)
N(6)	10497(2)	6191(2)	2014(1)	32(1)
N(1)	7205(2)	4247(2)	1560(1)	28(1)
C(125)	10295(3)	4262(3)	380(2)	48(1)
C(124)	9940(3)	4962(2)	340(2)	34(1)
C(140)	9777(2)	5031(2)	1845(2)	29(1)
C(148)	9249(3)	7783(3)	3304(2)	46(1)
C(128)	11259(3)	5426(3)	773(2)	50(1)
C(104)	5019(3)	5270(3)	507(2)	41(1)
C(105)	4692(4)	4554(3)	521(2)	60(2)
C(169)	4855(5)	7332(4)	2576(3)	72(2)
C(1)	7870(3)	3708(2)	1748(2)	34(1)
C(109)	5688(3)	5436(3)	135(2)	49(1)
C(100)	5436(3)	5378(2)	2305(2)	35(1)
C(126)	11125(4)	4145(3)	623(3)	60(2)
C(164)	5377(3)	7278(3)	3040(2)	51(1)
C(147)	9705(4)	7461(3)	3725(2)	60(2)
C(7)	6150(3)	4195(2)	2342(2)	33(1)
C(127)	11602(4)	4729(3)	812(2)	59(1)
C(8)	6294(3)	4018(2)	1749(2)	34(1)
C(165)	5047(4)	6914(3)	3480(3)	64(2)
C(166)	4183(5)	6609(4)	3449(4)	88(2)
C(106)	5028(5)	4043(4)	169(3)	73(2)
C(163)	6257(4)	8315(3)	3419(3)	61(1)
N(5)	8335(2)	4631(2)	301(1)	34(1)
C(121)	7965(3)	4772(2)	771(2)	29(1)
O(2)	8197(2)	5301(1)	1049(1)	28(1)
C(120)	7199(3)	4293(2)	967(2)	33(1)
C(122)	9034(3)	5102(2)	76(2)	35(1)
C(108)	6018(4)	4918(4)	-216(2)	66(2)
C(107)	5688(5)	4213(4)	-199(2)	73(2)
C(167)	3675(5)	6656(5)	2994(5)	98(3)
C(168)	3995(6)	7004(5)	2568(5)	109(4)
C(142)	10488(3)	6989(2)	2104(2)	36(1)
C(143)	11406(3)	7297(3)	1954(2)	53(1)
C(123)	9069(4)	5008(3)	-524(2)	59(2)
C(103)	3705(3)	6061(4)	749(3)	61(1)

Table 3. Bond lengths [A] and angles [deg] for 1.

O(11)-C(12S)	1.224(5)
O(12)-C(12S)	1.232(5)
O(21)-C(22S)	1.217(6)
O(22)-C(22S)	1.265(6)
O(31)-C(32S)	1.213(5)
O(32)-C(32S)	1.229(6)
O(41)-C(42S)	1.263(6)
O(42)-C(42S)	1.220(7)
C(12S)-C(11S)	1.557(7)
C(22S)-C(21S)	1.517(8)
C(32S)-C(31S)	1.521(8)
C(42S)-C(41S)	1.517(9)
C(11S)-F(11)	1.249(6)
C(11S)-F(12)	1.330(7)
C(11S)-F(13)	1.340(6)
C(21S)-F(21)	1.301(8)
C(21S)-F(22)	1.325(7)
C(21S)-F(23)	1.347(9)
C(31S)-F(31)	1.311(11)
C(31S)-F(33)	1.309(7)
C(31S)-F(32)	1.355(9)
C(41S)-F(41)	1.296(8)
C(41S)-F(43)	1.305(11)
C(41S)-F(42)	1.326(13)
N(1S)-C(2S)	1.471(11)
N(2S)-C(4S)	1.58(2)
C(1S)-C(2S)	1.144(9)
C(3S)-C(4S)	1.33(2)
Eu(1)-O(3)	2.352(2)
Eu(1)-O(5)	2.358(2)
Eu(1)-O(2)	2.374(3)
Eu(1)-O(4)	2.384(3)
Eu(1)-O(1)	2.425(2)
Eu(1)-N(3)	2.688(3)
Eu(1)-N(1)	2.694(3)
Eu(1)-N(4)	2.696(3)
Eu(1)-N(2)	2.717(3)
Eu(1)-C(101)	3.240(3)
Eu(1)-C(141)	3.249(3)
Eu(1)-C(161)	3.250(4)
O(4)-C(161)	1.244(5)
O(5)-C(101)	1.251(5)
N(8)-C(101)	1.318(5)
N(8)-C(102)	1.476(6)
N(8)-H(8)	.88
C(141)-O(3)	1.264(4)
C(141)-N(6)	1.307(5)
C(141)-C(140)	1.517(5)
C(5)-N(3)	1.486(5)
C(5)-C(6)	1.523(6)
C(5)-H(5A)	.99
C(5)-H(5B)	.99
N(2)-C(3)	1.488(5)
N(2)-C(140)	1.487(5)
N(2)-C(2)	1.494(5)
C(101)-C(100)	1.524(6)

N(3)-C(160)	1.480(5)
N(3)-C(4)	1.487(5)
C(6)-N(4)	1.493(5)
C(6)-H(6A)	.99
C(6)-H(6B)	.99
C(2)-C(1)	1.520(6)
C(2)-H(2A)	.99
C(2)-H(2B)	.99
C(4)-C(3)	1.529(6)
C(4)-H(4A)	.99
C(4)-H(4B)	.99
C(161)-N(7)	1.324(5)
C(161)-C(160)	1.519(6)
C(144)-C(145)	1.381(7)
C(144)-C(149)	1.385(7)
C(144)-C(142)	1.513(6)
C(3)-H(3A)	.99
C(3)-H(3B)	.99
N(7)-C(162)	1.466(6)
N(7)-H(7)	.88
N(4)-C(7)	1.484(5)
N(4)-C(100)	1.483(5)
C(160)-H(16A)	.99
C(160)-H(16B)	.99
C(102)-C(104)	1.509(7)
C(102)-C(103)	1.523(6)
C(102)-H(102)	1.00
C(145)-C(146)	1.409(8)
C(145)-H(145)	.95
C(149)-C(148)	1.396(7)
C(149)-H(149)	.95
C(162)-C(164)	1.506(7)
C(162)-C(163)	1.532(7)
C(162)-H(162)	1.00
C(146)-C(147)	1.375(9)
C(146)-H(146)	.95
C(129)-C(128)	1.375(7)
C(129)-C(124)	1.383(6)
C(129)-H(129)	.95
N(6)-C(142)	1.488(5)
N(6)-H(6)	.88
N(1)-C(120)	1.480(5)
N(1)-C(1)	1.483(5)
N(1)-C(8)	1.502(5)
C(125)-C(124)	1.398(7)
C(125)-C(126)	1.399(8)
C(125)-H(125)	.95
C(124)-C(122)	1.528(6)
C(140)-H(14A)	.99
C(140)-H(14B)	.99
C(148)-C(147)	1.385(9)
C(148)-H(148)	.95
C(128)-C(127)	1.385(8)
C(128)-H(128)	.95
C(104)-C(109)	1.399(7)
C(104)-C(105)	1.406(7)
C(105)-C(106)	1.381(9)
C(105)-H(105)	.95
C(169)-C(164)	1.398(9)
C(169)-C(168)	1.422(12)

C(169)-H(169)	.95
C(1)-H(1A)	.99
C(1)-H(1B)	.99
C(109)-C(108)	1.386(8)
C(109)-H(109)	.95
C(100)-H(10A)	.99
C(100)-H(10B)	.99
C(126)-C(127)	1.374(9)
C(126)-H(126)	.95
C(164)-C(165)	1.376(9)
C(147)-H(147)	.95
C(7)-C(8)	1.530(6)
C(7)-H(7A)	.99
C(7)-H(7B)	.99
C(127)-H(127)	.95
C(8)-H(8A)	.99
C(8)-H(8B)	.99
C(165)-C(166)	1.413(9)
C(165)-H(165)	.95
C(166)-C(167)	1.367(12)
C(166)-H(166)	.95
C(106)-C(107)	1.384(10)
C(106)-H(106)	.95
C(163)-H(16C)	.98
C(163)-H(16D)	.98
C(163)-H(16E)	.98
N(5)-C(121)	1.321(5)
N(5)-C(122)	1.470(5)
N(5)-H(5)	.88
C(121)-O(2)	1.245(5)
C(121)-C(120)	1.527(5)
C(120)-H(12A)	.99
C(120)-H(12B)	.99
C(122)-C(123)	1.505(6)
C(122)-H(122)	1.00
C(108)-C(107)	1.391(10)
C(108)-H(108)	.95
C(107)-H(107)	.95
C(167)-C(168)	1.331(14)
C(167)-H(167)	.95
C(168)-H(168)	.95
C(142)-C(143)	1.532(6)
C(142)-H(142)	1.00
C(143)-H(14C)	.98
C(143)-H(14D)	.98
C(143)-H(14E)	.98
C(123)-H(12C)	.98
C(123)-H(12D)	.98
C(123)-H(12E)	.98
C(103)-H(10C)	.98
C(103)-H(10D)	.98
C(103)-H(10E)	.98

O(11)-C(12S)-O(12)	128.5(5)
O(11)-C(12S)-C(11S)	117.7(4)
O(12)-C(12S)-C(11S)	113.8(4)
O(21)-C(22S)-O(22)	127.6(6)
O(21)-C(22S)-C(21S)	120.1(5)
O(22)-C(22S)-C(21S)	112.3(5)
O(31)-C(32S)-O(32)	127.1(5)

O(31)-C(32S)-C(31S)	114.3(4)
O(32)-C(32S)-C(31S)	118.5(5)
O(42)-C(42S)-O(41)	128.0(6)
O(42)-C(42S)-C(41S)	118.0(5)
O(41)-C(42S)-C(41S)	114.0(5)
F(11)-C(11S)-F(12)	108.0(6)
F(11)-C(11S)-F(13)	108.6(5)
F(12)-C(11S)-F(13)	103.0(5)
F(11)-C(11S)-C(12S)	114.8(5)
F(12)-C(11S)-C(12S)	109.0(5)
F(13)-C(11S)-C(12S)	112.6(4)
F(21)-C(21S)-F(22)	108.6(6)
F(21)-C(21S)-F(23)	105.1(7)
F(22)-C(21S)-F(23)	105.4(6)
F(21)-C(21S)-C(22S)	113.8(5)
F(22)-C(21S)-C(22S)	113.0(5)
F(23)-C(21S)-C(22S)	110.5(6)
F(31)-C(31S)-F(33)	108.0(8)
F(31)-C(31S)-F(32)	103.2(6)
F(33)-C(31S)-F(32)	108.2(6)
F(31)-C(31S)-C(32S)	111.4(6)
F(33)-C(31S)-C(32S)	114.4(5)
F(32)-C(31S)-C(32S)	111.0(6)
F(41)-C(41S)-F(43)	111.2(7)
F(41)-C(41S)-F(42)	106.5(8)
F(43)-C(41S)-F(42)	99.6(8)
F(41)-C(41S)-C(42S)	114.5(6)
F(43)-C(41S)-C(42S)	113.4(8)
F(42)-C(41S)-C(42S)	110.4(7)
C(1S)-C(2S)-N(1S)	176.4(9)
C(3S)-C(4S)-N(2S)	163(2)
O(3)-Eu(1)-O(5)	144.81(9)
O(3)-Eu(1)-O(2)	82.53(9)
O(5)-Eu(1)-O(2)	87.88(9)
O(3)-Eu(1)-O(4)	87.77(9)
O(5)-Eu(1)-O(4)	83.13(10)
O(2)-Eu(1)-O(4)	148.76(9)
O(3)-Eu(1)-O(1)	71.79(9)
O(5)-Eu(1)-O(1)	73.02(9)
O(2)-Eu(1)-O(1)	73.71(9)
O(4)-Eu(1)-O(1)	75.05(9)
O(3)-Eu(1)-N(3)	73.90(9)
O(5)-Eu(1)-N(3)	130.58(10)
O(2)-Eu(1)-N(3)	137.74(10)
O(4)-Eu(1)-N(3)	65.58(9)
O(1)-Eu(1)-N(3)	127.91(9)
O(3)-Eu(1)-N(1)	129.33(9)
O(5)-Eu(1)-N(1)	74.85(10)
O(2)-Eu(1)-N(1)	65.55(9)
O(4)-Eu(1)-N(1)	138.71(9)
O(1)-Eu(1)-N(1)	128.22(9)
N(3)-Eu(1)-N(1)	103.83(9)
O(3)-Eu(1)-N(4)	141.76(9)
O(5)-Eu(1)-N(4)	66.10(9)
O(2)-Eu(1)-N(4)	130.44(9)
O(4)-Eu(1)-N(4)	72.07(10)
O(1)-Eu(1)-N(4)	129.60(10)
N(3)-Eu(1)-N(4)	68.25(10)
N(1)-Eu(1)-N(4)	67.17(10)
O(3)-Eu(1)-N(2)	65.85(9)

O(5)-Eu(1)-N(2)	141.47(10)
O(2)-Eu(1)-N(2)	71.42(9)
O(4)-Eu(1)-N(2)	130.47(9)
O(1)-Eu(1)-N(2)	127.49(9)
N(3)-Eu(1)-N(2)	67.06(10)
N(1)-Eu(1)-N(2)	67.10(10)
N(4)-Eu(1)-N(2)	102.90(10)
O(3)-Eu(1)-C(101)	155.23(10)
O(5)-Eu(1)-C(101)	18.47(10)
O(2)-Eu(1)-C(101)	103.74(9)
O(4)-Eu(1)-C(101)	74.44(10)
O(1)-Eu(1)-C(101)	86.81(10)
N(3)-Eu(1)-C(101)	112.39(10)
N(1)-Eu(1)-C(101)	73.82(10)
N(4)-Eu(1)-C(101)	48.19(10)
N(2)-Eu(1)-C(101)	138.92(10)
O(3)-Eu(1)-C(141)	18.54(9)
O(5)-Eu(1)-C(141)	153.83(9)
O(2)-Eu(1)-C(141)	72.72(9)
O(4)-Eu(1)-C(141)	104.28(9)
O(1)-Eu(1)-C(141)	84.55(9)
N(3)-Eu(1)-C(141)	74.13(9)
N(1)-Eu(1)-C(141)	110.90(9)
N(4)-Eu(1)-C(141)	140.05(10)
N(2)-Eu(1)-C(141)	48.22(9)
C(101)-Eu(1)-C(141)	171.29(9)
O(3)-Eu(1)-C(161)	77.53(9)
O(5)-Eu(1)-C(161)	100.33(10)
O(2)-Eu(1)-C(161)	155.55(9)
O(4)-Eu(1)-C(161)	18.47(10)
O(1)-Eu(1)-C(161)	86.62(9)
N(3)-Eu(1)-C(161)	48.17(9)
N(1)-Eu(1)-C(161)	138.78(9)
N(4)-Eu(1)-C(161)	73.47(10)
N(2)-Eu(1)-C(161)	111.99(10)
C(101)-Eu(1)-C(161)	89.18(10)
C(141)-Eu(1)-C(161)	91.42(10)
C(161)-O(4)-Eu(1)	124.1(2)
C(101)-O(5)-Eu(1)	124.9(2)
C(101)-N(8)-C(102)	121.1(3)
C(101)-N(8)-H(8)	119.5(2)
C(102)-N(8)-H(8)	119.4(2)
O(3)-C(141)-N(6)	121.6(3)
O(3)-C(141)-C(140)	119.8(3)
N(6)-C(141)-C(140)	118.5(3)
O(3)-C(141)-Eu(1)	36.3(2)
N(6)-C(141)-Eu(1)	157.7(3)
C(140)-C(141)-Eu(1)	83.6(2)
N(3)-C(5)-C(6)	115.1(3)
N(3)-C(5)-H(5A)	108.5(2)
C(6)-C(5)-H(5A)	108.5(2)
N(3)-C(5)-H(5B)	108.5(2)
C(6)-C(5)-H(5B)	108.5(2)
H(5A)-C(5)-H(5B)	107.5
C(3)-N(2)-C(140)	110.2(3)
C(3)-N(2)-C(2)	109.1(3)
C(140)-N(2)-C(2)	109.0(3)
C(3)-N(2)-Eu(1)	111.7(2)
C(140)-N(2)-Eu(1)	105.6(2)
C(2)-N(2)-Eu(1)	111.2(2)

O(5)-C(101)-N(8)	121.8(4)
O(5)-C(101)-C(100)	119.6(3)
N(8)-C(101)-C(100)	118.6(3)
O(5)-C(101)-Eu(1)	36.7(2)
N(8)-C(101)-Eu(1)	158.4(3)
C(100)-C(101)-Eu(1)	83.0(2)
C(160)-N(3)-C(4)	109.4(3)
C(160)-N(3)-C(5)	110.4(3)
C(4)-N(3)-C(5)	109.1(3)
C(160)-N(3)-Eu(1)	106.2(2)
C(4)-N(3)-Eu(1)	111.8(2)
C(5)-N(3)-Eu(1)	110.0(2)
N(4)-C(6)-C(5)	111.4(3)
N(4)-C(6)-H(6A)	109.4(2)
C(5)-C(6)-H(6A)	109.4(2)
N(4)-C(6)-H(6B)	109.3(2)
C(5)-C(6)-H(6B)	109.3(2)
H(6A)-C(6)-H(6B)	108.0
N(2)-C(2)-C(1)	111.9(3)
N(2)-C(2)-H(2A)	109.2(2)
C(1)-C(2)-H(2A)	109.2(2)
N(2)-C(2)-H(2B)	109.2(2)
C(1)-C(2)-H(2B)	109.3(2)
H(2A)-C(2)-H(2B)	107.9
N(3)-C(4)-C(3)	111.8(3)
N(3)-C(4)-H(4A)	109.2(2)
C(3)-C(4)-H(4A)	109.2(2)
N(3)-C(4)-H(4B)	109.3(2)
C(3)-C(4)-H(4B)	109.3(2)
H(4A)-C(4)-H(4B)	107.9
O(4)-C(161)-N(7)	122.5(4)
O(4)-C(161)-C(160)	120.2(3)
N(7)-C(161)-C(160)	117.3(3)
O(4)-C(161)-Eu(1)	37.4(2)
N(7)-C(161)-Eu(1)	159.5(3)
C(160)-C(161)-Eu(1)	82.8(2)
C(145)-C(144)-C(149)	118.8(4)
C(145)-C(144)-C(142)	120.3(4)
C(149)-C(144)-C(142)	120.8(4)
N(2)-C(3)-C(4)	113.2(3)
N(2)-C(3)-H(3A)	108.9(2)
C(4)-C(3)-H(3A)	108.9(2)
N(2)-C(3)-H(3B)	109.0(2)
C(4)-C(3)-H(3B)	109.0(2)
H(3A)-C(3)-H(3B)	107.8
C(161)-N(7)-C(162)	121.2(4)
C(161)-N(7)-H(7)	119.4(2)
C(162)-N(7)-H(7)	119.4(2)
C(7)-N(4)-C(100)	109.9(3)
C(7)-N(4)-C(6)	109.2(3)
C(100)-N(4)-C(6)	108.6(3)
C(7)-N(4)-Eu(1)	112.7(2)
C(100)-N(4)-Eu(1)	105.7(2)
C(6)-N(4)-Eu(1)	110.6(2)
N(3)-C(160)-C(161)	111.3(3)
N(3)-C(160)-H(16A)	109.4(2)
C(161)-C(160)-H(16A)	109.3(2)
N(3)-C(160)-H(16B)	109.4(2)
C(161)-C(160)-H(16B)	109.4(2)
H(16A)-C(160)-H(16B)	108.0

N(8)-C(102)-C(104)	112.0(4)
N(8)-C(102)-C(103)	108.4(4)
C(104)-C(102)-C(103)	112.5(4)
N(8)-C(102)-H(102)	107.9(2)
C(104)-C(102)-H(102)	107.9(2)
C(103)-C(102)-H(102)	107.9(3)
C(144)-C(145)-C(146)	121.0(5)
C(144)-C(145)-H(145)	119.5(3)
C(146)-C(145)-H(145)	119.5(3)
C(144)-C(149)-C(148)	121.1(5)
C(144)-C(149)-H(149)	119.4(3)
C(148)-C(149)-H(149)	119.4(3)
N(7)-C(162)-C(164)	112.1(4)
N(7)-C(162)-C(163)	109.1(4)
C(164)-C(162)-C(163)	111.0(4)
N(7)-C(162)-H(162)	108.2(2)
C(164)-C(162)-H(162)	108.2(3)
C(163)-C(162)-H(162)	108.2(3)
C(147)-C(146)-C(145)	118.7(5)
C(147)-C(146)-H(146)	120.7(3)
C(145)-C(146)-H(146)	120.6(3)
C(141)-O(3)-Eu(1)	125.2(2)
C(128)-C(129)-C(124)	121.6(5)
C(128)-C(129)-H(129)	119.2(3)
C(124)-C(129)-H(129)	119.2(3)
C(141)-N(6)-C(142)	119.8(3)
C(141)-N(6)-H(6)	120.1(2)
C(142)-N(6)-H(6)	120.1(2)
C(120)-N(1)-C(1)	110.9(3)
C(120)-N(1)-C(8)	108.9(3)
C(1)-N(1)-C(8)	108.8(3)
C(120)-N(1)-Eu(1)	105.3(2)
C(1)-N(1)-Eu(1)	111.9(2)
C(8)-N(1)-Eu(1)	110.9(2)
C(124)-C(125)-C(126)	120.8(5)
C(124)-C(125)-H(125)	119.6(3)
C(126)-C(125)-H(125)	119.6(3)
C(129)-C(124)-C(125)	118.2(4)
C(129)-C(124)-C(122)	120.3(4)
C(125)-C(124)-C(122)	121.6(4)
N(2)-C(140)-C(141)	111.7(3)
N(2)-C(140)-H(14A)	109.3(2)
C(141)-C(140)-H(14A)	109.3(2)
N(2)-C(140)-H(14B)	109.3(2)
C(141)-C(140)-H(14B)	109.3(2)
H(14A)-C(140)-H(14B)	107.9
C(147)-C(148)-C(149)	118.9(5)
C(147)-C(148)-H(148)	120.5(3)
C(149)-C(148)-H(148)	120.6(3)
C(127)-C(128)-C(129)	119.7(5)
C(127)-C(128)-H(128)	120.2(3)
C(129)-C(128)-H(128)	120.2(3)
C(109)-C(104)-C(105)	118.0(5)
C(109)-C(104)-C(102)	120.7(4)
C(105)-C(104)-C(102)	121.2(5)
C(106)-C(105)-C(104)	119.8(6)
C(106)-C(105)-H(105)	120.1(4)
C(104)-C(105)-H(105)	120.1(3)
C(164)-C(169)-C(168)	119.2(8)
C(164)-C(169)-H(169)	120.4(4)

C(168)-C(169)-H(169)	120.4(6)
N(1)-C(1)-C(2)	113.7(3)
N(1)-C(1)-H(1A)	108.8(2)
C(2)-C(1)-H(1A)	108.8(2)
N(1)-C(1)-H(1B)	108.8(2)
C(2)-C(1)-H(1B)	108.8(2)
H(1A)-C(1)-H(1B)	107.7
C(108)-C(109)-C(104)	121.5(5)
C(108)-C(109)-H(109)	119.2(4)
C(104)-C(109)-H(109)	119.3(3)
N(4)-C(100)-C(101)	110.7(3)
N(4)-C(100)-H(10A)	109.4(2)
C(101)-C(100)-H(10A)	109.5(2)
N(4)-C(100)-H(10B)	109.6(2)
C(101)-C(100)-H(10B)	109.5(2)
H(10A)-C(100)-H(10B)	108.1
C(127)-C(126)-C(125)	119.2(5)
C(127)-C(126)-H(126)	120.4(3)
C(125)-C(126)-H(126)	120.4(3)
C(165)-C(164)-C(169)	119.5(6)
C(165)-C(164)-C(162)	120.6(5)
C(169)-C(164)-C(162)	119.9(6)
C(146)-C(147)-C(148)	121.3(5)
C(146)-C(147)-H(147)	119.3(3)
C(148)-C(147)-H(147)	119.3(3)
N(4)-C(7)-C(8)	112.8(3)
N(4)-C(7)-H(7A)	109.0(2)
C(8)-C(7)-H(7A)	109.0(2)
N(4)-C(7)-H(7B)	109.0(2)
C(8)-C(7)-H(7B)	109.1(2)
H(7A)-C(7)-H(7B)	107.8
C(128)-C(127)-C(126)	120.6(5)
C(128)-C(127)-H(127)	119.7(3)
C(126)-C(127)-H(127)	119.7(3)
N(1)-C(8)-C(7)	111.7(3)
N(1)-C(8)-H(8A)	109.3(2)
C(7)-C(8)-H(8A)	109.2(2)
N(1)-C(8)-H(8B)	109.3(2)
C(7)-C(8)-H(8B)	109.3(2)
H(8A)-C(8)-H(8B)	107.9
C(164)-C(165)-C(166)	118.6(7)
C(164)-C(165)-H(165)	120.7(3)
C(166)-C(165)-H(165)	120.7(5)
C(167)-C(166)-C(165)	122.0(8)
C(167)-C(166)-H(166)	119.0(5)
C(165)-C(166)-H(166)	119.0(5)
C(107)-C(106)-C(105)	121.8(6)
C(107)-C(106)-H(106)	119.1(4)
C(105)-C(106)-H(106)	119.1(4)
C(162)-C(163)-H(16C)	109.5(3)
C(162)-C(163)-H(16D)	109.5(3)
H(16C)-C(163)-H(16D)	109.5
C(162)-C(163)-H(16E)	109.5(3)
H(16C)-C(163)-H(16E)	109.5
H(16D)-C(163)-H(16E)	109.5
C(121)-N(5)-C(122)	121.3(3)
C(121)-N(5)-H(5)	119.3(2)
C(122)-N(5)-H(5)	119.4(2)
O(2)-C(121)-N(5)	122.0(4)
O(2)-C(121)-C(120)	118.8(3)

N(5)-C(121)-C(120)	119.1(3)
O(2)-C(121)-Eu(1)	36.7(2)
N(5)-C(121)-Eu(1)	158.7(3)
C(120)-C(121)-Eu(1)	82.2(2)
C(121)-O(2)-Eu(1)	125.0(2)
N(1)-C(120)-C(121)	110.5(3)
N(1)-C(120)-H(12A)	109.6(2)
C(121)-C(120)-H(12A)	109.6(2)
N(1)-C(120)-H(12B)	109.5(2)
C(121)-C(120)-H(12B)	109.6(2)
H(12A)-C(120)-H(12B)	108.1
N(5)-C(122)-C(123)	109.6(4)
N(5)-C(122)-C(124)	111.6(3)
C(123)-C(122)-C(124)	112.2(4)
N(5)-C(122)-H(122)	107.8(2)
C(123)-C(122)-H(122)	107.8(3)
C(124)-C(122)-H(122)	107.7(2)
C(109)-C(108)-C(107)	119.9(6)
C(109)-C(108)-H(108)	120.1(4)
C(107)-C(108)-H(108)	120.1(4)
C(106)-C(107)-C(108)	118.9(6)
C(106)-C(107)-H(107)	120.5(4)
C(108)-C(107)-H(107)	120.5(4)
C(168)-C(167)-C(166)	119.5(8)
C(168)-C(167)-H(167)	120.3(5)
C(166)-C(167)-H(167)	120.2(5)
C(167)-C(168)-C(169)	121.2(8)
C(167)-C(168)-H(168)	119.4(5)
C(169)-C(168)-H(168)	119.4(6)
N(6)-C(142)-C(144)	110.6(3)
N(6)-C(142)-C(143)	108.6(3)
C(144)-C(142)-C(143)	113.1(4)
N(6)-C(142)-H(142)	108.1(2)
C(144)-C(142)-H(142)	108.1(2)
C(143)-C(142)-H(142)	108.1(3)
C(142)-C(143)-H(14C)	109.5(3)
C(142)-C(143)-H(14D)	109.5(2)
H(14C)-C(143)-H(14D)	109.5
C(142)-C(143)-H(14E)	109.5(3)
H(14C)-C(143)-H(14E)	109.5
H(14D)-C(143)-H(14E)	109.5
C(122)-C(123)-H(12C)	109.5(3)
C(122)-C(123)-H(12D)	109.4(3)
H(12C)-C(123)-H(12D)	109.5
C(122)-C(123)-H(12E)	109.5(3)
H(12C)-C(123)-H(12E)	109.5
H(12D)-C(123)-H(12E)	109.5
C(102)-C(103)-H(10C)	109.4(3)
C(102)-C(103)-H(10D)	109.5(3)
H(10C)-C(103)-H(10D)	109.5
C(102)-C(103)-H(10E)	109.5(3)
H(10C)-C(103)-H(10E)	109.5
H(10D)-C(103)-H(10E)	109.5

Table 4. Anisotropic displacement parameters (A^2 x 10^3) for 1.
The anisotropic displacement factor exponent takes the form:
-2 pi^2 [h^2 a*^2 U11 + ... + 2 h k a* b* U12]

	U11	U22	U33	U23	U13	U12
O(11)	35(2)	74(2)	68(2)	17(2)	4(2)	11(2)
O(12)	34(2)	54(2)	103(3)	12(2)	19(2)	1(2)
O(21)	64(2)	57(2)	65(2)	10(2)	-27(2)	0(2)
O(22)	111(4)	74(3)	71(3)	-7(2)	-49(3)	35(3)
O(31)	87(3)	60(2)	37(2)	9(2)	9(2)	31(2)
O(32)	119(4)	68(3)	57(2)	-21(2)	-13(2)	36(3)
O(41)	66(3)	64(2)	70(3)	7(2)	27(2)	-18(2)
O(42)	70(3)	47(2)	84(3)	4(2)	36(2)	-6(2)
C(12S)	22(2)	43(2)	50(2)	-6(2)	-7(2)	2(2)
C(22S)	51(3)	52(3)	50(3)	7(2)	-12(2)	4(2)
C(32S)	44(2)	42(2)	46(2)	-14(2)	-1(2)	6(2)
C(42S)	55(3)	49(3)	65(3)	17(3)	16(3)	-1(2)
C(11S)	41(3)	60(3)	56(3)	11(2)	7(2)	6(2)
C(21S)	99(5)	57(3)	54(3)	2(3)	-12(3)	-6(3)
C(31S)	138(7)	73(4)	42(3)	-10(3)	26(4)	-37(4)
C(41S)	104(6)	66(4)	101(6)	-19(4)	53(5)	-29(4)
F(11)	80(3)	220(6)	101(3)	91(4)	-18(2)	6(3)
F(12)	185(6)	67(3)	179(6)	-10(3)	102(5)	-54(3)
F(13)	62(2)	140(4)	70(2)	32(2)	28(2)	19(2)
F(21)	213(6)	81(3)	85(3)	24(2)	-34(4)	-58(4)
F(22)	164(5)	91(3)	67(2)	-4(2)	-56(3)	-10(3)
F(23)	151(5)	115(4)	118(4)	-38(3)	28(4)	29(4)
F(31)	250(8)	127(4)	112(4)	49(3)	-110(5)	-37(5)
F(32)	205(7)	141(5)	81(3)	-35(3)	82(4)	-75(5)
F(33)	229(6)	78(3)	72(2)	4(2)	33(3)	-74(3)
F(41)	142(4)	101(3)	95(3)	-26(3)	64(3)	-44(3)
F(42)	206(8)	253(10)	159(6)	-109(7)	70(6)	-145(8)
F(43)	277(10)	80(4)	190(7)	7(4)	129(7)	27(5)
Eu(1)	20(1)	26(1)	23(1)	1(1)	0(1)	-1(1)
O(1)	28(1)	32(1)	38(1)	8(1)	2(1)	2(1)
O(4)	31(1)	31(1)	31(1)	-1(1)	4(1)	5(1)
O(5)	21(1)	40(2)	34(1)	6(1)	-2(1)	-2(1)
N(8)	23(2)	47(2)	45(2)	8(2)	3(1)	-6(2)
C(141)	21(2)	36(2)	24(2)	0(2)	-2(2)	1(1)
C(5)	36(2)	39(2)	25(2)	5(1)	1(2)	-5(2)
N(2)	27(2)	26(2)	32(2)	1(1)	0(1)	3(1)
C(101)	23(2)	31(2)	41(2)	3(2)	-1(2)	-3(2)
N(3)	28(2)	32(2)	27(2)	0(1)	1(1)	-1(1)
C(6)	33(2)	41(2)	29(2)	2(2)	9(2)	-6(2)
C(2)	34(2)	29(2)	31(2)	-1(2)	0(2)	4(2)
C(4)	32(2)	32(2)	27(2)	1(2)	-5(2)	2(2)
C(161)	29(2)	30(2)	31(2)	-2(1)	5(2)	-2(2)
C(144)	31(2)	37(2)	43(2)	-8(2)	-2(2)	-11(2)
C(3)	35(2)	33(2)	26(2)	4(2)	-1(1)	7(2)
N(7)	40(2)	37(2)	34(2)	-6(1)	4(1)	4(2)
N(4)	26(2)	37(2)	27(2)	3(1)	0(1)	-4(1)

C(160)	31(2)	37(2)	28(2)	-7(2)	-3(2)	1(2)
C(102)	26(2)	52(3)	49(3)	15(2)	-7(2)	-2(2)
C(145)	45(2)	47(2)	51(3)	-9(2)	-8(2)	-5(2)
C(149)	35(2)	35(2)	50(3)	-9(2)	2(2)	-8(2)
C(162)	48(2)	37(2)	50(3)	-3(2)	4(2)	11(2)
C(146)	63(3)	57(3)	45(3)	-5(2)	-9(2)	-12(3)
O(3)	24(1)	29(1)	29(1)	-2(1)	0(1)	0(1)
C(129)	38(2)	40(2)	34(2)	3(2)	5(2)	-2(2)
N(6)	24(2)	33(2)	40(2)	-4(1)	2(1)	0(1)
N(1)	30(2)	29(2)	25(2)	1(1)	1(1)	-4(1)
C(125)	50(3)	46(3)	49(3)	4(2)	12(2)	-5(2)
C(124)	34(2)	40(2)	27(2)	3(2)	7(2)	0(2)
C(140)	26(2)	34(2)	27(2)	0(2)	1(2)	2(1)
C(148)	41(3)	42(3)	56(3)	-17(2)	6(2)	-8(2)
C(128)	36(2)	66(3)	49(3)	7(2)	2(2)	-7(2)
C(104)	35(2)	47(3)	39(2)	8(2)	-15(2)	-2(2)
C(105)	54(3)	61(4)	64(3)	8(3)	-9(3)	-17(3)
C(169)	67(4)	73(4)	77(4)	-21(3)	-16(3)	32(3)
C(1)	39(2)	29(2)	34(2)	1(2)	0(2)	0(2)
C(109)	47(3)	51(3)	47(3)	12(2)	-7(2)	-2(2)
C(100)	22(2)	43(2)	39(2)	2(2)	3(2)	1(2)
C(126)	47(3)	52(3)	81(4)	19(3)	21(3)	13(2)
C(164)	41(2)	48(3)	65(3)	-19(3)	-1(2)	16(2)
C(147)	71(4)	60(3)	49(3)	-20(3)	16(3)	-29(3)
C(7)	35(2)	33(2)	33(2)	2(2)	5(2)	-5(2)
C(127)	35(3)	75(4)	67(4)	23(3)	5(2)	0(2)
C(8)	32(2)	34(2)	37(2)	3(2)	0(2)	-9(2)
C(165)	48(3)	74(4)	70(4)	-15(3)	9(3)	-3(3)
C(166)	56(4)	91(5)	118(6)	-24(5)	22(4)	-12(4)
C(106)	85(5)	61(4)	72(4)	-15(3)	-25(4)	-7(3)
C(163)	59(3)	42(3)	83(4)	-17(3)	11(3)	7(2)
N(5)	34(2)	41(2)	27(2)	-5(1)	1(1)	-7(1)
C(121)	28(2)	33(2)	26(2)	4(2)	-4(2)	-1(2)
O(2)	29(1)	30(1)	24(1)	-3(1)	-2(1)	-3(1)
C(120)	35(2)	35(2)	28(2)	-2(2)	-2(2)	-5(2)
C(122)	38(2)	41(2)	25(2)	4(2)	1(2)	-5(2)
C(108)	70(4)	92(5)	36(3)	10(3)	-3(3)	16(3)
C(107)	88(5)	80(5)	51(3)	-15(3)	-23(3)	17(4)
C(167)	43(3)	101(6)	149(9)	-58(6)	-4(5)	5(4)
C(168)	63(5)	113(7)	153(9)	-75(7)	-44(5)	43(5)
C(142)	30(2)	34(2)	45(2)	-1(2)	2(2)	-4(2)
C(143)	44(3)	40(2)	74(3)	-4(2)	13(3)	-13(2)
C(123)	59(3)	96(5)	23(2)	5(2)	0(2)	-27(3)
C(103)	33(2)	80(4)	68(3)	21(3)	-10(2)	7(2)

Table 5. Hydrogen coordinates (x 10^4) and isotropic displacement parameters (A^2 x 10^3) for 1.

	x	y	z	U(eq)
H(8)	4191(2)	5494(2)	1614(1)	46
H(5A)	7428(3)	4992(2)	3599(1)	40
H(5B)	7513(3)	4422(2)	3119(1)	40
H(6A)	6006(3)	4737(2)	3250(2)	41
H(6B)	6234(3)	5577(2)	3155(2)	41
H(2A)	9234(3)	3590(2)	1853(2)	37
H(2B)	8987(3)	4074(2)	1340(2)	37
H(4A)	9015(3)	4917(2)	3374(2)	37
H(4B)	9395(3)	5462(2)	2929(2)	37
H(3A)	9688(3)	4251(2)	2670(1)	38
H(3B)	8648(3)	4059(2)	2707(1)	38
H(7)	7197(2)	7207(2)	3581(1)	44
H(16A)	8607(3)	6383(2)	3119(2)	39
H(16B)	7945(3)	6096(2)	3578(2)	39
H(102)	5046(3)	6284(3)	846(2)	51
H(145)	11151(3)	6533(3)	3033(2)	57
H(149)	9186(3)	7832(2)	2488(2)	48
H(162)	6443(3)	7793(2)	2689(2)	54
H(146)	10717(4)	6779(3)	3926(2)	66
H(129)	10216(3)	6015(3)	502(2)	45
H(6)	11009(2)	5958(2)	1990(1)	39
H(125)	9970(3)	3862(3)	240(2)	58
H(14A)	9827(2)	4963(2)	1452(2)	35
H(14B)	10313(2)	4816(2)	2014(2)	35
H(148)	8770(3)	8109(3)	3372(2)	56
H(128)	11587(3)	5826(3)	910(2)	60
H(105)	4241(4)	4423(3)	771(2)	71
H(169)	5073(5)	7584(4)	2271(3)	87
H(1A)	7814(3)	3263(2)	1527(2)	41
H(1B)	7732(3)	3575(2)	2124(2)	41
H(109)	5922(3)	5915(3)	123(2)	58
H(10A)	5388(3)	5829(2)	2519(2)	42
H(10B)	4905(3)	5075(2)	2383(2)	42
H(126)	11357(4)	3667(3)	657(3)	72
H(147)	9528(4)	7562(3)	4083(2)	72
H(7A)	5542(3)	4039(2)	2449(2)	40
H(7B)	6584(3)	3915(2)	2560(2)	40
H(127)	12171(4)	4655(3)	971(2)	71
H(8A)	6222(3)	3489(2)	1693(2)	41
H(8B)	5833(3)	4269(2)	1532(2)	41
H(165)	5394(4)	6869(3)	3797(3)	77
H(166)	3948(5)	6364(4)	3753(4)	106
H(106)	4799(5)	3562(4)	180(3)	87
H(16C)	5815(19)	8659(9)	3278(9)	74
H(16D)	6848(8)	8543(12)	3421(13)	74
H(16E)	6092(25)	8175(4)	3785(4)	74
H(5)	8160(2)	4247(2)	118(1)	41
H(12A)	6623(3)	4498(2)	845(2)	39
H(12B)	7261(3)	3800(2)	813(2)	39
H(122)	8863(3)	5617(2)	152(2)	42
H(108)	6469(4)	5044(4)	-467(2)	79

H(107)	5912(5)	3853(4)	-437(2)	88
H(167)	3098(5)	6442(5)	2983(5)	117
H(168)	3642(6)	7035(5)	2251(5)	131
H(142)	10034(3)	7207(2)	1857(2)	43
H(14C)	11870(4)	7044(13)	2159(10)	63
H(14D)	11423(8)	7816(5)	2038(13)	63
H(14E)	11511(10)	7226(17)	1569(4)	63
H(12C)	9515(19)	5340(15)	-675(2)	71
H(12D)	8481(8)	5118(20)	-677(2)	71
H(12E)	9233(25)	4507(7)	-609(2)	71
H(10C)	3682(6)	6263(20)	386(6)	73
H(10D)	3499(9)	6427(16)	1007(10)	73
H(10E)	3317(6)	5633(5)	770(15)	73

Appendix 5 Crystal data for $(Eu.13b)^{3+}$

$C_{57}H_{75}EuF_9N_{11}O_{14}S_9$, M = 1557.42 orthorhombic, space group $P2_12_12_1$, a = 15.7764(2), b = 20.4123(2), c = 21.7840(2) Å, U = 7015.1(1)Å^3, Z = 4, $\rho_{calcd.}$ = 1.371 g cm^{-3}, F (000) = 3192, μ = 10.74 cm^{-1}, crystal dimensions 0.2×0.3×0.4 mm, Mo-K_α radiation (λ=0.71073Å), measurement at 150(2) K. Final R (on F) and wR_2 (on F^2) were 0.051 and 0.1477 respectively for all 14716 unique data. Final GOF = 0.915, and the final difference Fourier map showed no feature > +0.92 and < -1.68 e Å^{-3}. A Flack x parameter of -0.02(1) showed the refinement had been carried out with the correct polarity.

Intensity data were collected on a *Siemens* SMART automated 3-circle diffractometer equipped with a CCD (512 x 512 pixels) area detector for all four complexes. The structures were solved using Patterson and Fourier methods (SHELXS86)[1] and refined on F^2 using all unique data by full - matrix least - squares (SHELXL93)[2]. All non-hydrogen atoms were refined with anisotropic displacement parameters. Hydrogen atoms were generated in calculated positions and refined using a riding model.

Table 1. Crystal data and structure refinement for 1.

Empirical formula	C57 H75 Eu F9 N11 O14 S3
Formula weight	1557.42
Temperature	150(2) K
Wavelength	.71073 A
Crystal system	Orthorhombic
Space group	P2(1)2(1)2(1)
Unit cell dimensions	a = 15.7764(2) A alpha = 90 deg. b = 20.4123(2) A beta = 90 deg. c = 21.7840(2) A gamma = 90 deg.
Volume	7015.2(1) A^3
Z	4
Number of reflexions used	7574
Crystal description	block
Crystal colour	colourless
Density (calculated)	1.475 Mg/m^3
Absorption coefficient	1.074 mm^-1
F(000)	3192
Crystal size	0.4 x 0.3 x 0.2 mm
Theta range for data collection	1.37 to 28.16 deg.
Index ranges	-19<=h<=18, -24<=k<=26, -28<=l<=26
Experiment device	Siemens SMART-CCD
Experiment methods	Omega scans
Reflections collected	55315
Independent reflections	14735 [R(int) = 0.0709]
Absorption correction	Semi-empirical from psi-scans
Refinement method	Full-matrix least-squares on F^2
Data / restraints / parameters	14716 / 0 / 815
Goodness-of-fit on F^2	0.915
Final R indices [I>2sigma(I)]	R1 = 0.0510, wR2 = 0.1210
R indices (all data)	R1 = 0.0750, wR2 = 0.1477

Absolute structure parameter	-.02(1)
Largest diff. peak and hole	0.918 and -1.674 e.A^-3

Table 2. Atomic coordinates (x 10^4) and equivalent isotropic displacement parameters (A^2 x 10^3) for 1. U(eq) is defined as one third of the trace of the orthogonalized Uij tensor.

	x	y	z	U(eq)
Eu	1181(1)	88(1)	866(1)	31(1)
N(1)	715(3)	-206(2)	-264(2)	35(1)
N(2)	2857(3)	363(2)	760(2)	34(1)
N(3)	2088(4)	-912(3)	415(2)	34(1)
N(4)	1488(4)	1076(2)	84(2)	33(1)
N(5)	-660(4)	1652(3)	264(3)	41(1)
N(6)	2622(4)	1618(3)	1941(3)	39(1)
N(7)	-633(4)	-1521(3)	264(3)	40(1)
N(8)	2550(4)	-1422(3)	1989(2)	36(1)
O(1)	1884(3)	-525(2)	1622(2)	34(1)
O(2)	1642(3)	982(2)	1470(2)	35(1)
O(3)	-20(3)	759(2)	659(2)	41(1)
O(4)	207(3)	-832(2)	805(2)	38(1)
C(1)	1341(5)	-655(3)	-565(3)	39(2)
C(2)	1669(5)	-1196(3)	-138(3)	38(2)
C(3)	2962(5)	-728(3)	246(3)	40(2)
C(4)	3360(4)	-248(3)	694(3)	36(1)
C(5)	3013(5)	786(3)	205(3)	37(2)
C(6)	2358(4)	1328(3)	150(3)	36(2)
C(7)	1363(5)	860(3)	-566(3)	37(2)
C(8)	623(4)	393(3)	-653(3)	38(2)
S(1)	-313(2)	2724(1)	-1132(1)	75(1)
F(1)	1088(5)	3340(7)	-1408(4)	198(6)
O(14)	321(3)	142(2)	1794(2)	40(1)
S(2)	4016(2)	-2704(1)	1339(1)	60(1)
F(2)	135(4)	3966(4)	-1049(5)	159(4)
S(3)	1376(2)	372(1)	3491(1)	69(1)
F(3)	824(4)	3325(5)	-444(4)	124(3)
F(4)	5144(6)	-3306(3)	1994(4)	130(3)
F(5)	5633(4)	-2864(4)	1143(3)	97(2)
O(5)	178(6)	2131(4)	-1127(3)	121(4)
F(6)	5339(4)	-2293(3)	1950(3)	87(2)
O(6)	-692(5)	2898(4)	-1704(3)	98(3)
F(7)	-169(7)	813(6)	3548(4)	181(5)
O(7)	-857(4)	2810(3)	-603(3)	66(2)
F(8)	-46(6)	-185(5)	3738(6)	176(5)
O(8)	3849(4)	-3280(3)	996(3)	81(2)
F(9)	317(4)	541(5)	4407(3)	114(3)
O(9)	4083(4)	-2110(3)	945(3)	76(2)
O(10)	3509(4)	-2616(2)	1881(2)	54(1)
O(11)	1720(7)	1016(3)	3648(4)	113(3)
O(12)	1251(6)	267(5)	2853(3)	128(4)
O(13)	1789(4)	-131(3)	3814(2)	71(2)
C(100)	877(4)	1595(3)	239(3)	38(2)
C(101)	19(5)	1310(3)	390(3)	39(2)
C(102)	-1514(5)	1425(4)	428(4)	52(2)
C(103)	-2104(5)	2018(4)	440(5)	61(2)
C(104)	-1823(6)	884(4)	-5(6)	70(3)
C(105)	-1707(6)	930(5)	-634(6)	75(3)
C(106)	-2006(8)	449(6)	-1012(8)	113(5)

C(107)	-2411(10)	-67(9)	-771(13)	169(10)
C(108)	-2534(11)	-148(9)	-172(12)	167(10)
C(109)	-2232(8)	351(6)	249(8)	121(5)
C(120)	-138(5)	-531(3)	-231(3)	41(2)
C(121)	-166(4)	-984(3)	328(3)	35(1)
C(122)	-755(5)	-1998(3)	766(3)	45(2)
C(123)	-1488(5)	-2456(4)	600(4)	57(2)
C(124)	56(5)	-2372(3)	895(3)	43(2)
C(125)	493(5)	-2693(4)	432(4)	50(2)
C(126)	1222(7)	-3036(4)	551(4)	62(2)
C(126)	1551(6)	-3077(4)	1139(5)	65(2)
C(128)	1116(7)	-2756(4)	1619(4)	68(2)
C(129)	369(6)	-2415(4)	1489(4)	53(2)
C(140)	2095(4)	-1416(3)	916(3)	38(1)
C(141)	2195(5)	-1088(3)	1536(3)	34(1)
C(142)	2620(5)	-1169(3)	2621(3)	38(2)
C(143)	2487(5)	-1720(4)	3072(3)	49(2)
C(144)	3467(5)	-814(3)	2683(3)	41(2)
C(145)	4228(6)	-1153(4)	2691(4)	59(2)
C(146)	5004(6)	-826(6)	2709(4)	69(3)
C(147)	5017(7)	-148(6)	2711(4)	82(3)
C(148)	4258(7)	198(4)	2710(3)	73(3)
C(149)	3488(6)	-129(4)	2703(3)	55(2)
C(160)	3117(4)	706(3)	1315(3)	38(2)
C(161)	2402(5)	1127(3)	1574(3)	37(2)
C(162)	1964(5)	1993(4)	2289(3)	45(2)
C(163)	2440(5)	2414(4)	2761(3)	55(2)
C(164)	1417(4)	2393(3)	1858(3)	43(2)
C(165)	1759(6)	2858(4)	1450(4)	54(2)
C(166)	1244(7)	3219(4)	1080(4)	61(2)
C(167)	382(7)	3143(5)	1094(4)	68(3)
C(168)	14(6)	2690(5)	1495(5)	72(3)
C(169)	540(5)	2315(4)	1883(4)	55(2)
C(200)	480(7)	3371(8)	-1000(6)	112(5)
C(300)	5078(7)	-2780(5)	1607(4)	80(3)
C(400)	310(8)	376(6)	3828(6)	89(3)
N(1S)	-2767(8)	1018(7)	2479(6)	130(4)
N(2S)	-4437(14)	-821(10)	1055(10)	207(8)
C(3S)	-3538(18)	-1105(12)	1059(12)	189(9)
C(4S)	-2832(19)	-1272(14)	1029(14)	221(11)
C(2S)	-1225(8)	959(5)	2062(5)	79(3)
C(1S)	-1878(7)	980(5)	2235(5)	75(3)
N(3S)	-1055(9)	-899(6)	2399(6)	119(4)
C(6S)	-1917(13)	-709(9)	2391(9)	138(6)
C(5S)	-2628(16)	-597(11)	2396(11)	183(9)

Table 3. Bond lengths [A] and angles [deg] for 1.

Eu-O(1)	2.348(4)
Eu-O(2)	2.364(4)
Eu-O(3)	2.381(5)
Eu-O(4)	2.430(4)
Eu-O(14)	2.437(4)
Eu-N(1)	2.638(5)
Eu-N(3)	2.678(5)
Eu-N(4)	2.684(5)
Eu-N(2)	2.713(5)
Eu-C(141)	3.233(6)
Eu-C(161)	3.255(7)
Eu-C(101)	3.265(7)
N(1)-C(8)	1.494(8)
N(1)-C(1)	1.497(8)
N(1)-C(120)	1.501(9)
N(2)-C(160)	1.456(8)
N(2)-C(4)	1.486(8)
N(2)-C(5)	1.506(8)
N(3)-C(3)	1.476(9)
N(3)-C(2)	1.491(8)
N(3)-C(140)	1.499(8)
N(4)-C(100)	1.472(8)
N(4)-C(6)	1.473(9)
N(4)-C(7)	1.497(8)
N(5)-C(101)	1.308(9)
N(5)-C(102)	1.469(9)
N(5)-H(5)	.88
N(6)-C(161)	1.329(8)
N(6)-C(162)	1.496(9)
N(6)-H(6)	.88
N(7)-C(121)	1.329(8)
N(7)-C(122)	1.476(8)
N(7)-H(7)	.88
N(8)-C(141)	1.324(8)
N(8)-C(142)	1.474(8)
N(8)-H(8)	.88
O(1)-C(141)	1.263(7)
O(2)-C(161)	1.256(9)
O(3)-C(101)	1.271(8)
O(4)-C(121)	1.234(8)
C(1)-C(2)	1.534(9)
C(1)-H(1A)	.99
C(1)-H(1B)	.99
C(2)-H(2A)	.99
C(2)-H(2B)	.99
C(3)-C(4)	1.519(9)
C(3)-H(3A)	.99
C(3)-H(3B)	.99
C(4)-H(4A)	.99
C(4)-H(4B)	.99
C(5)-C(6)	1.520(9)
C(5)-H(5A)	.99
C(5)-H(5B)	.99
C(6)-H(6A)	.99
C(6)-H(6B)	.99
C(7)-C(8)	1.519(9)

C(7)-H(7A)	.99
C(7)-H(7B)	.99
C(8)-H(8A)	.99
C(8)-H(8B)	.99
S(1)-O(6)	1.427(6)
S(1)-O(5)	1.437(7)
S(1)-O(7)	1.448(6)
S(1)-C(200)	1.84(2)
F(1)-C(200)	1.309(13)
S(2)-O(8)	1.417(6)
S(2)-O(10)	1.438(5)
S(2)-O(9)	1.490(6)
S(2)-C(300)	1.781(11)
F(2)-C(200)	1.33(2)
S(3)-O(13)	1.405(6)
S(3)-O(12)	1.419(6)
S(3)-O(11)	1.463(8)
S(3)-C(400)	1.834(13)
F(3)-C(200)	1.331(14)
F(4)-C(300)	1.370(13)
F(5)-C(300)	1.349(11)
F(6)-C(300)	1.309(11)
F(7)-C(400)	1.319(13)
F(8)-C(400)	1.29(2)
F(9)-C(400)	1.305(13)
C(100)-C(101)	1.509(10)
C(100)-H(10A)	.99
C(100)-H(10B)	.99
C(102)-C(103)	1.526(11)
C(102)-C(104)	1.531(13)
C(102)-H(102)	1.00
C(103)-H(10C)	.98
C(103)-H(10D)	.98
C(103)-H(10E)	.98
C(104)-C(109)	1.38(2)
C(104)-C(105)	1.39(2)
C(105)-C(106)	1.36(2)
C(105)-H(105)	.95
C(106)-C(107)	1.34(2)
C(106)-H(106)	.95
C(107)-C(108)	1.33(3)
C(107)-H(107)	.95
C(108)-C(109)	1.45(2)
C(108)-H(108)	.95
C(109)-H(109)	.95
C(120)-C(121)	1.529(9)
C(120)-H(12A)	.99
C(120)-H(12B)	.99
C(122)-C(124)	1.517(10)
C(122)-C(123)	1.530(10)
C(122)-H(122)	1.00
C(123)-H(12C)	.98
C(123)-H(12D)	.98
C(123)-H(12E)	.98
C(124)-C(129)	1.388(10)
C(124)-C(125)	1.387(10)
C(125)-C(126)	1.371(12)
C(125)-H(125)	.95
C(126)-C(126)	1.385(12)
C(126)-H(126)	.95

C(126)-C(128)	1.413(13)
C(126)-H(12F)	.95
C(128)-C(129)	1.398(13)
C(128)-H(128)	.95
C(129)-H(129)	.95
C(140)-C(141)	1.516(9)
C(140)-H(14A)	.99
C(140)-H(14B)	.99
C(142)-C(143)	1.507(9)
C(142)-C(144)	1.527(10)
C(142)-H(142)	1.00
C(143)-H(14C)	.98
C(143)-H(14D)	.98
C(143)-H(14E)	.98
C(144)-C(145)	1.385(11)
C(144)-C(149)	1.398(10)
C(145)-C(146)	1.395(12)
C(145)-H(145)	.95
C(146)-C(147)	1.38(2)
C(146)-H(146)	.95
C(147)-C(148)	1.39(2)
C(147)-H(147)	.95
C(148)-C(149)	1.387(12)
C(148)-H(148)	.95
C(149)-H(149)	.95
C(160)-C(161)	1.525(10)
C(160)-H(16A)	.99
C(160)-H(16B)	.99
C(162)-C(164)	1.513(10)
C(162)-C(163)	1.536(10)
C(162)-H(162)	1.00
C(163)-H(16C)	.98
C(163)-H(160)	.98
C(163)-H(16E)	.98
C(164)-C(169)	1.395(11)
C(164)-C(165)	1.408(10)
C(165)-C(166)	1.361(12)
C(165)-H(165)	.95
C(166)-C(167)	1.368(14)
C(166)-H(166)	.95
C(167)-C(168)	1.397(14)
C(167)-H(167)	.95
C(168)-C(169)	1.412(13)
C(168)-H(168)	.95
C(169)-H(169)	.95
N(1S)-C(1S)	1.50(2)
N(2S)-C(3S)	1.53(3)
C(3S)-C(4S)	1.17(3)
C(2S)-C(1S)	1.098(14)
N(3S)-C(6S)	1.41(2)
C(6S)-C(5S)	1.14(3)

O(1)-Eu-O(2)	82.8(2)
O(1)-Eu-O(3)	144.6(2)
O(2)-Eu-O(3)	84.6(2)
O(1)-Eu-O(4)	85.7(2)
O(2)-Eu-O(4)	145.2(2)
O(3)-Eu-O(4)	86.0(2)
O(1)-Eu-O(14)	72.8(2)
O(2)-Eu-O(14)	71.0(2)

O(3)-Eu-O(14)	71.8(2)
O(4)-Eu-O(14)	74.2(2)
O(1)-Eu-N(1)	131.72(14)
O(2)-Eu-N(1)	141.3(2)
O(3)-Eu-N(1)	74.5(2)
O(4)-Eu-N(1)	66.3(2)
O(14)-Eu-N(1)	129.0(2)
O(1)-Eu-N(3)	66.34(14)
O(2)-Eu-N(3)	128.8(2)
O(3)-Eu-N(3)	142.6(2)
O(4)-Eu-N(3)	74.3(2)
O(14)-Eu-N(3)	129.5(2)
N(1)-Eu-N(3)	68.5(2)
O(1)-Eu-N(4)	139.5(2)
O(2)-Eu-N(4)	73.6(2)
O(3)-Eu-N(4)	65.9(2)
O(4)-Eu-N(4)	131.4(2)
O(14)-Eu-N(4)	126.4(2)
N(1)-Eu-N(4)	68.3(2)
N(3)-Eu-N(4)	104.1(2)
O(1)-Eu-N(2)	73.1(2)
O(2)-Eu-N(2)	65.6(2)
O(3)-Eu-N(2)	129.9(2)
O(4)-Eu-N(2)	140.5(2)
O(14)-Eu-N(2)	127.1(2)
N(1)-Eu-N(2)	103.9(2)
N(3)-Eu-N(2)	66.8(2)
N(4)-Eu-N(2)	67.3(2)
O(1)-Eu-C(141)	18.8(2)
O(2)-Eu-C(141)	99.7(2)
O(3)-Eu-C(141)	155.0(2)
O(4)-Eu-C(141)	76.3(2)
O(14)-Eu-C(141)	86.2(2)
N(1)-Eu-C(141)	113.0(2)
N(3)-Eu-C(141)	48.4(2)
N(4)-Eu-C(141)	139.0(2)
N(2)-Eu-C(141)	73.1(2)
O(1)-Eu-C(161)	74.6(2)
O(2)-Eu-C(161)	18.4(2)
O(3)-Eu-C(161)	100.7(2)
O(4)-Eu-C(161)	154.6(2)
O(14)-Eu-C(161)	84.6(2)
N(1)-Eu-C(161)	139.1(2)
N(3)-Eu-C(161)	110.7(2)
N(4)-Eu-C(161)	72.8(2)
N(2)-Eu-C(161)	47.8(2)
C(141)-Eu-C(161)	88.6(2)
O(1)-Eu-C(101)	153.6(2)
O(2)-Eu-C(101)	76.1(2)
O(3)-Eu-C(101)	18.9(2)
O(4)-Eu-C(101)	102.6(2)
O(14)-Eu-C(101)	85.2(2)
N(1)-Eu-C(101)	73.8(2)
N(3)-Eu-C(101)	140.0(2)
N(4)-Eu-C(101)	47.6(2)
N(2)-Eu-C(101)	111.2(2)
C(141)-Eu-C(101)	171.3(2)
C(161)-Eu-C(101)	89.1(2)
C(8)-N(1)-C(1)	108.5(5)
C(8)-N(1)-C(120)	107.6(5)

C(1)-N(1)-C(120)	110.0(5)
C(8)-N(1)-Eu	111.7(3)
C(1)-N(1)-Eu	111.3(4)
C(120)-N(1)-Eu	107.7(4)
C(160)-N(2)-C(4)	109.5(5)
C(160)-N(2)-C(5)	110.1(5)
C(4)-N(2)-C(5)	108.4(5)
C(160)-N(2)-Eu	107.7(4)
C(4)-N(2)-Eu	110.8(3)
C(5)-N(2)-Eu	110.3(4)
C(3)-N(3)-C(2)	108.1(5)
C(3)-N(3)-C(140)	110.4(5)
C(2)-N(3)-C(140)	108.9(5)
C(3)-N(3)-Eu	113.4(4)
C(2)-N(3)-Eu	110.8(4)
C(140)-N(3)-Eu	105.1(4)
C(100)-N(4)-C(6)	109.7(5)
C(100)-N(4)-C(7)	110.0(5)
C(6)-N(4)-C(7)	108.5(5)
C(100)-N(4)-Eu	106.1(4)
C(6)-N(4)-Eu	111.7(4)
C(7)-N(4)-Eu	110.8(3)
C(101)-N(5)-C(102)	122.1(6)
C(101)-N(5)-H(5)	118.9(4)
C(102)-N(5)-H(5)	118.9(3)
C(161)-N(6)-C(162)	120.7(6)
C(161)-N(6)-H(6)	119.7(4)
C(162)-N(6)-H(6)	119.7(3)
C(121)-N(7)-C(122)	122.6(6)
C(121)-N(7)-H(7)	118.7(4)
C(122)-N(7)-H(7)	118.7(3)
C(141)-N(8)-C(142)	123.2(5)
C(141)-N(8)-H(8)	118.4(4)
C(142)-N(8)-H(8)	118.4(3)
C(141)-O(1)-Eu	124.3(4)
C(161)-O(2)-Eu	125.2(4)
C(101)-O(3)-Eu	123.9(5)
C(121)-O(4)-Eu	122.7(4)
N(1)-C(1)-C(2)	113.4(5)
N(1)-C(1)-H(1A)	108.9(3)
C(2)-C(1)-H(1A)	108.9(4)
N(1)-C(1)-H(1B)	108.9(3)
C(2)-C(1)-H(1B)	108.9(3)
H(1A)-C(1)-H(1B)	107.7
N(3)-C(2)-C(1)	111.1(5)
N(3)-C(2)-H(2A)	109.4(3)
C(1)-C(2)-H(2A)	109.4(4)
N(3)-C(2)-H(2B)	109.4(3)
C(1)-C(2)-H(2B)	109.4(3)
H(2A)-C(2)-H(2B)	108.0
N(3)-C(3)-C(4)	112.9(5)
N(3)-C(3)-H(3A)	109.0(3)
C(4)-C(3)-H(3A)	109.0(3)
N(3)-C(3)-H(3B)	109.0(3)
C(4)-C(3)-H(3B)	109.0(4)
H(3A)-C(3)-H(3B)	107.8
N(2)-C(4)-C(3)	112.5(5)
N(2)-C(4)-H(4A)	109.1(3)
C(3)-C(4)-H(4A)	109.1(3)
N(2)-C(4)-H(4B)	109.1(3)

C(3)-C(4)-H(4B)	109.1(4)
H(4A)-C(4)-H(4B)	107.8
N(2)-C(5)-C(6)	111.7(5)
N(2)-C(5)-H(5A)	109.3(3)
C(6)-C(5)-H(5A)	109.3(4)
N(2)-C(5)-H(5B)	109.3(3)
C(6)-C(5)-H(5B)	109.3(4)
H(5A)-C(5)-H(5B)	107.9
N(4)-C(6)-C(5)	112.7(5)
N(4)-C(6)-H(6A)	109.0(3)
C(5)-C(6)-H(6A)	109.0(4)
N(4)-C(6)-H(6B)	109.0(3)
C(5)-C(6)-H(6B)	109.0(4)
H(6A)-C(6)-H(6B)	107.8
N(4)-C(7)-C(8)	113.8(5)
N(4)-C(7)-H(7A)	108.8(3)
C(8)-C(7)-H(7A)	108.8(4)
N(4)-C(7)-H(7B)	108.8(3)
C(8)-C(7)-H(7B)	108.8(3)
H(7A)-C(7)-H(7B)	107.7
N(1)-C(8)-C(7)	111.7(5)
N(1)-C(8)-H(8A)	109.3(3)
C(7)-C(8)-H(8A)	109.3(4)
N(1)-C(8)-H(8B)	109.3(3)
C(7)-C(8)-H(8B)	109.3(3)
H(8A)-C(8)-H(8B)	107.9
O(6)-S(1)-O(5)	116.2(4)
O(6)-S(1)-O(7)	114.6(4)
O(5)-S(1)-O(7)	114.6(4)
O(6)-S(1)-C(200)	104.0(5)
O(5)-S(1)-C(200)	103.7(6)
O(7)-S(1)-C(200)	101.1(5)
O(8)-S(2)-O(10)	115.7(4)
O(8)-S(2)-O(9)	112.6(4)
O(10)-S(2)-O(9)	114.2(4)
O(8)-S(2)-C(300)	106.0(5)
O(10)-S(2)-C(300)	105.4(4)
O(9)-S(2)-C(300)	101.1(5)
O(13)-S(3)-O(12)	116.4(4)
O(13)-S(3)-O(11)	111.6(5)
O(12)-S(3)-O(11)	114.5(6)
O(13)-S(3)-C(400)	103.1(5)
O(12)-S(3)-C(400)	105.4(6)
O(11)-S(3)-C(400)	104.0(5)
N(4)-C(100)-C(101)	111.1(5)
N(4)-C(100)-H(10A)	109.4(3)
C(101)-C(100)-H(10A)	109.4(4)
N(4)-C(100)-H(10B)	109.4(3)
C(101)-C(100)-H(10B)	109.4(4)
H(10A)-C(100)-H(10B)	108.0
O(3)-C(101)-N(5)	121.9(7)
O(3)-C(101)-C(100)	119.1(6)
N(5)-C(101)-C(100)	118.9(6)
O(3)-C(101)-Eu	37.3(3)
N(5)-C(101)-Eu	159.1(5)
C(100)-C(101)-Eu	82.0(4)
N(5)-C(102)-C(103)	108.3(6)
N(5)-C(102)-C(104)	111.7(7)
C(103)-C(102)-C(104)	112.8(7)
N(5)-C(102)-H(102)	108.0(4)

C(103)-C(102)-H(102)	108.0(5)
C(104)-C(102)-H(102)	108.0(5)
C(102)-C(103)-H(10C)	109.5(5)
C(102)-C(103)-H(10D)	109.5(4)
H(10C)-C(103)-H(10D)	109.5
C(102)-C(103)-H(10E)	109.5(5)
H(10C)-C(103)-H(10E)	109.5
H(10D)-C(103)-H(10E)	109.5
C(109)-C(104)-C(105)	120.7(11)
C(109)-C(104)-C(102)	118.1(11)
C(105)-C(104)-C(102)	121.2(8)
C(106)-C(105)-C(104)	120.1(12)
C(106)-C(105)-H(105)	120.0(9)
C(104)-C(105)-H(105)	119.9(6)
C(107)-C(106)-C(105)	120(2)
C(107)-C(106)-H(106)	120.2(13)
C(105)-C(106)-H(106)	120.1(9)
C(108)-C(107)-C(106)	124(2)
C(108)-C(107)-H(107)	118.2(11)
C(106)-C(107)-H(107)	118.2(13)
C(107)-C(108)-C(109)	119(2)
C(107)-C(108)-H(108)	120.6(11)
C(109)-C(108)-H(108)	120.5(11)
C(104)-C(109)-C(108)	117(2)
C(104)-C(109)-H(109)	121.5(9)
C(108)-C(109)-H(109)	121.5(11)
N(1)-C(120)-C(121)	109.3(5)
N(1)-C(120)-H(12A)	109.8(3)
C(121)-C(120)-H(12A)	109.8(3)
N(1)-C(120)-H(12B)	109.8(3)
C(121)-C(120)-H(12B)	109.8(4)
H(12A)-C(120)-H(12B)	108.3
O(4)-C(121)-N(7)	124.0(6)
O(4)-C(121)-C(120)	120.4(6)
N(7)-C(121)-C(120)	115.6(6)
O(4)-C(121)-Eu	38.7(3)
N(7)-C(121)-Eu	162.0(5)
C(120)-C(121)-Eu	82.1(4)
N(7)-C(122)-C(124)	111.0(6)
N(7)-C(122)-C(123)	109.1(6)
C(124)-C(122)-C(123)	111.9(6)
N(7)-C(122)-H(122)	108.2(4)
C(124)-C(122)-H(122)	108.2(4)
C(123)-C(122)-H(122)	108.2(4)
C(122)-C(123)-H(12C)	109.5(5)
C(122)-C(123)-H(12D)	109.5(4)
H(12C)-C(123)-H(12D)	109.5
C(122)-C(123)-H(12E)	109.5(4)
H(12C)-C(123)-H(12E)	109.5
H(12D)-C(123)-H(12E)	109.5
C(129)-C(124)-C(125)	118.2(7)
C(129)-C(124)-C(122)	120.3(7)
C(125)-C(124)-C(122)	121.5(6)
C(126)-C(125)-C(124)	121.4(7)
C(126)-C(125)-H(125)	119.3(5)
C(124)-C(125)-H(125)	119.3(4)
C(125)-C(126)-C(126)	121.3(8)
C(125)-C(126)-H(126)	119.3(5)
C(126)-C(126)-H(126)	119.3(5)
C(126)-C(126)-C(128)	118.4(8)

C(126)-C(126)-H(12F)	120.8(5)
C(128)-C(126)-H(12F)	120.8(5)
C(129)-C(128)-C(126)	119.4(8)
C(129)-C(128)-H(128)	120.3(5)
C(126)-C(128)-H(128)	120.3(5)
C(124)-C(129)-C(128)	121.3(8)
C(124)-C(129)-H(129)	119.4(5)
C(128)-C(129)-H(129)	119.3(5)
N(3)-C(140)-C(141)	110.2(5)
N(3)-C(140)-H(14A)	109.6(3)
C(141)-C(140)-H(14A)	109.6(4)
N(3)-C(140)-H(14B)	109.6(3)
C(141)-C(140)-H(14B)	109.6(4)
H(14A)-C(140)-H(14B)	108.1
O(1)-C(141)-N(8)	121.4(6)
O(1)-C(141)-C(140)	119.6(6)
N(8)-C(141)-C(140)	118.7(5)
O(1)-C(141)-Eu	36.9(3)
N(8)-C(141)-Eu	158.2(4)
C(140)-C(141)-Eu	82.8(3)
N(8)-C(142)-C(143)	109.7(5)
N(8)-C(142)-C(144)	108.3(5)
C(143)-C(142)-C(144)	114.7(6)
N(8)-C(142)-H(142)	108.0(4)
C(143)-C(142)-H(142)	108.0(4)
C(144)-C(142)-H(142)	108.0(4)
C(142)-C(143)-H(14C)	109.5(4)
C(142)-C(143)-H(14D)	109.5(4)
H(14C)-C(143)-H(14D)	109.5
C(142)-C(143)-H(14E)	109.5(4)
H(14C)-C(143)-H(14E)	109.5
H(14D)-C(143)-H(14E)	109.5
C(145)-C(144)-C(149)	118.6(7)
C(145)-C(144)-C(142)	121.5(6)
C(149)-C(144)-C(142)	119.8(7)
C(144)-C(145)-C(146)	121.4(8)
C(144)-C(145)-H(145)	119.3(4)
C(146)-C(145)-H(145)	119.3(6)
C(147)-C(146)-C(145)	119.5(10)
C(147)-C(146)-H(146)	120.2(6)
C(145)-C(146)-H(146)	120.3(6)
C(146)-C(147)-C(148)	119.7(9)
C(146)-C(147)-H(147)	120.2(6)
C(148)-C(147)-H(147)	120.2(6)
C(149)-C(148)-C(147)	120.6(9)
C(149)-C(148)-H(148)	119.7(6)
C(147)-C(148)-H(148)	119.7(6)
C(148)-C(149)-C(144)	120.2(8)
C(148)-C(149)-H(149)	119.9(6)
C(144)-C(149)-H(149)	119.9(5)
N(2)-C(160)-C(161)	111.7(6)
N(2)-C(160)-H(16A)	109.3(3)
C(161)-C(160)-H(16A)	109.3(4)
N(2)-C(160)-H(16B)	109.3(3)
C(161)-C(160)-H(16B)	109.3(3)
H(16A)-C(160)-H(16B)	107.9
O(2)-C(161)-N(6)	122.5(6)
O(2)-C(161)-C(160)	120.4(6)
N(6)-C(161)-C(160)	117.1(7)
O(2)-C(161)-Eu	36.4(3)

N(6)-C(161)-Eu	158.7(5)
C(160)-C(161)-Eu	84.0(4)
N(6)-C(162)-C(164)	111.0(5)
N(6)-C(162)-C(163)	106.6(6)
C(164)-C(162)-C(163)	113.1(6)
N(6)-C(162)-H(162)	108.7(3)
C(164)-C(162)-H(162)	108.7(4)
C(163)-C(162)-H(162)	108.7(4)
C(162)-C(163)-H(16C)	109.5(4)
C(162)-C(163)-H(160)	109.4(4)
H(16C)-C(163)-H(160)	109.5
C(162)-C(163)-H(16E)	109.5(4)
H(16C)-C(163)-H(16E)	109.5
H(160)-C(163)-H(16E)	109.5
C(169)-C(164)-C(165)	118.8(8)
C(169)-C(164)-C(162)	118.7(7)
C(165)-C(164)-C(162)	122.5(7)
C(166)-C(165)-C(164)	120.7(8)
C(166)-C(165)-H(165)	119.6(6)
C(164)-C(165)-H(165)	119.7(5)
C(165)-C(166)-C(167)	121.2(8)
C(165)-C(166)-H(166)	119.4(6)
C(167)-C(166)-H(166)	119.4(5)
C(166)-C(167)-C(168)	120.1(9)
C(166)-C(167)-H(167)	119.9(5)
C(168)-C(167)-H(167)	119.9(6)
C(167)-C(168)-C(169)	119.3(9)
C(167)-C(168)-H(168)	120.3(6)
C(169)-C(168)-H(168)	120.4(6)
C(164)-C(169)-C(168)	119.8(9)
C(164)-C(169)-H(169)	120.1(5)
C(168)-C(169)-H(169)	120.1(6)
F(1)-C(200)-F(2)	106.8(11)
F(1)-C(200)-F(3)	108.4(10)
F(2)-C(200)-F(3)	107.7(14)
F(1)-C(200)-S(1)	110.9(13)
F(2)-C(200)-S(1)	111.3(8)
F(3)-C(200)-S(1)	111.6(8)
F(6)-C(300)-F(5)	108.7(10)
F(6)-C(300)-F(4)	102.7(8)
F(5)-C(300)-F(4)	108.2(8)
F(6)-C(300)-S(2)	114.6(7)
F(5)-C(300)-S(2)	112.1(7)
F(4)-C(300)-S(2)	109.9(9)
F(8)-C(400)-F(9)	112.3(14)
F(8)-C(400)-F(7)	106.3(12)
F(9)-C(400)-F(7)	106.0(10)
F(8)-C(400)-S(3)	109.5(9)
F(9)-C(400)-S(3)	112.3(9)
F(7)-C(400)-S(3)	110.1(11)
C(4S)-C(3S)-N(2S)	174(3)
C(2S)-C(1S)-N(1S)	179.0(12)
C(5S)-C(6S)-N(3S)	175(2)

Table 4. Anisotropic displacement parameters (A^2 x 10^3) for 1.
The anisotropic displacement factor exponent takes the form:
-2 pi^2 [h^2 a*^2 U11 + ... + 2 h k a* b* U12]

	U11	U22	U33	U23	U13	U12
Eu	38(1)	25(1)	29(1)	0(1)	1(1)	-1(1)
N(1)	42(3)	26(3)	35(3)	2(2)	0(2)	-2(2)
N(2)	39(3)	28(2)	34(3)	1(2)	1(2)	-1(2)
N(3)	44(3)	31(3)	27(3)	1(2)	-1(2)	-1(2)
N(4)	40(3)	23(2)	36(3)	1(2)	1(2)	0(2)
N(5)	37(4)	36(3)	50(3)	6(2)	0(3)	3(3)
N(6)	39(3)	37(3)	41(3)	-8(2)	-4(2)	-7(2)
N(7)	50(4)	33(3)	35(3)	1(2)	-3(3)	-7(3)
N(8)	45(3)	30(3)	33(3)	-3(2)	-1(2)	4(2)
O(1)	44(3)	28(2)	31(2)	0(2)	-6(2)	5(2)
O(2)	38(3)	32(2)	36(2)	-7(2)	2(2)	-2(2)
O(3)	51(3)	32(2)	39(3)	5(2)	2(2)	1(2)
O(4)	44(3)	36(2)	34(2)	-2(2)	-3(2)	-6(2)
C(1)	54(5)	31(3)	32(3)	0(2)	-2(3)	0(3)
C(2)	48(4)	32(3)	33(3)	-5(2)	0(3)	1(3)
C(3)	43(4)	37(3)	39(4)	2(3)	2(3)	-2(3)
C(4)	36(4)	34(3)	40(3)	2(2)	3(2)	1(3)
C(5)	33(4)	36(3)	42(4)	5(3)	3(3)	-1(3)
C(6)	38(4)	32(3)	37(3)	5(3)	0(3)	2(3)
C(7)	49(5)	33(3)	30(3)	3(2)	2(3)	2(3)
C(8)	47(4)	31(3)	35(3)	-3(2)	-4(3)	-1(3)
S(1)	84(2)	91(2)	49(1)	17(1)	10(1)	53(2)
F(1)	70(5)	374(16)	151(7)	131(9)	32(5)	34(8)
O(14)	45(3)	38(2)	36(2)	3(2)	5(2)	-8(2)
S(2)	66(2)	68(1)	46(1)	-11(1)	7(1)	10(1)
F(2)	69(4)	119(6)	288(13)	99(7)	-36(6)	-24(4)
S(3)	105(2)	66(1)	36(1)	-6(1)	-7(1)	35(1)
F(3)	69(4)	170(8)	132(6)	39(6)	-6(4)	19(5)
F(4)	190(8)	81(4)	118(6)	6(4)	-44(6)	62(5)
F(5)	65(4)	131(6)	94(4)	-42(4)	2(3)	31(4)
O(5)	167(8)	136(7)	59(4)	-7(4)	-12(5)	118(7)
F(6)	83(4)	94(4)	83(4)	-34(3)	-22(3)	20(3)
O(6)	91(5)	146(7)	56(4)	28(4)	5(3)	72(5)
F(7)	182(9)	250(11)	111(6)	-46(7)	-47(6)	163(9)
O(7)	86(5)	48(3)	63(3)	6(3)	26(3)	13(3)
F(8)	121(7)	134(8)	274(13)	-46(8)	-27(8)	-41(6)
O(8)	80(4)	83(4)	81(4)	-33(3)	17(4)	-1(4)
F(9)	85(5)	199(8)	59(3)	-20(4)	8(3)	27(5)
O(9)	88(5)	68(4)	71(4)	22(3)	1(3)	11(3)
O(10)	75(4)	43(3)	45(3)	-5(2)	11(3)	14(3)
O(11)	175(9)	53(4)	112(6)	-3(4)	25(6)	-9(5)
O(12)	162(8)	181(8)	41(3)	-40(4)	-37(4)	107(7)
O(13)	79(4)	81(4)	53(3)	3(3)	-17(3)	30(4)
C(100)	45(4)	28(3)	41(3)	2(3)	1(3)	0(3)
C(101)	42(4)	37(4)	37(3)	4(3)	0(3)	2(3)
C(102)	41(4)	48(4)	66(5)	14(4)	6(4)	4(3)

C(103)	43(5)	50(5)	91(6)	2(4)	7(4)	9(4)
C(104)	47(5)	36(4)	125(9)	-5(5)	5(5)	4(4)
C(105)	51(6)	65(6)	109(8)	-11(5)	-26(5)	9(4)
C(106)	73(8)	103(9)	163(14)	-42(9)	-34(8)	5(7)
C(107)	84(10)	112(13)	310(30)	-65(21)	36(15)	-54(9)
C(108)	110(12)	80(9)	310(29)	-38(15)	76(16)	-55(9)
C(109)	90(9)	63(6)	210(16)	-14(9)	39(9)	-32(6)
C(120)	49(4)	33(3)	40(3)	1(3)	-2(3)	0(3)
C(121)	39(4)	32(3)	36(3)	-6(3)	0(3)	-6(3)
C(122)	66(5)	37(3)	33(3)	2(3)	0(3)	-16(3)
C(123)	59(5)	54(4)	58(4)	6(4)	-3(4)	-19(4)
C(124)	61(4)	31(3)	38(3)	-1(3)	-5(3)	-11(3)
C(125)	66(5)	36(4)	49(4)	0(3)	-3(4)	3(4)
C(126)	76(6)	40(4)	69(5)	-1(3)	1(5)	10(5)
C(126)	69(6)	36(4)	89(6)	8(4)	-9(5)	1(4)
C(128)	79(6)	55(4)	70(5)	27(4)	-25(5)	-13(5)
C(129)	74(6)	39(4)	45(4)	11(3)	0(4)	-8(4)
C(140)	55(4)	28(3)	30(3)	-1(3)	-5(3)	-1(3)
C(141)	40(4)	31(3)	29(3)	5(2)	3(3)	2(3)
C(142)	47(4)	36(3)	30(3)	-5(3)	-3(3)	-1(3)
C(143)	67(5)	48(4)	34(4)	5(3)	-6(3)	-11(4)
C(144)	51(4)	43(4)	29(3)	-2(3)	-4(3)	-2(3)
C(145)	63(5)	62(5)	50(4)	-19(4)	4(4)	0(4)
C(146)	40(5)	101(8)	67(6)	-21(5)	0(4)	-10(5)
C(147)	76(7)	117(9)	53(5)	5(6)	-1(4)	-45(7)
C(148)	121(9)	54(5)	42(4)	6(4)	-15(4)	-40(6)
C(149)	86(6)	39(3)	40(3)	4(3)	-12(3)	-8(4)
C(160)	42(4)	34(3)	37(3)	0(3)	-1(3)	-4(3)
C(161)	50(5)	27(3)	33(3)	2(2)	3(3)	-3(3)
C(162)	51(5)	42(4)	42(4)	-6(3)	3(3)	-7(3)
C(163)	64(5)	54(4)	46(4)	-18(3)	-2(4)	2(4)
C(164)	45(4)	44(4)	41(3)	-10(3)	4(3)	4(3)
C(165)	62(5)	45(4)	54(4)	-7(4)	-2(4)	-11(4)
C(166)	73(6)	45(4)	66(5)	-3(3)	-1(5)	2(4)
C(167)	82(7)	56(5)	66(5)	-5(4)	-11(5)	23(5)
C(168)	50(6)	79(6)	86(7)	-33(5)	1(5)	15(5)
C(169)	45(5)	59(5)	59(5)	-22(4)	11(4)	0(4)
C(200)	60(7)	172(14)	104(9)	77(9)	18(6)	33(8)
C(300)	92(8)	83(7)	64(6)	-25(5)	-8(5)	29(6)
C(400)	78(8)	80(7)	110(9)	-19(6)	-18(6)	28(6)

Table 5. Hydrogen coordinates (x 10^4) and isotropic displacement parameters (A^2 x 10^3) for 1.

	x	y	z	U(eq)
H(5)	-603(4)	2030(3)	74(3)	50
H(6)	3160(4)	1724(3)	1980(3)	47
H(7)	-879(4)	-1596(3)	-92(3)	48
H(8)	2754(4)	-1814(3)	1909(2)	43
H(1A)	1828(5)	-393(3)	-713(3)	47
H(1B)	1070(5)	-860(3)	-927(3)	47
H(2A)	1189(5)	-1476(3)	-7(3)	45
H(2B)	2079(5)	-1473(3)	-362(3)	45
H(3A)	2958(5)	-530(3)	-169(3)	48
H(3B)	3315(5)	-1129(3)	228(3)	48
H(4A)	3413(4)	-461(3)	1101(3)	44
H(4B)	3937(4)	-136(3)	551(3)	44
H(5A)	2996(5)	510(3)	-169(3)	44
H(5B)	3585(5)	982(3)	234(3)	44
H(6A)	2388(4)	1610(3)	519(3)	43
H(6B)	2496(4)	1603(3)	-211(3)	43
H(7A)	1888(5)	644(3)	-711(3)	45
H(7B)	1269(5)	1252(3)	-826(3)	45
H(8A)	89(4)	620(3)	-545(3)	45
H(8B)	589(4)	262(3)	-1090(3)	45
H(10A)	822(4)	1900(3)	-113(3)	45
H(10B)	1089(4)	1848(3)	595(3)	45
H(102)	-1489(5)	1240(4)	852(4)	62
H(10C)	-1881(21)	2346(13)	725(22)	92
H(10D)	-2670(11)	1880(7)	574(27)	92
H(10E)	-2141(31)	2207(18)	27(7)	92
H(105)	-1419(6)	1297(5)	-803(6)	90
H(106)	-1926(8)	480(6)	-1443(8)	136
H(107)	-2622(10)	-392(9)	-1043(13)	203
H(108)	-2816(11)	-527(9)	-22(12)	200
H(109)	-2311(8)	312(6)	680(8)	145
H(12A)	-240(5)	-788(3)	-610(3)	49
H(12B)	-587(5)	-194(3)	-197(3)	49
H(122)	-914(5)	-1751(3)	1145(3)	54
H(12C)	-2021(7)	-2209(8)	604(26)	85
H(12D)	-1519(24)	-2812(16)	901(16)	85
H(12E)	-1394(19)	-2639(22)	190(12)	85
H(125)	283(5)	-2675(4)	23(4)	61
H(126)	1507(7)	-3250(4)	223(4)	74
H(12F)	2056(6)	-3316(4)	1217(5)	78
H(128)	1329(7)	-2772(4)	2027(4)	82
H(129)	69(6)	-2208(4)	1814(4)	63
H(14A)	2570(4)	-1725(3)	848(3)	46
H(14B)	1560(4)	-1668(3)	907(3)	46
H(142)	2157(5)	-841(3)	2684(3)	45
H(14C)	2473(35)	-1543(5)	3490(4)	74
H(14D)	2953(19)	-2035(14)	3036(18)	74
H(14E)	1949(18)	-1940(18)	2983(16)	74
H(145)	4221(6)	-1618(4)	2683(4)	70
H(146)	5519(6)	-1066(6)	2721(4)	83
H(147)	5542(7)	80(6)	2712(4)	99

H(148)	4266(7)	664(4)	2714(3)	87
H(149)	2973(6)	112(4)	2713(3)	66
H(16A)	3610(4)	989(3)	1220(3)	45
H(16B)	3295(4)	383(3)	1628(3)	45
H(162)	1594(5)	1676(4)	2513(3)	54
H(16C)	2030(5)	2645(22)	3021(17)	82
H(160)	2797(28)	2733(19)	2547(3)	82
H(16E)	2796(28)	2131(5)	3017(17)	82
H(165)	2355(6)	2921(4)	1433(4)	65
H(166)	1487(7)	3530(4)	807(4)	73
H(167)	34(7)	3399(5)	832(4)	82
H(168)	-584(6)	2636(5)	1505(5)	86
H(169)	296(5)	2009(4)	2161(4)	66

Appendix 6 Crystal data for $(Dy.13b)^{3+}$

$C_{57}H_{78}DyF_9N_{11}O_{14}S_3$, M = 1570.98, orthorhombic, space group $P2_12_12_1$, a = 15.7679(4), b = 20.3133(4), c = 21.7304(4) Å, U = 6960.2(3)Å^3, Z = 4, $\rho_{calcd.}$ = 1.499 g cm^{-3}, F (000) = 3216, μ = 12.55 cm^{-1}, crystal 0.2×0.3×0.3 mm, MoK-α radiation (λ=0.71073 Å), measurement at 150(2)K. Final R (on F) and wR_2 (on F^2) were 0.042 and 0.1174 respectively for all 12017 unique data. Final GOF = 1.094, and the final difference fourier map showed no feature > +0.99 and < -1.09 e Å^{-3}. A Flack x parameter of -0.021(9) showed the refinement had been carried out with the correct polarity.

Intensity data were collected on a *Siemens* SMART automated 3-circle diffractometer equipped with a CCD (512 x 512 pixels) area detector for all four complexes. The structures were solved using Patterson and Fourier methods (SHELXS86)[1] and refined on F^2 using all unique data by full - matrix least - squares (SHELXL93)[2]. All non-hydrogen atoms were refined with anisotropic displacement parameters. Hydrogen atoms were generated in calculated positions and refined using a riding model.

Table 1. Crystal data and structure refinement for 1.

Empirical formula	C57 H78 Dy F9 N11 O14 S3
Formula weight	1570.98
Temperature	150(2) K
Wavelength	.71073 A
Crystal system	Orthorhombic
Space group	P2(1)2(1)2(1)
Unit cell dimensions	a = 15.7679(4) A alpha = 90 deg. b = 20.3133(4) A beta = 90 deg. c = 21.7304(4) A gamma = 90 deg.
Volume	6960.2(3) A^3
Z	4
Number of reflexions used	8192
Crystal description	block
Crystal colour	colourless
Density (calculated)	1.499 Mg/m^3
Absorption coefficient	1.255 mm^-1
F(000)	3216
Crystal size	0.3 x 0.3 x 0.2 mm
Theta range for data collection	1.37 to 25.79 deg.
Index ranges	-18<=h<=11, -24<=k<=23, -26<=l<=26
Experiment device	Siemens SMART-CCD
Experiment methods	Omega scans
Reflections collected	31346
Independent reflections	12047 [R(int) = 0.0590]
Absorption correction	Semi-empirical from psi-scans
Refinement method	Full-matrix least-squares on F^2
Data / restraints / parameters	12017 / 0 / 859
Goodness-of-fit on F^2	1.097
Final R indices [I>2sigma(I)]	R1 = 0.0422, wR2 = 0.1033
R indices (all data)	R1 = 0.0498, wR2 = 0.1174

Absolute structure parameter	-.021(9)
Largest diff. peak and hole	0.993 and -1.088 e.A^-3

Table 2. Atomic coordinates (x 10^4) and equivalent isotropic displacement parameters (A^2 x 10^3) for 1. U(eq) is defined as one third of the trace of the orthogonalized Uij tensor.

	x	y	z	U(eq)
Dy	6201(1)	5088(1)	10835(1)	28(1)
O(4)	5001(3)	5736(2)	10640(2)	34(1)
O(3)	6623(3)	5976(2)	11438(2)	34(1)
N(5)	7585(3)	6610(3)	11935(2)	38(1)
O(2)	6891(3)	4490(2)	11587(2)	31(1)
O(1)	5257(3)	4174(2)	10782(2)	35(1)
N(3)	5742(3)	4805(2)	9713(2)	32(1)
N(8)	4382(4)	3485(3)	10258(2)	37(1)
N(1)	6499(3)	6085(2)	10074(2)	29(1)
O(14)	5338(2)	5124(2)	11757(2)	35(1)
N(6)	7544(3)	3594(2)	11967(2)	33(1)
N(7)	4343(3)	6632(3)	10269(3)	41(1)
N(2)	7099(3)	4093(2)	10394(2)	29(1)
N(4)	7853(3)	5371(2)	10741(2)	31(1)
C(101)	5030(4)	6289(3)	10388(3)	32(1)
C(4)	8012(4)	5805(3)	10196(3)	34(1)
C(121)	7376(4)	6132(3)	11564(3)	30(1)
C(122)	6925(4)	6987(3)	12276(3)	42(2)
C(2)	6378(4)	5869(3)	9420(3)	35(1)
C(8)	6358(4)	4353(3)	9411(3)	35(1)
C(120)	8099(4)	5715(3)	11300(3)	33(1)
C(3)	7363(4)	6354(3)	10145(3)	33(1)
C(1)	5641(4)	5402(3)	9330(3)	34(1)
C(126)	6247(6)	8238(4)	11064(3)	58(2)
C(5)	8369(4)	4767(3)	10679(3)	35(1)
C(140)	7116(4)	3592(3)	10892(3)	31(1)
C(124)	6388(4)	7401(3)	11840(3)	41(2)
C(164)	5080(4)	2638(3)	10887(3)	42(1)
C(168)	6144(6)	2254(4)	11623(4)	61(2)
C(167)	6566(5)	1927(4)	11141(4)	60(2)
C(166)	6262(5)	1971(3)	10554(4)	56(2)
C(125)	6739(5)	7852(4)	11443(3)	51(2)
C(162)	4273(4)	3012(3)	10760(3)	40(1)
C(141)	7188(4)	3924(3)	11516(3)	31(1)
C(7)	6683(4)	3810(3)	9837(3)	34(1)
C(163)	3540(5)	2553(4)	10597(3)	55(2)
C(100)	5873(4)	6596(3)	10233(3)	33(1)
C(169)	5401(5)	2600(4)	11490(3)	51(2)
C(160)	4886(4)	4471(3)	9752(3)	37(1)
C(123)	7373(5)	7397(4)	12759(3)	53(2)
C(165)	5513(5)	2309(4)	10426(3)	51(2)
C(161)	4862(4)	4027(3)	10311(3)	31(1)
C(128)	5005(6)	7719(5)	11467(4)	70(3)
C(127)	5375(6)	8168(5)	11071(4)	66(2)
C(148)	9257(6)	5226(4)	12704(3)	60(2)
C(142)	7609(4)	3857(3)	12599(3)	34(1)
C(149)	8475(5)	4886(4)	12694(3)	51(2)
C(144)	8465(4)	4216(3)	12667(3)	38(1)
C(143)	7474(5)	3297(4)	13053(3)	46(2)
C(103)	2891(4)	6971(4)	10467(4)	62(2)

C(105)	3292(6)	5911(5)	9373(5)	75(3)
C(6)	7984(4)	4285(3)	10227(3)	34(1)
C(102)	3490(4)	6377(4)	10438(4)	51(2)
C(106)	2997(7)	5421(7)	8980(7)	114(5)
C(104)	3193(5)	5848(4)	10001(6)	68(3)
C(147)	9995(6)	4877(6)	12702(3)	75(3)
C(145)	9211(5)	3867(4)	12678(3)	52(2)
C(146)	9994(5)	4196(5)	12704(4)	69(3)
C(129)	5510(4)	7324(4)	11861(4)	52(2)
S(2)	3638(2)	10368(1)	11524(1)	63(1)
S(3)	4024(1)	2700(1)	8659(1)	58(1)
S(1)	-377(2)	7324(1)	11139(1)	68(1)
O(9S)	3862(4)	3277(3)	9005(3)	81(2)
F(9)	5349(3)	2276(3)	8048(3)	83(2)
O(6S)	3239(3)	9847(3)	11201(2)	65(2)
O(8S)	3510(3)	2605(2)	8120(2)	53(1)
O(5S)	3766(5)	10267(4)	12164(2)	108(3)
O(3S)	-891(4)	7216(3)	10603(2)	62(2)
O(7S)	4106(4)	2100(3)	9056(3)	70(2)
O(4S)	3272(5)	11010(3)	11364(3)	93(2)
F(3)	807(4)	6739(4)	10484(3)	119(3)
F(8)	5641(3)	2858(3)	8838(3)	91(2)
O(2S)	-770(4)	7151(4)	11707(3)	92(2)
F(6)	4699(4)	10547(4)	10614(3)	108(2)
O(1S)	90(5)	7934(4)	11133(3)	101(3)
F(2)	122(4)	6093(4)	11092(5)	151(4)
F(1)	1042(4)	6750(6)	11460(4)	189(5)
F(5)	5175(5)	10832(5)	11481(3)	150(4)
C(2S)	4700(6)	10393(5)	11194(5)	75(3)
F(7)	5126(6)	3296(3)	7991(3)	131(3)
C(1S)	441(6)	6694(7)	11033(6)	106(5)
F(4)	5084(5)	9842(5)	11281(5)	164(4)
C(3S)	5085(7)	2767(5)	8376(4)	80(3)
C(109)	2783(8)	5311(6)	10239(7)	115(5)
C(107)	2604(9)	4897(9)	9219(12)	181(10)
C(108)	2467(12)	4833(10)	9805(12)	182(10)
N(3W)	3810(7)	5941(5)	12046(4)	91(2)
C(3W)	3144(7)	5992(5)	12230(5)	72(3)
N(9W)	3949(9)	4112(5)	12413(6)	123(4)
C(4W)	2280(7)	6049(6)	12460(6)	100(4)
C(9W)	3048(12)	4305(7)	12378(8)	119(5)
N(8W)	5600(10)	793(9)	8953(9)	208(8)
C(8W)	6480(16)	1070(11)	8939(8)	180(9)
C(7W)	7087(17)	1359(15)	8960(11)	316(22)
C(6W)	2352(11)	4414(10)	12364(13)	210(12)

Table 3. Bond lengths [A] and angles [deg] for 1.

Dy-O(2)	2.307(4)
Dy-O(3)	2.326(4)
Dy-O(4)	2.342(4)
Dy-O(1)	2.382(4)
Dy-O(14)	2.421(4)
Dy-N(3)	2.609(4)
Dy-N(2)	2.648(5)
Dy-N(1)	2.657(5)
Dy-N(4)	2.676(5)
O(4)-C(101)	1.252(7)
O(3)-C(121)	1.259(8)
N(5)-C(121)	1.305(8)
N(5)-C(122)	1.490(8)
O(2)-C(141)	1.250(7)
O(1)-C(161)	1.235(7)
N(3)-C(1)	1.479(7)
N(3)-C(8)	1.489(7)
N(3)-C(160)	1.512(8)
N(8)-C(161)	1.342(8)
N(8)-C(162)	1.464(8)
N(1)-C(100)	1.474(7)
N(1)-C(3)	1.476(8)
N(1)-C(2)	1.500(7)
N(6)-C(141)	1.314(8)
N(6)-C(142)	1.479(7)
N(7)-C(101)	1.314(8)
N(7)-C(102)	1.488(8)
N(2)-C(140)	1.487(7)
N(2)-C(7)	1.492(7)
N(2)-C(6)	1.493(8)
N(4)-C(120)	1.455(7)
N(4)-C(5)	1.478(7)
N(4)-C(4)	1.498(7)
C(101)-C(100)	1.507(9)
C(4)-C(3)	1.519(9)
C(121)-C(120)	1.531(8)
C(122)-C(123)	1.514(9)
C(122)-C(124)	1.524(10)
C(2)-C(1)	1.511(8)
C(8)-C(7)	1.528(8)
C(126)-C(125)	1.377(11)
C(126)-C(127)	1.382(12)
C(5)-C(6)	1.515(8)
C(140)-C(141)	1.519(8)
C(124)-C(125)	1.375(10)
C(124)-C(129)	1.395(10)
C(164)-C(165)	1.384(10)
C(164)-C(169)	1.408(10)
C(164)-C(162)	1.507(9)
C(168)-C(169)	1.395(11)
C(168)-C(167)	1.407(12)
C(167)-C(166)	1.365(11)
C(166)-C(165)	1.394(11)
C(162)-C(163)	1.526(9)
C(160)-C(161)	1.514(9)
C(128)-C(127)	1.382(13)

C(128)-C(129)	1.417(12)
C(148)-C(147)	1.362(13)
C(148)-C(149)	1.414(11)
C(142)-C(143)	1.521(9)
C(142)-C(144)	1.541(9)
C(149)-C(144)	1.361(10)
C(144)-C(145)	1.375(10)
C(103)-C(102)	1.534(10)
C(105)-C(104)	1.380(14)
C(105)-C(106)	1.391(14)
C(102)-C(104)	1.509(12)
C(106)-C(107)	1.34(2)
C(104)-C(109)	1.369(14)
C(147)-C(146)	1.385(14)
C(145)-C(146)	1.404(11)
S(2)-O(6S)	1.418(5)
S(2)-O(5S)	1.419(5)
S(2)-O(4S)	1.467(7)
S(2)-C(2S)	1.822(11)
S(3)-O(9S)	1.417(6)
S(3)-O(8S)	1.437(5)
S(3)-O(7S)	1.500(6)
S(3)-C(3S)	1.788(10)
S(1)-O(2S)	1.425(6)
S(1)-O(3S)	1.437(5)
S(1)-O(1S)	1.440(6)
S(1)-C(1S)	1.832(14)
F(9)-C(3S)	1.293(11)
F(3)-C(1S)	1.327(13)
F(8)-C(3S)	1.347(11)
F(6)-C(2S)	1.298(11)
F(2)-C(1S)	1.328(14)
F(1)-C(1S)	1.332(12)
F(5)-C(2S)	1.321(11)
C(2S)-F(4)	1.288(13)
F(7)-C(3S)	1.364(12)
C(109)-C(108)	1.44(2)
C(107)-C(108)	1.30(3)
N(3W)-C(3W)	1.129(13)
C(3W)-C(4W)	1.46(2)
N(9W)-C(9W)	1.47(2)
C(9W)-C(6W)	1.12(2)
N(8W)-C(8W)	1.50(2)
C(8W)-C(7W)	1.12(2)

O(2)-Dy-O(3)	82.8(2)
O(2)-Dy-O(4)	143.54(14)
O(3)-Dy-O(4)	84.1(2)
O(2)-Dy-O(1)	85.34(14)
O(3)-Dy-O(1)	144.1(2)
O(4)-Dy-O(1)	85.7(2)
O(2)-Dy-O(14)	72.28(14)
O(3)-Dy-O(14)	70.84(14)
O(4)-Dy-O(14)	71.29(14)
O(1)-Dy-O(14)	73.3(2)
O(2)-Dy-N(3)	132.56(14)
O(3)-Dy-N(3)	141.0(2)
O(4)-Dy-N(3)	74.4(2)
O(1)-Dy-N(3)	67.0(2)
O(14)-Dy-N(3)	128.61(13)

O(2)-Dy-N(2)	66.58(14)
O(3)-Dy-N(2)	130.0(2)
O(4)-Dy-N(2)	142.6(2)
O(1)-Dy-N(2)	73.9(2)
O(14)-Dy-N(2)	128.5(2)
N(3)-Dy-N(2)	69.0(2)
O(2)-Dy-N(1)	139.31(14)
O(3)-Dy-N(1)	73.12(14)
O(4)-Dy-N(1)	66.58(14)
O(1)-Dy-N(1)	132.4(2)
O(14)-Dy-N(1)	126.27(14)
N(3)-Dy-N(1)	68.56(14)
N(2)-Dy-N(1)	105.13(14)
O(2)-Dy-N(4)	73.03(14)
O(3)-Dy-N(4)	66.31(14)
O(4)-Dy-N(4)	130.7(2)
O(1)-Dy-N(4)	140.53(14)
O(14)-Dy-N(4)	127.14(14)
N(3)-Dy-N(4)	104.22(14)
N(2)-Dy-N(4)	67.4(2)
N(1)-Dy-N(4)	67.4(2)
C(101)-O(4)-Dy	123.7(4)
C(121)-O(3)-Dy	126.0(4)
C(121)-N(5)-C(122)	120.9(6)
C(141)-O(2)-Dy	125.0(4)
C(161)-O(1)-Dy	122.9(4)
C(1)-N(3)-C(8)	109.1(4)
C(1)-N(3)-C(160)	107.7(4)
C(8)-N(3)-C(160)	109.3(5)
C(1)-N(3)-Dy	112.0(3)
C(8)-N(3)-Dy	111.5(3)
C(160)-N(3)-Dy	107.0(3)
C(161)-N(8)-C(162)	122.8(5)
C(100)-N(1)-C(3)	109.4(5)
C(100)-N(1)-C(2)	110.0(5)
C(3)-N(1)-C(2)	109.0(5)
C(100)-N(1)-Dy	105.8(3)
C(3)-N(1)-Dy	112.4(3)
C(2)-N(1)-Dy	110.2(3)
C(141)-N(6)-C(142)	122.5(5)
C(101)-N(7)-C(102)	120.8(5)
C(140)-N(2)-C(7)	109.6(4)
C(140)-N(2)-C(6)	109.8(5)
C(7)-N(2)-C(6)	108.3(5)
C(140)-N(2)-Dy	105.6(3)
C(7)-N(2)-Dy	110.6(3)
C(6)-N(2)-Dy	112.8(3)
C(120)-N(4)-C(5)	109.2(4)
C(120)-N(4)-C(4)	109.5(4)
C(5)-N(4)-C(4)	108.9(4)
C(120)-N(4)-Dy	107.4(3)
C(5)-N(4)-Dy	111.4(3)
C(4)-N(4)-Dy	110.5(3)
O(4)-C(101)-N(7)	122.2(6)
O(4)-C(101)-C(100)	120.1(5)
N(7)-C(101)-C(100)	117.6(5)
N(4)-C(4)-C(3)	112.1(5)
O(3)-C(121)-N(5)	124.0(6)
O(3)-C(121)-C(120)	118.9(5)
N(5)-C(121)-C(120)	117.0(6)

N(5)-C(122)-C(123)	107.6(5)
N(5)-C(122)-C(124)	111.2(5)
C(123)-C(122)-C(124)	112.8(6)
N(1)-C(2)-C(1)	113.8(5)
N(3)-C(8)-C(7)	113.4(5)
N(4)-C(120)-C(121)	112.3(5)
N(1)-C(3)-C(4)	110.9(5)
N(3)-C(1)-C(2)	111.0(4)
C(125)-C(126)-C(127)	119.6(8)
N(4)-C(5)-C(6)	112.0(5)
N(2)-C(140)-C(141)	110.3(5)
C(125)-C(124)-C(129)	119.6(7)
C(125)-C(124)-C(122)	122.3(6)
C(129)-C(124)-C(122)	118.0(7)
C(165)-C(164)-C(169)	118.0(7)
C(165)-C(164)-C(162)	121.9(6)
C(169)-C(164)-C(162)	120.1(7)
C(169)-C(168)-C(167)	118.8(7)
C(166)-C(167)-C(168)	119.9(8)
C(167)-C(166)-C(165)	121.1(8)
C(124)-C(125)-C(126)	121.9(7)
N(8)-C(162)-C(164)	111.6(5)
N(8)-C(162)-C(163)	108.5(5)
C(164)-C(162)-C(163)	111.9(5)
O(2)-C(141)-N(6)	122.6(6)
O(2)-C(141)-C(140)	119.4(5)
N(6)-C(141)-C(140)	118.0(5)
N(2)-C(7)-C(8)	111.2(5)
N(1)-C(100)-C(101)	110.6(5)
C(168)-C(169)-C(164)	121.5(8)
N(3)-C(160)-C(161)	109.6(5)
C(164)-C(165)-C(166)	120.7(7)
O(1)-C(161)-N(8)	123.6(6)
O(1)-C(161)-C(160)	120.5(5)
N(8)-C(161)-C(160)	115.8(5)
C(127)-C(128)-C(129)	120.8(8)
C(126)-C(127)-C(128)	119.7(8)
C(147)-C(148)-C(149)	119.4(8)
N(6)-C(142)-C(143)	108.8(5)
N(6)-C(142)-C(144)	108.7(5)
C(143)-C(142)-C(144)	114.5(5)
C(144)-C(149)-C(148)	120.0(8)
C(149)-C(144)-C(145)	120.3(7)
C(149)-C(144)-C(142)	119.2(6)
C(145)-C(144)-C(142)	120.5(6)
C(104)-C(105)-C(106)	120.1(12)
N(2)-C(6)-C(5)	112.7(5)
N(7)-C(102)-C(104)	111.9(6)
N(7)-C(102)-C(103)	107.0(6)
C(104)-C(102)-C(103)	113.4(7)
C(107)-C(106)-C(105)	119(2)
C(109)-C(104)-C(105)	120.1(11)
C(109)-C(104)-C(102)	118.5(11)
C(105)-C(104)-C(102)	121.4(8)
C(148)-C(147)-C(146)	121.2(8)
C(144)-C(145)-C(146)	120.5(8)
C(147)-C(146)-C(145)	118.5(9)
C(124)-C(129)-C(128)	118.3(8)
O(6S)-S(2)-O(5S)	116.1(4)
O(6S)-S(2)-O(4S)	111.7(4)

O(5S)-S(2)-O(4S)	114.7(5)
O(6S)-S(2)-C(2S)	103.5(4)
O(5S)-S(2)-C(2S)	105.0(5)
O(4S)-S(2)-C(2S)	104.0(5)
O(9S)-S(3)-O(8S)	116.3(4)
O(9S)-S(3)-O(7S)	112.4(4)
O(8S)-S(3)-O(7S)	114.2(3)
O(9S)-S(3)-C(3S)	106.7(4)
O(8S)-S(3)-C(3S)	104.9(4)
O(7S)-S(3)-C(3S)	100.4(5)
O(2S)-S(1)-O(3S)	114.8(3)
O(2S)-S(1)-O(1S)	116.3(4)
O(3S)-S(1)-O(1S)	114.4(4)
O(2S)-S(1)-C(1S)	104.0(5)
O(3S)-S(1)-C(1S)	100.8(5)
O(1S)-S(1)-C(1S)	103.8(5)
F(4)-C(2S)-F(6)	110.6(12)
F(4)-C(2S)-F(5)	104.5(9)
F(6)-C(2S)-F(5)	107.3(8)
F(4)-C(2S)-S(2)	110.5(7)
F(6)-C(2S)-S(2)	112.8(7)
F(5)-C(2S)-S(2)	110.8(8)
F(2)-C(1S)-F(3)	108.4(13)
F(2)-C(1S)-F(1)	106.3(10)
F(3)-C(1S)-F(1)	108.1(8)
F(2)-C(1S)-S(1)	111.3(7)
F(3)-C(1S)-S(1)	111.8(8)
F(1)-C(1S)-S(1)	110.7(11)
F(9)-C(3S)-F(8)	107.8(9)
F(9)-C(3S)-F(7)	104.8(8)
F(8)-C(3S)-F(7)	108.6(8)
F(9)-C(3S)-S(3)	115.6(6)
F(8)-C(3S)-S(3)	111.3(6)
F(7)-C(3S)-S(3)	108.4(8)
C(104)-C(109)-C(108)	116.9(14)
C(108)-C(107)-C(106)	122(2)
C(107)-C(108)-C(109)	121(2)
N(3W)-C(3W)-C(4W)	178.9(13)
C(6W)-C(9W)-N(9W)	176(2)
C(7W)-C(8W)-N(8W)	170(3)

Table 4. Anisotropic displacement parameters (A^2 x 10^3) for 1.
The anisotropic displacement factor exponent takes the form:
-2 pi^2 [h^2 a*^2 U11 + ... + 2 h k a* b* U12]

	U11	U22	U33	U23	U13	U12
Dy	30(1)	25(1)	28(1)	0(1)	1(1)	-1(1)
O(4)	34(2)	29(2)	38(2)	7(2)	4(2)	7(2)
O(3)	34(2)	29(2)	38(2)	-3(2)	1(2)	-5(2)
N(5)	37(3)	40(3)	36(3)	-9(2)	1(2)	-8(2)
O(2)	39(2)	24(2)	29(2)	1(2)	-1(2)	1(2)
O(1)	40(2)	34(2)	31(2)	-1(2)	-3(2)	-4(2)
N(3)	37(2)	25(3)	33(2)	2(2)	-2(2)	-7(2)
N(8)	44(3)	36(3)	32(3)	-1(2)	-5(2)	-6(2)
N(1)	31(2)	26(3)	29(2)	1(2)	0(2)	2(2)
O(14)	36(2)	37(2)	31(2)	3(2)	4(2)	-8(2)
N(6)	41(3)	29(3)	29(3)	-2(2)	-3(2)	6(2)
N(7)	36(3)	34(3)	54(4)	7(3)	2(3)	5(2)
N(2)	35(3)	27(3)	26(2)	1(2)	0(2)	-1(2)
N(4)	30(2)	30(2)	32(3)	-3(2)	4(2)	1(2)
C(101)	33(3)	31(3)	33(3)	1(3)	0(3)	5(3)
C(4)	32(3)	37(4)	33(3)	5(3)	4(3)	0(3)
C(121)	38(3)	28(3)	24(3)	-3(2)	2(3)	-3(3)
C(122)	41(3)	46(4)	39(3)	-12(3)	7(3)	-5(3)
C(2)	39(4)	30(3)	36(3)	4(2)	1(3)	2(3)
C(8)	46(4)	32(3)	27(3)	-3(2)	1(3)	4(3)
C(120)	26(3)	28(3)	45(4)	-2(3)	-7(3)	-4(2)
C(3)	36(3)	26(3)	37(3)	6(3)	-3(3)	-2(3)
C(1)	34(3)	33(3)	34(3)	3(2)	-5(2)	3(2)
C(126)	67(5)	48(4)	59(4)	-4(3)	-3(4)	3(4)
C(5)	34(3)	32(3)	38(3)	-2(2)	3(2)	1(2)
C(140)	39(3)	21(3)	33(3)	-2(3)	-3(3)	-1(2)
C(124)	44(4)	40(4)	40(3)	-13(3)	3(3)	1(3)
C(164)	52(4)	29(3)	45(4)	6(3)	-7(3)	-13(3)
C(168)	63(5)	51(4)	68(5)	26(4)	-24(5)	-14(4)
C(167)	57(5)	34(4)	89(6)	14(4)	-14(4)	-4(4)
C(166)	58(5)	41(4)	70(5)	1(3)	2(4)	2(4)
C(125)	49(4)	48(5)	57(4)	-12(4)	1(3)	-4(3)
C(162)	57(4)	29(3)	32(3)	5(3)	1(3)	-14(3)
C(141)	36(3)	27(3)	30(3)	4(2)	0(3)	-1(3)
C(7)	45(4)	29(3)	26(3)	-3(2)	3(3)	0(3)
C(163)	64(5)	42(4)	60(4)	7(3)	-2(4)	-26(4)
C(100)	37(3)	26(3)	37(3)	3(2)	4(3)	-2(2)
C(169)	68(5)	47(4)	37(4)	10(3)	-3(3)	-15(4)
C(160)	39(3)	37(4)	35(3)	-4(3)	-8(3)	-1(3)
C(123)	63(5)	50(4)	44(4)	-16(3)	4(3)	-5(4)
C(165)	65(5)	38(4)	50(4)	-4(3)	-1(4)	-5(4)
C(161)	31(3)	26(3)	35(3)	-1(2)	0(3)	-1(3)
C(128)	48(5)	85(7)	76(6)	-27(5)	12(4)	10(5)
C(127)	66(5)	61(6)	71(6)	-6(4)	-12(4)	19(4)
C(148)	92(6)	46(5)	44(4)	5(3)	-14(4)	-24(4)
C(142)	40(3)	40(4)	23(3)	-3(2)	-3(2)	6(3)

C(149)	75(5)	45(4)	32(3)	3(3)	-7(3)	-15(4)
C(144)	45(3)	43(4)	27(3)	-1(3)	-3(3)	-5(3)
C(143)	55(4)	49(4)	33(3)	2(3)	0(3)	-12(3)
C(103)	31(4)	61(5)	94(6)	0(4)	9(4)	14(4)
C(105)	48(5)	72(6)	103(8)	-16(5)	-24(5)	6(4)
C(6)	30(3)	33(3)	40(4)	3(3)	5(3)	0(3)
C(102)	34(3)	47(4)	72(5)	13(4)	10(3)	9(3)
C(106)	66(6)	109(10)	168(13)	-61(9)	-36(7)	17(7)
C(104)	33(4)	39(4)	132(9)	-4(5)	4(4)	2(3)
C(147)	79(6)	101(8)	47(4)	-3(5)	4(4)	-47(6)
C(145)	44(4)	63(5)	48(4)	-8(4)	1(3)	1(4)
C(146)	45(4)	99(8)	64(6)	-26(5)	1(4)	-10(5)
C(129)	41(4)	62(5)	54(4)	-16(4)	11(3)	1(4)
S(2)	85(2)	67(1)	36(1)	5(1)	-7(1)	-34(1)
S(3)	57(1)	73(1)	45(1)	-13(1)	-8(1)	-11(1)
S(1)	67(1)	88(2)	49(1)	12(1)	-7(1)	-45(1)
O(9S)	78(4)	93(4)	73(4)	-36(3)	-15(3)	4(4)
F(9)	77(3)	88(4)	85(4)	-34(3)	22(3)	-24(3)
O(6S)	72(3)	69(4)	53(3)	-6(3)	-14(2)	-24(3)
O(8S)	70(3)	46(3)	42(3)	-1(2)	-17(2)	-14(3)
O(5S)	134(6)	145(7)	45(3)	31(4)	-35(4)	-84(6)
O(3S)	70(3)	53(3)	64(3)	9(2)	-21(3)	-12(3)
O(7S)	72(4)	74(4)	65(4)	24(3)	-4(3)	-13(3)
O(4S)	123(6)	61(4)	96(5)	8(4)	11(4)	-2(4)
F(3)	56(3)	172(7)	129(5)	40(5)	13(4)	-6(4)
F(8)	58(3)	125(5)	92(4)	-45(4)	1(3)	-30(3)
O(2S)	80(4)	141(7)	54(3)	20(4)	-3(3)	-62(4)
F(6)	65(3)	192(8)	67(3)	20(4)	3(3)	-23(4)
O(1S)	117(6)	115(6)	71(4)	-9(4)	13(4)	-85(5)
F(2)	57(3)	118(6)	277(11)	94(7)	24(5)	17(4)
F(1)	55(4)	358(14)	155(7)	121(8)	-35(4)	-28(6)
F(5)	131(6)	209(9)	111(5)	28(5)	-33(4)	-123(6)
C(2S)	70(6)	74(7)	80(7)	15(5)	-18(5)	-18(5)
F(7)	186(8)	89(5)	117(5)	10(4)	47(5)	-64(5)
C(1S)	50(5)	155(12)	114(9)	76(8)	-19(6)	-34(6)
F(4)	94(5)	139(8)	259(10)	49(7)	-15(6)	38(6)
C(3S)	81(7)	92(8)	68(6)	-32(6)	11(5)	-35(6)
C(109)	96(8)	63(7)	186(13)	-5(8)	36(9)	-30(6)
C(107)	97(9)	121(14)	324(29)	-86(20)	52(15)	-64(9)
C(108)	132(15)	109(14)	305(28)	-56(17)	97(17)	-63(12)
N(3W)	80(6)	101(7)	92(6)	-9(5)	12(6)	12(6)
C(3W)	80(7)	72(7)	64(5)	-8(5)	2(5)	12(5)
N(9W)	135(10)	92(7)	141(9)	7(6)	40(8)	-25(7)
C(4W)	81(7)	120(9)	99(8)	-23(7)	-7(6)	30(7)
C(9W)	128(13)	76(9)	152(14)	-6(8)	-12(11)	-16(9)
N(8W)	148(13)	243(19)	234(19)	40(15)	-45(13)	-87(13)
C(8W)	250(26)	179(19)	112(12)	5(11)	9(14)	-89(19)
C(7W)	323(34)	436(47)	188(22)	-25(25)	49(21)	-301(36)
C(6W)	93(12)	141(17)	395(37)	-3(20)	-30(18)	-16(12)

Table 5. Hydrogen coordinates (x 10^4) and isotropic displacement parameters (A^2 x 10^3) for 1.

	x	y	z	U(eq)
H(5A)	8111(3)	6709(3)	11983(2)	45
H(8A)	4127(4)	3412(3)	9915(2)	44
H(6A)	7747(3)	3209(2)	11891(2)	39
H(7A)	4387(3)	7009(3)	10091(3)	49
H(4A)	7995(4)	5540(3)	9824(3)	41
H(4B)	8574(4)	5995(3)	10229(3)	41
H(12A)	6552(4)	6673(3)	12486(3)	50
H(2A)	6893(4)	5655(3)	9279(3)	42
H(2B)	6290(4)	6255(3)	9165(3)	42
H(8B)	6837(4)	4608(3)	9264(3)	42
H(8C)	6089(4)	4152(3)	9056(3)	42
H(12B)	8579(4)	5999(3)	11212(3)	40
H(12C)	8276(4)	5396(3)	11606(3)	40
H(3A)	7387(4)	6626(3)	10512(3)	40
H(3B)	7497(4)	6630(3)	9794(3)	40
H(1B)	5118(4)	5623(3)	9440(3)	40
H(1C)	5606(4)	5277(3)	8900(3)	40
H(12D)	6499(6)	8545(4)	10804(3)	69
H(5B)	8420(4)	4557(3)	11079(3)	42
H(5C)	8934(4)	4885(3)	10542(3)	42
H(14A)	7595(4)	3299(3)	10832(3)	37
H(14B)	6602(4)	3330(3)	10877(3)	37
H(16A)	6356(6)	2240(4)	12022(4)	73
H(16B)	7051(5)	1681(4)	11222(4)	72
H(16C)	6560(5)	1772(3)	10235(4)	67
H(12E)	7326(5)	7898(4)	11429(3)	62
H(16D)	4119(4)	3255(3)	11133(3)	48
H(7B)	6212(4)	3533(3)	9962(3)	40
H(7C)	7086(4)	3538(3)	9616(3)	40
H(16E)	3039(5)	2808(4)	10521(3)	83
H(16F)	3438(5)	2256(4)	10933(3)	83
H(16G)	3683(5)	2305(4)	10236(3)	83
H(10A)	5805(4)	6895(3)	9888(3)	40
H(10B)	6076(4)	6849(3)	10582(3)	40
H(16H)	5112(5)	2809(4)	11807(3)	61
H(16I)	4787(4)	4214(3)	9383(3)	45
H(16J)	4443(4)	4801(3)	9783(3)	45
H(12F)	7700(5)	7114(4)	13022(3)	79
H(12G)	6961(5)	7629(4)	13001(3)	79
H(12H)	7742(5)	7707(4)	12561(3)	79
H(16K)	5303(5)	2314(4)	10026(3)	61
H(12I)	4418(6)	7675(5)	11474(4)	84
H(12J)	5039(6)	8421(5)	10812(4)	79
H(14C)	9268(6)	5684(4)	12711(3)	73
H(14D)	7154(4)	4180(3)	12658(3)	41
H(14E)	7968(5)	5119(4)	12705(3)	61
H(14F)	6930(5)	3099(4)	12981(3)	69
H(14G)	7496(5)	3465(4)	13465(3)	69
H(14H)	7910(5)	2972(4)	12998(3)	69
H(10C)	3113(4)	7290(4)	10752(4)	93
H(10D)	2341(4)	6830(4)	10603(4)	93

H(10E)	2846(4)	7166(4)	10066(4)	93
H(10F)	3557(6)	6282(5)	9212(5)	89
H(6B)	7982(4)	4482(3)	9820(3)	41
H(6C)	8334(4)	3893(3)	10210(3)	41
H(10G)	3526(4)	6185(4)	10851(4)	61
H(10H)	3073(7)	5458(7)	8557(7)	137
H(14I)	10510(6)	5101(6)	12699(3)	91
H(14J)	9198(5)	3409(4)	12667(3)	62
H(14K)	10500(5)	3961(5)	12723(4)	83
H(12K)	5261(4)	7022(4)	12127(4)	63
H(109)	2712(8)	5257(6)	10661(7)	138
H(10K)	2422(9)	4565(9)	8955(12)	217
H(10L)	2159(12)	4474(10)	9948(12)	219
H(4W1)	2081(21)	6490(13)	12395(37)	150
H(4W2)	2273(11)	5951(43)	12893(10)	150
H(4W3)	1917(13)	5745(31)	12247(29)	150
H(7W1)	7524(42)	1079(63)	8799(153)	474
H(7W2)	7228(121)	1486(154)	9373(23)	474
H(7W3)	7038(81)	1745(90)	8708(131)	474
H(6WA)	2272(19)	4760(69)	12069(68)	315
H(6WB)	2145(28)	4554(95)	12759(25)	315
H(6WC)	2043(16)	4031(31)	12234(90)	315

Appendix 7 Crystal data for $(Na.13c)^+$

M = 1194.36; orthorhombic, space group $P2_12_12_1$, a = 15.0215(12), b = 17.1363(14), c = 23.8997(14) Å, U = 6152.1(8)Å^3, Z = 4, $\rho_{calcd.}$ = 1.290 g cm^3, F (000) = 2528, μ = 0.96 cm^{-1}, crystal 0.2×0.3×0.25 mm, radiation MoK-α radiation (λ=0.71073Å), measurement at 150(2)K. Final R (on F) and $wR2$ (on F^2) were 0.071 and 0.2096 respectively for all 8046 unique data. Final GOF = 1.037, and the final difference fourier map showed no feature > +0.65 and < -0.53 e Å^{-3}. A Flack x parameter of -0.5(9) revealed that the absolute configuration of this molecule could not be determined from the X-ray experiment.

Intensity data were collected on a *Siemens* SMART automated 3-circle diffractometer equipped with a CCD (512 x 512 pixels) area detector for all four complexes. The structures were solved using Patterson and Fourier methods (SHELXS86)[1] and refined on F^2 using all unique data by full - matrix least - squares (SHELXL93)[2]. All non-hydrogen atoms were refined with anisotropic displacement parameters. Hydrogen atoms were generated in calculated positions and refined using a riding model.

Table 1. Crystal data and structure refinement for 1.

Identification code	96srv087
Empirical formula	C68 H75 F3 N9 Na O6
Formula weight	1194.36
Temperature	150(2) K
Wavelength	.71073 A
Crystal system	Orthorhombic
Space group	P2(1)2(1)2(1)
Unit cell dimensions	a = 15.0215(12) A alpha = 90 deg. b = 17.1363(14) A beta = 90 deg. c = 23.8997(14) A gamma = 90 deg.
Volume	6152.1(8) A^3
Z	4
Number of reflexions used	7346
Crystal description	Block
Crystal colour	Colourless
Density (calculated)	1.290 Mg/m^3
Absorption coefficient	0.096 mm^-1
F(000)	2528
Crystal size	0.20 x 0.30 x 0.25 mm
Theta range for data collection	1.46 to 22.50 deg.
Index ranges	-18<=h<=18, -20<=k<=19, -27<=l<=28
Experiment device	SMART
Experiment methods	Omega scans
Reflections collected	26944
Independent reflections	8046 [R(int) = 0.0748]
Refinement method	Full-matrix least-squares on F^2
Data / restraints / parameters	7364 / 0 / 745
Goodness-of-fit on F^2	1.037
Final R indices [I>2sigma(I)]	R1 = 0.0705, wR2 = 0.1713
R indices (all data)	R1 = 0.1149, wR2 = 0.2096

Absolute structure parameter	-.5(9)
Largest diff. peak and hole	0.654 and -0.526 e.A^-3

Table 2. Atomic coordinates (x 10^4) and equivalent isotropic displacement parameters (A^2 x 10^3) for 1. U(eq) is defined as one third of the trace of the orthogonalized Uij tensor.

	x	y	z	U(eq)
Na	2585(1)	4916(1)	4620(1)	34(1)
O(1)	3955(3)	5436(2)	4163(2)	38(1)
O(2)	1985(3)	6096(2)	4177(2)	40(1)
O(3)	1179(3)	4463(2)	4210(2)	39(1)
O(4)	3115(3)	3692(3)	4215(2)	40(1)
N(1)	4015(3)	5037(3)	5298(2)	31(1)
N(2)	2519(3)	6197(3)	5299(2)	31(1)
N(3)	1205(3)	4863(3)	5351(2)	32(1)
N(4)	2714(3)	3706(3)	5356(2)	31(1)
N(5)	5448(3)	5627(3)	4191(2)	36(1)
N(6)	1744(3)	7393(3)	4169(2)	41(1)
N(7)	-280(3)	4153(3)	4303(2)	36(1)
N(8)	3385(3)	2390(3)	4257(2)	38(1)
C(1)	4096(4)	5833(3)	5516(3)	36(2)
C(2)	3223(4)	6170(4)	5728(3)	38(2)
C(3)	1629(4)	6238(4)	5547(3)	38(2)
C(4)	1288(4)	5473(3)	5775(3)	35(2)
C(5)	1165(4)	4085(3)	5608(3)	36(2)
C(6)	2054(4)	3774(4)	5802(2)	34(2)
C(7)	3628(4)	3683(3)	5583(2)	32(2)
C(8)	3969(4)	4479(3)	5764(3)	34(2)
C(11)	4750(4)	4865(4)	4931(3)	41(2)
C(12)	4679(4)	5338(3)	4391(3)	36(2)
C(13)	5456(4)	6008(4)	3641(3)	38(2)
C(14)	6407(4)	6208(5)	3467(3)	55(2)
C(15)	4870(4)	6736(4)	3630(2)	37(2)
C(21)	2660(4)	6851(4)	4919(2)	39(2)
C(22)	2100(4)	6742(4)	4387(2)	33(2)
C(23)	1259(4)	7359(4)	3636(3)	41(2)
C(24)	1076(4)	8185(4)	3430(3)	47(2)
C(25)	400(4)	6880(4)	3690(3)	39(2)
C(31)	413(4)	4988(4)	5004(2)	39(2)
C(32)	476(4)	4513(3)	4475(3)	34(2)
C(33)	-307(4)	3779(4)	3748(2)	33(2)
C(34)	-1271(4)	3564(4)	3620(3)	47(2)
C(35)	298(4)	3084(4)	3716(3)	37(2)
C(41)	2552(4)	3005(3)	5013(2)	34(2)
C(42)	3049(4)	3057(4)	4461(3)	35(2)
C(43)	3752(4)	2393(4)	3678(2)	38(2)
C(44)	3929(4)	1540(4)	3503(3)	46(2)
C(45)	4596(4)	2898(4)	3642(3)	37(2)
C(151)	4905(4)	7244(4)	4070(3)	42(2)
C(152)	4380(5)	7932(4)	4076(3)	50(2)
C(153)	3826(5)	8095(4)	3636(3)	48(2)
C(154)	3761(4)	7581(4)	3173(3)	43(2)
C(155)	3200(4)	7737(4)	2713(3)	42(2)
C(156)	3139(4)	7234(4)	2264(3)	48(2)
C(157)	3668(4)	6574(4)	2256(3)	43(2)
C(158)	4218(4)	6402(4)	2691(3)	48(2)
C(159)	4292(4)	6895(4)	3161(2)	34(2)

C(251)	-119(4)	6942(4)	4164(3)	45(2)
C(252)	-889(4)	6510(4)	4237(3)	51(2)
C(253)	-1164(4)	5995(4)	3837(3)	52(2)
C(254)	-691(5)	5921(4)	3334(3)	51(2)
C(255)	-969(6)	5421(4)	2889(4)	69(3)
C(256)	-509(6)	5347(5)	2404(4)	74(3)
C(257)	274(6)	5794(5)	2331(3)	65(2)
C(258)	565(4)	6294(4)	2737(3)	51(2)
C(259)	110(4)	6381(4)	3249(3)	46(2)
C(351)	396(4)	2580(4)	4167(3)	41(2)
C(352)	941(4)	1900(4)	4129(3)	53(2)
C(353)	1395(4)	1744(4)	3650(3)	45(2)
C(354)	1343(4)	2233(4)	3182(3)	43(2)
C(355)	1826(4)	2084(4)	2675(3)	47(2)
C(356)	1762(5)	2563(4)	2229(3)	52(2)
C(357)	1208(5)	3221(4)	2248(3)	50(2)
C(358)	727(4)	3391(4)	2722(3)	41(2)
C(359)	779(4)	2910(4)	3203(3)	40(2)
C(451)	5200(4)	2903(4)	4080(3)	42(2)
C(452)	5964(4)	3379(4)	4056(3)	46(2)
C(453)	6110(4)	3861(4)	3613(3)	45(2)
C(454)	5518(4)	3856(4)	3151(3)	46(2)
C(455)	5658(5)	4356(4)	2668(3)	54(2)
C(456)	5082(6)	4347(4)	2233(3)	60(2)
C(457)	4347(5)	3847(5)	2236(3)	55(2)
C(458)	4173(5)	3365(4)	2688(3)	49(2)
C(459)	4757(4)	3366(4)	3159(3)	41(2)
F(1)	6835(4)	5027(3)	5789(2)	105(2)
F(2)	8201(4)	5185(4)	5821(3)	118(2)
F(3)	7411(4)	5957(4)	5341(3)	121(2)
O(1S)	7196(3)	4882(3)	4550(2)	63(1)
O(2S)	8096(3)	4111(3)	5043(2)	50(1)
N(1S)	2644(4)	5046(3)	7034(2)	50(2)
C(1S)	7518(4)	5191(4)	5455(3)	44(2)
C(2S)	7614(4)	4693(4)	4974(3)	36(2)
C(3S)	2510(5)	5128(4)	8112(3)	52(2)
C(4S)	2578(4)	5079(4)	7509(3)	43(2)

Table 3. Bond lengths [A] and angles [deg] for 1.

Na-O(4)	2.443(5)
Na-O(3)	2.453(4)
Na-O(2)	2.454(5)
Na-O(1)	2.493(4)
Na-N(1)	2.700(5)
Na-N(3)	2.712(5)
Na-N(4)	2.728(5)
Na-N(2)	2.733(5)
O(1)-C(12)	1.227(7)
O(2)-C(22)	1.228(7)
O(3)-C(32)	1.233(7)
O(4)-C(42)	1.239(7)
N(1)-C(11)	1.441(7)
N(1)-C(1)	1.465(7)
N(1)-C(8)	1.470(7)
N(2)-C(21)	1.458(7)
N(2)-C(3)	1.463(7)
N(2)-C(2)	1.473(7)
N(3)-C(4)	1.461(7)
N(3)-C(31)	1.467(7)
N(3)-C(5)	1.469(7)
N(4)-C(6)	1.459(7)
N(4)-C(41)	1.475(7)
N(4)-C(7)	1.476(7)
N(5)-C(12)	1.344(7)
N(5)-C(13)	1.468(7)
N(5)-H(5C)	.88
N(6)-C(22)	1.342(7)
N(6)-C(23)	1.469(8)
N(6)-H(6C)	.88
N(7)-C(32)	1.356(7)
N(7)-C(33)	1.472(7)
N(7)-H(7C)	.88
N(8)-C(42)	1.342(8)
N(8)-C(43)	1.489(7)
N(8)-H(8C)	.88
C(1)-C(2)	1.520(8)
C(1)-H(1B)	.99
C(1)-H(1A)	.99
C(2)-H(2B)	.99
C(2)-H(2A)	.99
C(3)-C(4)	1.510(8)
C(3)-H(3B)	.99
C(3)-H(3A)	.99
C(4)-H(4B)	.99
C(4)-H(4A)	.99
C(5)-C(6)	1.510(8)
C(5)-H(5B)	.99
C(5)-H(5A)	.99
C(6)-H(6B)	.99
C(6)-H(6A)	.99
C(7)-C(8)	1.522(8)
C(7)-H(7B)	.99
C(7)-H(7A)	.99
C(8)-H(8B)	.99
C(8)-H(8A)	.99

C(11)-C(12)	1.528(8)
C(11)-H(11B)	.99
C(11)-H(11A)	.99
C(13)-C(14)	1.527(8)
C(13)-C(15)	1.527(9)
C(13)-H(13)	1.00
C(14)-H(14C)	.98
C(14)-H(14B)	.98
C(14)-H(14A)	.98
C(15)-C(151)	1.365(8)
C(15)-C(159)	1.443(8)
C(21)-C(22)	1.536(8)
C(21)-H(21B)	.99
C(21)-H(21A)	.99
C(23)-C(24)	1.524(9)
C(23)-C(25)	1.536(9)
C(23)-H(23)	1.00
C(24)-H(24C)	.98
C(24)-H(24B)	.98
C(24)-H(24A)	.98
C(25)-C(251)	1.380(9)
C(25)-C(259)	1.425(9)
C(31)-C(32)	1.507(8)
C(31)-H(31B)	.99
C(31)-H(31A)	.99
C(33)-C(35)	1.501(8)
C(33)-C(34)	1.525(8)
C(33)-H(33)	1.00
C(34)-H(34C)	.98
C(34)-H(34B)	.98
C(34)-H(34A)	.98
C(35)-C(351)	1.388(8)
C(35)-C(359)	1.456(9)
C(41)-C(42)	1.519(8)
C(41)-H(41B)	.99
C(41)-H(41A)	.99
C(43)-C(45)	1.538(9)
C(43)-C(44)	1.544(9)
C(43)-H(43)	1.00
C(44)-H(44C)	.98
C(44)-H(44B)	.98
C(44)-H(44A)	.98
C(45)-C(451)	1.384(8)
C(45)-C(459)	1.427(9)
C(151)-C(152)	1.418(9)
C(151)-H(151)	.95
C(152)-C(153)	1.370(9)
C(152)-H(152)	.95
C(153)-C(154)	1.418(9)
C(153)-H(153)	.95
C(154)-C(155)	1.412(9)
C(154)-C(159)	1.420(9)
C(155)-C(156)	1.379(9)
C(155)-H(155)	.95
C(156)-C(157)	1.383(9)
C(156)-H(156)	.95
C(157)-C(158)	1.360(9)
C(157)-H(157)	.95
C(158)-C(159)	1.410(9)
C(158)-H(158)	.95

C(251)-C(252)	1.383(9)
C(251)-H(251)	.95
C(252)-C(253)	1.365(10)
C(252)-H(252)	.95
C(253)-C(254)	1.402(10)
C(253)-H(253)	.95
C(254)-C(255)	1.428(11)
C(254)-C(259)	1.453(10)
C(255)-C(256)	1.354(12)
C(255)-H(255)	.95
C(256)-C(257)	1.415(12)
C(256)-H(256)	.95
C(257)-C(258)	1.365(10)
C(257)-H(257)	.95
C(258)-C(259)	1.410(9)
C(258)-H(258)	.95
C(351)-C(352)	1.427(9)
C(351)-H(351)	.95
C(352)-C(353)	1.359(9)
C(352)-H(352)	.95
C(353)-C(354)	1.400(9)
C(353)-H(353)	.95
C(354)-C(355)	1.436(9)
C(354)-C(359)	1.438(9)
C(355)-C(356)	1.350(10)
C(355)-H(355)	.95
C(356)-C(357)	1.403(9)
C(356)-H(356)	.95
C(357)-C(358)	1.373(9)
C(357)-H(357)	.95
C(358)-C(359)	1.415(9)
C(358)-H(358)	.95
C(451)-C(452)	1.409(9)
C(451)-H(451)	.95
C(452)-C(453)	1.362(9)
C(452)-H(452)	.95
C(453)-C(454)	1.418(9)
C(453)-H(453)	.95
C(454)-C(459)	1.419(9)
C(454)-C(455)	1.453(9)
C(455)-C(456)	1.351(10)
C(455)-H(455)	.95
C(456)-C(457)	1.397(10)
C(456)-H(456)	.95
C(457)-C(458)	1.384(10)
C(457)-H(457)	.95
C(458)-C(459)	1.427(9)
C(458)-H(458)	.95
F(1)-C(1S)	1.330(8)
F(2)-C(1S)	1.348(8)
F(3)-C(1S)	1.350(8)
O(1S)-C(2S)	1.237(7)
O(2S)-C(2S)	1.243(7)
N(1S)-C(4S)	1.140(8)
C(1S)-C(2S)	1.440(9)
C(3S)-C(4S)	1.448(9)
C(3S)-H(3SA)	.98
C(3S)-H(3SB)	.98
C(3S)-H(3SC)	.98

O(4)-Na-O(3)	81.4(2)
O(4)-Na-O(2)	131.0(2)
O(3)-Na-O(2)	76.9(2)
O(4)-Na-O(1)	82.2(2)
O(3)-Na-O(1)	130.5(2)
O(2)-Na-O(1)	79.6(2)
O(4)-Na-N(1)	92.5(2)
O(3)-Na-N(1)	161.6(2)
O(2)-Na-N(1)	119.2(2)
O(1)-Na-N(1)	65.06(14)
O(4)-Na-N(3)	118.4(2)
O(3)-Na-N(3)	65.7(2)
O(2)-Na-N(3)	91.5(2)
O(1)-Na-N(3)	157.6(2)
N(1)-Na-N(3)	102.9(2)
O(4)-Na-N(4)	65.1(2)
O(3)-Na-N(4)	94.5(2)
O(2)-Na-N(4)	158.6(2)
O(1)-Na-N(4)	119.7(2)
N(1)-Na-N(4)	67.3(2)
N(3)-Na-N(4)	67.2(2)
O(4)-Na-N(2)	159.5(2)
O(3)-Na-N(2)	117.4(2)
O(2)-Na-N(2)	65.24(14)
O(1)-Na-N(2)	90.2(2)
N(1)-Na-N(2)	67.0(2)
N(3)-Na-N(2)	67.4(2)
N(4)-Na-N(2)	103.3(2)
C(12)-O(1)-Na	119.3(4)
C(22)-O(2)-Na	121.0(4)
C(32)-O(3)-Na	120.7(4)
C(42)-O(4)-Na	122.7(4)
C(11)-N(1)-C(1)	110.1(5)
C(11)-N(1)-C(8)	111.4(4)
C(1)-N(1)-C(8)	109.9(5)
C(11)-N(1)-Na	103.2(3)
C(1)-N(1)-Na	110.6(3)
C(8)-N(1)-Na	111.5(3)
C(21)-N(2)-C(3)	110.3(5)
C(21)-N(2)-C(2)	110.7(5)
C(3)-N(2)-C(2)	112.1(4)
C(21)-N(2)-Na	104.0(3)
C(3)-N(2)-Na	108.2(3)
C(2)-N(2)-Na	111.2(3)
C(4)-N(3)-C(31)	110.9(4)
C(4)-N(3)-C(5)	111.2(5)
C(31)-N(3)-C(5)	109.6(5)
C(4)-N(3)-Na	111.0(3)
C(31)-N(3)-Na	104.5(3)
C(5)-N(3)-Na	109.4(3)
C(6)-N(4)-C(41)	111.1(4)
C(6)-N(4)-C(7)	111.5(4)
C(41)-N(4)-C(7)	109.6(5)
C(6)-N(4)-Na	111.2(3)
C(41)-N(4)-Na	104.4(3)
C(7)-N(4)-Na	108.9(3)
C(12)-N(5)-C(13)	119.3(5)
C(12)-N(5)-H(5C)	120.4(3)
C(13)-N(5)-H(5C)	120.4(3)
C(22)-N(6)-C(23)	120.1(5)

C(22)-N(6)-H(6C)	119.9(3)
C(23)-N(6)-H(6C)	119.9(3)
C(32)-N(7)-C(33)	119.6(5)
C(32)-N(7)-H(7C)	120.2(3)
C(33)-N(7)-H(7C)	120.2(3)
C(42)-N(8)-C(43)	118.2(5)
C(42)-N(8)-H(8C)	120.9(4)
C(43)-N(8)-H(8C)	120.9(3)
N(1)-C(1)-C(2)	113.6(5)
N(1)-C(1)-H(1B)	108.8(3)
C(2)-C(1)-H(1B)	108.8(3)
N(1)-C(1)-H(1A)	108.9(3)
C(2)-C(1)-H(1A)	108.8(3)
H(1B)-C(1)-H(1A)	107.7
N(2)-C(2)-C(1)	113.6(5)
N(2)-C(2)-H(2B)	108.8(3)
C(1)-C(2)-H(2B)	108.8(3)
N(2)-C(2)-H(2A)	108.8(3)
C(1)-C(2)-H(2A)	108.8(3)
H(2B)-C(2)-H(2A)	107.7
N(2)-C(3)-C(4)	114.5(5)
N(2)-C(3)-H(3B)	108.6(3)
C(4)-C(3)-H(3B)	108.6(3)
N(2)-C(3)-H(3A)	108.6(3)
C(4)-C(3)-H(3A)	108.6(3)
H(3B)-C(3)-H(3A)	107.6
N(3)-C(4)-C(3)	113.5(5)
N(3)-C(4)-H(4B)	108.9(3)
C(3)-C(4)-H(4B)	108.9(3)
N(3)-C(4)-H(4A)	108.9(3)
C(3)-C(4)-H(4A)	108.9(3)
H(4B)-C(4)-H(4A)	107.7
N(3)-C(5)-C(6)	114.3(5)
N(3)-C(5)-H(5B)	108.7(3)
C(6)-C(5)-H(5B)	108.7(3)
N(3)-C(5)-H(5A)	108.7(3)
C(6)-C(5)-H(5A)	108.7(3)
H(5B)-C(5)-H(5A)	107.6
N(4)-C(6)-C(5)	113.9(5)
N(4)-C(6)-H(6B)	108.8(3)
C(5)-C(6)-H(6B)	108.8(3)
N(4)-C(6)-H(6A)	108.8(3)
C(5)-C(6)-H(6A)	108.8(3)
H(6B)-C(6)-H(6A)	107.7
N(4)-C(7)-C(8)	113.2(5)
N(4)-C(7)-H(7B)	108.9(3)
C(8)-C(7)-H(7B)	108.9(3)
N(4)-C(7)-H(7A)	108.9(3)
C(8)-C(7)-H(7A)	108.9(3)
H(7B)-C(7)-H(7A)	107.8
N(1)-C(8)-C(7)	112.6(5)
N(1)-C(8)-H(8B)	109.1(3)
C(7)-C(8)-H(8B)	109.1(3)
N(1)-C(8)-H(8A)	109.1(3)
C(7)-C(8)-H(8A)	109.1(3)
H(8B)-C(8)-H(8A)	107.8
N(1)-C(11)-C(12)	110.6(5)
N(1)-C(11)-H(11B)	109.5(3)
C(12)-C(11)-H(11B)	109.5(3)
N(1)-C(11)-H(11A)	109.5(3)

C(12)-C(11)-H(11A)	109.5(3)
H(11B)-C(11)-H(11A)	108.1
O(1)-C(12)-N(5)	123.6(5)
O(1)-C(12)-C(11)	120.6(5)
N(5)-C(12)-C(11)	115.8(5)
N(5)-C(13)-C(14)	110.5(5)
N(5)-C(13)-C(15)	111.9(5)
C(14)-C(13)-C(15)	110.6(5)
N(5)-C(13)-H(13)	107.9(3)
C(14)-C(13)-H(13)	107.9(4)
C(15)-C(13)-H(13)	107.9(3)
C(13)-C(14)-H(14C)	109.5(4)
C(13)-C(14)-H(14B)	109.5(4)
H(14C)-C(14)-H(14B)	109.5
C(13)-C(14)-H(14A)	109.5(3)
H(14C)-C(14)-H(14A)	109.5
H(14B)-C(14)-H(14A)	109.5
C(151)-C(15)-C(159)	120.0(6)
C(151)-C(15)-C(13)	119.1(6)
C(159)-C(15)-C(13)	120.9(6)
N(2)-C(21)-C(22)	110.0(5)
N(2)-C(21)-H(21B)	109.7(3)
C(22)-C(21)-H(21B)	109.7(3)
N(2)-C(21)-H(21A)	109.7(3)
C(22)-C(21)-H(21A)	109.7(3)
H(21B)-C(21)-H(21A)	108.2
O(2)-C(22)-N(6)	122.3(5)
O(2)-C(22)-C(21)	121.7(5)
N(6)-C(22)-C(21)	116.0(5)
N(6)-C(23)-C(24)	109.5(5)
N(6)-C(23)-C(25)	111.4(5)
C(24)-C(23)-C(25)	111.8(5)
N(6)-C(23)-H(23)	108.0(3)
C(24)-C(23)-H(23)	108.0(4)
C(25)-C(23)-H(23)	108.0(4)
C(23)-C(24)-H(24C)	109.5(3)
C(23)-C(24)-H(24B)	109.5(4)
H(24C)-C(24)-H(24B)	109.5
C(23)-C(24)-H(24A)	109.5(4)
H(24C)-C(24)-H(24A)	109.5
H(24B)-C(24)-H(24A)	109.5
C(251)-C(25)-C(259)	118.8(6)
C(251)-C(25)-C(23)	120.2(6)
C(259)-C(25)-C(23)	121.0(6)
N(3)-C(31)-C(32)	110.2(5)
N(3)-C(31)-H(31B)	109.6(3)
C(32)-C(31)-H(31B)	109.6(3)
N(3)-C(31)-H(31A)	109.6(3)
C(32)-C(31)-H(31A)	109.6(3)
H(31B)-C(31)-H(31A)	108.1
O(3)-C(32)-N(7)	122.0(5)
O(3)-C(32)-C(31)	121.4(5)
N(7)-C(32)-C(31)	116.5(5)
N(7)-C(33)-C(35)	112.0(5)
N(7)-C(33)-C(34)	108.2(5)
C(35)-C(33)-C(34)	111.9(5)
N(7)-C(33)-H(33)	108.2(3)
C(35)-C(33)-H(33)	108.2(3)
C(34)-C(33)-H(33)	108.2(4)
C(33)-C(34)-H(34C)	109.5(3)

C(33)-C(34)-H(34B)	109.5(4)
H(34C)-C(34)-H(34B)	109.5
C(33)-C(34)-H(34A)	109.5(3)
H(34C)-C(34)-H(34A)	109.5
H(34B)-C(34)-H(34A)	109.5
C(351)-C(35)-C(359)	118.3(6)
C(351)-C(35)-C(33)	121.3(6)
C(359)-C(35)-C(33)	120.4(6)
N(4)-C(41)-C(42)	110.8(5)
N(4)-C(41)-H(41B)	109.5(3)
C(42)-C(41)-H(41B)	109.5(3)
N(4)-C(41)-H(41A)	109.5(3)
C(42)-C(41)-H(41A)	109.5(3)
H(41B)-C(41)-H(41A)	108.1
O(4)-C(42)-N(8)	123.1(6)
O(4)-C(42)-C(41)	120.2(6)
N(8)-C(42)-C(41)	116.7(6)
N(8)-C(43)-C(45)	111.1(5)
N(8)-C(43)-C(44)	108.2(5)
C(45)-C(43)-C(44)	112.0(5)
N(8)-C(43)-H(43)	108.5(3)
C(45)-C(43)-H(43)	108.5(3)
C(44)-C(43)-H(43)	108.5(3)
C(43)-C(44)-H(44C)	109.5(3)
C(43)-C(44)-H(44B)	109.5(3)
H(44C)-C(44)-H(44B)	109.5
C(43)-C(44)-H(44A)	109.5(3)
H(44C)-C(44)-H(44A)	109.5
H(44B)-C(44)-H(44A)	109.5
C(451)-C(45)-C(459)	119.8(6)
C(451)-C(45)-C(43)	120.1(6)
C(459)-C(45)-C(43)	120.1(6)
C(15)-C(151)-C(152)	121.1(6)
C(15)-C(151)-H(151)	119.5(4)
C(152)-C(151)-H(151)	119.5(4)
C(153)-C(152)-C(151)	120.0(7)
C(153)-C(152)-H(152)	120.0(4)
C(151)-C(152)-H(152)	120.0(4)
C(152)-C(153)-C(154)	120.9(7)
C(152)-C(153)-H(153)	119.6(4)
C(154)-C(153)-H(153)	119.6(4)
C(155)-C(154)-C(153)	122.1(6)
C(155)-C(154)-C(159)	118.5(6)
C(153)-C(154)-C(159)	119.4(6)
C(156)-C(155)-C(154)	121.8(6)
C(156)-C(155)-H(155)	119.1(4)
C(154)-C(155)-H(155)	119.1(4)
C(155)-C(156)-C(157)	118.9(6)
C(155)-C(156)-H(156)	120.6(4)
C(157)-C(156)-H(156)	120.6(4)
C(158)-C(157)-C(156)	121.1(7)
C(158)-C(157)-H(157)	119.5(4)
C(156)-C(157)-H(157)	119.5(4)
C(157)-C(158)-C(159)	121.8(6)
C(157)-C(158)-H(158)	119.1(4)
C(159)-C(158)-H(158)	119.1(4)
C(158)-C(159)-C(154)	117.9(6)
C(158)-C(159)-C(15)	123.6(6)
C(154)-C(159)-C(15)	118.6(6)
C(25)-C(251)-C(252)	122.2(7)

C(25)-C(251)-H(251)	118.9(4)
C(252)-C(251)-H(251)	118.9(4)
C(253)-C(252)-C(251)	120.8(7)
C(253)-C(252)-H(252)	119.6(4)
C(251)-C(252)-H(252)	119.6(4)
C(252)-C(253)-C(254)	120.4(7)
C(252)-C(253)-H(253)	119.8(4)
C(254)-C(253)-H(253)	119.8(4)
C(253)-C(254)-C(255)	123.1(7)
C(253)-C(254)-C(259)	119.4(7)
C(255)-C(254)-C(259)	117.6(7)
C(256)-C(255)-C(254)	123.0(8)
C(256)-C(255)-H(255)	118.5(5)
C(254)-C(255)-H(255)	118.5(5)
C(255)-C(256)-C(257)	118.6(8)
C(255)-C(256)-H(256)	120.7(5)
C(257)-C(256)-H(256)	120.7(5)
C(258)-C(257)-C(256)	121.2(8)
C(258)-C(257)-H(257)	119.4(5)
C(256)-C(257)-H(257)	119.4(5)
C(257)-C(258)-C(259)	121.9(7)
C(257)-C(258)-H(258)	119.1(5)
C(259)-C(258)-H(258)	119.1(4)
C(258)-C(259)-C(25)	123.9(6)
C(258)-C(259)-C(254)	117.7(7)
C(25)-C(259)-C(254)	118.4(6)
C(35)-C(351)-C(352)	121.3(6)
C(35)-C(351)-H(351)	119.4(4)
C(352)-C(351)-H(351)	119.4(4)
C(353)-C(352)-C(351)	120.2(7)
C(353)-C(352)-H(352)	119.9(4)
C(351)-C(352)-H(352)	119.9(4)
C(352)-C(353)-C(354)	121.8(6)
C(352)-C(353)-H(353)	119.1(4)
C(354)-C(353)-H(353)	119.1(4)
C(353)-C(354)-C(355)	122.6(6)
C(353)-C(354)-C(359)	119.3(6)
C(355)-C(354)-C(359)	118.1(6)
C(356)-C(355)-C(354)	121.5(7)
C(356)-C(355)-H(355)	119.2(4)
C(354)-C(355)-H(355)	119.2(4)
C(355)-C(356)-C(357)	120.3(7)
C(355)-C(356)-H(356)	119.8(4)
C(357)-C(356)-H(356)	119.8(4)
C(358)-C(357)-C(356)	120.6(7)
C(358)-C(357)-H(357)	119.7(4)
C(356)-C(357)-H(357)	119.7(4)
C(357)-C(358)-C(359)	121.2(6)
C(357)-C(358)-H(358)	119.4(4)
C(359)-C(358)-H(358)	119.4(4)
C(358)-C(359)-C(354)	118.3(6)
C(358)-C(359)-C(35)	122.6(6)
C(354)-C(359)-C(35)	119.1(6)
C(45)-C(451)-C(452)	120.5(6)
C(45)-C(451)-H(451)	119.8(4)
C(452)-C(451)-H(451)	119.8(4)
C(453)-C(452)-C(451)	120.9(6)
C(453)-C(452)-H(452)	119.5(4)
C(451)-C(452)-H(452)	119.5(4)
C(452)-C(453)-C(454)	120.0(6)

C(452)-C(453)-H(453)	120.0(4)
C(454)-C(453)-H(453)	120.0(4)
C(453)-C(454)-C(459)	119.9(6)
C(453)-C(454)-C(455)	121.6(7)
C(459)-C(454)-C(455)	118.4(6)
C(456)-C(455)-C(454)	120.7(7)
C(456)-C(455)-H(455)	119.6(5)
C(454)-C(455)-H(455)	119.6(4)
C(455)-C(456)-C(457)	120.6(7)
C(455)-C(456)-H(456)	119.7(5)
C(457)-C(456)-H(456)	119.7(4)
C(458)-C(457)-C(456)	121.3(7)
C(458)-C(457)-H(457)	119.4(5)
C(456)-C(457)-H(457)	119.4(4)
C(457)-C(458)-C(459)	119.8(7)
C(457)-C(458)-H(458)	120.1(5)
C(459)-C(458)-H(458)	120.1(4)
C(454)-C(459)-C(458)	119.1(6)
C(454)-C(459)-C(45)	118.7(6)
C(458)-C(459)-C(45)	122.2(6)
F(1)-C(1S)-F(2)	101.3(6)
F(1)-C(1S)-F(3)	103.6(6)
F(2)-C(1S)-F(3)	103.2(6)
F(1)-C(1S)-C(2S)	115.5(6)
F(2)-C(1S)-C(2S)	115.9(6)
F(3)-C(1S)-C(2S)	115.3(6)
O(1S)-C(2S)-O(2S)	127.9(6)
O(1S)-C(2S)-C(1S)	116.6(6)
O(2S)-C(2S)-C(1S)	115.4(6)
C(4S)-C(3S)-H(3SA)	109.5(4)
C(4S)-C(3S)-H(3SB)	109.5(4)
H(3SA)-C(3S)-H(3SB)	109.5
C(4S)-C(3S)-H(3SC)	109.5(4)
H(3SA)-C(3S)-H(3SC)	109.5
H(3SB)-C(3S)-H(3SC)	109.5
N(1S)-C(4S)-C(3S)	179.0(7)

Table 4. Anisotropic displacement parameters (A^2 x 10^3) for 1.
The anisotropic displacement factor exponent takes the form:
-2 pi^2 [h^2 a*^2 U11 + ... + 2 h k a* b* U12]

	U11	U22	U33	U23	U13	U12
Na	35(1)	36(1)	30(1)	2(1)	-1(1)	-2(1)
O(1)	35(3)	42(2)	38(3)	8(2)	-3(2)	0(2)
O(2)	46(3)	37(3)	38(3)	-6(2)	-10(2)	2(2)
O(3)	33(2)	47(3)	38(3)	-8(2)	9(2)	-10(2)
O(4)	42(2)	44(3)	35(2)	6(2)	9(2)	8(2)
N(1)	31(3)	32(3)	29(3)	2(3)	2(2)	3(2)
N(2)	35(3)	30(3)	27(3)	1(2)	-2(2)	1(2)
N(3)	34(3)	30(3)	32(3)	-2(3)	1(2)	0(2)
N(4)	28(3)	40(3)	26(3)	7(2)	3(2)	-1(2)
N(5)	32(3)	49(3)	27(3)	5(3)	3(3)	-1(2)
N(6)	60(3)	25(3)	37(3)	-3(3)	-14(3)	-1(3)
N(7)	27(3)	48(3)	32(3)	-12(3)	4(3)	-8(2)
N(8)	45(3)	36(3)	33(3)	-2(3)	7(3)	4(3)
C(1)	41(4)	33(4)	33(4)	10(3)	-1(3)	-9(3)
C(2)	44(4)	40(4)	32(4)	4(3)	-7(3)	-4(3)
C(3)	34(4)	42(4)	36(4)	-2(3)	4(3)	2(3)
C(4)	36(3)	37(4)	32(4)	-7(3)	2(3)	3(3)
C(5)	38(4)	29(3)	40(4)	1(3)	5(3)	-9(3)
C(6)	38(4)	33(3)	32(4)	-1(3)	6(3)	1(3)
C(7)	43(4)	27(3)	28(3)	4(3)	0(3)	5(3)
C(8)	29(3)	40(4)	31(4)	15(3)	-6(3)	5(3)
C(11)	34(4)	49(4)	39(4)	15(3)	2(3)	2(3)
C(12)	37(4)	37(4)	32(4)	6(3)	5(3)	4(3)
C(13)	37(4)	40(4)	35(4)	9(3)	6(3)	0(3)
C(14)	38(4)	80(5)	48(4)	12(4)	6(3)	4(4)
C(15)	41(4)	44(4)	27(4)	2(3)	5(3)	-14(3)
C(21)	38(4)	41(4)	38(4)	10(3)	1(3)	-8(3)
C(22)	32(3)	39(4)	28(4)	2(3)	1(3)	1(3)
C(23)	37(4)	39(4)	45(4)	4(3)	5(3)	1(3)
C(24)	48(4)	56(5)	38(4)	6(4)	0(3)	-2(4)
C(25)	37(4)	43(4)	36(4)	11(3)	-4(3)	5(3)
C(31)	34(3)	49(4)	33(4)	-13(3)	2(3)	3(3)
C(32)	40(4)	30(3)	33(4)	2(3)	2(3)	1(3)
C(33)	31(3)	37(4)	31(4)	1(3)	2(3)	-5(3)
C(34)	37(4)	49(4)	54(4)	-2(4)	-3(3)	-6(3)
C(35)	33(4)	42(4)	37(4)	-4(3)	-6(3)	-6(3)
C(41)	45(4)	26(3)	30(3)	1(3)	1(3)	-3(3)
C(42)	33(4)	37(4)	36(4)	6(3)	-1(3)	1(3)
C(43)	38(4)	49(4)	28(4)	-9(3)	6(3)	-1(3)
C(44)	39(4)	53(4)	45(4)	-17(4)	-1(3)	4(3)
C(45)	35(4)	39(4)	36(4)	-3(3)	-7(3)	10(3)
C(151)	49(4)	41(4)	36(4)	6(4)	-7(3)	-9(3)
C(152)	65(5)	40(4)	46(5)	-3(4)	5(4)	-14(4)
C(153)	54(4)	45(4)	46(5)	14(4)	15(4)	0(4)
C(154)	49(4)	44(4)	35(4)	2(3)	2(3)	-6(4)
C(155)	43(4)	41(4)	42(4)	13(4)	6(4)	3(3)

C(156)	45(4)	66(5)	33(4)	8(4)	-7(3)	-3(4)
C(157)	51(4)	40(4)	38(4)	0(3)	-7(4)	2(3)
C(158)	43(4)	55(5)	46(4)	9(4)	10(4)	6(4)
C(159)	40(4)	32(4)	30(4)	1(3)	-4(3)	2(3)
C(251)	43(4)	51(4)	42(4)	-2(4)	2(4)	12(3)
C(252)	34(4)	70(5)	48(5)	0(4)	4(4)	12(4)
C(253)	23(4)	63(5)	70(5)	17(4)	-5(4)	0(3)
C(254)	41(4)	42(4)	69(5)	6(4)	-16(4)	3(3)
C(255)	68(6)	46(5)	94(7)	7(5)	-43(5)	-7(4)
C(256)	91(7)	66(6)	64(6)	-22(5)	-32(5)	13(5)
C(257)	79(6)	70(6)	47(5)	-12(4)	-13(5)	23(5)
C(258)	45(4)	71(5)	37(4)	-8(4)	-6(4)	15(4)
C(259)	48(4)	44(4)	47(4)	4(4)	-3(4)	14(4)
C(351)	44(4)	38(4)	41(4)	11(4)	-6(3)	-10(3)
C(352)	51(4)	42(4)	66(5)	7(4)	-6(4)	-6(4)
C(353)	44(4)	45(4)	47(4)	0(4)	-7(4)	9(3)
C(354)	39(4)	32(4)	57(5)	-3(4)	-8(4)	-1(3)
C(355)	39(4)	52(5)	51(5)	-11(4)	1(4)	-3(3)
C(356)	53(5)	53(5)	50(5)	-18(4)	5(4)	-10(4)
C(357)	59(5)	50(5)	40(4)	4(4)	5(4)	-7(4)
C(358)	46(4)	42(4)	36(4)	0(3)	4(3)	-5(3)
C(359)	33(4)	44(4)	42(4)	-2(3)	1(3)	-11(3)
C(451)	38(4)	49(4)	38(4)	10(3)	1(3)	8(3)
C(452)	46(4)	51(4)	40(4)	-2(4)	-10(3)	8(3)
C(453)	37(4)	42(4)	55(5)	-10(4)	3(4)	5(3)
C(454)	39(4)	49(4)	49(5)	-6(4)	5(4)	8(4)
C(455)	49(4)	62(5)	49(5)	9(4)	11(4)	5(4)
C(456)	72(6)	60(5)	49(5)	11(4)	12(5)	18(5)
C(457)	56(5)	78(6)	31(4)	8(4)	4(4)	21(4)
C(458)	48(4)	65(5)	34(4)	0(4)	4(4)	14(4)
C(459)	39(4)	47(4)	35(4)	3(3)	-2(3)	13(3)

Table 5. Hydrogen coordinates (x 10^4) and isotropic displacement parameters (A^2 x 10^3) for 1.

	x	y	z	U(eq)
H(5C)	5941(3)	5589(3)	4388(2)	60(23)
H(6C)	1802(3)	7841(3)	4346(2)	31(17)
H(7C)	-751(3)	4144(3)	4521(2)	40(18)
H(8C)	3388(3)	1961(3)	4460(2)	42(20)
H(1B)	4331(4)	6175(3)	5217(3)	43
H(1A)	4534(4)	5834(3)	5826(3)	43
H(2B)	3012(4)	5851(4)	6047(3)	46
H(2A)	3331(4)	6705(4)	5868(3)	46
H(3B)	1207(4)	6428(4)	5259(3)	45
H(3A)	1638(4)	6626(4)	5854(3)	45
H(4B)	1698(4)	5290(3)	6072(3)	42
H(4A)	699(4)	5560(3)	5949(3)	42
H(5B)	909(4)	3715(3)	5334(3)	43
H(5A)	757(4)	4106(3)	5933(3)	43
H(6B)	2292(4)	4124(4)	6096(2)	41
H(6A)	1964(4)	3254(4)	5972(2)	41
H(7B)	4032(4)	3468(3)	5294(2)	39
H(7A)	3642(4)	3325(3)	5908(2)	39
H(8B)	3571(4)	4691(3)	6058(3)	40
H(8A)	4569(4)	4419(3)	5930(3)	40
H(11B)	4751(4)	4301(4)	4841(3)	49
H(11A)	5317(4)	4991(4)	5122(3)	49
H(13)	5212(4)	5630(4)	3361(3)	45
H(14C)	6764(9)	5729(6)	3455(18)	83
H(14B)	6666(11)	6571(21)	3739(11)	83
H(14A)	6402(5)	6451(24)	3096(9)	83
H(21B)	3298(4)	6885(4)	4819(2)	47
H(21A)	2489(4)	7344(4)	5107(2)	47
H(23)	1650(4)	7096(4)	3355(3)	49
H(24C)	1640(5)	8465(9)	3385(16)	71
H(24B)	704(23)	8459(9)	3704(9)	71
H(24A)	765(25)	8163(4)	3070(9)	71
H(31B)	361(4)	5548(4)	4909(2)	46
H(31A)	-126(4)	4833(4)	5215(2)	46
H(33)	-106(4)	4169(4)	3464(2)	40
H(34C)	-1632(7)	4039(4)	3600(17)	70
H(34B)	-1501(9)	3225(20)	3917(9)	70
H(34A)	-1299(5)	3289(21)	3261(9)	70
H(41B)	1906(4)	2953(3)	4940(2)	41
H(41A)	2751(4)	2536(3)	5220(2)	41
H(43)	3293(4)	2618(4)	3421(2)	46
H(44C)	3367(6)	1250(7)	3498(16)	69
H(44B)	4339(21)	1297(8)	3770(10)	69
H(44A)	4195(25)	1531(4)	3128(7)	69
H(151)	5287(4)	7135(4)	4376(3)	51
H(152)	4412(5)	8279(4)	4385(3)	60
H(153)	3481(5)	8560(4)	3640(3)	58
H(155)	2854(4)	8201(4)	2712(3)	50
H(156)	2740(4)	7340(4)	1965(3)	57
H(157)	3647(4)	6234(4)	1942(3)	51
H(158)	4562(4)	5937(4)	2678(3)	57

H(251)	58(4)	7294(4)	4451(3)	54
H(252)	-1229(4)	6573(4)	4569(3)	61
H(253)	-1679(4)	5685(4)	3900(3)	62
H(255)	-1500(6)	5127(4)	2935(4)	83
H(256)	-709(6)	5002(5)	2120(4)	88
H(257)	604(6)	5746(5)	1994(3)	78
H(258)	1089(4)	6591(4)	2673(3)	61
H(351)	94(4)	2690(4)	4507(3)	49
H(352)	987(4)	1556(4)	4439(3)	64
H(353)	1756(4)	1289(4)	3632(3)	54
H(355)	2198(4)	1637(4)	2653(3)	57
H(356)	2094(5)	2454(4)	1899(3)	63
H(357)	1164(5)	3553(4)	1931(3)	60
H(358)	354(4)	3838(4)	2727(3)	49
H(451)	5098(4)	2583(4)	4398(3)	50
H(452)	6382(4)	3363(4)	4354(3)	55
H(453)	6610(4)	4202(4)	3613(3)	54
H(455)	6159(5)	4694(4)	2657(3)	64
H(456)	5178(6)	4682(4)	1923(3)	73
H(457)	3959(5)	3839(5)	1922(3)	66
H(458)	3665(5)	3034(4)	2684(3)	59
H(3SA)	2138(22)	4700(14)	8251(3)	78
H(3SB)	2241(25)	5628(11)	8216(3)	78
H(3SC)	3105(5)	5088(23)	8278(3)	78